ORNL/TM-2002/93

OAK RIDGE
NATIONAL LABORATORY

MANAGED BY UT-BATTELLE
FOR THE DEPARTMENT OF ENERGY

ANALYSIS OF THE JASPER AXIAL SHIELD EXPERIMENT

September 2002

C. O. Slater
Oak Ridge National Laboratory

UT-BATTELLE

ORNL-27 (4-00)

DOCUMENT AVAILABILITY

Reports produced after January 1, 1996, are generally available free via the U.S. Department of Energy (DOE) Information Bridge:

Web site: http://www.osti.gov/bridge

Reports produced before January 1, 1996, may be purchased by members of the public from the following source:

National Technical Information Service
5285 Port Royal Road
Springfield, VA 22161
Telephone: 703-605-6000 (1-800-553-6847)
TDD: 703-487-4639
Fax: 703-605-6900
E-mail: info@ntis.fedworld.gov
Web site: http://www.ntis.gov/support/ordernowabout.htm

Reports are available to DOE employees, DOE contractors, Energy Technology Data Exchange (ETDE) representatives, and International Nuclear Information System (INIS) representatives from the following source:

Office of Scientific and Technical Information
P.O. Box 62
Oak Ridge, TN 37831
Telephone: 865-576-8401
Fax: 865-576-5728
E-mail: reports@adonis.osti.gov
Web site: http://www.osti.gov/contact.html

This report was prepared as an account of work sponsored by an agency of the United States Government. Neither the United States government nor any agency thereof, nor any of their employees, makes any warranty, express or implied, or assumes any legal liability or responsibility for the accuracy, completeness, or usefulness of any information, apparatus, product, or process disclosed, or represents that its use would not infringe privately owned rights. Reference herein to any specific commercial product, process, or service by trade name, trademark, manufacturer, or otherwise, does not necessarily constitute or imply its endorsement, recommendation, or favoring by the United States Government or any agency thereof. The views and opinions of authors expressed herein do not necessarily state or reflect those of the United States Government or any agency thereof.

ORNL/TM-2002/93

Nuclear Science and Technology Division (94)

ANALYSIS OF THE JASPER AXIAL SHIELD EXPERIMENT

C. O. Slater
Oak Ridge National Laboratory
Oak Ridge, TN 37831

Date Published: September 2002

LIMITATION ON DISCLOSURE

This document contains information developed and furnished under the provisions of the USDOE/PNC Agreement on the Japanese-American Reactor Shielding Research Program, dated September 26, 1985. This information shall not be disseminated outside the Power Reactor and Nuclear Fuel Development Corporation (PNC), their contractors and licensees, and concerned agencies of the Government of Japan without prior approval in writing from the United States Department of Energy (USDOE). The information shall furthermore not be disseminated outside the USDOE and its contractors without prior approval in writing from PNC. This notice shall be marked on any reproduction hereof, in whole or in part.

Prepared by the
OAK RIDGE NATIONAL LABORATORY
P.O. Box 2008
Oak Ridge, Tennessee 37831-6285
managed by
UT-Battelle, LLC
for the
U.S. DEPARTMENT OF ENERGY
under contract DE-AC05-00OR22725

Page Intentionally Blank

TABLE OF CONTENTS

LIST OF TABLES v

LIST OF FIGURES vii

ABSTRACT xiii

1. INTRODUCTION 1

2.0 DESCRIPTION OF THE EXPERIMENT 3
- 2.1 Original Configurations 3
- 2.2 Remeasurement Configurations 6

3.0 THE ANALYSIS 7
- 3.1 Neutron Source 7
- 3.2 Data 7
- 3.3 Methods 11
- 3.4 Results 12
  - 3.4.1 Original Configurations 12
    - 3.4.1.1 Bonner Ball Count Rates on Centerline 30 cm Behind Configurations 12
    - 3.4.1.2 Bonner Ball Count Rates on Centerline 150 cm Behind Configurations 15
    - 3.4.1.3 Neutron Spectra Behind Configurations 17
    - 3.4.1.4 Bonner Ball Count Rates at the Spectrum Measurement Locations 17
    - 3.4.1.5 Hornyak Button and Bonner Ball Count Rate Radial Traverses Behind Configurations 17
    - 3.4.1.6 Neutron Streaming Factors 18
    - 3.4.1.7 Shield Attenuation 18
    - 3.4.1.8 Radiation Background 19
  - 3.4.2 Remeasurement Configurations 30
    - 3.4.2.1 Bonner Ball Count Rates on Centerline 30 cm Behind Configurations 30
    - 3.4.2.2 Bonner Ball Count Rates on Centerline 150 cm Behind Configurations 30
    - 3.4.2.3 Neutron Spectra Behind Configurations 30
    - 3.4.2.4 Bonner Ball Count Rates at the Spectrum Measurement Locations 31
    - 3.4.2.5 Hornyak Button and Bonner Ball Count Rate Radial Traverses Behind Configurations 31
    - 3.4.2.6 Neutron Streaming Factors 31
    - 3.4.2.7 Radiation Background 31

4.0 SUMMARY 35

REFERENCES 37

APPENDIX A 39

APPENDIX B 47

APPENDIX C 61

APPENDIX D 65

APPENDIX E 73

APPENDIX F 77

APPENDIX G 107

LIST OF TABLES

Table 1. Atomic densities ($b^{-1} \cdot cm^{-1}$) for constituents of materials used in the experiment calculations..... 9
Table 2. Macro mixture compositions formed from base mixtures in Table 1..... 11
Table E1. Bonner Ball count rate response functions (cm^2). 75
Table E2. Hornyak Button response functions ($erg \cdot g^{-1} \cdot cm^2$) with various energy cutoffs to simulate detector bias settings. 76
Table F1. Comparison of calculated and measured 3-inch Bonner ball count rates on centerline 30 cm behind various original configurations. 79
Table F2. Comparison of calculated and measured 4-inch Bonner ball count rates on centerline 30 cm behind various original configurations. 80
Table F3. Comparison of calculated and measured 5-inch Bonner ball count rates on centerline 30 cm behind various original configurations. 81
Table F4. Comparison of calculated and measured 8-inch Bonner ball count rates on centerline 30 cm behind various original configurations. 82
Table F5. Comparison of calculated and measured 10-inch Bonner ball count rates on centerline 30 cm behind various original configurations. 83
Table F6. Comparison of calculated and measured 12-inch Bonner ball count rates on centerline 30 cm behind various original configurations. 84
Table F7. Comparison of calculated and measured 3-inch Bonner ball count rates on centerline 150 cm behind various original configurations. 85
Table F8. Comparison of calculated and measured 4-inch Bonner ball count rates on centerline 150 cm behind various original configurations. 86
Table F9. Comparison of calculated and measured 5-inch Bonner ball count rates on centerline 150 cm behind various original configurations. 87
Table F10. Comparison of calculated and measured 8-inch Bonner ball count rates on centerline 150 cm behind various original configurations. 88
Table F11. Comparison of calculated and measured 10-inch Bonner ball count rates on centerline 150 cm behind various original configurations. 89
Table F12. Comparison of calculated and measured 12-inch Bonner ball count rates on centerline 150 cm behind various original configurations. 90
Table F13. Comparison of calculated and measured Bonner ball count rates and the integrated spectrum at the spectrum measurement location 179.1 cm behind original Axial Shield Experiment Configuration I.A. 91
Table F14. Comparison of calculated and measured Bonner ball count rates and the integrated spectrum at the spectrum measurement location 25 cm behind original Axial Shield Experiment Configurations II.A and II.B (with lead). 92
Table F15. Comparison of calculated and measured Bonner ball count rates and the integrated spectrum at the spectrum measurement location 98.3 cm behind original Axial Shield Experiment Configuration II.B (no lead). 93
Table F16. Heterogeneous-to-homogeneous Bonner ball count-rate ratios (streaming factors) for various Axial Shield Experiment original configurations. 94
Table F17. Comparison of calculated and measured 3-inch Bonner ball count rates on centerline 30 cm behind various remeasurement configurations. 95
Table F18. Comparison of calculated and measured 4-inch Bonner ball count rates on centerline 30 cm behind various remeasurement configurations. 95
Table F19. Comparison of calculated and measured 5-inch Bonner ball count rates on centerline 30 cm behind various remeasurement configurations. 96
Table F20. Comparison of calculated and measured 8-inch Bonner ball count rates on centerline 30 cm behind various remeasurement configurations. 96
Table F21. Comparison of calculated and measured 10-inch Bonner ball count rates on centerline 30 cm behind various remeasurement configurations. 97

Table F22. Comparison of calculated and measured 12-inch Bonner ball count rates on centerline 30 cm behind various remeasurement configurations. 97
Table F23. Comparison of calculated and measured 3-inch Bonner ball count rates on centerline 150 cm behind various remeasurement configurations. 98
Table F24. Comparison of calculated and measured 4-inch Bonner ball count rates on centerline 150 cm behind various remeasurement configurations. 99
Table F25. Comparison of calculated and measured 5-inch Bonner ball count rates on centerline 150 cm behind various remeasurement configurations. 100
Table F26. Comparison of calculated and measured 8-inch Bonner ball count rates on centerline 150 cm behind various remeasurement configurations. 101
Table F27. Comparison of calculated and measured 10-inch Bonner ball count rates on centerline 150 cm behind various remeasurement configurations. 102
Table F28. Comparison of calculated and measured 12-inch Bonner ball count rates on centerline 150 cm behind various remeasurement configurations. 103
Table F29. Comparison of calculated and remeasured Bonner ball count rates and the integrated spectrum at the spectrum measurement location 25 cm behind remeasurement Axial Shield Experiment Configurations II.A, II.B, and III.A. 104
Table F30. Heterogeneous-to-homogeneous Bonner ball count-rate ratios (streaming factors) for various Axial Shield Experiment remeasurement configurations. 105

LIST OF FIGURES

Figure 1. Plan view of the Tower Shield Reactor-II (TSR-II) with its wide-beam collimator. 3
Figure 2. Overview of the hexagonal shield assemblies used in the JASPER Axial Shield Experiment. 5
Figure 3. Neutron response functions in the VELM61 group structure for three Bonner balls and the Hornyak button 8
Figure 4. Comparison of the ^{11}B total cross section for ENDF/B-VI-based VITAMIN-B6 and ENDF/B-V-based VELM61 cross-section libraries. 13
Figure 5. Comparison of VITAMIN-B6 and VELM61 neutron spectra transmitted through B_4C. 14
Figure 6. Comparison of VITAMIN-E and VELM61 neutron spectra transmitted through B_4C. 15
Figure 7. Lithiated paraffin shield used to perform background measurements for the original JASPER Axial Shield Experiment configurations. 16
Figure 8. Isoplot of the calculated 5-inch Bonner ball count rate for JASPER Axial Shield Experiment original Configuration II.A using standard-weighted UO_2 cross sections. 20
Figure 9. Isoplot of the calculated 5-inch Bonner ball count rate for JASPER Axial Shield Experiment original Configuration II.A using self-shielded UO_2 cross sections. 21
Figure 10. Isoplot of the calculated 5-inch Bonner ball count rate for JASPER Axial Shield Experiment original Configuration II.B using standard-weighted UO_2 cross sections. 22
Figure 11. Isoplot of the calculated 5-inch Bonner ball count rate for JASPER Axial Shield Experiment original Configuration II.B using self-shielded UO_2 cross sections. 23
Figure 12. Isoplot of the calculated 5-inch Bonner ball count rate due to fission for JASPER Axial Shield Experiment original Configuration II.A using standard-weighted UO_2 cross sections. 24
Figure 13. Isoplot of the calculated 5-inch Bonner ball count rate due to fission for JASPER Axial Shield Experiment original Configuration II.A using self-shielded UO_2 cross sections. 25
Figure 14. Isoplot of the calculated fission neutron production in the UO_2 blankets of JASPER Axial Shield Experiment original Configuration II.A using standard-weighted UO_2 cross sections. 26
Figure 15. Isoplot of the calculated fission neutron production in the UO_2 blankets of JASPER Axial Shield Experiment original Configuration II.A using self-shielded UO_2 cross sections. 27
Figure 16. Isoplot of the calculated fission neutron production in the UO_2 blankets of JASPER Axial Shield Experiment original Configuration II.B using standard-weighted UO_2 cross sections. 28
Figure 17. Isoplot of the calculated fission neutron production in the UO_2 blankets of JASPER Axial Shield Experiment original Configuration II.B using self-shielded UO_2 cross sections. 29
Figure 18. Isoplot of the calculated 5-inch Bonner ball count rate for JASPER Axial Shield Experiment remeasurement Configuration II.A using standard-weighted UO_2 cross sections. 32
Figure 19. Isoplot of the calculated fission neutron production in the UO_2 blankets of JASPER Axial Shield Experiment remeasurement Configuration II.A using standard-weighted UO_2 cross sections. 33
Figure B1. Spectrum modifier for the JASPER Axial Shield Experiment Configurations (Configuration I.A of the Experiment Program Plan). 49
Figure B2. Details of the UO_2 blankets in the spectrum modifier for the JASPER Axial Shield Experiment Configurations. 50
Figure B3. Details of the aluminum-framed, B_4C-surrounded, seven-hexagon support for the axial shield assemblies of the JASPER Axial Shield Experiment Configurations. 51
Figure B4. Details of the stainless steel homogeneous assembly used in the JASPER Axial Shield Experiment Configurations. 52

Figure B5. Details of the B_4C homogeneous assembly used in the JASPER Axial Shield Experiment Configurations. 52
Figure B6. Details of the stainless steel rod bundle assembly used in the JASPER Axial Shield Experiment Configurations. 53
Figure B7. Details of the B_4C rod bundle assembly used in the JASPER Axial Shield Experiment Configurations. 53
Figure B8. Details of the stainless steel central sodium channel assembly used in the JASPER Axial Shield Experiment Configurations. 54
Figure B9. Details of the B_4C central sodium channel assembly used in the JASPER Axial Shield Experiment Configurations. 54
Figure B10. Details of the stainless steel central blockage assembly used in the JASPER Axial Shield Experiment Configurations. 55
Figure B11. Details of the B_4C central blockage assembly used in the JASPER Axial Shield Experiment Configurations. 55
Figure B12. Plan view for most of the configurations used in the original measurement program for the JASPER Axial Shield Experiment. 56
Figure B13. Plan view for those configurations for which neutron spectra were measured in the original measurement program for the JASPER Axial Shield Experiment. 57
Figure B14. Plan view for the configuration containing the fission gas plenum mockup in the original measurement program for the JASPER Axial Shield Experiment. 58
Figure B15. Details of the fission gas plenum mockup used in the JASPER Axial Shield Experiment Configuration III.E. 59
Figure D1. Details of the collimating lithiated-paraffin shield used in configurations for the remeasurement program for the JASPER Axial Shield Experiment. 67
Figure D2. Elevation view of the collimating lithiated-paraffin shield superimposed on the outline of the seven axial shield assembly mockup for the remeasurement program for the JASPER Axial Shield Experiment. 68
Figure D3. Plan view for the spectrum modifier plus a collimating lithiated-paraffin shield for the remeasurement program for the JASPER Axial Shield Experiment (Configuration I.A). 69
Figure D4. Plan view for the spectrum modifier plus a collimating lithiated-paraffin shield plus the B_4C homogeneous axial shield mockup for the remeasurement program for the JASPER Axial Shield Experiment (Configuration II.B). 70
Figure D5. Plan view of configurations consisting of the spectrum modifier plus axial shield mockups preceded and followed by collimating lithiated-paraffin shields for the remeasurement program for the JASPER Axial Shield Experiment (Configurations II.A, III.A, IV.A, and V.A). 71
Figure G1. Comparison of neutron spectra behind a one-dimensional model of the spectrum modifier for self-shielded and unshielded UO_2 cross sections. 109
Figure G2. Comparison of gamma-ray spectra behind a one-dimensional model of the spectrum modifier for self-shielded and unshielded UO_2 cross sections. 110
Figure G3. Comparison of neutron spectra behind a two-dimensional model of the spectrum modifier for self-shielded and unshielded UO_2 cross sections. 111
Figure G4. Comparison of neutron spectra due to neutrons from a 22-cm-diameter region of a two-dimensional model of the spectrum modifier for self-shielded and unshielded UO_2 cross sections. 112
Figure G5. Comparison of calculated and measured neutron spectra behind Jasper Axial Shield Experiment original Configuration I.A. 113
Figure G6. Comparison of calculated and measured neutron spectra behind Jasper Axial Shield Experiment original Configuration II.A. 114
Figure G7. Comparison of calculated and measured neutron spectra behind Jasper Axial Shield Experiment original Configuration II.B with lead slabs. 115

Figure G8. Comparison of calculated and measured neutron spectra behind Jasper Axial Shield Experiment original Configuration II.B without lead slabs 116
Figure G9. Comparison of calculated and measured 3-inch Bonner Ball count rates for a radial traverse 30 cm behind Jasper Axial Shield Experiment original Configuration I.A. 117
Figure G10. Comparison of calculated and measured 5-inch Bonner Ball count rates for a radial traverse 30 cm behind Jasper Axial Shield Experiment original Configuration I.A. 118
Figure G11. Comparison of calculated and measured 10-inch Bonner Ball count rates for a radial traverse 30 cm behind Jasper Axial Shield Experiment original Configuration I.A. 119
Figure G12. Comparison of calculated and measured Bonner Ball count rates and Hornyak button responses for radial traverses 30 cm behind Jasper Axial Shield Experiment original Configuration II.A and calculations using standard-weighted UO_2 cross sections. 120
Figure G13. Comparison of calculated and measured Bonner Ball count rates and Hornyak button responses for radial traverses 30 cm behind Jasper Axial Shield Experiment original Configuration II.B and calculations using standard-weighted UO_2 cross sections. 121
Figure G14. Comparison of calculated and measured Bonner Ball count rates and Hornyak button responses for radial traverses 30 cm behind Jasper Axial Shield Experiment original Configuration III.A and calculations using standard-weighted UO_2 cross sections. 122
Figure G15. Comparison of calculated and measured Bonner Ball count rates and Hornyak button responses for radial traverses 30 cm behind Jasper Axial Shield Experiment original Configuration III.B and calculations using standard-weighted UO_2 cross sections. 123
Figure G16. Comparison of calculated and measured Bonner Ball count rates and Hornyak button responses for radial traverses 30 cm behind Jasper Axial Shield Experiment original Configuration III.C and calculations using standard-weighted UO_2 cross sections. 124
Figure G17. Comparison of calculated and measured Bonner Ball count rates and Hornyak button responses for radial traverses 30 cm behind Jasper Axial Shield Experiment original Configuration III.D and calculations using standard-weighted UO_2 cross sections. 125
Figure G18. Comparison of calculated and measured Bonner Ball count rates and Hornyak button responses for radial traverses 30 cm behind Jasper Axial Shield Experiment original Configuration III.E and calculations using standard-weighted UO_2 cross sections. 126
Figure G19. Comparison of calculated and measured Bonner Ball count rates and Hornyak button responses for radial traverses 30 cm behind Jasper Axial Shield Experiment original Configuration IV.A and calculations using standard-weighted UO_2 cross sections. 127
Figure G20. Comparison of calculated and measured Bonner Ball count rates and Hornyak button responses for radial traverses 30 cm behind Jasper Axial Shield Experiment original Configuration IV.B and calculations using standard-weighted UO_2 cross sections. 128
Figure G21. Comparison of calculated and measured Bonner Ball count rates and Hornyak button responses for radial traverses 30 cm behind Jasper Axial Shield Experiment original Configuration V.A and calculations using standard-weighted UO_2 cross sections. 129
Figure G22. Comparison of calculated and measured Bonner Ball count rates and Hornyak button responses for radial traverses 30 cm behind Jasper Axial Shield Experiment original Configuration V.B and calculations using standard-weighted UO_2 cross sections. 130
Figure G23. Calculated-to-measured (C/E) response ratios for radial traverses 30 cm behind Jasper Axial Shield Experiment original Configuration I.A and calculations using self-shielded UO_2 cross sections. 131
Figure G24. Calculated-to-measured (C/E) response ratios for radial traverses 30 cm behind Jasper Axial Shield Experiment original Configuration I.A and calculations using standard-weighted UO_2 cross sections. 132

Figure G25. Calculated-to-measured (C/E) response ratios for radial traverses 30 cm behind Jasper Axial Shield Experiment original Configuration II.A and calculations using standard-weighted UO_2 cross sections. 133
Figure G26. Calculated-to-measured (C/E) response ratios for radial traverses 30 cm behind Jasper Axial Shield Experiment original Configuration II.B and calculations using standard-weighted UO_2 cross sections. 134
Figure G27. Calculated-to-measured (C/E) response ratios for radial traverses 30 cm behind Jasper Axial Shield Experiment original Configuration III.A and calculations using standard-weighted UO_2 cross sections. 135
Figure G28. Calculated-to-measured (C/E) response ratios for radial traverses 30 cm behind Jasper Axial Shield Experiment original Configuration III.B and calculations using standard-weighted UO_2 cross sections. 136
Figure G29. Calculated-to-measured (C/E) response ratios for radial traverses 30 cm behind Jasper Axial Shield Experiment original Configuration III.C and calculations using standard-weighted UO_2 cross sections. 137
Figure G30. Calculated-to-measured (C/E) response ratios for radial traverses 30 cm behind Jasper Axial Shield Experiment original Configuration III.D and calculations using standard-weighted UO_2 cross sections. 138
Figure G31. Calculated-to-measured (C/E) response ratios for radial traverses 30 cm behind Jasper Axial Shield Experiment original Configuration III.E and calculations using standard-weighted UO_2 cross sections. 139
Figure G32. Calculated-to-measured (C/E) response ratios for radial traverses 30 cm behind Jasper Axial Shield Experiment original Configuration IV.A and calculations using standard-weighted UO_2 cross sections. 140
Figure G33. Calculated-to-measured (C/E) response ratios for radial traverses 30 cm behind Jasper Axial Shield Experiment original Configuration IV.B and calculations using standard-weighted UO_2 cross sections. 141
Figure G34. Calculated-to-measured (C/E) response ratios for radial traverses 30 cm behind Jasper Axial Shield Experiment original Configuration V.A and calculations using standard-weighted UO_2 cross sections. 142
Figure G35. Calculated-to-measured (C/E) response ratios for radial traverses 30 cm behind Jasper Axial Shield Experiment original Configuration V.B and calculations using standard-weighted UO_2 cross sections. 143
Figure G36. Comparison of calculated and measured neutron spectra behind Jasper Axial Shield Experiment remeasurement Configuration II.A. 144
Figure G37. Comparison of calculated and measured neutron spectra behind Jasper Axial Shield Experiment remeasurement Configuration II.B. 145
Figure G38. Comparison of calculated and measured neutron spectra behind Jasper Axial Shield Experiment remeasurement Configuration III.A. 146
Figure G39. Comparison of calculated and measured Bonner Ball count rates for radial traverses 30 cm behind Jasper Axial Shield Experiment remeasurement Configuration I.A and calculations using standard-weighted UO_2 cross sections. 147
Figure G40. Comparison of calculated and measured Bonner Ball count rates and Hornyak button responses for radial traverses 30 cm behind Jasper Axial Shield Experiment remeasurement Configuration II.A and calculations using standard-weighted UO_2 cross sections. 148
Figure G41. Comparison of calculated and measured Bonner Ball count rates and Hornyak button responses for radial traverses 30 cm behind Jasper Axial Shield Experiment remeasurement Configuration II.B and calculations using standard-weighted UO_2 cross sections. 149

Figure G42. Comparison of calculated and measured Bonner Ball count rates and Hornyak button responses for radial traverses 30 cm behind Jasper Axial Shield Experiment remeasurement Configuration III.A and calculations using standard-weighted UO_2 cross sections. 150
Figure G43. Comparison of calculated and measured Bonner Ball count rates and Hornyak button responses for radial traverses 30 cm behind Jasper Axial Shield Experiment remeasurement Configuration IV.A and calculations using standard-weighted UO_2 cross sections. 151
Figure G44. Comparison of calculated and measured Bonner Ball count rates and Hornyak button responses for radial traverses 30 cm behind Jasper Axial Shield Experiment remeasurement Configuration V.A and calculations using standard-weighted UO_2 cross sections. 152
Figure G45. Calculated-to-measured (C/E) response ratios for radial traverses 30 cm behind Jasper Axial Shield Experiment remeasurement Configuration I.A and calculations using standard-weighted UO_2 cross sections. 153
Figure G46. Calculated-to-measured (C/E) response ratios for radial traverses 30 cm behind Jasper Axial Shield Experiment remeasurement Configuration II.A and calculations using standard-weighted UO_2 cross sections. 154
Figure G47. Calculated-to-measured (C/E) response ratios for radial traverses 30 cm behind Jasper Axial Shield Experiment remeasurement Configuration II.B and calculations using standard-weighted UO_2 cross sections. 155
Figure G48. Calculated-to-measured (C/E) response ratios for radial traverses 30 cm behind Jasper Axial Shield Experiment remeasurement Configuration III.A and calculations using standard-weighted UO_2 cross sections. 156
Figure G49. Calculated-to-measured (C/E) response ratios for radial traverses 30 cm behind Jasper Axial Shield Experiment remeasurement Configuration IV.A and calculations using standard-weighted UO_2 cross sections. 157
Figure G50. Calculated-to-measured (C/E) response ratios for radial traverses 30 cm behind Jasper Axial Shield Experiment remeasurement Configuration V.A and calculations using standard-weighted UO_2 cross sections. 158

Page Intentionally Blank

ABSTRACT

The results of the analysis of the Axial Shield Experiment are presented. This experiment is the third in a series of several experiments (eight planned initially) comprising a joint U.S. DOE-Japan PNC Shielding Research Program (JASPER). Experiments previously performed under the program included the Radial Shield Attenuation and the Fission Gas Plenum Experiments. The Axial Shield Experiment was designed to examine the shielding effectiveness of various B_4C and steel axial shield designs proposed for liquid sodium cooled fast reactors. Initially, eleven configurations were measured. Then, because of the significant background from the concrete surrounding the axial shield mockups and the large uncertainties in the concrete composition, six additional configurations were measured. These configurations included lithiated paraffin collimator shields before and after the axial shield mockup in order to reduce background from the axial shield concrete. Calculated results were obtained using the DORT two-dimensional discrete ordinates radiation transport code and several auxiliary codes, and the calculated and measured results were compared. Calculated results for the configurations without B_4C were in generally good agreement with the measured results. For those configurations with B_4C, the calculated results for remeasurement configurations with the lithiated paraffin shields still overpredicted the Bonner ball count rates and spectra, while they underpredicted for the low-energy responses at the distant detectors. In light of the problems experienced with B_4C in the analysis of the Radial Shield Attenuation Experiment, it appears that the ^{11}B cross-section data may be responsible for part of the disagreement. However, the uncertainty in the axial shield concrete composition may have also contributed to the disagreement. Overall, the analysis indicates a need for (1) better ^{11}B cross-section data, (2) greater certainty in the axial shield concrete composition, particularly the water content, and (3) spatially-dependent weighting of the ^{235}U and ^{238}U cross sections over several regions of the depleted UO_2 radial blankets. While weighted uranium cross sections obtained using a 1-D spectrum modifier model improved the agreement between calculated and measured results behind the spectrum modifier, the same cross sections led to calculated responses that greatly overpredicted the measured responses for the other configurations. This overprediction was believed to be due mainly to the neutron reflection by the axial shield or plenum concrete, reflection that was not factored into the cross-section weighting model. It can be inferred from the comparisons of the calculated and measured results that design calculations should be reasonably accurate for stainless steel shields and a bit conservative for B_4C shields.

Page Intentionally Blank

1. INTRODUCTION

Compared to the years of experience with thermal reactors, fast reactors have relatively little experience on which to base their shield designs. In an effort to verify the shielding designs for liquid sodium cooled fast reactors, the United States Department of Energy and Japan's Power Reactor and Nuclear Fuel Development Corporation (PNC) developed a cooperative program called JASPER[a]. The Axial Shield Experiment is the third of several experiments planned under the program. Previously performed experiments included the Radial Shield Attenuation Experiment[1,2] and the Fission Gas Plenum Experiment.[3,4] The Axial Shield Experiment was designed to examine the shielding effectiveness of various B_4C and steel axial shield designs proposed for liquid sodium cooled fast reactors. Initially, eleven configurations were measured. Then, because of the significant background from the concrete surrounding the axial shield mockups and the large uncertainties in the concrete composition, six additional configurations were measured. These configurations included lithiated paraffin collimator shields before and after[b] the axial shield mockup in order to reduce background from the axial shield concrete. As with the Fission Gas Plenum Experiment, a major goal of this experiment was to verify the accuracy of the calculated axial neutron leakage from the fission gas plenum and axial shield regions of a typical liquid metal reactor (LMR). Overly conservative calculated neutron fluxes could lead to an overprediction of the shielding requirements. The shielding could have a significant impact on the fuel-assembly length and the longer fuel assemblies could force an increase in the vessel height. With the increased vessel height come higher costs due to (1) the extra steel required for the vessel, (2) the additional weight to be transported, (3) a larger sodium inventory, and (4) the extra material required for other scaled-up components in the reactor building. When the calculated neutron fluxes are highly accurate, less conservatism is required in the shield design and costs are lower. Thus, reasonably accurate calculated neutron fluxes are highly desirable. The measured data from this experiment[5] serve as a benchmark for judging the adequacy of the calculational methods and data. This report presents (1) a description of the experiment, (2) a discussion of the methods and data used in the calculations, (3) the results of calculations for this experiment and their comparisons with the measured data, and (4) a few implications of the analysis for data needs and shield design.

---

[a]Japanese-American Shielding Program of Experimental Research

[b]There was no lithiated paraffin collimator shield after the axial shield mockup in remeasurement Configuration II.B.

Page Intentionally Blank

2. 0 DESCRIPTION OF THE EXPERIMENT

2.1 Original Configurations

As stated previously, eleven configurations were included in the original measurements. The configurations consisted of either a spectrum modifier only or a spectrum modifier followed by an axial shield mockup. The configurations were centered in front of the wide-beam portal of the Tower Shielding Reactor II (TSR-II) at the ORNL Tower Shielding Facility (TSF). A schematic drawing of the TSR-II is shown in Figure 1. The spectrum modifier is 152.4 cm on each side and, as shown in Figure B1, consists of slabs of material totaling approximately 10 cm of carbon steel, 9 cm of aluminum, 2.5 cm of boral, and 20 cm of depleted UO_2 radial blanket material. For reactor background shielding, the slabs were surrounded by a 20.3-cm-thick layer of lithiated paraffin and a very thick concrete layer. The UO_2 blankets are shown in Figure B2. The spectrum modifier by itself is designated as Configuration I.A.

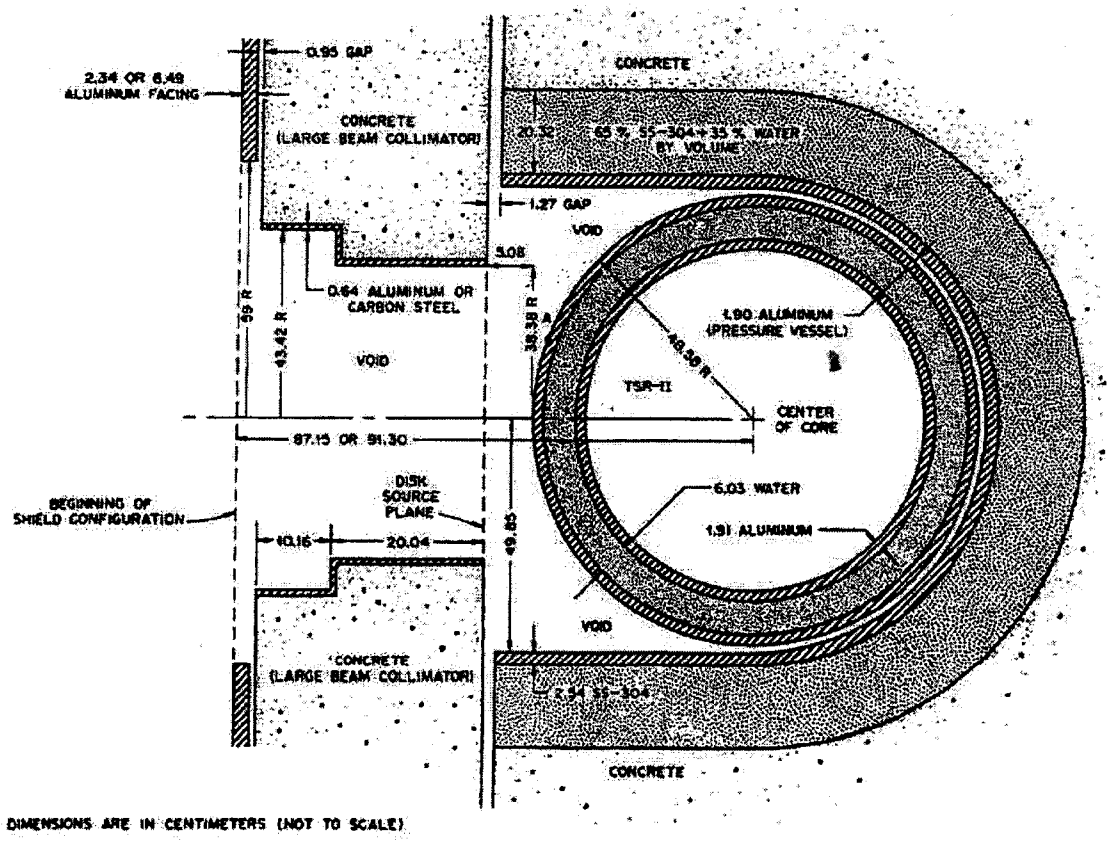

Figure 1. Plan view of the Tower Shielding Reactor-II (TSR-II) with its wide-beam collimator.

The other configurations consisted of the spectrum modifier followed by an axial shield mockup. The approximately 45-cm-thick axial shield mockup included seven hexagonal-shaped assemblies in an aluminum mesh that was surrounded by boron carbide (B_4C) and concrete lined by carbon steel as shown in Figure B3. There were eight types of assemblies (four types each for B_4C and stainless steel assemblies). The assemblies are shown in Figure 2 and more detailed descriptions are given in Figures B4-B11. Shown in Figures B4 and B5 are the stainless steel and B_4C homogeneous assemblies. Figures B6 and B7 show the stainless steel and B_4C rod bundle assemblies; Figures B8 and B9 show the stainless steel and B_4C central sodium channel assemblies; and Figures B10 and B11 show the stainless steel and B_4C central blockage assemblies. In each case, the aluminum was used to represent sodium and was included at about half the sodium volume fraction found in an LMR so that the neutron attenuation was about the same as that for the equivalent sodium. Basically, the configurations are described in the Experimental Program Plan in Appendix A. The axial shield configurations included ones with (1) seven homogeneous B_4C assemblies (II.A), (2) seven homogeneous stainless steel assemblies (II.B), (3) one B_4C central blockage assembly surrounded by six homogeneous B_4C assemblies (III.A), (4) seven B_4C central blockage assemblies (III.B), (5) one stainless steel central blockage assembly surrounded by six homogeneous stainless steel assemblies (III.C), (6) seven stainless steel central blockage assemblies (III.D), (7) seven B_4C central blockage assemblies with a fission-gas plenum mockup preceding the axial shield mockup (III.E), (8) one B_4C rod bundle assembly surrounded by six homogeneous B_4C assemblies (IV.A), (9) one stainless steel rod bundle assembly surrounded by six homogeneous stainless steel assemblies (IV.B), (10) one B_4C central sodium channel assembly surrounded by six homogeneous B_4C assemblies (V.A), and (11) one stainless steel central sodium channel assembly surrounded by six homogeneous stainless steel assemblies (V.B). The configuration layouts are shown in Figure B12 for most configurations, in Figure B13 for those configurations for which the neutron spectrum was measured (Configurations II.A and II.B), and in Figure B14 for Configuration III.E (the only configuration containing the fission-gas-plenum mockup). The design for the fission-gas-plenum mockup used in Configuration III.E is shown in Figure B15. More detailed descriptions of the configurations are found in the measurement report.[5]

Integral measurements were made on centerline behind the configurations with the Bonner ball system (3-, 4-, 5-, 8-, 10-, and 12-in. Bonner balls). Radial traverse integral measurements were made using the 3-, 5-, and 8-in. Bonner balls and a 0.635-cm-dia. × 0.159-cm-thick Hornyak button. The Hornyak button was used to map very localized spatial variations in the neutron flux while the Bonner balls were used to measure responses that were more global in nature, each measurement being influenced by contributions from large spatial regions. Neutron spectrum measurements were made on centerline as close as feasible behind the selected configurations using the NE-213 and Hydrogen Counter (or Benjamin) spectrometers, and 3-, 5-, and 10-in. Bonner ball measurements were made at the spectrum locations.

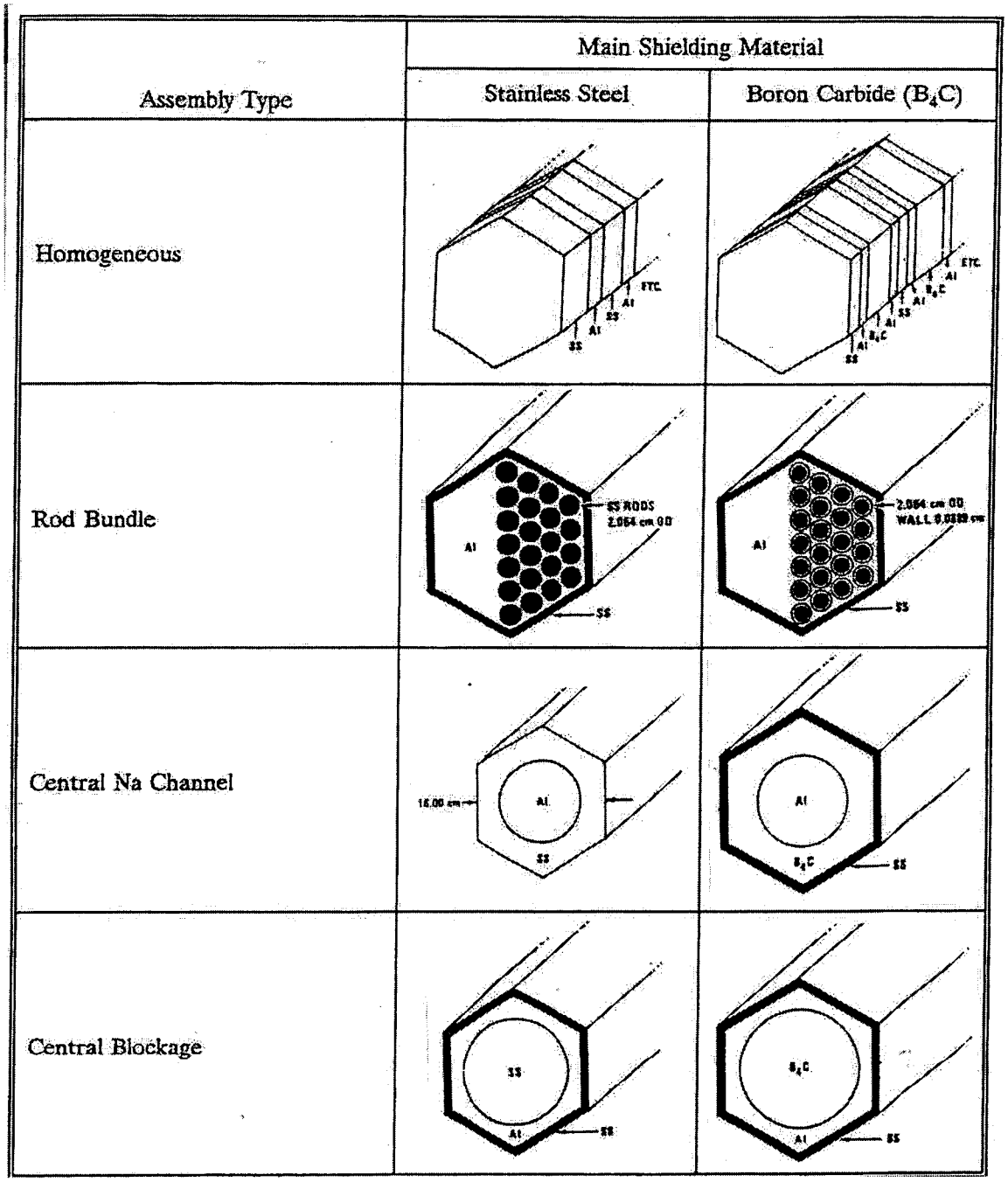

Figure 2. Overview of the hexagonal shield assemblies used in the JASPER Axial Shielding Experiment.

2.2 Remeasurement Configurations

Because the B_4C axial shield assemblies are much better neutron attenuators than is concrete, high background neutron leakage from the concrete was observed in the measurements. Since there may be large uncertainties in the concrete composition, a dominant neutron leakage from the concrete could translate to large uncertainties in the calculated neutron responses. Therefore, configurations, believed capable of greatly reducing the background leakage from the concrete were designed and a remeasurement program was carried out. The Experimental Program Plan for the remeasurements is shown in Appendix C and drawings for the configurations are shown in Appendix D. Figure D1 shows a collimating lithiated paraffin shield that was used to reduce the concrete background. The collimating shield was designed with an opening about the size of the seven axial shield assemblies, and the superimposed outline of the opening on the outline of the axial shield assemblies in Figure D2 demonstrates a reasonably good fit. Configuration I.A shown in Figure D3 has the spectrum modifier followed by the collimating shield. The other configurations consist of Configuration I.A followed by an axial shield mockup (Figure D4) or Configuration I.A followed by an axial shield mockup and another collimating shield (Figure D5). Figures D4 and D5 also show lead behind the mockups for which neutron spectra were measured. All the configurations with axial shield mockups contain B_4C assemblies and all except Configuration II.B have a collimating shield following the axial shield mockup. Configurations II.A and II.B consist of Configuration I.A followed by an axial shield mockup having seven homogeneous B_4C assemblies, Configuration II.A differing from Configuration II.B in that a collimating shield follows the axial shield mockup. Configurations III.A, IV.A, and V.A are like Configuration II.A except that the central shield assembly is replaced by a B_4C rod bundle assembly (III.A), a B_4C central blockage assembly (IV.A), or a B_4C central sodium channel assembly (V.A). More detailed descriptions of the configurations are found in the measurement report.[6] Measurements were made with the same detectors used with the original configurations (section 2.1).

3.0 THE ANALYSIS

3.1 Neutron Source

The neutron source was provided by the TSR-II with its wide-beam configuration as shown in Figure 1. The effective boundary source on a plane just upstream of the spectrum modifier was obtained from a previous analysis.[7] In that analysis, the one-dimensional angular fluxes on the reactor's spherical surface, as determined by Maerker,[8] were projected onto the side and end surfaces of a cylinder surrounding the hemisphere of the reactor nearest the opening. Those fluxes were then used as internal boundary sources for a DORT[9] calculation through a mockup of the reactor, its housing and collimator, and the spectrum modifier (without the UO_2 blankets). The boundary fluxes used as a source for this experiment were output by the above DORT calculation at the interface between the collimator and the spectrum modifier (the location labeled "beginning of the shield configuration" in Figure 1). In the previous analysis, the boundary fluxes were computed for a 51-group structure. Boundary fluxes for the 61-group structure used in the present analysis were converted by the code CHBSGP[c] using lethargy weighting.

3.2 Data

The source of the cross-section data used is the VELM61 library[10]. Detector response functions were obtained from the VELM61 two-dimensional response function array. Ref. 10 lists the sources of most of the response function data. For the Hornyak button, two response functions are given. They are based on a first-collision dose response function with estimated energy cutoffs of 120 and 270 keV corresponding to the bias setting of the detector. (Actually, beyond truncating the response below a certain energy, one should also reduce the response values by the fraction of light pulses that would have energies below the cutoff energy, since those pulses would not be counted.) For this analysis, higher energy cutoffs were explored because calculated results consistently overpredicted measured responses in previous experimental analyses. New response functions were obtained from the VELM61 response functions by zeroing out the response for groups with energies below the cutoff energy. The additional response functions were generated for cutoff energies of 302, 498, and 743 keV. Response functions are given in Tables E1 and E2 in Appendix E. The Hornyak button response function with the 743 keV energy cutoff was selected to obtain the calculated responses to be compared with the measurements. Note that the normalization factors for the response functions depend on the units of the neutron flux. Since the units of the neutron source are per minute per watt, the fluxes have units of $cm^{-2} \cdot min^{-1} \cdot W^{-1}$. Therefore, after the response functions are folded with the fluxes, the Bonner ball count rates are multiplied by 0.0166667 to obtain count rates per second per watt and the Hornyak button dose rate is multiplied by 60.0 to obtain a dose rate with the units "ergs per gram per hour per watt". Plots of the Hornyak button and the 3-, 5-, and 10-inch Bonner ball response functions in the VELM61 neutron group structure are shown in Figure 3.

Material composition data are shown in Table 1. They were based mainly on the analyses given in Tables 1-14 of Ref. 5. Compositions for some materials were retained from previous experimental analyses. The compositions of mixtures formed by combining portions of one or more of the basic mixtures of Table 1 (i.e., macromixtures) are shown in Table 2. For the axial shield region, the inner six walls of the support mesh were separated into one cylindrical annular region, and the 18 exterior walls of the support mesh were separated into an outer annular region. The remaining six walls of the support mesh were homogenized with the shield materials in the outer six axial shield assemblies to form some of the macromixtures shown in Table 2. While the central blockage and central sodium channel assemblies in the center position could be separated into two or three heterogeneous regions, the rod bundle had to be homogenized and is one of the macromixtures in Table 2.

---

[c]Undocumented code written by author.

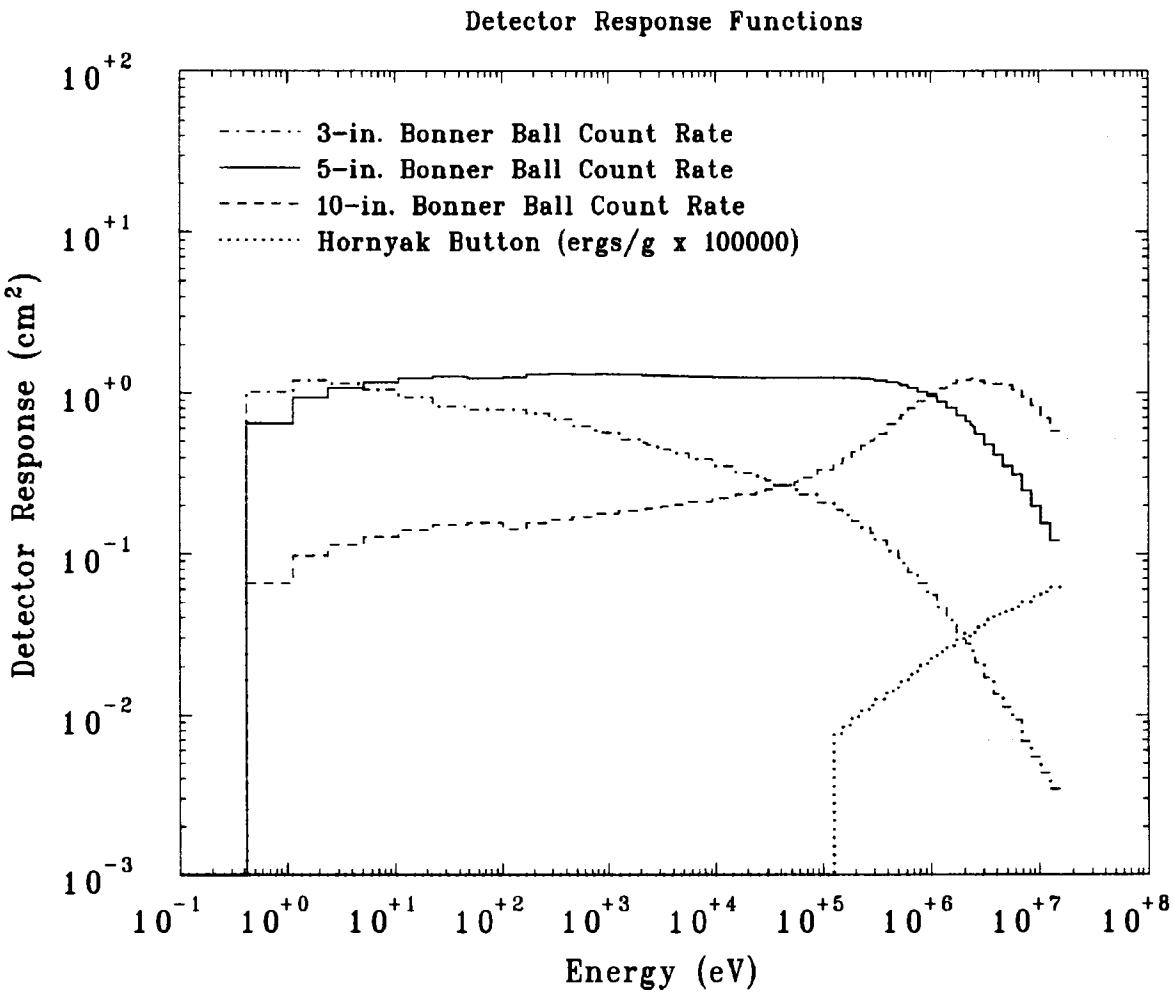

Figure 3. Neutron response functions in the VELM61 group structure for three Bonner balls and the Hornyak button.

Table 1. Atomic densities ($b^{-1} \cdot cm^{-1}$) for constituents of materials used in the experiment calculations.

Element	Material							
	Carbon Steel	Aluminum Slab	Boral	UO_2 Blanket Mixture	Lithiated Paraffin	Lead	B_4C (1.0 g/cm^3)	Gas Plenum Aluminum
H					5.930-2			
6Li					5.625-4			
^{7}Li					6.938-3			
^{10}B			5.130-3				8.713-3	
^{11}B			2.077-2				3.529-2	
C	9.854-4[a]		6.450-3		3.340-2		1.003-2	
N							4.369-4	
O				2.963-2	1.130-2			
Na				5.592-3				
Mg		5.752-4						6.956-4
Al		5.875-2	3.650-2	6.880-3				5.854-2
Si	4.214-4	3.648-4						3.937-4
P								
S								
K								
Ca								
Ti		1.426-5						8.488-6
Cr	1.366-4	6.881-5						5.317-5
Mn	8.617-4	2.960-6						3.256-5
Fe	8.329-2	1.369-4	7.700-4	1.995-5				1.223-4
Ni	4.032-5			3.635-5				
Cu	2.235-5	7.678-5						1.101-4
Mo	9.869-6							
Pb						3.299-2		
^{235}U				1.056-4				
^{238}U				1.471-2				

[a]Read as 9.854×10^{-4}.

Table 1. (continued).

Element	Material						
	SS304	B_4C Rod Bundle SS	Gas Plenum SS	Gas Plenum Concrete	Axial Shield Concrete[a]	Axial Shield Concrete[b]	Block Concrete
H				6.160-3	7.883-3	1.257-2	6.400-3
^{6}Li							
^{7}Li							
^{10}B							
^{11}B							
C				1.080-2	1.057-2	1.025-2	1.010-2
N							
O				4.520-2	4.503-2	4.611-2	4.480-2
Na				8.280-5	1.026-5	9.945-6	
Mg				5.010-3	4.733-3	4.588-3	2.180-3
Al				6.980-4	4.452-4	4.315-4	6.240-4
Si		5.265-4	7.813-4	2.080-3	2.264-3	2.195-3	4.350-3
P				6.190-6	2.037-5	1.974-5	
S				9.680-5	2.889-5	2.800-5	5.780-5
K				1.770-4	1.627-4	1.577-4	1.110-4
Ca				9.600-3	9.527-3	9.234-3	9.890-3
Ti		4.979-5	1.992-5				
Cr	1.530-2[c]	1.679-2	1.752-2				
Mn	1.760-3	1.077-3	1.302-3				
Fe	6.000-2	6.005-2	5.913-2	5.270-4	1.702-4	1.650-4	1.090-4
Ni	7.800-3	7.402-3	7.475-3				
Cu		2.778-4	1.952-4				
Mo		1.591-4	1.144-4				
Pb							
^{235}U							
^{238}U							

[a]Water content is 4.912% by weight.

[b]Water content is 7.83% by weight.

[c]Read as 1.530×10^{-2}.

Table 2. Macro mixture compositions formed from base mixtures in Table 1.

Macro Mixture	Macro Mixture Composition
60% Carbon Steel	0.6 × Carbon Steel
B_4C (ρ=1.3, 1.33, 1.38, 1.39, and 1.41 g/cm^3)	$\rho \times B_4C$ (1.0 g/cm^3)
B_4C + Al Mix #1	0.035676 × Al Slab + 0.96432 × B_4C (1.41 g/cm^3)
B_4C + Al Mix #2	0.1043 × Al Slab + 0.89570 × B_4C (1.41 g/cm^3)
SS + Al Mix #1	0.36467 × Al Slab + 0.63533 × SS304
SS + Al Mix #2	0.88447 × Al Slab + 0.11553 × SS304
SS + Al Mix #2	0.07719 × Al Slab + 0.92281 × SS304
B_4C + Al + SS	0.36467 × Al Slab + 0.09865 × SS304 + 0.53668 × B_4C (1.3 g/cm^3)
SS + Al Plenum Mix #1	0.17989 × Gas Plenum Al + 0.15963 × Gas Plenum SS
SS + Al Plenum Mix #2	0.18175 × Gas Plenum Al + 0.15716 × Gas Plenum SS

3.3 Methods

The shielding analyses were performed using the DORT two-dimensional discrete ordinates radiation transport code.[9] The calculations were performed with 61 neutron groups, a symmetric S_{12} quadrature set (96 directions), and a P_3 Legendre polynomial expansion of the cross-section scattering moments. The S_{12} quadrature set was deemed adequate for transport through the configurations because there were no streaming paths. Further, it was deemed adequate for calculating fluxes in the void short distances behind the configurations (less than 50 cm), since most rays from the source plane to the detector location would lie within the bounds of the discrete quadrature directions. Thus, the same quadrature was used to calculate the neutron fluxes in the void region behind the configuration.

Several auxiliary codes were used to either prepare input for DORT or to process output from DORT. Cross sections were mixed and a group-independent cross-section file was prepared for DORT using the AXMIX code.[11] RTFLUM[12] was used to prepare a restart flux guess for DORT. Plotting of the measured and calculated data was performed with the ASPECT code.[13] Auxiliary codes written by the author, including BSPRP2, VFX2BD, DSKTRN, DTWTPN, PSPECT, and XPANVF, were used to process DORT data files. BSPRP2 was used to optionally change the mesh and/or quadrature on a boundary flux file while preparing an input source for DORT. VFX2BD was used to copy boundary fluxes from a DORT flux moments file (VARFLM format) and create a disk boundary source file for a DORT calculation through a void region behind a configuration. This code (a modification to the VFL2BD code) also calculates the integrated source by group for both the +Z and -Z directions. DSKTRN and DTWTPN used DORT flux files and response functions to calculate detector responses. DTWTPN averages responses over finite-sized spherical detectors located within the DORT geometry while DSKTRN integrates the angular flux on the cylindrical end surfaces of the DORT geometry to calculate responses at detectors outside the geometry. Traditionally, DTWTPN has averaged responses over the detector hemisphere facing the source, and this hemisphere was used for all locations along a radial traverse. However, at the suggestion of J. A. Bucholz, the code was altered so that the responses would be averaged over the hemisphere having a polar axis facing a specified location (generally, a point at the center of the end of the configuration). Compared to the traditional method, this method tends to increase responses at detectors on the fringes of a radial traverse and bring them into better agreement with measured results. PSPECT was used to print and "punch" (i.e. output formatted 80-column data to a file) fluxes at selected input locations and print cumulative flux sums (integrals) by group at those locations. The flux spectra were then plotted and compared against the measured spectra, and the flux sums were compared against the integrals of the measured spectra. Finally, XPANVF was used to combine the flux files from DORT calculations through the configurations with those for DORT calculations through void regions behind the configurations. The purpose for such a combination is to create a flux file for a DTWTPN calculation. The combined flux file is for a geometry which envelops all the Bonner ball detector position, something

which neither individual geometry does. Using the combined flux file, the DTWTPN calculation thus avoids using extrapolation to calculate the response at any location on the spherical surface of interest.

In addition to the above codes which preprocess or postprocess DORT data, one other code (MDSPEC) written by the author was used strictly for processing the measured spectrum data. This code accepts the measured spectrum data from the unfolding codes in free-field format but in a certain order. The code then integrates the flux, bins it over a specified group structure, computes a cumulative flux sum by group, and punches the measured spectra along with FIDO[d] array numbers and data block terminators. This data then becomes input for a user-modified version of ASPECT plotting code[13] (i.e., a version with a user-written INSERT subroutine replacing the default subroutine). In the output 1$ array, the "number of data points" entry is tagged negative to indicate hydrogen counter data for which average fluxes and percent deviations are expected. By contrast, upper and lower bound flux values (plus or minus one standard deviation about the mean values) are expected for the NE-213 data, and the 1$ array contains a positive entry. The code also eliminates flux pairs from both the integrals and the spectral data whenever the lower flux level of the pair is negative. The negatives generally occur in the upper and lower energy regions where poor counting statistics usually lead to spectral unfolding difficulties that then lead to nonphysical fluxes in some energy regions. Therefore, one is justified in eliminating those fluxes from data used for comparison.

3.4 Results

3.4.1 Original Configurations

3.4.1.1 Bonner Ball Count Rates on Centerline 30 cm Behind Configurations. Bonner ball count rates on centerline 30 cm behind the configurations were calculated using the DTWTPN code. Results are presented in Tables F1-F6 for the 3-, 4-, 5-, 8-, 10-, and 12-inch Bonner balls, respectively. For Configuration I.A, results are given for both standard-weighted and self-shielded uranium cross sections. The self-shielded cross sections seemed to improve results, even though the count rates are overpredicted by about the same amount that the standard-weighted cross sections underpredict the count rates. In general, the results for all configurations are in good to excellent agreement. The worst overall agreement is the 47% overprediction of the 3-in. Bonner ball count rate for Configuration III.D. Also, the differences between the calculated and measured results tended to be larger for the B_4C assemblies than for the stainless steel assemblies.

The larger differences seen for the B_4C assemblies may be due to possible uncertainties in the ^{11}B cross section. Figure 4 shows a plot of the ^{11}B total cross section in the ENDF/B-VI-based VITAMIN-B6 fine-group library[14] group structure versus that for the ENDF/B-V-based VELM61 library. It is seen that there are a few resonances above 0.3 MeV and that both libraries represent them reasonably well. The libraries differ in the peak cross-section values at 0.2 MeV and 10 keV and in the cross-section values for energies below 10 keV. One dimensional calculations were performed using a 45-cm-thick region containing the homogeneous axial shield mixture and using as a source the DORT-calculated spectrum incident on the axial shield assembly. These calculations were performed using the VELM61 and the VITAMIN-B6 libraries as well as the ENDF-V-based VITAMIN-E fine-group library[15] from which the VELM61 library was derived. The purpose of the calculations was to determine if the differences in the ^{11}B total cross sections were enough to change significantly the C/E ratios for Bonner balls behind B_4C axial shield mockups. Figures 5 and 6 compare the VELM61 transmitted spectrum with the transmitted spectra for the VITAMIN-B6 and VITAMIN-E libraries, respectively. For both the fine-group libraries, the VELM61 library gives more transmitted neutron flux in the energy region below 2 keV and above 7 MeV. The flux is about the same in the energy range 2 keV $\leq E \leq$ 7 MeV. If the flux below 2 keV weren't such a small part of the total neutron flux, the higher low-energy neutron flux calculated by VELM61 would partially explain the overprediction of the count rates for the smaller Bonner balls behind the axial shield assemblies containing B_4C. However, when the fluxes were folded with the Bonner ball response functions, the results for the fine-group libraries differed by only a few percent from the results for the VELM61 library. Thus, if there is a problem with the ^{11}B cross sections, it is common to all three libraries. Likely, the ^{11}B cross sections from ENDF/B-V were passed to ENDF/B-VI with little or no change.

---

[d]FIDO is a method for inputting data arrays into computer codes like ASPECT. The rules are explained in a section of Ref. 13 and elsewhere.

As for the effect of cross-section self-shielding on neutron and gamma-ray fluxes, Figures G1-G4 demonstrate significant changes that occur in the spectra. For the one-dimensional model used to self-shield the cross sections, Figure G1 shows large differences in the neutron spectrum below 1 keV while Figure G2 shows much smaller differences for the gamma-ray spectrum. Figures G3 and G4 show large differences in the neutron spectrum below 1 keV for a two-dimensional model of the spectrum modifier, both for a spectrum from the full spectrum modifier and for one from a 22-cm-diameter circle at the center of the spectrum modifier. The differences are amplified when the spectrum is obtained from the smaller section of the spectrum modifier (Figure G4).

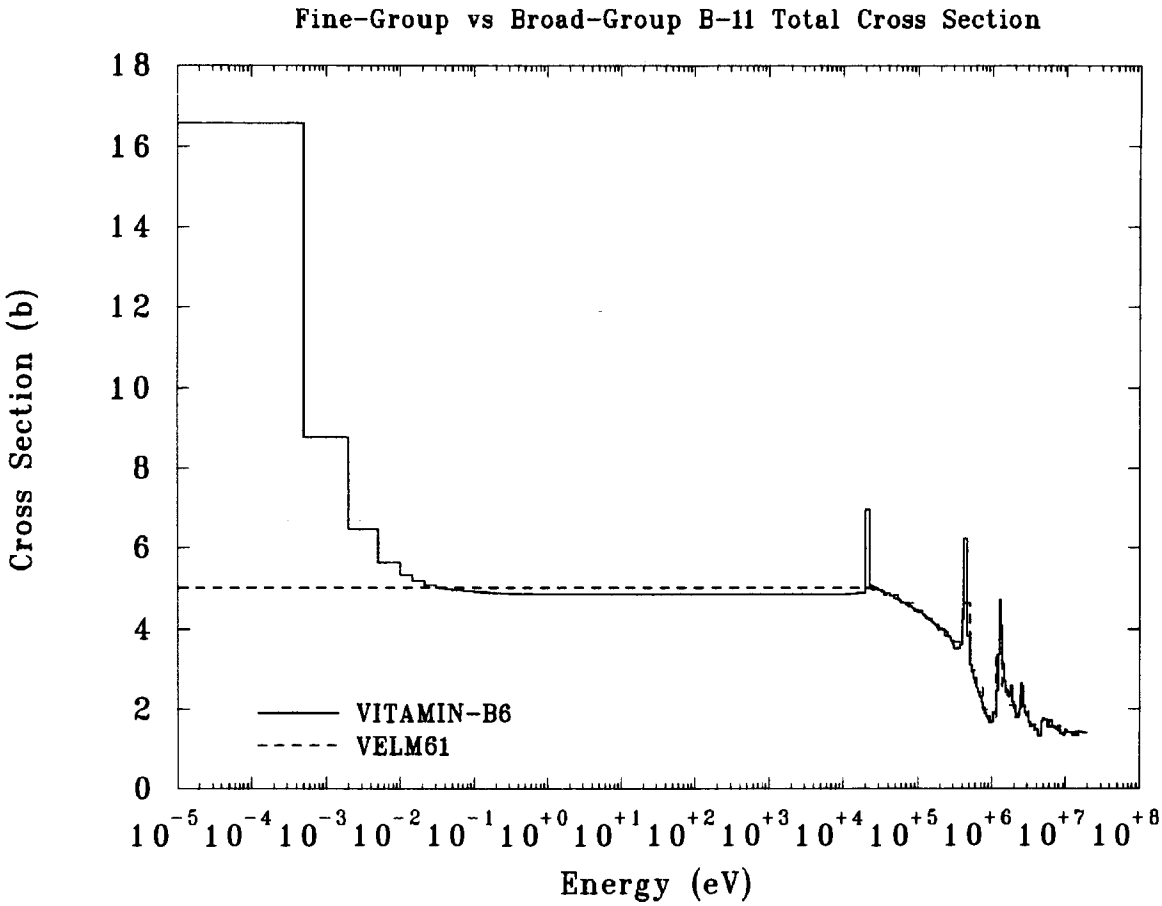

Figure 4. Comparison of the ^{11}B total cross section for ENDF/B-VI-based VITAMIN-B6 and ENDF/B-V-based VELM61 cross-section libraries.

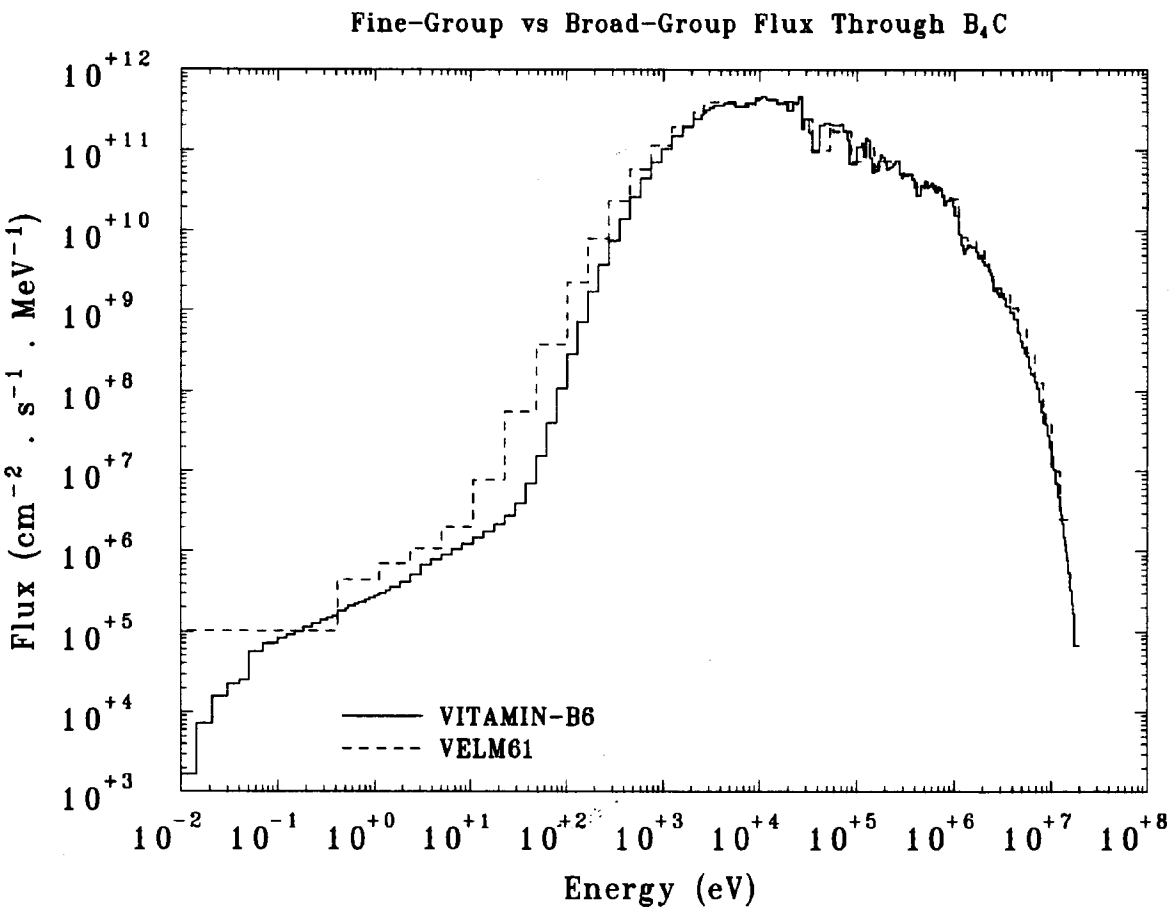

Figure 5. Comparison of VITAMIN-B6 and VELM61 neutron spectra transmitted through B_4C.

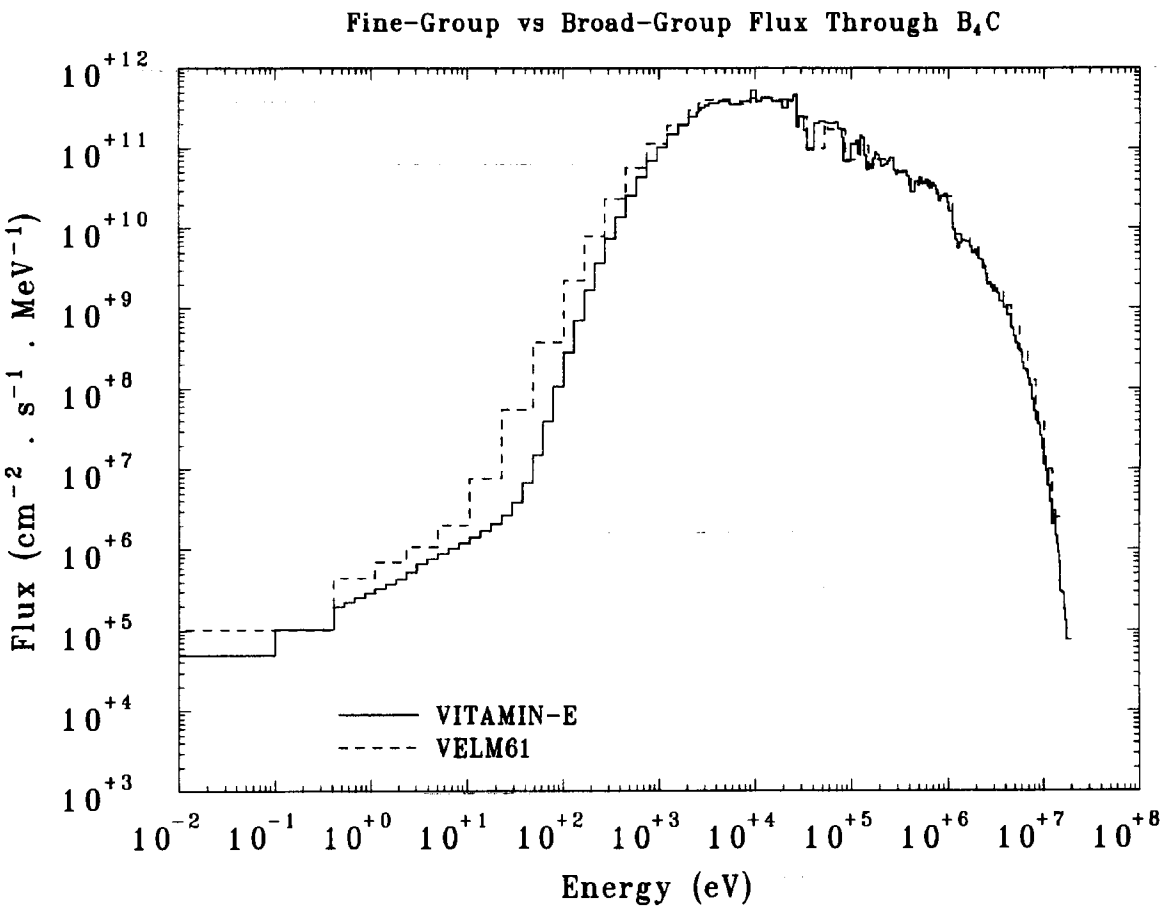

Figure 6. Comparison of VITAMIN-E and VELM61 neutron spectra transmitted through B_4C.

3.4.1.2 Bonner Ball Count Rates on Centerline 150 cm Behind Configurations. Bonner ball count rates on centerline 150 cm behind the configurations were calculated using the DSKTRN computer code with no interpolation of the angular fluxes. Count rates were calculated at the "centers of detection"[16] for each of six Bonner balls used in the measurements. Background count rates were estimated by binning contributions from regions not shadowed by the shadow shield into a separate region. For the six Bonner balls, Tables F7-F12 show the measured and calculated count rates (both foreground and net), along with the calculation-to-experiment ratios. Note that two "net" values are given for all configurations except I.A. For those configurations, Net(1) corresponds to contributions from radii less than or equal to the equivalent cylindrical radius of the shadow shield. Net(2) corresponds to contributions from an even smaller radius, indicating some region of significant neutron penetration through the shadow shield. This radius was arbitrarily chosen as the radial boundary nearest that calculated by projecting back to the source plane a ray from the detector location through a point on the cylindrical shadow-shield surface 5 cm from the outer radius. The shadow shield is shown in Figure 7. It is 50.8 cm thick and is shaped to barely cover the seven hexagonal assemblies and the surrounding B_4C collar. The equivalent radius of the shadow shield is 30.33 cm. A projection from 150 cm behind the shield back to the axial shield assembly through r=30.33 cm and z=50.8 cm yields a shadowed radius of 45.9 cm for Net(1). A projection through r=25 cm and z=50.8 cm yields a shadowed radius of 37.8 cm for Net(2). The closest radial boundaries in the problem geometry were selected, giving a radius of 45.26 cm for Net(1) and 37.88 cm for Net(2).

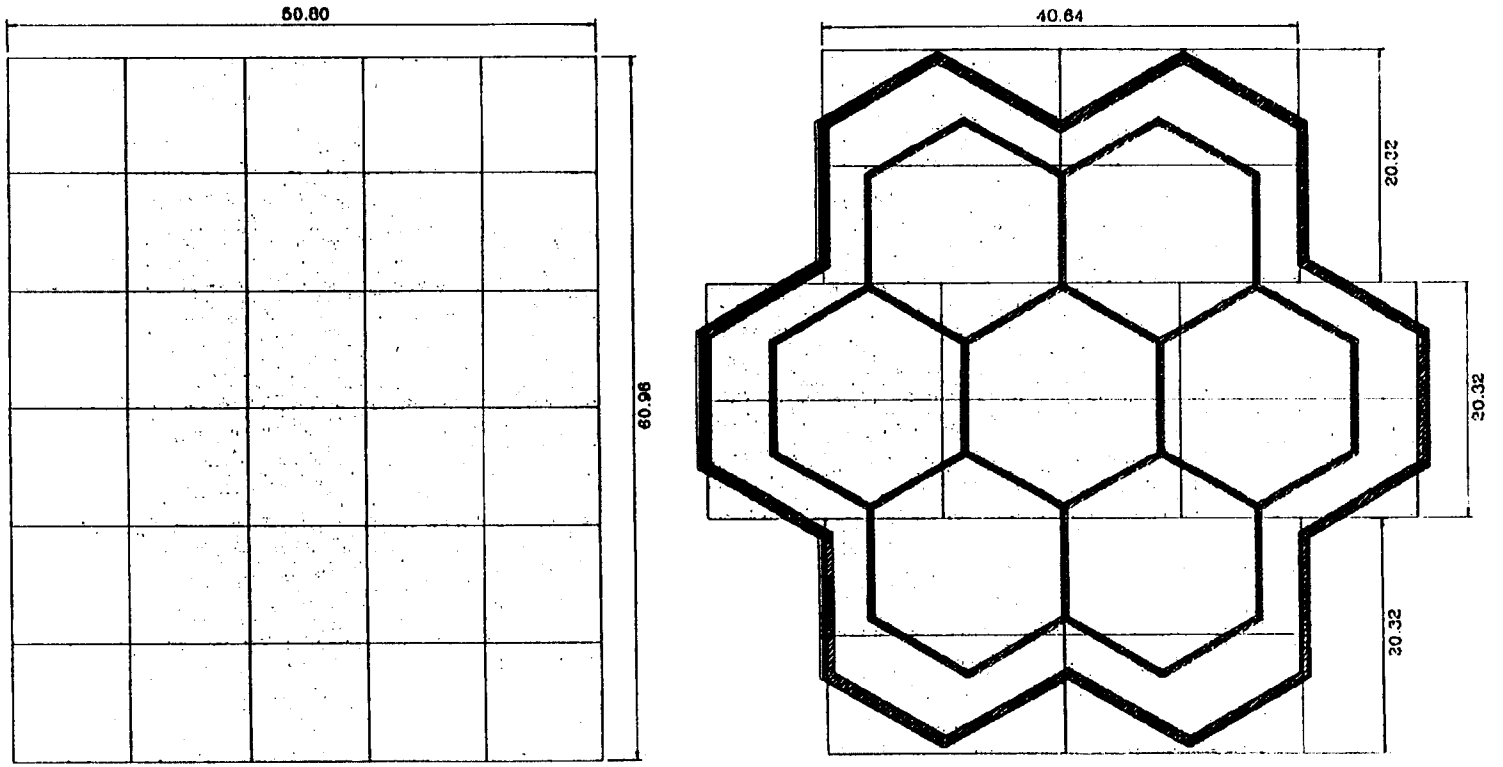

Figure 7. Lithiated paraffin shield used to perform background measurements for the original JASPER Axial Shield Experiment configurations.

For the spectrum modifier (Configuration I.A), the calculated results underpredict the measured results by 6 to 13% using the standard-weighted UO_2 cross sections and overpredict by 1 to 12% using the self-shielded UO_2 cross sections. The results using the self-shielded cross sections agree better overall than those obtained using the standard-weighted cross sections. For the other configurations, the agreement is fair to good. Agreement tends to worsen with decreasing ball size (except for the 3-in. ball). According to the results in the tables, the Net(2) calculations appear to remove too much flux from that which is assumed to contribute to the responses. The foreground measured and calculated results are in good agreement for some configurations, while the Net(1) calculated results agree about the same or better with the measured results. When there is a significant background contribution and a shadow shield is used to make background measurements, it is very difficult to translate the physical model to an equivalent calculational model. The method chosen for the Net(1) results seemed to be the most logical choice.

3.4.1.3 Neutron Spectra Behind Configurations. As mentioned earlier, spectra were measured at positions as close as possible behind the configuration. This location varied by configuration and was selected to minimize gamma-ray contributions to the detector response. Most configurations included lead slabs to reduce the gamma-ray contributions. The measured spectra are compared with the calculated spectra in Figures G5-G8. The calculated spectra are plotted as histograms while the measured spectra are plotted as curves representing plus or minus one standard deviation on the flux above 0.9 MeV (NE-213) and three histograms with plus or minus one standard deviation error bars on the flux below 1.0 MeV (1-, 3-, and 10-atm hydrogen counter data). The calculated spectra behind Configurations I.A and II.B are in good agreement with the measured results while the integral of the calculated spectrum behind Configuration II.A is about 25% higher than measured (there is definite overprediction in the 3-8 MeV energy range). The trend is the same as that shown for the Bonner ball count rates. First, the results using the self-shielded UO_2 cross sections agree better than those using the standard-weighted UO_2 cross sections. Second, the results for the stainless steel assemblies agree better than those for the B_4C assemblies.

3.4.1.4 Bonner Ball Count Rates at the Spectrum Measurement Locations. As a check on the spectrum measurements, 3-, 5-, and 10-inch Bonner ball measurements were made at the same locations where the spectrum measurements were made. Results are compared in Tables F13-F15. There is good agreement behind the spectrum modifier and behind the steel assemblies. Calculated results overpredict Bonner ball count rates behind the B_4C assemblies. Agreement is good behind the spectrum modifier (Configuration I.A) with the self-shielded UO_2 cross sections giving the better agreement. Agreement also improves when results are compared with background removed, with the self-shielded UO_2 results being in nearly perfect agreement. For Configuration II.B with the lead shield, all results except the 3-inch Bonner ball count rate agree within 20%. For Configuration II.B without the lead shield, the measured and calculated foreground results are in excellent agreement, and agreement is still good when the results are compared with background removed.

3.4.1.5 Hornyak Button and Bonner Ball Count Rate Radial Traverses Behind Configurations. Hornyak button radial traverses were made 2.37 cm behind the configurations (except for the 1.85-cm traverse behind Configuration III.E). Bonner ball radial traverses with the 3-, 5-, and 8-inch Bonner balls were made with the balls centered 30 cm behind the configurations. Behind Configuration I.A, a traverse was made with the 10-inch Bonner ball instead of the 8-inch Bonner ball as listed in the Program Plan. Calculated results for these traverses are plotted against measured results in Figures G9-G22 and ratios of the calculated-to-measured count rates are shown in Figures G23-G35. The latter figures have a solid line drawn at an ordinate of 1.0 (perfect agreement) and two dashed lines drawn at ordinates of 0.8 and 1.2, marking the region of good agreement of calculation with measurement (±20%). For Bonner ball count rates behind the spectrum modifier (Configuration I.A), most of the ratios for the self-shielded UO_2 cross-section data fall within the region of good agreement while 50% or less of the ratios for the standard-weighted UO_2 cross sections fall within that range. For the other configurations, the calculated Bonner ball count rates are generally higher than measured, with differences being largest behind the B_4C axial shield configurations. For some configurations, the ratios for the 3-inch Bonner ball fall slightly above the region of good agreement. As has been observed in other analyses,[4] the calculated Hornyak button responses in some cases greatly overpredict the measured responses (as large as a factor of 1.75). A few values along some traverses do fall within or below the range of good agreement. These values lie at the edges of the traverse where the Bonner ball count-rare ratios also drop

sharply. Hence, the good agreement results from the tendency of the calculations to underpredict at the edges of the traverse, thus bringing the overprediction seen along the centerline within range at the edge of the traverse. Likewise, the Bonner ball ratios that are within range along the centerline tend to fall below range at the edges of the traverse.

While the self-shielded uranium cross sections improved results for Configuration I.A, the same cross sections caused count rates for the shield configurations to be overestimated due to fission hot spots near the interface between the radial blanket and the axial shield assembly. The fission density is believed to be too high because in the self-shielding of the UO_2 cross sections, the contributions of the shield configurations to the shielded cross sections were not included. Therefore, the standard-weighted UO_2 cross sections were used in calculations for the shield configurations.

3.4.1.6 Neutron Streaming Factors. Differences in the densities of the coolant and the shield material result in the preferential transport of neutrons along the coolant pathways through the shield (i.e. neutron streaming). Heterogeneous calculations should record flux differences in the coolant and in the shield materials, while the homogeneous calculations would show no differences. By comparing detector responses for the heterogeneous models to those for the homogeneous model, one can get an idea of the neutron streaming for each of the heterogeneous models. Properly performed calculations should show results similar to the measured results. Table F15 shows ratios of the Bonner ball count rates for the heterogeneous models to those for the equivalent homogeneous model. Ratios (for both the calculated and measured values) are shown for the 3-inch Bonner ball (low-energy neutron flux), the 5-inch Bonner ball (total neutron flux), and the 10-inch Bonner ball (fast neutron flux). The results indicate first that the greatest streaming effects occur for the central sodium channel assemblies. Second, the larger streaming effects occur at low neutron energies. Third, of the configurations with only one heterogeneous axial shield assembly (configurations labeled A, C, and D in the table), only those with the central sodium channel assembly have significant streaming effects (the others show an effect of 12% or less). If the trend seen for the one versus seven central blockage assembly comparison held for the other assembly types, then one should see even larger streaming effects for assemblies having seven central sodium channel assemblies. For instance, heterogeneous-to-homogeneous 5-inch Bonner ball count rate ratios would be 1.48 and 1.41 for the stainless steel and B_4C assemblies, respectively. Fourth, the central blockage and rod bundle assemblies exhibit similar streaming effects, although one might expect the central blockage assembly to allow more streaming because of the larger lumped coolant region. It is noted that the streaming factors decrease with detector size. The radii of the larger Bonner balls are greater than the equivalent cylindrical radius of the inner hexagon. Therefore, streaming might be masked partially by contributions from the homogeneous axial shield region. In addition, the cross sections for neutrons detected by those balls are not drastically different among the various materials. Hence, there is less preferential transmission through the lower density regions.

Streaming factors based on calculated count rates are generally lower than those based on the measured count rates. However, ratios for the seven central blockage B_4C assemblies are similar, while ratios of the calculated 3-inch and 5-inch Bonner ball count rates for the stainless steel assemblies are higher than the ratios of the measured count rates. In any case, one needs to find suitable scale factors to apply to fluxes or dose rates calculated using the homogeneous models.

3.4.1.7 Shield Attenuation. From the Bonner ball count rates behind the configurations, one can make observations regarding the attenuation characteristics of the shield assemblies. First, the B_4C shield assemblies are better attenuators than the steel assemblies. The attenuation factors for the high-energy neutron flux (10-inch Bonner ball count rate) are more than two times larger than those for the steel assemblies. The attenuation factors for the low-energy neutron flux (3-inch Bonner ball count rate) are four to five times those for the steel assemblies. Second, the central blockage and rod bundle assemblies attenuate almost equally, and they attenuate better than the central sodium channel type assemblies.

3.4.1.8 Radiation Background. To get a true picture of the attenuation characteristics of the axial shield assemblies, one would like the background radiation levels (i.e. contributions from any region outside the region of the shield mockup) to be as small as possible. If the axial shields are better attenuators than the

background shield (concrete), then one can expect high background detector responses. This is believed to be the case for the configurations originally measured. Isoplots of the 5-inch Bonner ball count rate for Configuration II.A (homogeneous B_4C assemblies) are shown in Figures 8-9 for standard-weighted and self-shielded UO_2 cross sections, respectively. Results for Configuration II.B (homogeneous stainless steel assemblies) are shown in Figures 10-11. These results show that radiation levels in the concrete background shield are not insignificant when compared to those at the same depth into the axial shield. While the B_4C collar around the axial shield mockups may depress the flux levels, the flux levels continue to build up in the concrete surrounding the collar. One can see that the self-shielded UO_2 cross sections result in slightly higher flux levels in the axial shield region (as well as in the concrete shield) than do the standard-weighted UO_2 cross sections.

In addition, the resonance processing for the UO_2 cross sections was performed without regard for the material that would follow the radial blanket mockup. Therefore, the use of the self-shielded cross sections in calculations for configurations containing axial shield assemblies is probably inappropriate. Separate sets of cross sections should have been created for geometry mockups having the radial blankets followed by an axial shield region and for the blankets followed by the background concrete.

The effects of the cross sections on the calculated fission neutron production within the radial blanket mockup were studied also. Figures 13-14 show isoplots of the 5-inch Bonner ball count rate for Configuration II.A due to fission only for standard-weighted and self-shielded UO_2 cross sections, respectively. The count rate due to fission is 38.4% of the total count rate for the standard-weighted UO_2 cross sections and 44.9% of the total for the self-shielded UO_2 cross sections. While the total count rate for the self-shielded UO_2 cross sections is 12% higher than that for the standard-weighted UO_2 cross sections, the count rate due to fission is 31% higher. Thus, the fission neutron distribution can have a great impact on how the calculated dose rates compare with the measured ones. Isoplots of the calculated fission neutron production in the UO_2 radial blankets of Configurations II.A and II.B for both sets of cross sections are shown in Figures 14-17. The B_4C assemblies in Configuration II.A tended to depress production levels in the second blanket (Figures 14-15) when compared to levels for the stainless steel assemblies (Figures 16-17). The self-shielded UO_2 cross sections yielded higher neutron production than did the standard weighted cross sections. Differences in the fission distribution are seen throughout the blanket region, and the self-shielded cross sections result in slightly higher production levels near the outer radius of the blankets. One can also note that if one did an axial traverse along the centerline of the blankets, one would see a monotonic decrease in the fission neutron production. If one did an axial traverse near the outer radius of the blanket mockup, one would see a monotonic decrease in the fission neutron production through the first blanket and then an increase through the second blanket. For example, the maximum production along the centerline of the second blanket is about 3000 $cm^{-3} \cdot min^{-1}$. Peak values at the interface with the concrete shield are as high as 5000 $cm^{-3} \cdot min^{-1}$ for the standard-weighted UO_2 cross sections and as high as 6300 $cm^{-3} \cdot min^{-1}$ for the self-shielded UO_2 cross sections. The largest value for production in the first blanket is about 8000 $cm^{-3} \cdot min^{-1}$. So, the concrete greatly enhances the fission source in the blankets. Fission neutron production along the centerline at the interface between the radial blanket and the axial shield fall between 1000 and 1250 $cm^{-3} \cdot min^{-1}$ for Configuration II.A using standard-weighted UO_2 cross sections and between 1250 and 1580 $cm^{-3} \cdot min^{-1}$ for Configuration II.A using the self-shielded UO_2 cross sections. For Configuration II.B, the ranges are 1250 to 1580 $cm^{-3} \cdot min^{-1}$ for the standard-weighted UO_2 cross sections and 1990 to 2510 $cm^{-3} \cdot min^{-1}$ for the self-shielded UO_2 cross sections. The peak values are thus 3 to 6 times those along the centerline, and if the axial shield is a better attenuator than concrete is, then one would expect the fission neutrons to contribute a high background count rate. Any effort that could lower the fission rate in the outer radial portion of the blanket region should help to reduce the background count rate. The remeasurement program sought first to reduce the background by limiting the low-energy neutron backscatter from the concrete to the radial blanket region and the fissions that result therefrom. The program sought also to further reduce the population of those neutrons from the reactor that penetrate the background shield.

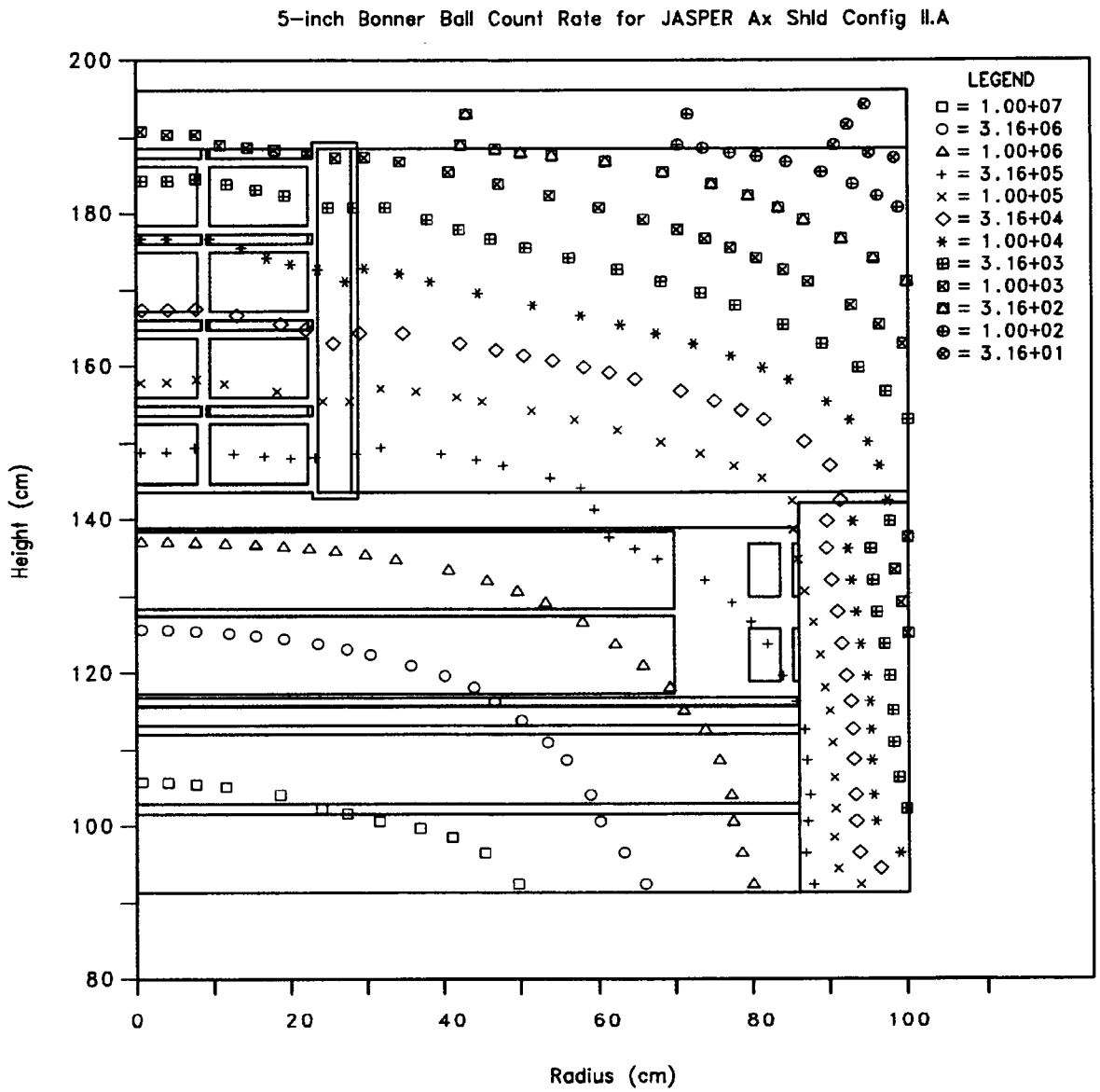

Figure 8. Isoplot of the calculated 5-inch Bonner ball count rate for JASPER Axial Shield Experiment original Configuration II.A using standard-weighted UO_2 cross sections.

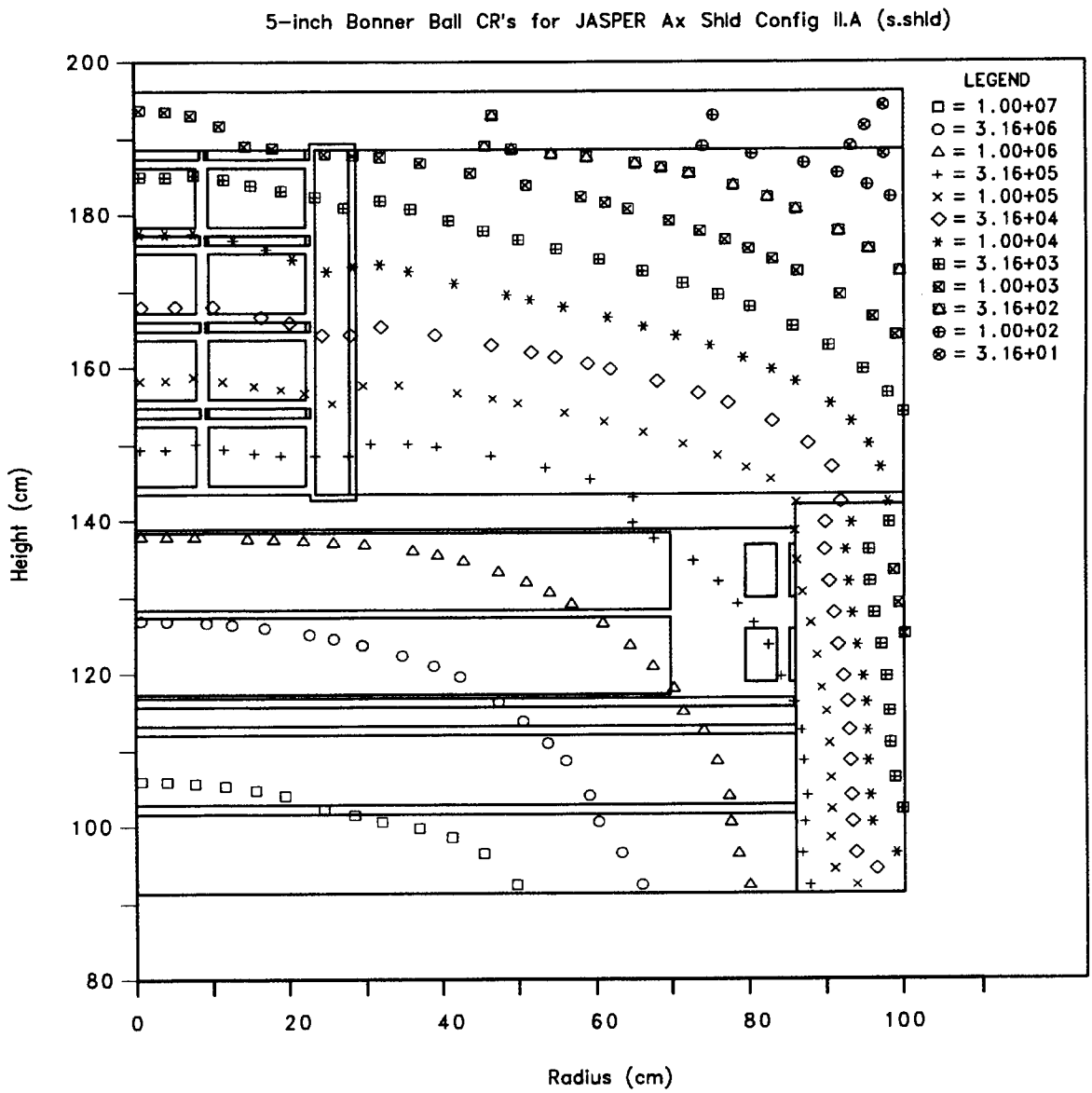

Figure 9. Isoplot of the calculated 5-inch Bonner ball count rate for JASPER Axial Shield Experiment original Configuration II.A using self-shielded UO_2 cross sections.

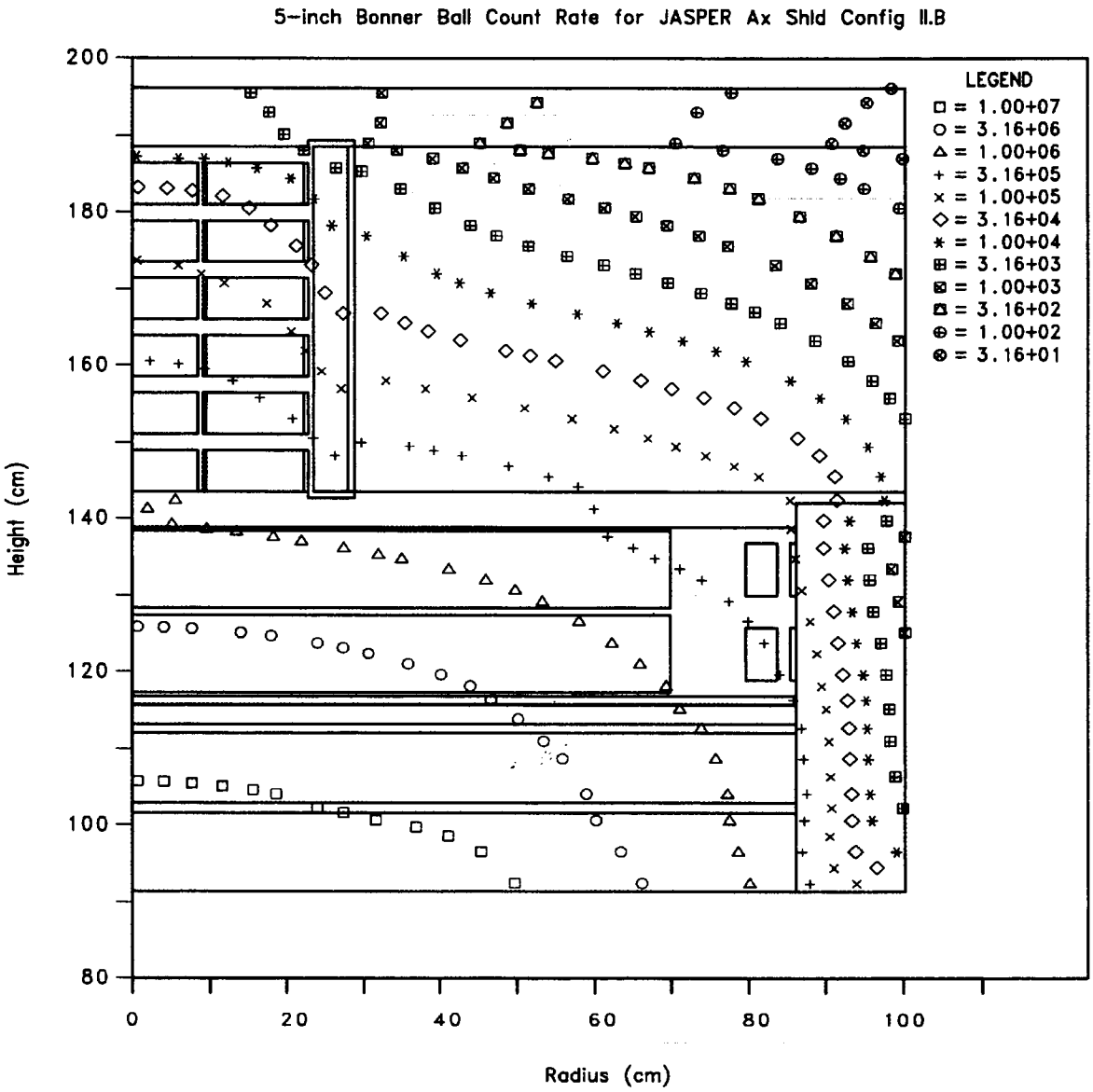

Figure 10. Isoplot of the calculated 5-inch Bonner ball count rate for JASPER Axial Shield Experiment original Configuration II.B using standard-weighted UO_2 cross sections.

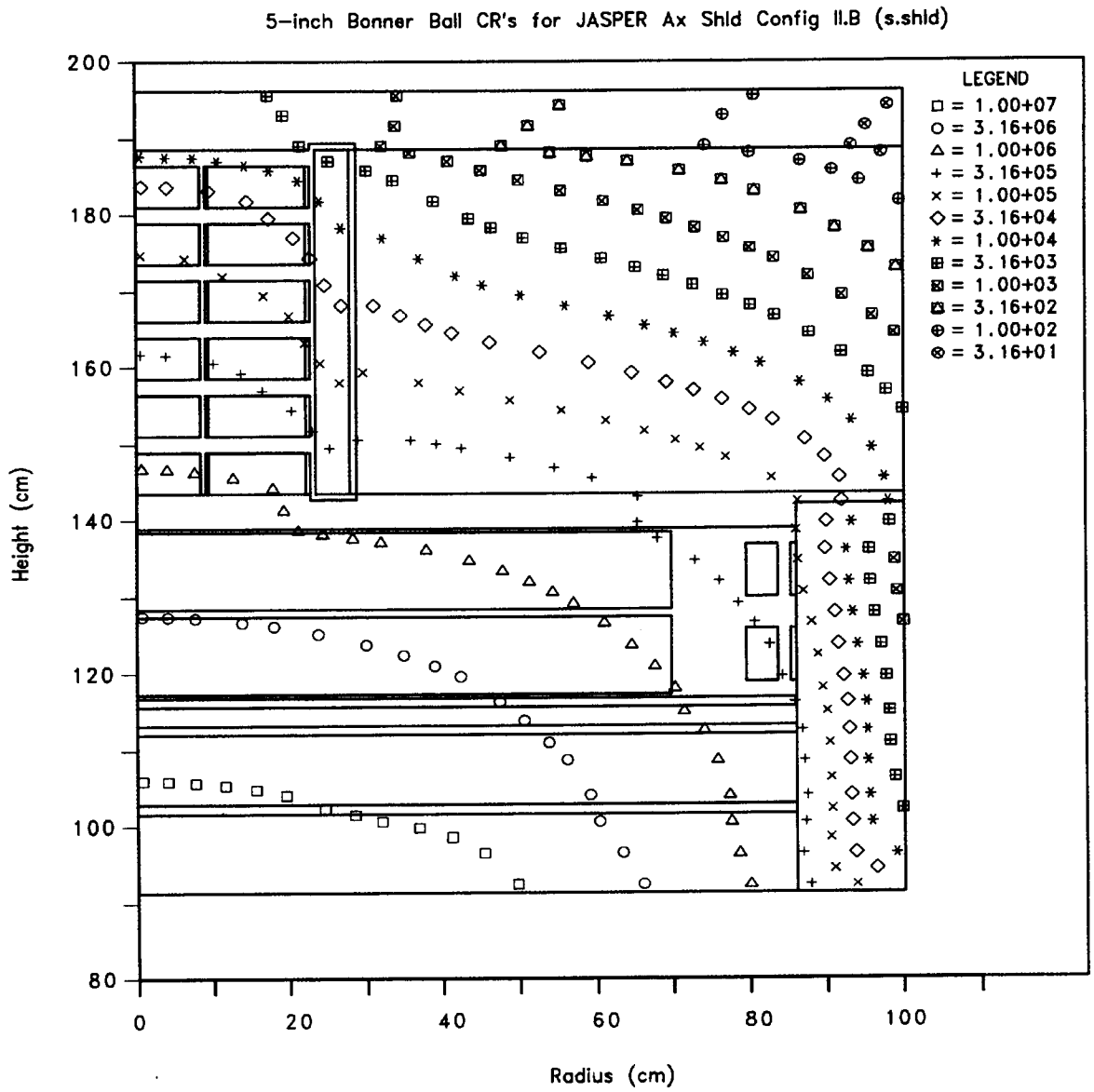

Figure 11. Isoplot of the calculated 5-inch Bonner ball count rate for JASPER Axial Shield Experiment original Configuration II.B using self-shielded UO_2 cross sections.

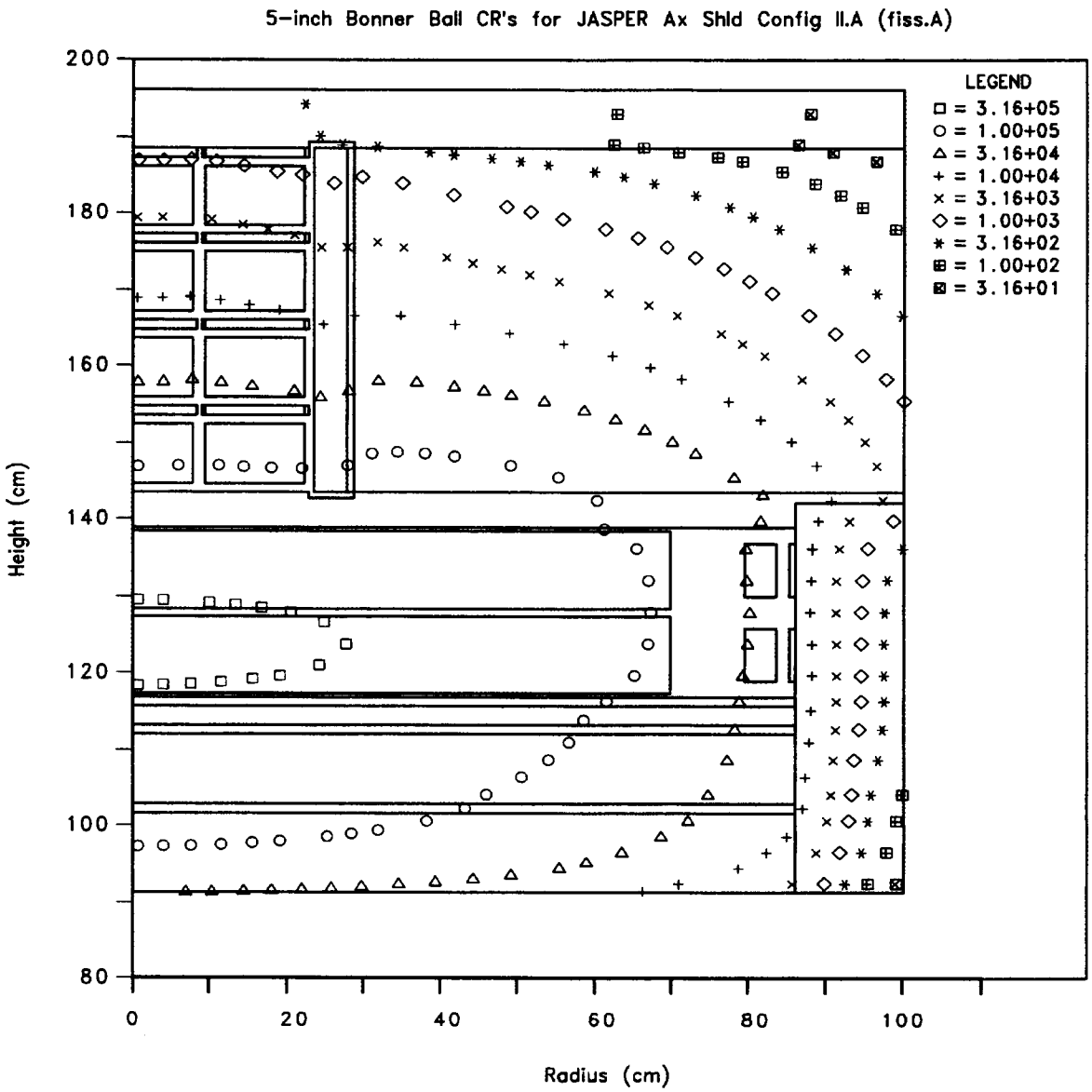

Figure 12. Isoplot of the calculated 5-inch Bonner ball count rate due to fission for JASPER Axial Shield Experiment original Configuration II.A using standard-weighted UO_2 cross sections.

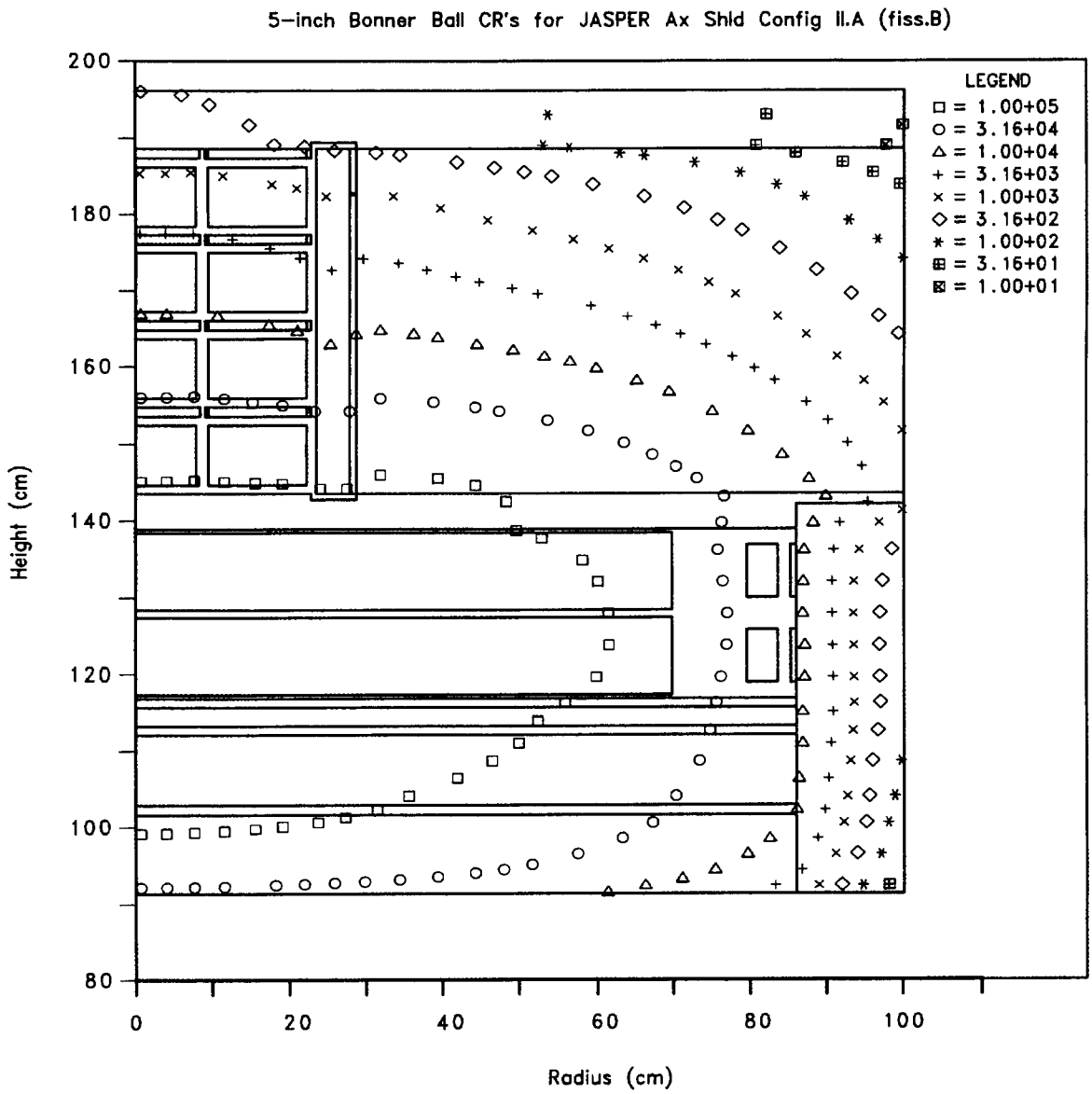

Figure 13. Isoplot of the calculated 5-inch Bonner ball count rate due to fission for JASPER Axial Shield Experiment original Configuration II.A using self-shielded UO_2 cross sections.

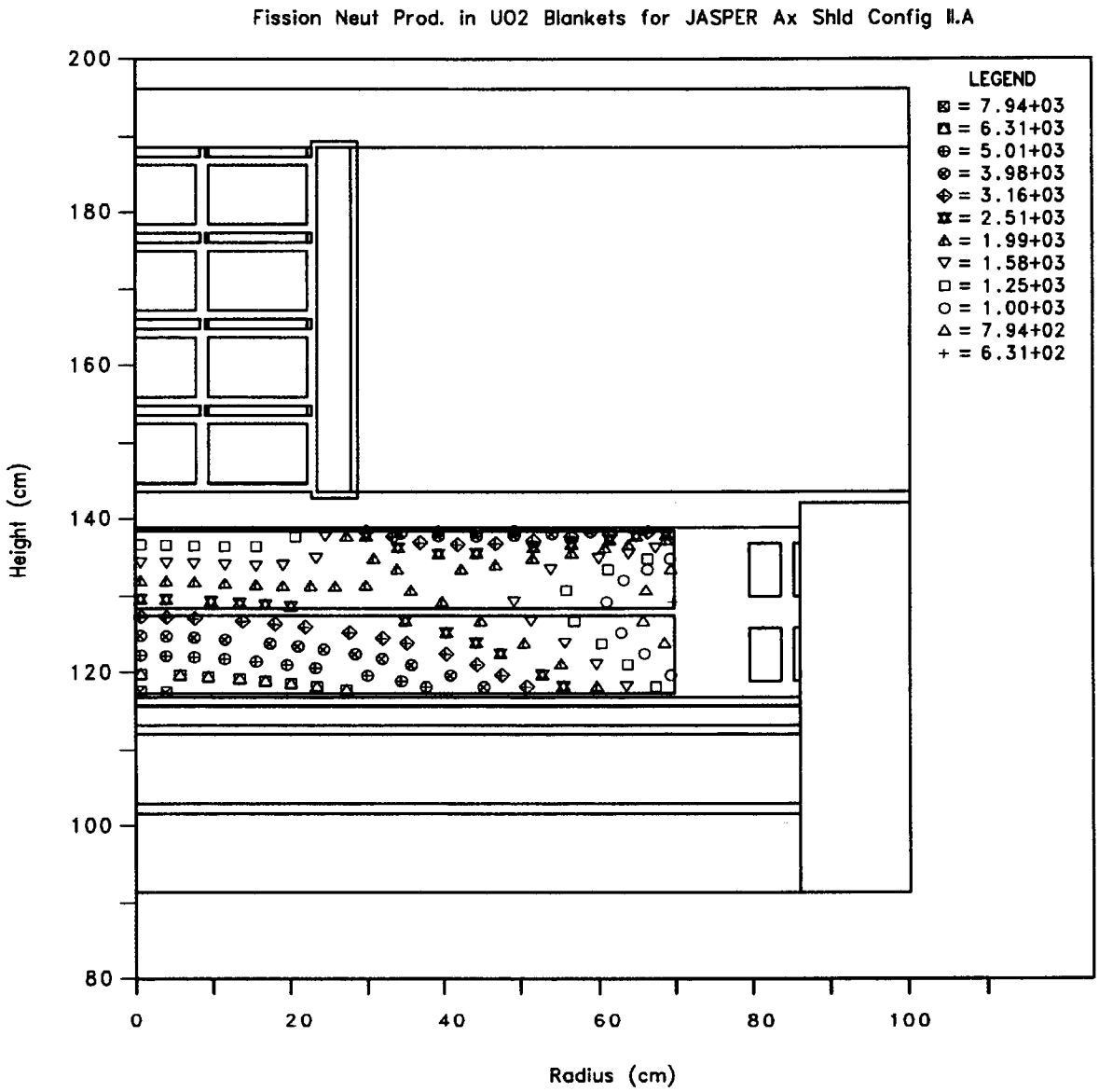

Figure 14. Isoplot of the calculated fission neutron production in the UO_2 blankets of JASPER Axial Shield Experiment original Configuration II.A using standard-weighted UO_2 cross sections.

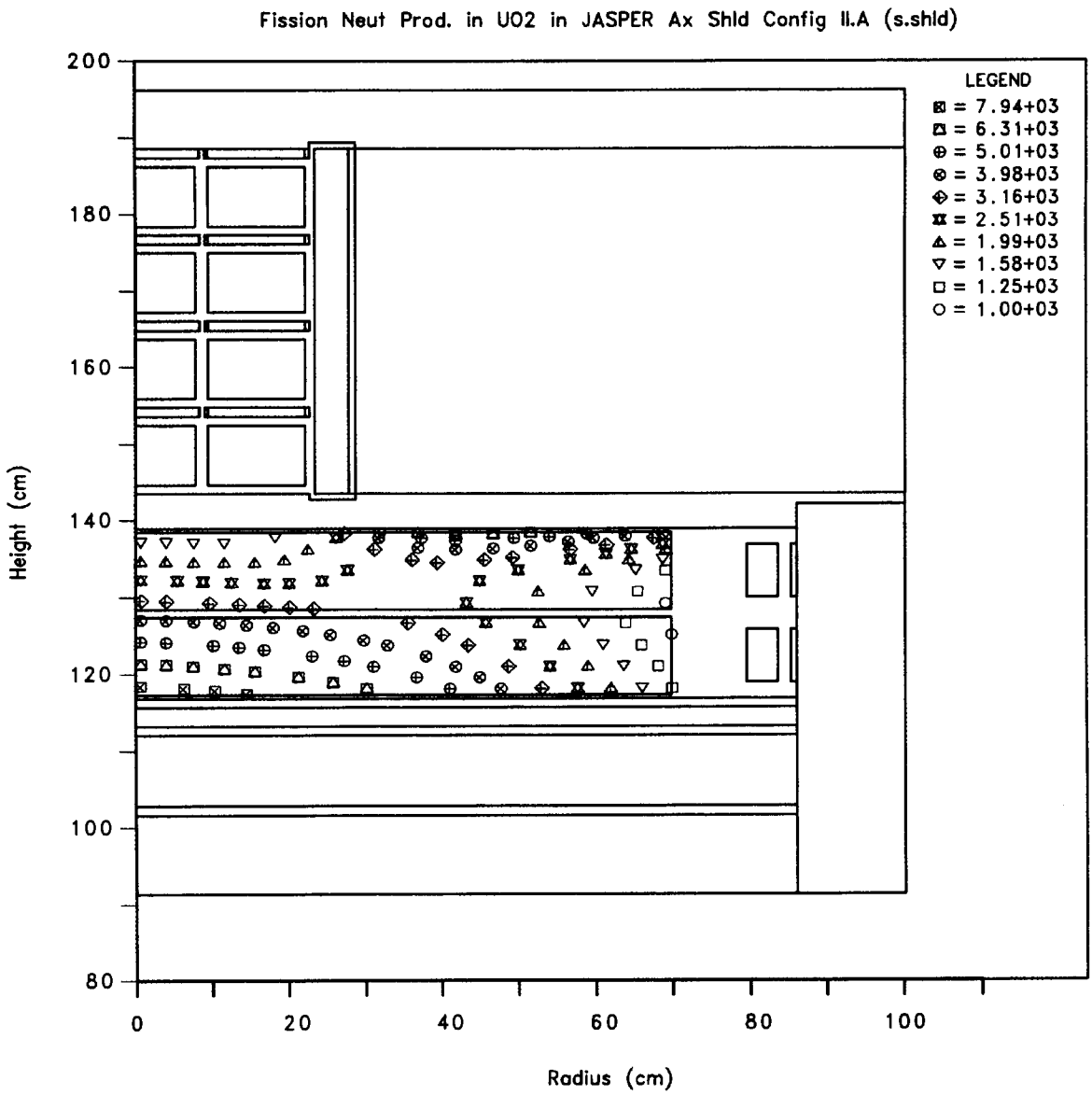

Figure 15. Isoplot of the calculated fission neutron production in the UO_2 blankets of JASPER Axial Shield Experiment original Configuration II.A using self-shielded UO_2 cross sections.

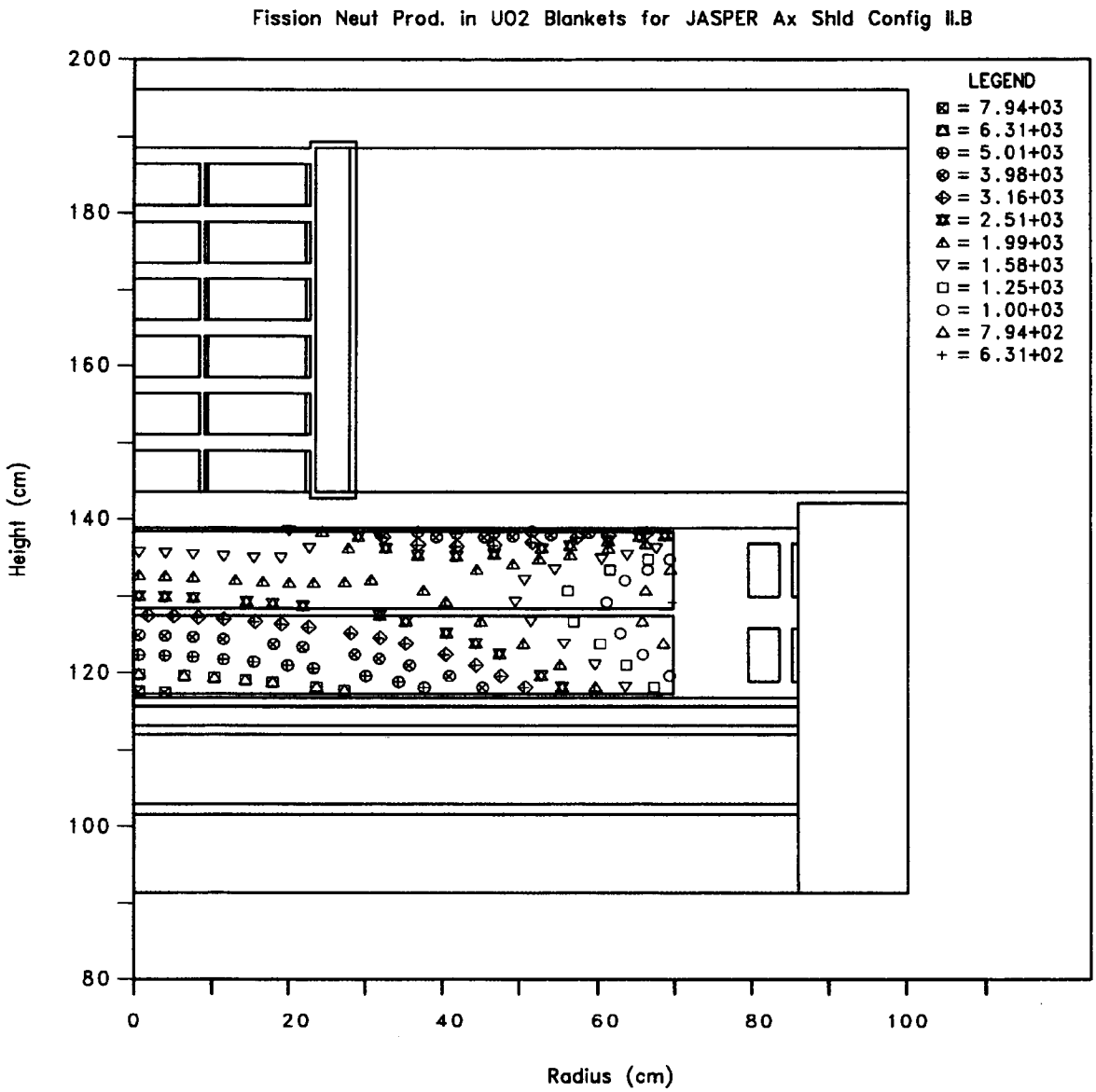

Figure 16. Isoplot of the calculated fission neutron production in the UO_2 blankets of JASPER Axial Shield Experiment original Configuration II.B using standard-weighted UO_2 cross sections.

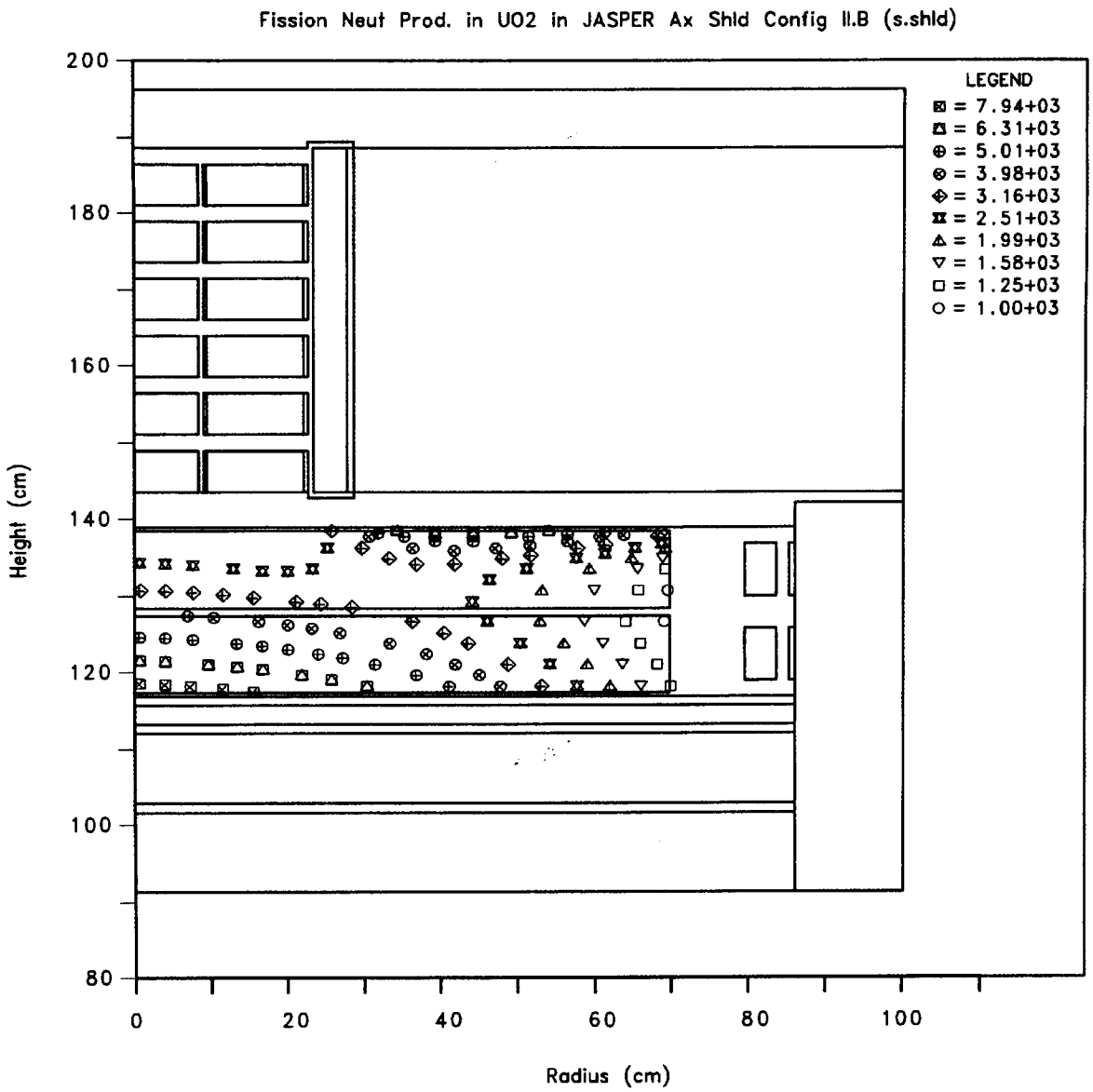

Figure 17. Isoplot of the calculated fission neutron production in the UO_2 blankets of JASPER Axial Shield Experiment original Configuration II.B using self-shielded UO_2 cross sections.

3.4.2 Remeasurement Configurations

3.4.2.1 Bonner Ball Count Rates on Centerline 30 cm Behind Configurations. As was the case for the original configurations, Bonner ball count rates on centerline 30 cm behind the configurations were calculated using the DTWTPN code. Results are presented in Tables F17-F22 for the 3-, 4-, 5-, 8-, 10-, and 12-inch Bonner balls, respectively. Note that the configuration identifiers now have the meanings ascribed in Section 2.2. The calculated and measured data are in good to excellent agreement for the 3-, 4-, 5-, and 8-inch Bonner balls with calculation-to-experiment ratios (C/Es) ranging from 0.85 to 1.28. C/Es range from 0.97 to 1.44 for the 10- and 12-inch Bonner balls. Comparing these count rates to those for the original configurations (Tables F1-F6), one sees that the collimator removes about half the count rate behind the shield configurations for all balls, slightly more than half for the smaller balls, and sometimes less for the larger balls. For the spectrum modifier, there is little effect for the 3-inch Bonner ball, but there is about a 20% reduction for the 10- and 12-inch Bonner balls.

3.4.2.2 Bonner Ball Count Rates on Centerline 150 cm Behind Configurations. Bonner ball count rates on centerline 150 cm behind the remeasurement configurations were calculated using the DTWTPN code. DORT fluxes were calculated in an extended void region behind each of the configurations, and detector responses were averaged over the forward hemisphere of each detector. Results are shown in Tables F23-F28. Calculated and measured results for the 8-, 10-, and 12-inch Bonner balls (Tables F26-F28) are in good to excellent agreement behind all configurations. For the other three balls (Tables F23-F25), there is a slight overprediction behind Configuration I.A and a somewhat greater underprediction behind Configuration V.A. Also, the calculation overpredicted the 3-inch Bonner ball count rate for Configuration II.B and underpredicted the 4- and 5-inch Bonner ball count rates behind Configuration III.A. Otherwise, the calculated and measured 3-, 4-, and 5-inch Bonner ball count rates show good to excellent agreement (within ±20%) for Configurations II.B, III.A, and IV.A. Background was eliminated from the calculations by calculating the DORT fluxes in the void region behind the configurations based on neutron leakage from the region bounded by r=37.88 cm. This radius is an equivalent radius of the shadow shield opening determined by projecting a line from the 150-cm position through a radius of 25 cm at the shadow-shield surface and then to the axial shield surface. The intersection with the axial shield surface is the equivalent radius, and it is about 7.5 cm larger than the equivalent radius used in DORT, that radius being one that gives the same cross-sectional area as the opening. Attempts to calculate detector count rates with DSKTRN using neutron leakages from the same region resulted in substantially lower calculated count rates (some C/Es less than 0.5, even as low as 0.36). No explanation for the underprediction could be found. One is trying to calculate angular fluxes on the axis of a cylinder for directions having an azimuthal cosine of -1.0. Traditionally, the flux calculated on axis by DSKTRN will be less than that calculated at an off-axis position. The DTWTPN calculation encompasses a host of off-axis detector positions in the averaging process and could thus be expected to give higher results.

3.4.2.3 Neutron Spectra Behind Configurations. Neutron spectra were measured for three of the remeasurement configurations (II.A, II.B, and III.A). The calculated and measured spectra are compared in Figures G36-G38. The shapes of the measured and calculated curves are similar. However, like the results for the original configurations, the calculated results still overpredict by 17 to 26%, which is comparable to the 25% overprediction for the original Configuration II.A. The introduction of the shadow shield to reduce the effects of background leakage from the concrete did not improve the agreement between calculation and measurement. One might then attribute the overprediction to the boron cross sections, since good agreement was achieved for the steel shields. The material densities should be reasonably accurate, so there should be little error due to incorrect density, or one would not expect great changes in the neutron flux for density changes within the uncertainty bounds.

3.4.2.4 Bonner Ball Count Rates at the Spectrum Measurement Locations. Bonner ball count rates were measured on centerline behind the configurations at the same locations at which the spectrum measurements were made. Bonner ball count rates were also calculated at these same locations, and the calculated and measured neutron flux spectra were integrated over their common energy interval (E > 52.4 keV). The calculated and measured Bonner ball count rates and integrated fluxes are compared in Table F29. As was the case for the original B_4C configurations, the calculations overpredict fluxes and count rates by 20 to 40% in general. Again, the background shields did not improve the agreement between measurement and calculation.

3.4.2.5 Hornyak Button and Bonner Ball Count Rate Radial Traverses Behind Configurations. Per the program plan, radial traverse measurements were made 2.4 cm behind the remeasurement configurations using the Hornyak button and 30 cm behind the configurations using the 3-, 5-, and 8-in. Bonner balls. Radial profiles of the calculated and measured Bonner ball count rates and Hornyak button dose rates are shown in Figures G39-G44 and radial profiles of the calculated-to-measured count rate ratios are shown in Figures G45-G50. Ratios near the centerline are similar to those for the original configurations. Ratios at the outer edges of the traverses are somewhat lower due to the calculational models that result in the shadow shield opening being such that Bonner balls "see" less of the axial shield surface than they "see" in the actual geometry.

3.4.2.6 Neutron Streaming Factors. Neutron streaming factors for the various shield configurations were estimated by the ratios of the Bonner ball count rates for the heterogeneous configurations to those for the homogeneous configuration. Values were obtained for both the measured and calculated Bonner ball count rates and are presented in Table F30. The streaming factors obtained from the calculated data are generally lower than those obtained from the measured data. For the central blockage configuration, the streaming factors from the calculated data are very close to those obtained from the measured data. They are also smaller than the factors for the other two axial shield designs. For the original configurations, the best comparisons between the factors from the calculated and measured data were those for the heterogeneous configuration containing seven central blockage assemblies. The comparisons for the original configuration with the single central blockage assembly surrounded by six homogeneous assemblies were similar to those for the other heterogeneous assemblies. Calculated streaming for the original rod bundle assemblies was virtually nonexistent. For the remeasurement configuration, the streaming factors range from 1.02 to 1.07 compared to 0.96 to 1.03 for the original configurations. Perhaps, the background shielding did place more emphasis on neutron transmission through the axial shields rather than through the concrete shields.

3.4.2.7 Radiation Background. For the original Configuration II.A, the fission neutron production in the UO_2 radial blankets was examined for its effect on the detector count rates behind the Configuration (Section 3.4.1.8). A similar analysis was performed for the remeasurement Configuration II.A. Figure 18 shows an isoplot of the 5-inch Bonner ball count rate and Figure 19 shows an isoplot of the fission neutron production in the UO_2 blankets. The lithiated paraffin collimator following the radial blanket did indeed reduce the count rates in the concrete relative to the levels within the axial shield (Figure 18). Also, the fission neutron production at the outer radius of the blanket region is comparable to that along the centerline (Figure 19). While the collimator affected the fission neutron production everywhere in the blanket region, the greater effect appears to be that portion of the blanket that previously interfaced with the concrete background shield. Measurements for the remeasurement configurations should be more indicative of the transmission through the axial shield mockups than through the background concrete as was the case for the original B_4C shield configurations.

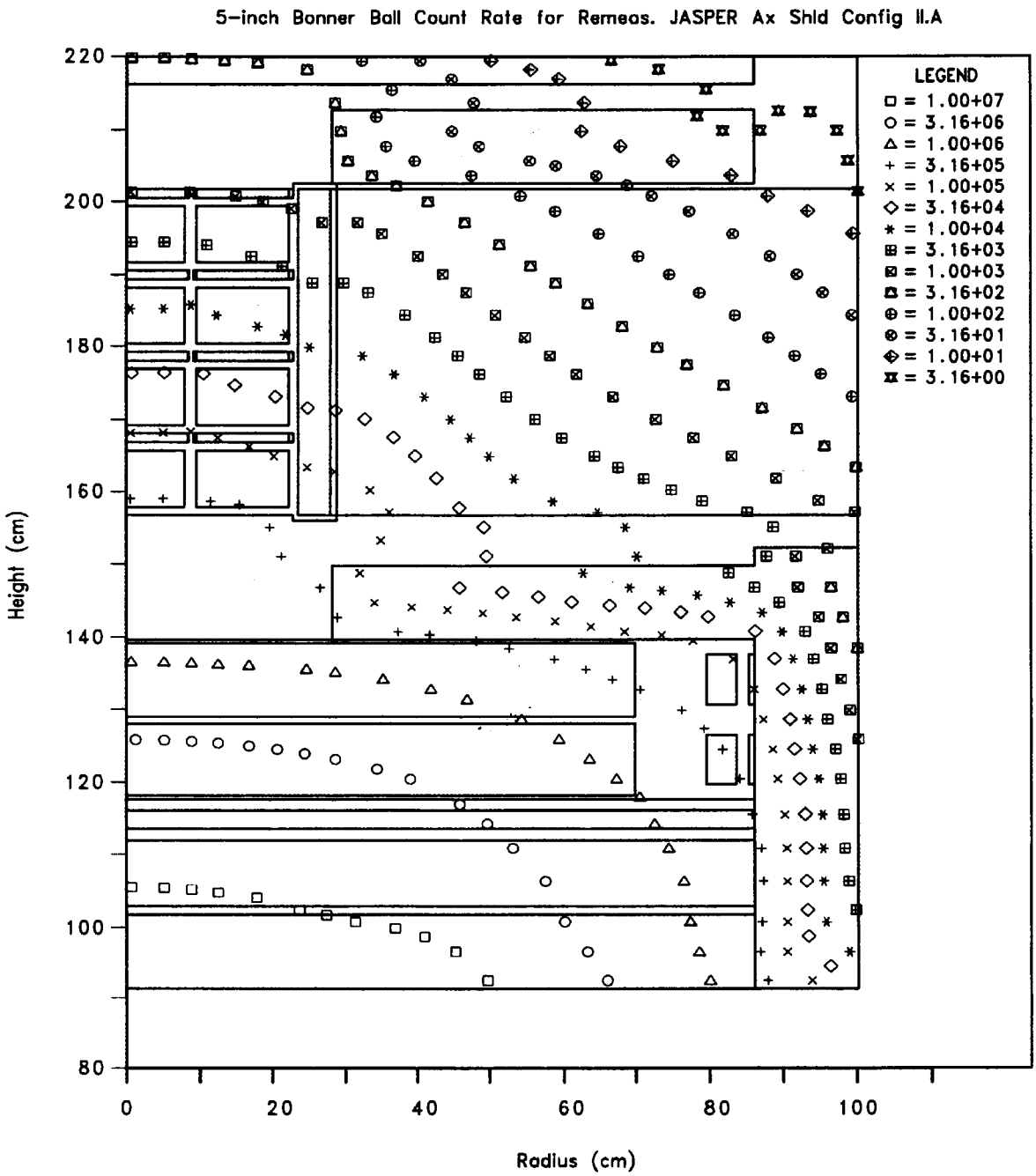

Figure 18. Isoplot of the calculated 5-inch Bonner ball count rate for JASPER Axial Shield Experiment remeasurement Configuration II.A using standard-weighted UO_2 cross sections.

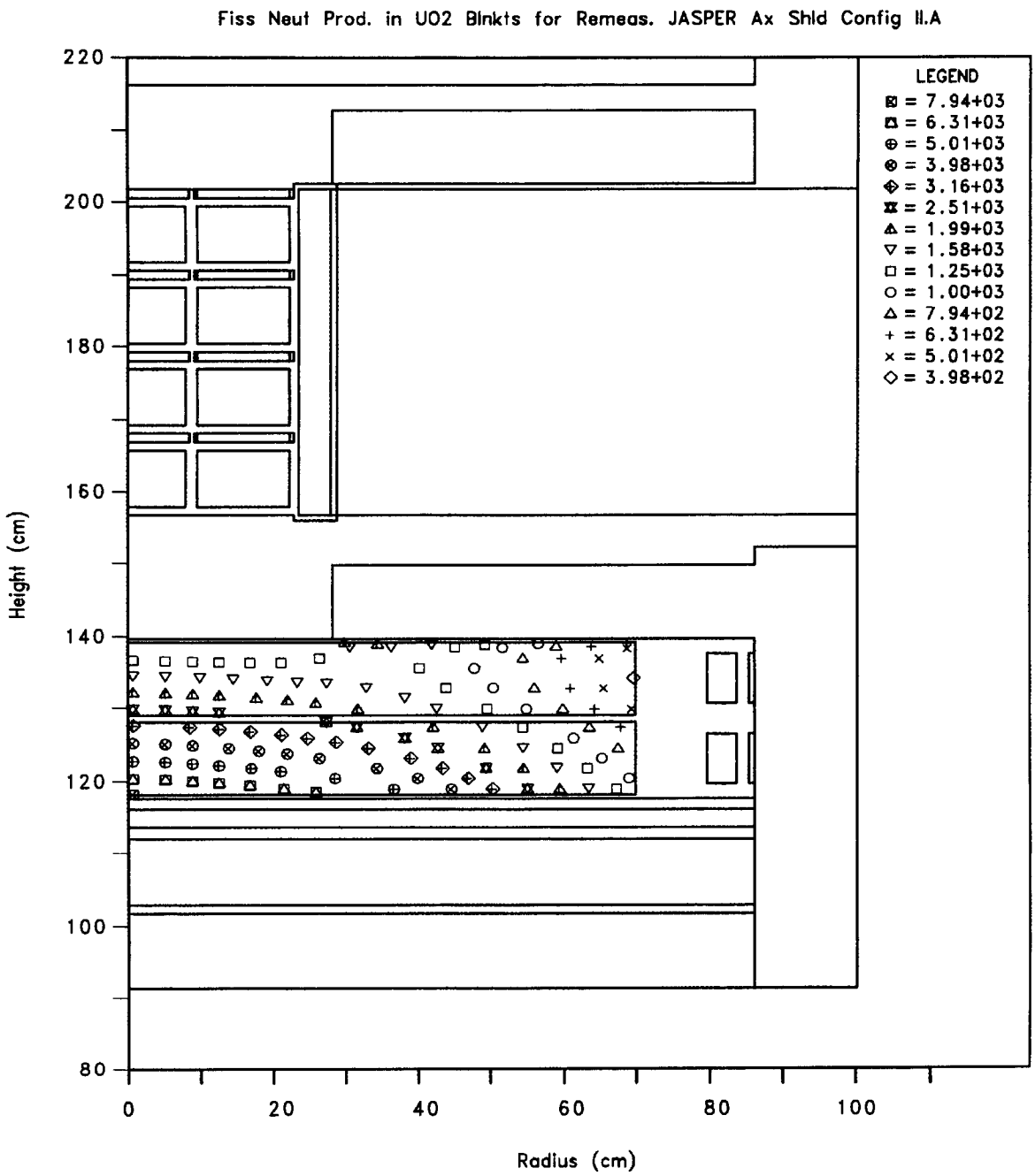

Figure 19. Isoplot of the calculated fission neutron production in the UO_2 blankets of JASPER Axial Shield Experiment remeasurement Configuration II.A using standard-weighted UO_2 cross sections.

Page Intentionally Blank

4.0 SUMMARY

Experiments were performed at the ORNL Tower Shielding Facility on mockups of several possible axial shield designs for sodium cooled fast reactors. The shields were based on either B_4C or stainless steel, with aluminum representing the sodium coolant. The shield configurations consisted of (1) seven homogeneous hexagonal assemblies, (2) one heterogeneous hexagonal assembly surrounded by six homogeneous hexagonal assemblies, or (3) seven heterogeneous hexagonal assemblies. Because the B_4C shields attenuated the neutron flux better than the concrete used as a background shield, a remeasurement program was carried out for the B_4C shield configurations. Both integral and spectral measurements were made. Calculations were performed for each of these configurations using a transport code typically used in the design analysis (e.g. DORT). Calculated results were compared to the measured results to see if the calculations could predict the measured results, and to infer from those comparisons whether design calculations using such a transport code give reasonable results, particularly because of data deficiencies and the approximations one makes in order to convert the three-dimensional geometries to equivalent two-dimensional geometries. The central hexagon was represented by a cylinder with equal cross-sectional area and the heterogeneous shields were modeled as concentric annular regions of shield material and coolant (aluminum) or vice versa. The outer six hexagons were modeled as a cylindrical annulus of equal cross-sectional area with the heterogeneous shields being represented as alternating annular regions of shield material and coolant. The rod bundle assembly was homogenized, although the container walls were modeled as a separate region. For a reactor, one might homogenize the shield region and apply scale factors derived from a heterogeneous model of one assembly. Results from the calculations compared favorably for the stainless steel configurations. Results for the both the original and remeasurement B_4C configurations in general were more than 20% higher than the measured results, ±20% being considered good agreement. However, both the calculations and measurements identified the shield designs with the larger streaming factors and those for which streaming was not very significant. As was the case for the Radial Shield Attenuation Experiment, there does appear to be a problem with boron cross sections. However, since the calculations overpredicted the measured results, one would expect design calculations to yield conservative results. In most cases, this is desirable. A B_4C shield shown by calculations to satisfy shielding criteria would have some margin of safety built in. Finally, the calculations and measurements showed that the B_4C shields attenuated neutrons better than the stainless steel shields did. Because transmission factors differed by as much as a factor of 4.0, one would have to have a very compelling reason to choose the stainless steel assemblies rather than the B_4C assemblies.

Page Intentionally Blank

REFERENCES

1. F. J. Muckenthaler et al., *Measurements for the JASPER Program Radial Shield Attenuation Experiment*, ORNL/TM-10731 (May 1987).

2. C. O. Slater, *Analysis of the JASPER Program Radial Shield Attenuation Experiment*, ORNL/TM-10701 (January 1993).

3. F. J. Muckenthaler et al., *Measurements for the JASPER Program Fission Gas Plenum Experiment*, ORNL/TM-10422 (June 1987).

4. C. O. Slater, *JASPER USDOE/PNC Shielding Research Program - Analysis of the JASPER Fission Gas Plenum Experiment*, ORNL/TM-10681 (May 1990).

5. F. J. Muckenthaler et al., *Measurements for the JASPER Program Axial Shield Experiment*, ORNL/TM-11839 (August 1991).

6. F. J. Muckenthaler et al., *Measurements for the JASPER Program Axial Shield Re-measurement Experiment*, ORNL/TM-12276 (March 1993).

7. C. O. Slater, *Analysis of the ORNL/TSF Alternate Shielding Materials Experiment*, ORNL/TM-10183 (April 1987).

8. R. E. Maerker and F. J. Muckenthaler, *The Absolute Neutron Spectrum Emerging Through the Large Beam Collimator from the TSR-II Reactor at the Tower Shielding Facility*, ORNL/TM-5183 (January 1976).

9. W. A. Rhoades and R. L. Childs, "The DORT Two-Dimensional Discrete Ordinates Transport Code," *Nucl. Sci. Eng.* **99**, 88-89 (May 1988).

10. C. Y. Fu and D. T. Ingersoll, *VELM61 and VELM22: Multigroup Cross-Section Libraries for Sodium-Cooled Reactor Shield Analysis*, ORNL/TM-5296 (April 1987).

11. G. C. Haynes, "The AXMIX Program for Cross Section Mixing and Library Arrangement," ORNL Central Files Number 74-12-2 (December 2, 1974).

12. W. A. Rhoades, "RTFLUM: A Module for Converting, Expanding, and Editing Standard Data Files," Section 4 of W. A. Rhoades and M. B. Emmett, *DOS: The Discrete Ordinates System*, ORNL/TM-8362 (August 1982).

13. D. T. Ingersoll and C. O. Slater, *DOGS - A Collection of Graphics for Support of Discrete Ordinates Codes*, ORNL/TM-7188 (March 1980).

14. J. E. White et al., *Production and Testing of the Revised VITAMIN-B6 Fine-Group and the BUGLE-96 Broad-Group Neutron/Photon Cross-Section Libraries Derived From ENDF/B-VI.3 Nuclear Data*, NUREG/CR-6214, Rev. 1 (ORNL/TM-6795/R1) (April 2000).

15. R. W. Roussin, *VITAMIN-E: A Coupled 174-Neutron, 38-Gamma-Ray Multigroup Library for Deriving Application-Dependent Working Libraries for Radiation Transport Calculations*, RSIC Data Library Collection DLC-113 (December 5, 1984).

16. R. E. Maerker et al., *Final Report on a Benchmark Experiment for Neutron Transport in Thick Sodium*, ORNL-4880 (1974).

Page Intentionally Blank

APPENDIX A

Experimental Program Plan for the JASPER Axial Shield Experiment Original Measurements

Page Intentionally Blank

EXPERIMENTAL PROGRAM PLAN
FOR THE JASPER AXIAL SHIELD EXPERIMENT

I. Spectrum Modifier (SM) Mockup

A. 10cm Fe + 10cm Al + 2.5cm boral + 20cm radial blanket

1. 3-, 4-, 5-, 8-, 10-, and 12-in. Bonner ball measurements on centerline:

   a. at 30 cm behind shield mockup
   b. at 150 cm behind shield mockup

2. 3-, 5-, and 8-in. Bonner ball horizontal traverse at 30 cm behind shield mockup

3. NE-213 and hydrogen counter spectrum measurements on centerline as close as feasible behind shield mockup

4. 3-, 5-, and 10-in. Bonner ball measurements on centerline at location of NE-213/H spectrum measurements

II. Homogeneous Shield Mockup

A. SM + 45-cm-thick B_4C homogeneous type assemblies in all seven shield positions

1. 3-, 4-, 5-, 8-, 10-, and 12-in. Bonner ball measurements on centerline:

   a. at 30 cm behind shield mockup

   b. at 150 cm behind shield mockup

2. 3-, 5-, and 8-in. Bonner ball horizontal traverse at 30 cm behind shield mockup

3. 0.6-cm Hornyak button horizontal traverse as close as possible behind shield mockup

4. NE-213 and hydrogen counter spectrum measurements on centerline as close as feasible behind shield mockup

5. 3-, 5-, and 10-in. Bonner ball measurements on centerline at location of NE-213/H spectrum measurements

B. SM + 45-cm-thick SS-304 homogeneous type assemblies in all seven shield positions

1. 3-, 4-, 5-, 8-, 10-, and 12-in. Bonner ball measurements on centerline:

a. at 30 cm behind shield mockup

b. at 150 cm behind shield mockup

2. 3-, 5-, and 8-in. Bonner ball horizontal traverse at 30 cm behind shield mockup

3. 0.6-cm Hornyak button horizontal traverse as close as possible behind shield mockup

4. NE-213 and hydrogen counter spectrum measurements on centerline as close as feasible behind shield mockup

5. 3-, 5-, and 10-in. Bonner ball measurements on centerline at location of NE-213/H spectrum measurements

III. Central Blockage Shield Mockup

A. SM + 45-cm-thick B_4C central blockage type assembly in center shield position with B_4C homogeneous type assemblies in outer six shield positions

1. 3-, 4-, 5-, 8-, 10-, and 12-in. Bonner ball measurements on centerline:

a. at 30 cm behind shield mockup

b. at 150 cm behind shield mockup

2. 3-, 5-, and 8-in. Bonner ball horizontal traverse at 30 cm behind shield mockup

3. 0.6-cm Hornyak button horizontal traverse as close as possible behind shield mockup

B. SM + 45-cm-thick B_4C central blockage type assemblies in all seven shield positions

1. 3-, 4-, 5-, 8-, 10-, and 12-in. Bonner ball measurements on centerline:

   a. at 30 cm behind shield mockup

   b. at 150 cm behind shield mockup

2. 3-, 5-, and 8-in. Bonner ball horizontal traverse at 30 cm behind shield mockup

3. 0.6-cm Hornyak button horizontal traverse as close as possible behind shield mockup

C. SM + 45-cm-thick SS-304 central blockage type assembly in center shield position with SS-304 homogeneous type assemblies in outer six shield positions

1. 3-, 4-, 5-, 8-, 10-, and 12-in. Bonner ball measurements on centerline:

   a. at 30 cm behind shield mockup

   b. at 150 cm behind shield mockup

2. 3-, 5-, and 8-in. Bonner ball horizontal traverse at 30 cm behind shield mockup

3. 0.6-cm Hornyak button horizontal traverse as close as possible behind shield mockup

D. SM + 45-cm-thick SS304 central blockage type assemblies in all seven shield positions

1. 3-, 4-, 5-, 8-, 10-, and 12-in. Bonner ball measurements on centerline:

   a. at 30 cm behind shield mockup

   b. at 150 cm behind shield mockup

2. 3-, 5-, and 8-in. Bonner ball horizontal traverse at 30 cm behind shield mockup

3. 0.6-cm Hornyak button horizontal traverse as close as possible behind shield mockup

E. SM + 20-cm-thick fission gas plenum mockup + 45-cm-thick B_4C central blockage type assemblies in all seven shield positions

1. 3-, 4-, 5-, 8-, 10-, and 12-in. Bonner ball measurements on centerline:

   a. at 30 cm behind shield mockup

   b. at 150 cm behind shield mockup

2. 3-, 5-, and 8-in. Bonner ball horizontal traverse at 30 cm behind shield mockup

3. 0.6-cm Hornyak button horizontal traverse as close as possible behind shield mockup

IV. Rod Bundle Shield Mockup

A. SM + 45-cm-thick B_4C rod bundle type assembly in center shield position with B_4C homogeneous type assemblies in outer six shield positions

1. 3-, 4-, 5-, 8-, 10-, and 12-in. Bonner ball measurements on centerline:

   a. at 30 cm behind shield mockup

   b. at 150 cm behind shield mockup

2. 3-, 5-, and 8-in. Bonner ball horizontal traverse at 30 cm behind shield mockup

3. 0.6-cm Hornyak button horizontal traverse as close as possible behind shield mockup

B. SM + 45-cm-thick SS-304 rod bundle type assembly in center shield position with SS-304 homogeneous type assemblies in outer six shield positions

1. 3-, 4-, 5-, 8-, 10-, and 12-in. Bonner ball measurements on centerline:

   a. at 30 cm behind shield mockup

   b. at 160 cm behind shield mockup

2. 3-, 5-, and 8-in. Bonner ball horizontal traverse at 30 cm behind shield mockup

3. 0.6-cm Hornyak button horizontal traverse as close as possible behind shield mockup

V. Central Sodium Channel Shield Mockup

A. SM + 45-cm-thick B_4C central sodium channel type assembly in center shield position with B_4C homogeneous type assemblies in outer six shield positions

1. 3-, 4-, 5-, 8-, 10-, and 12-in. Bonner ball measurements on centerline:

   a. at 30 cm behind shield mockup

   b. at 150 cm behind shield mockup

2. 3-, 5-, and 8-in. Bonner ball horizontal traverse at 30 cm behind shield mockup

3. 0.6-cm Hornyak button horizontal traverse as close as possible behind shield mockup

B. SM + 45-cm-thick SS-304 central sodium channel type assembly in center shield position with SS-304 homogeneous type assemblies in outer six shield positions

1. 3-, 4-, 5-, 8-, 10-, and 12-in. Bonner ball measurements on centerline:

   a. at 30 cm behind shield mockup

   b. at 150 cm behind shield mockup

2. 3-, 5-, and 8-in. Bonner ball horizontal traverse at 30 cm behind shield mockup

3. 0.6-cm Hornyak button horizontal traverse as close as possible behind shield mockup

Page Intentionally Blank

APPENDIX B

Pictorial Descriptions of the Configurations for the
JASPER Axial Experiment Original Measurement Program

Page Intentionally Blank

ORNL-DWG 90M-14862

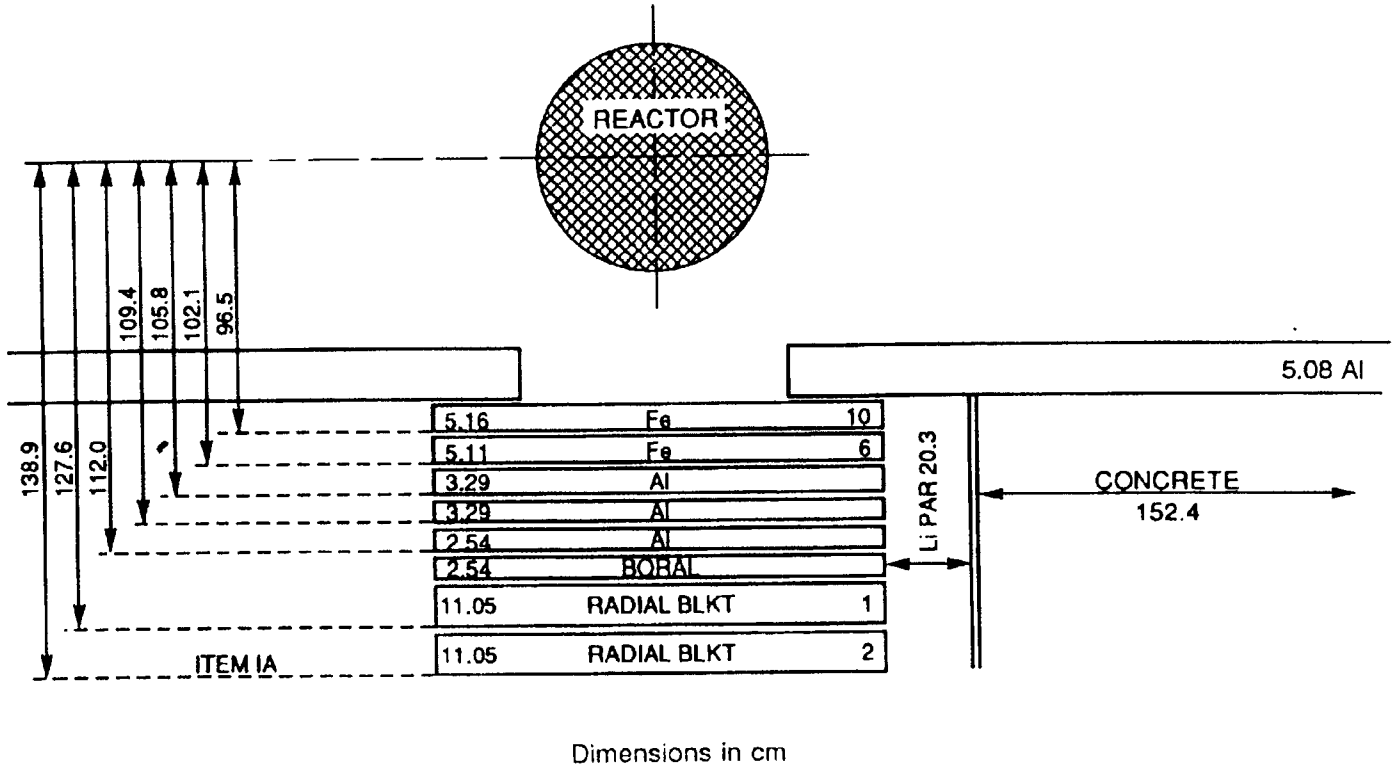

Figure B1. Spectrum modifier for the JASPER Axial Shield Experiment Configurations (Configuration I.A of the Experiment Program Plan).

ORNL DWG 87-7281

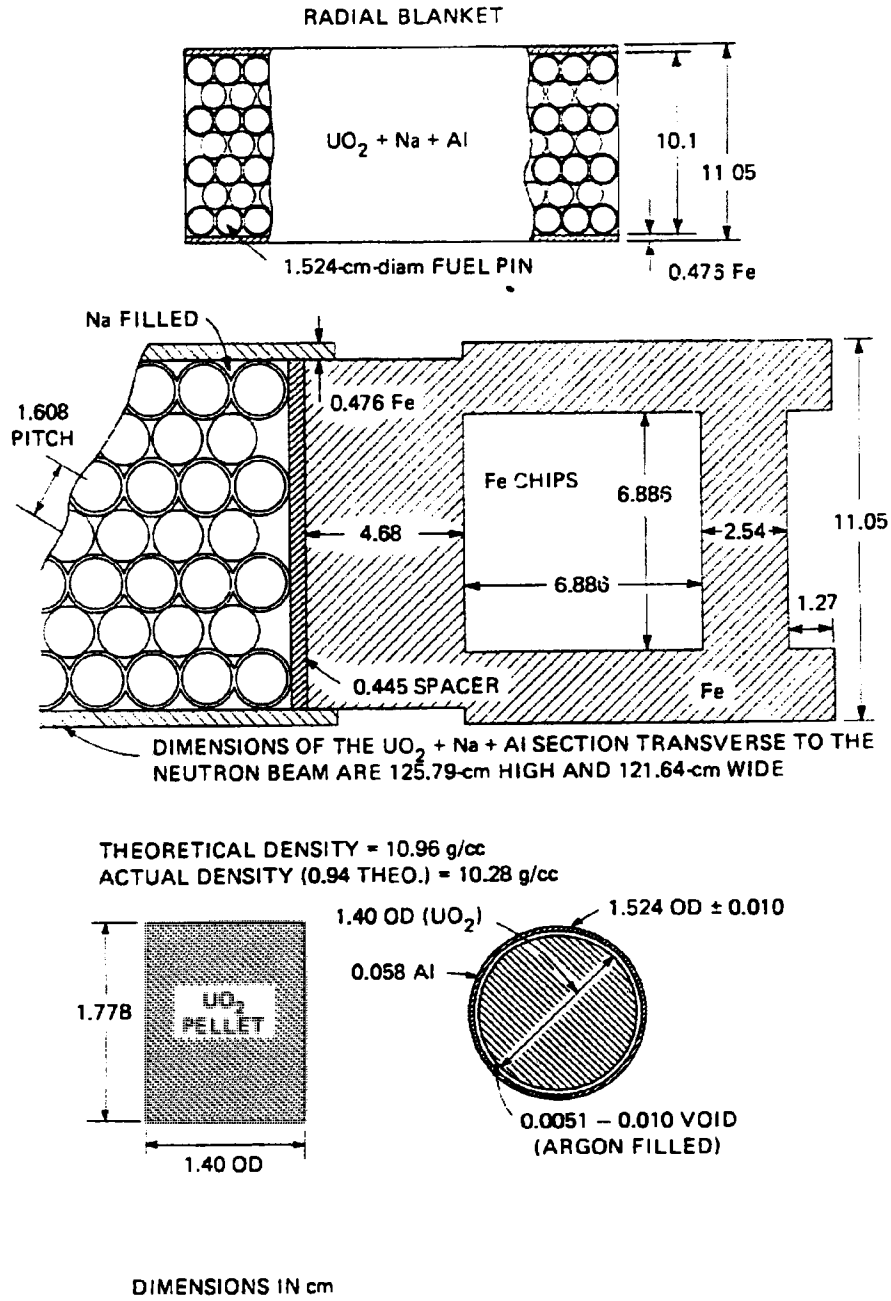

Figure B2. Details of the UO_2 blankets in the spectrum modifier for the JASPER Axial Shield Experiment Configurations.

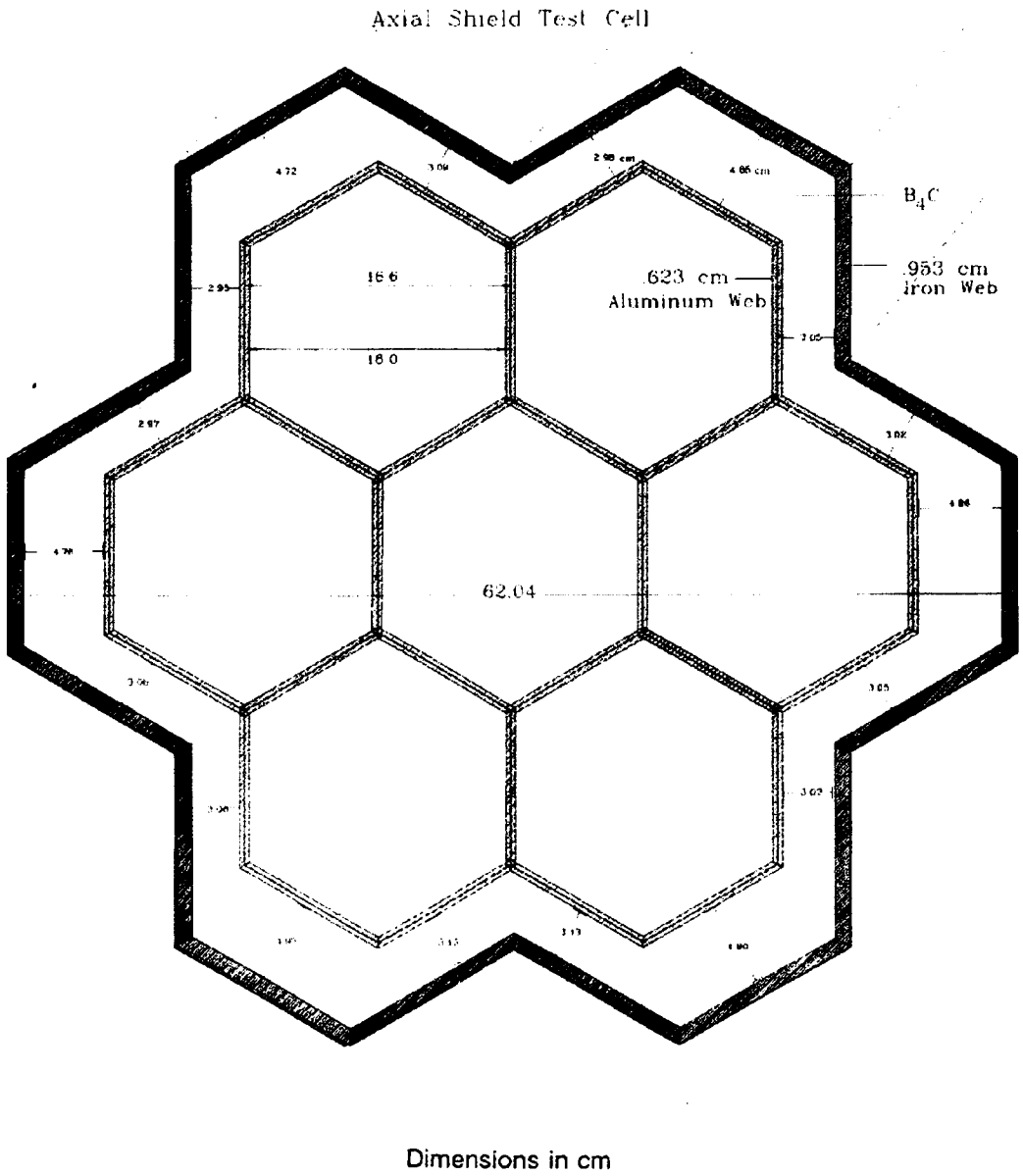

Figure B3. Details of the aluminum-framed, B_4C-surrounded, seven-hexagon support for the axial shield assemblies of the JASPER Axial Shield Experiment Configurations.

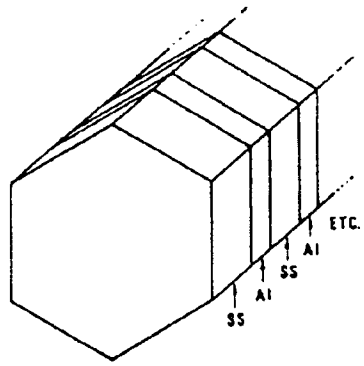

Thickness of Al pieces: 2.136 cm (6 total)
Thickness of SS pieces: 5.357 cm (6 total)
Width of assembly (flat surface to flat surface): 15.99 cm

Figure B4. Details of the stainless steel homogeneous assembly used in the JASPER Axial Shield Experiment Configurations.

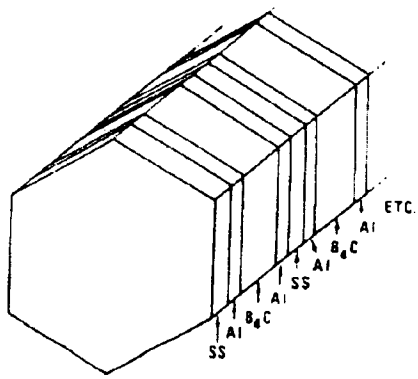

Depth of B_4C in container: 7.77 cm (4 total)
Width of B_4C: 14.73 cm
End plate thickness: 1.123 cm
Wall thickness of container: .627 cm
Width of container (flat surface to flat surface: 15.98 cm
Density of B_4C: 1.41 g/cc
Thickness of SS pieces: 1.25 cm (4 total)

Figure B5. Details of the B_4C homogeneous assembly used in the JASPER Axial Shield Experiment Configurations.

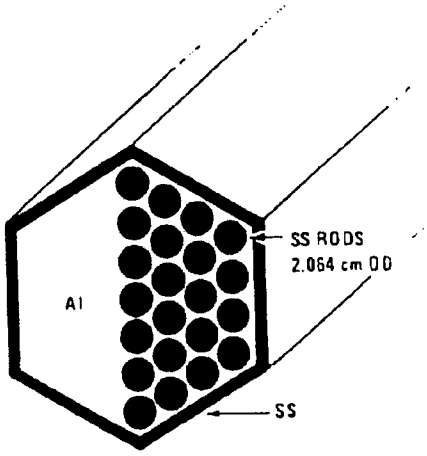

Diam of rod: 2.041 cm
Diam of hole: 2.064 cm
Length of aluminum: 44.97 cm
Thickness of SS wrapper: .452 cm
Pitch of rods: 2.38 cm
Width of aluminum (flat surface to flat surface): 15.00 cm

Figure B6. Details of the stainless steel rod bundle assembly used in the JASPER Axial Shield Experiment Configurations.

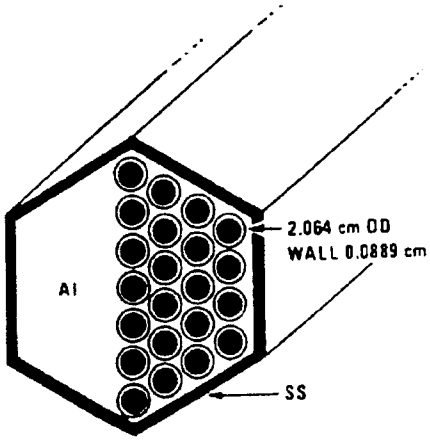

OD of rod: 2.06 cm
ID of rod wall: 1.897 cm
Rod wall thickness: .0813 cm
Thickness of rod cap: .159 cm
Length of B_4C in rod: 44.7 cm
Volume of B_4C rod: 126.28 cc
Average density of B_4C: 1.30 g/cc
Thickness of SS wrapper: .465 cm
Rod pitch: 2.38 cm
Width of Al (flat surface to flat surface): 15.00 cm
Width of assembly (flat surface to flat surface): 15.93 cm

Figure B7. Details of the B_4C rod bundle assembly used in the JASPER Axial Shield Experiment Configurations.

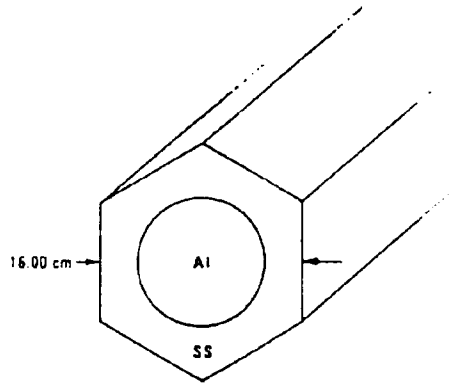

Diam of aluminum cylinder: 8.96 cm
Length of aluminum cylinder: 44.97 cm
Width of assembly (flat surface to flat surface): 16.03 cm

Figure B8. Details of the stainless steel central sodium channel assembly used in the JASPER Axial Shield Experiment Configurations.

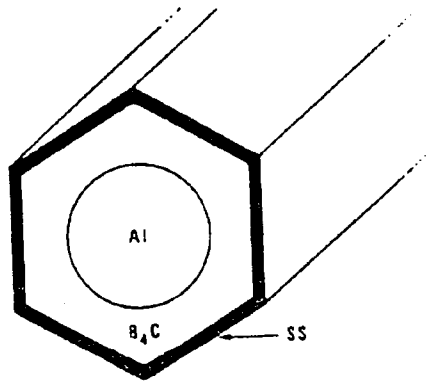

Diam of Al cylinder: 8.96 cm
Length of Al cylinder: 43.412 cm
Width of hexagon (flat surface to flat surface): 15.99 cm
Thickness of SS wrapper: .452 cm
Length of SS wrapper: 45 cm
Volume of B_4C: 5760.1 cc
Density of B_4C: 1.39 g/cc
Thickness of Al covers over end of B_4C: .794 cm

Figure B9. Details of the B_4C central sodium channel assembly used in the JASPER Axial Shield Experiment Configurations.

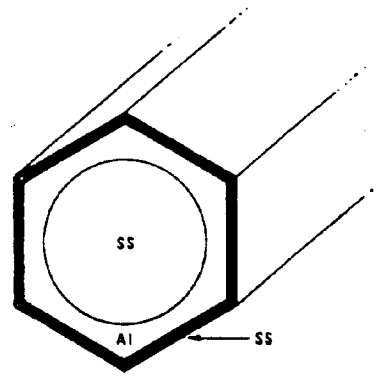

Diam of SS cylinder: 12.98 cm
Width of hexagon (flat wall to flat wall): 15.974 cm
Thickness of SS wrapper: .462 cm
Diam of Al void: 13.0 cm
Width of aluminum (flat surface to flat surface): 15.05 cm
Length of assembly: 45 cm

Figure B10. Details of the stainless steel central blockage assembly used in the JASPER Axial Shield Experiment Configurations.

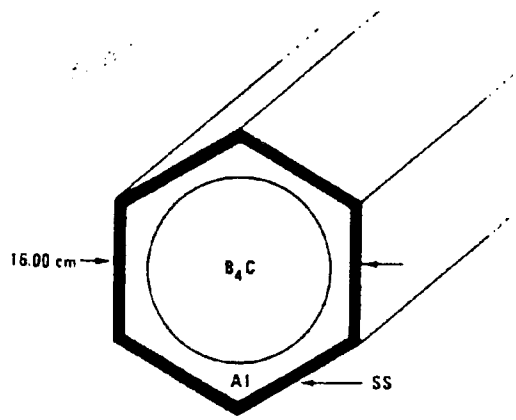

Width of container (flat surface to flat surface): 16.00 cm
Width of Al (flat surface to flat surface): 15.05 cm
Thickness of end plates: .476 cm
Diam of B_4C: 13 cm
Length of B_4C: 44.05 cm
Volume of B_4C: 5846.9 cc
Density of B_4C: 1.38 g/cc

Figure B11. Details of the B_4C central blockage assembly used in the JASPER Axial Shield Experiment Configurations.

ORNL-DWG 90M-15719Ra

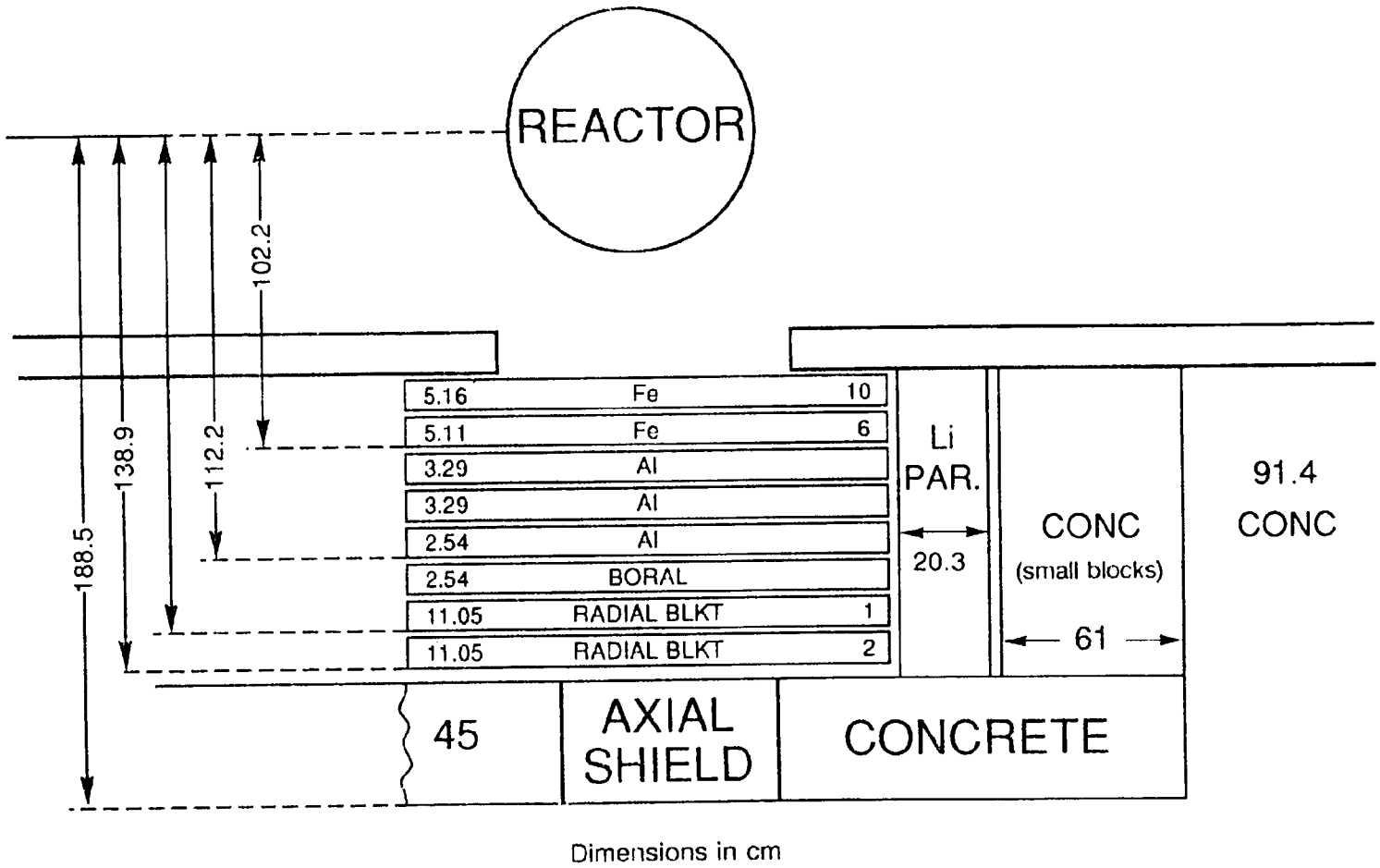

Figure B12. Plan view for most of the configurations used in the original measurement program for the JASPER Axial Shield Experiment.

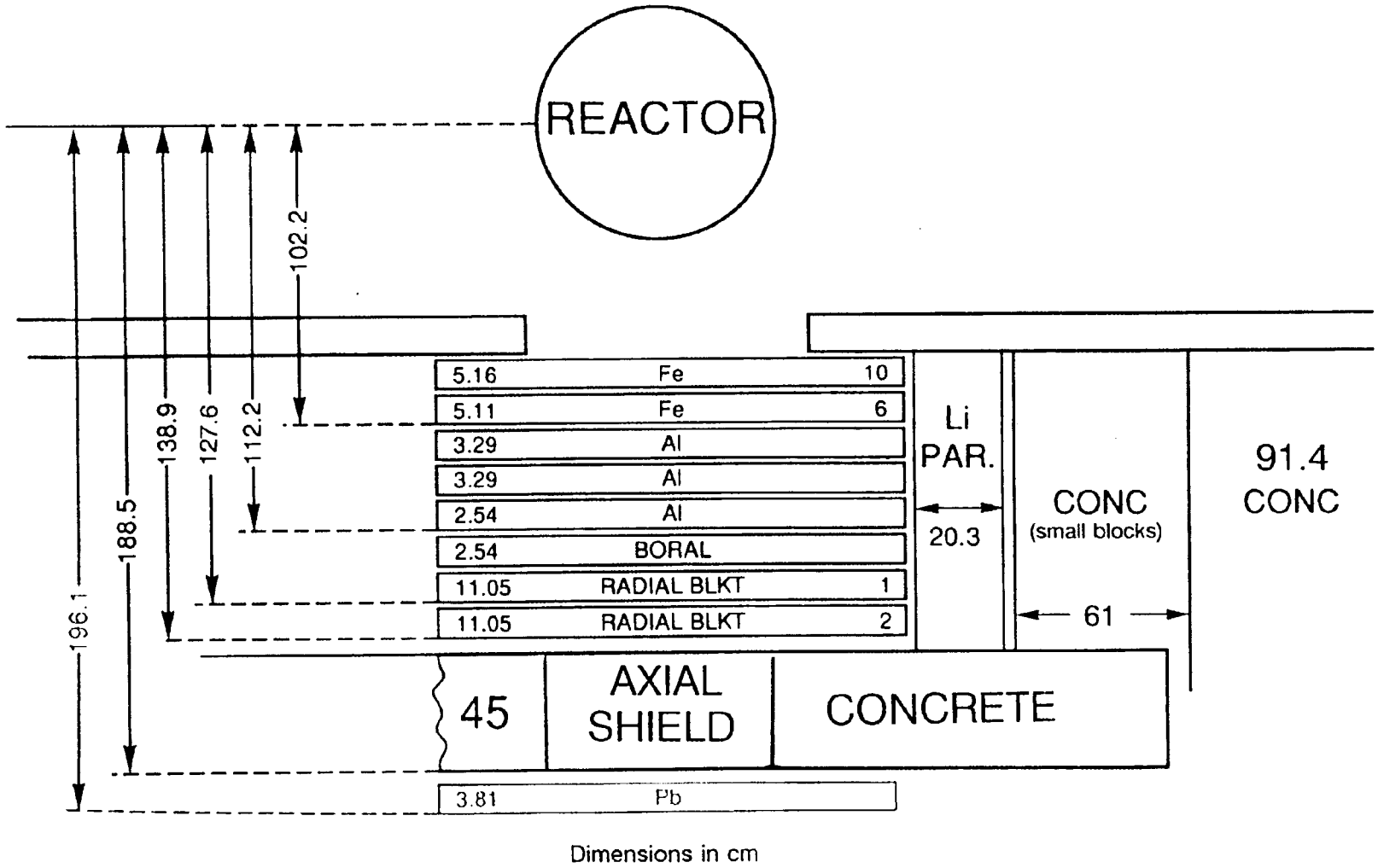

Figure B13. Plan view for those configurations for which neutron spectra were measured in the original measurement program for the JASPER Axial Shield Experiment.

ORNL-DWG 90M-16106

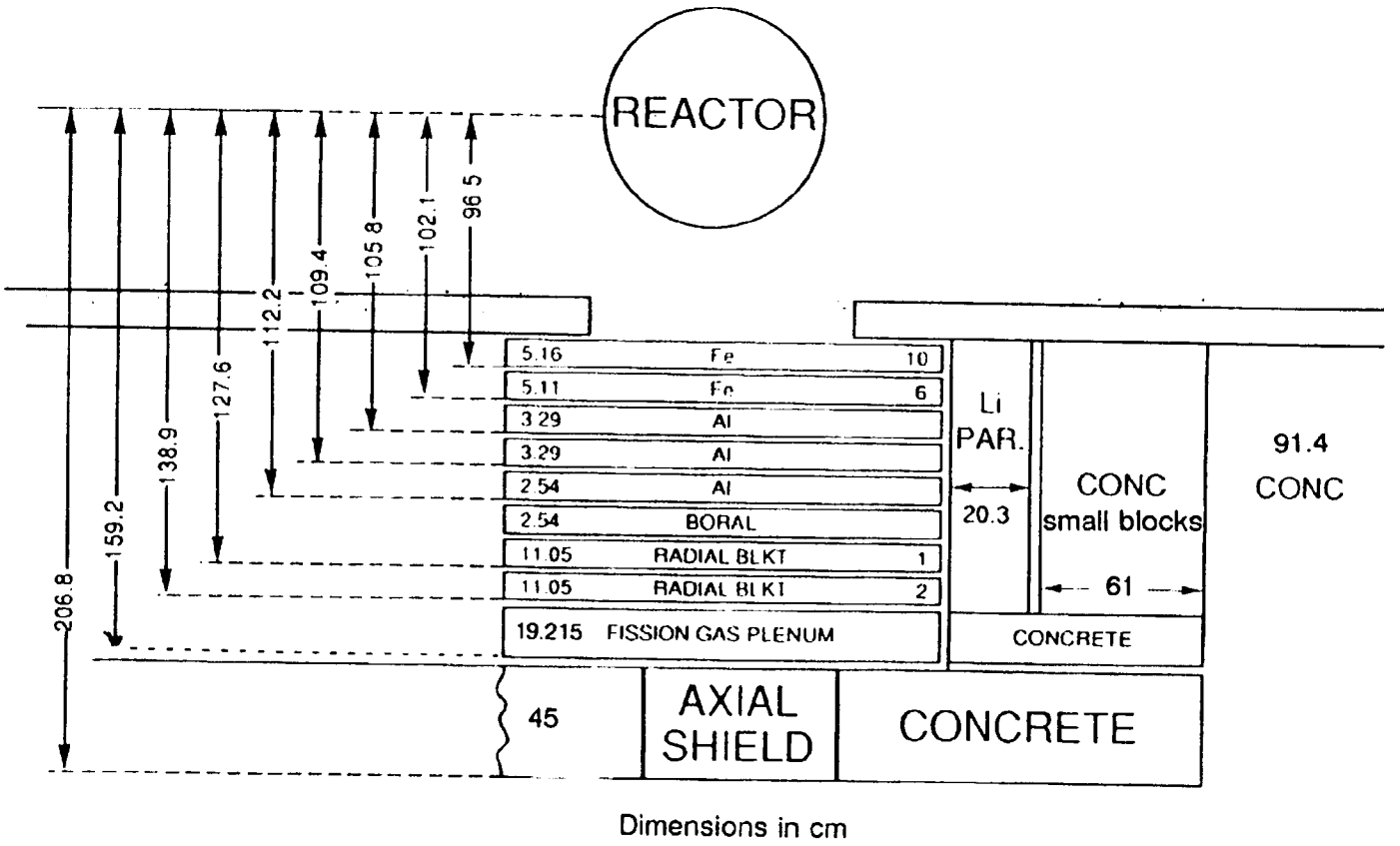

Figure B14. Plan view for the configuration containing the fission gas plenum mockup in the original measurement program for the JASPER Axial Shield Experiment.

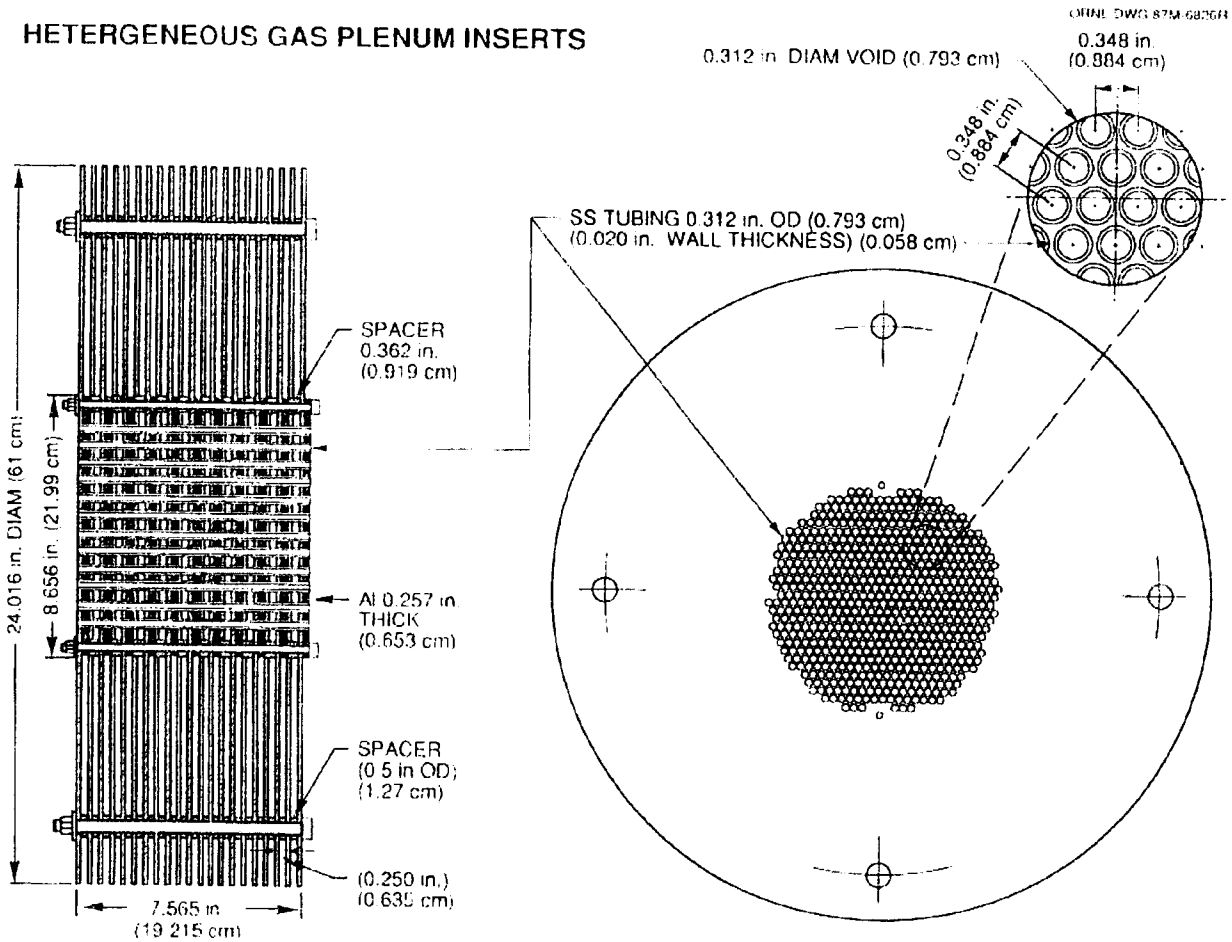

Figure B15. Details of the fission gas plenum mockup used in the JASPER Axial Shield Experiment Configuration III.E.

Page Intentionally Blank

APPENDIX C

Experimental Program Plan for the JASPER Axial Shield Remeasurement Experiment

Page Intentionally Blank

EXPERIMENTAL PROGRAM PLAN FOR THE JASPER AXIAL SHIELD RE-MEASUREMENT EXPERIMENT

I. Spectrum Modifier
   A. Spectrum Modifier (SM-1) (10 cm Fe + 9 cm Al + 2.5 cm boral + 20 cm Radial Blanket) + 10 cm lithiated paraffin with iris (see II)
      1. 3-, 4-, 5-, 8-, 10-, and 12-in Bonner ball measurements on centerline:
         a. 30 cm behind radial blanket
         b. 150 cm behind radial blanket (foreground and background)
      2. 3-, 5-, and 8-in Bonner ball horizontal traverses at 30 cm behind the radial blanket

II. Homogeneous Axial Shield Mockup
   A. SM-1 + 7 B_4C homogeneous-type assemblies (10 cm lithiated paraffin slab preceding and following axial shield)
      1. NE 213/hydrogen counter spectrum measurements on centerline as close as feasible behind the axial shield
      2. 3-, 5-, and 10-in Bonner ball on centerline at NE 213 location
      3. 3-, 4-, 5-, 8-, 10, and 12-in Bonner ball measurements on centerline:
         a. 30 cm behind axial shield
         b. 150 cm behind axial shield (foreground and background)
      4. 3-, 5-, and 8-in Bonner ball horizontal traverses at 30 cm behind axial shield
      5. Hornyak button (0.25-in-diameter) horizontal traverse as close as feasible behind axial shield
   B. SM-1 + 7 B_4C homogeneous-type assemblies (10 cm lithiated paraffin slab preceding axial shield only)
      1. NE 213/hydrogen counter spectrum measurements on centerline as close as feasible behind the axial shield
      2. 3-, 5-, and 10-in Bonner ball on centerline at NE 213 location
      3. 3-, 4-, 5-, 8-, 10-, and 12-in Bonner ball measurements on centerline:
         a. 30 cm behind axial shield
         b. 150 cm behind axial shield (foreground and background)
      4. 3-, 5-, and 8-in Bonner ball horizontal traverses at 30 cm behind axial shield
      5. Hornyak button (0.25-in-diameter) horizontal traverse as close as feasible behind axial shield

III. Rod Bundle Axial Shield Mockup

A. SM-1 + 6 B_4C homogeneous-type assemblies around one B_4C rod bundle hexagon assembly (10 cm lithiated paraffin slabs preceding and following axial shield)

1. NE 213/hydrogen counter spectrum measurements on centerline as close as feasible behind axial shield
2. 3-, 5-, and 10-in Bonner ball on centerline at NE 213 location
3. 3-, 4-, 5-, 8-, 10-, and 12-in Bonner ball measurements on centerline:
   a. 30 cm behind axial shield
   b. 150 cm behind axial shield (foreground and background)
4. 3-, 5-, and 8-in Bonner ball horizontal traverses at 30 cm behind axial shield
5. Hornyak button (0.25-in-diameter) horizontal traverse as close as feasible behind axial shield

IV. Central Blockage Shield Mockup

A. SM-1 + six B_4C homogeneous-type assemblies around one B_4C central blockage hexagon assembly (10 cm lithiated paraffin slabs preceding and following axial shield)

1. 3-, 4-, 5-, 8-, 10-, and 12-in Bonner ball measurements on centerline:
   a. 30 cm behind axial shield
   b. 150 cm behind axial shield (foreground and background)
2. 3-, 5-, and 8-in Bonner ball horizontal traverses at 30 cm behind axial shield
3. Hornyak button (0.25-in-diam) horizontal traverse as close as feasible behind axial shield

V. Central Sodium Channel Shield Mockup (lithiated paraffin as in IIA)

A. SM-1 + six B_4C homogeneous-type assemblies around one B_4C central sodium hexagon assembly (10 cm lithiated paraffin slab preceding and following axial shield)

1. 3-, 4-, 5-, 8-, 10-, and 12-in Bonner ball measurements on centerline:
   a. 30 cm behind axial shield
   b. 150 cm behind axial shield (foreground and background)
2. 3-, 5-, and 8-in Bonner ball horizontal traverses at 30 cm behind axial shield
3. Hornyak button (0.25-in-diam) horizontal traverse as close as feasible behind axial shield

APPENDIX D

Pictorial Descriptions of the Configurations for the
JASPER Axial Shield Remeasurement Experiment

Page Intentionally Blank

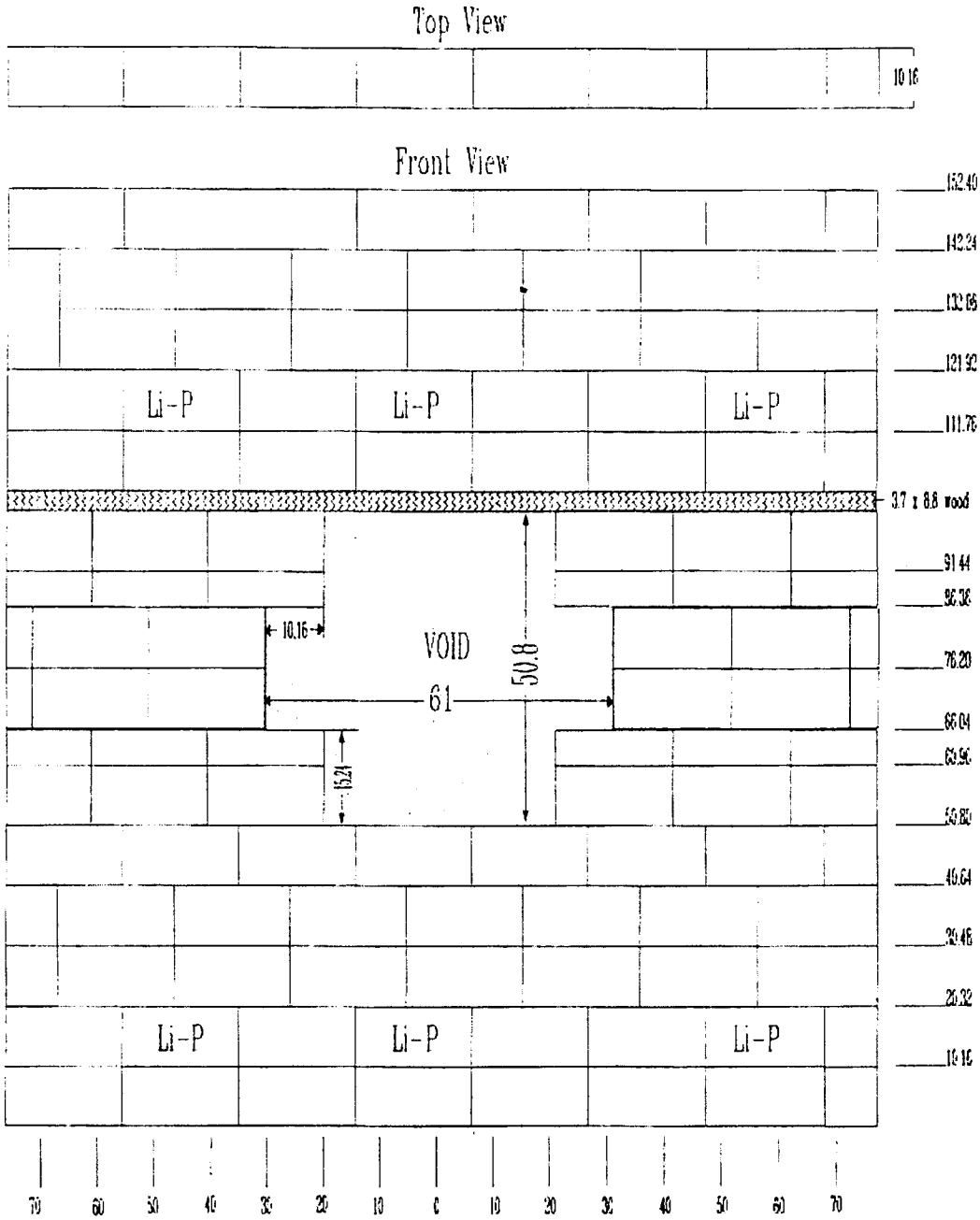

Figure D1. Details of the collimating lithiated-paraffin shield used in configurations for the remeasurement program for the JASPER Axial Shield Experiment.

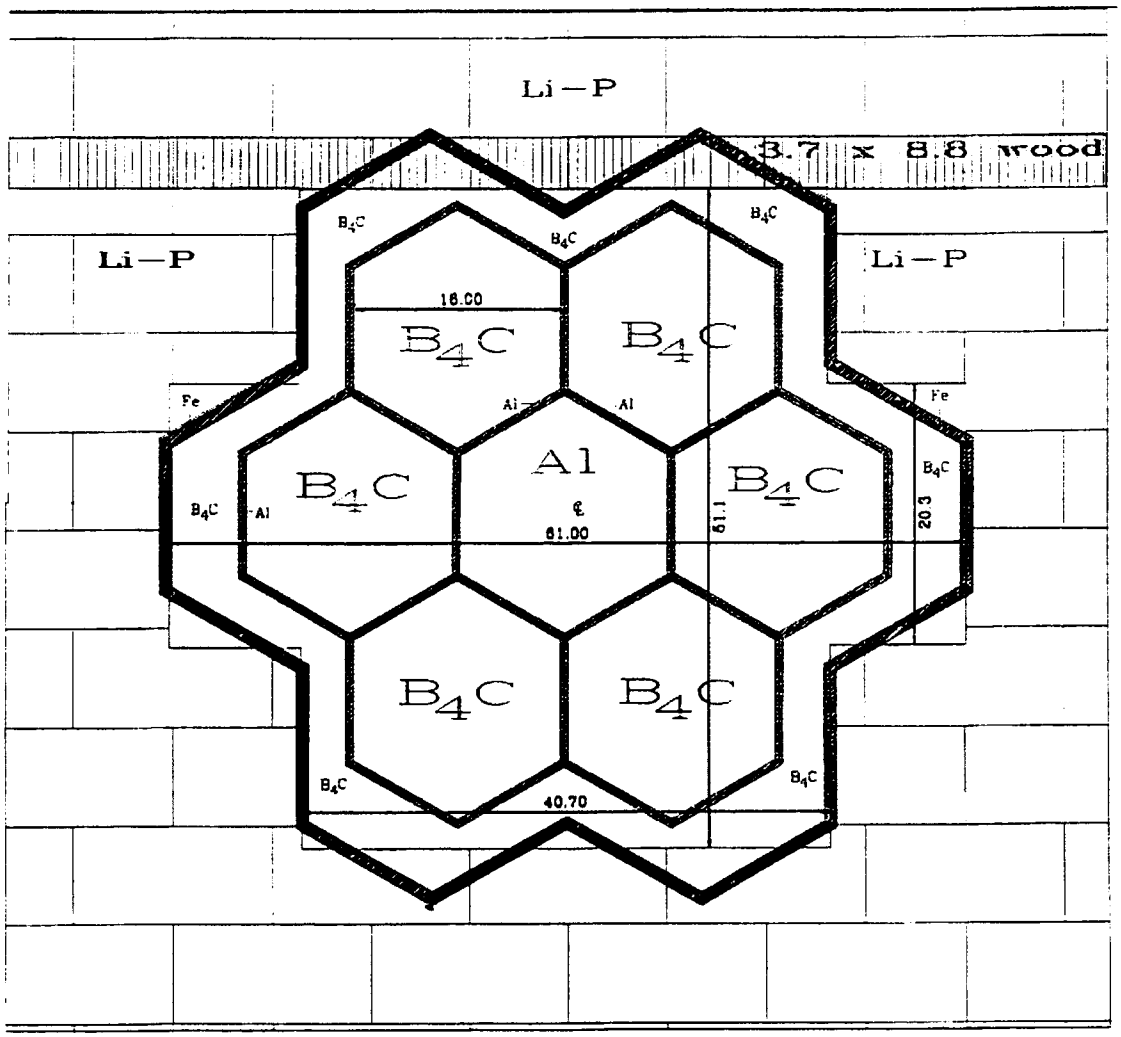

Figure D2. Elevation view of the collimating lithiated-paraffin shield superimposed on the outline of the seven axial shield assembly mockup for the remeasurement program for the JASPER Axial Shield Experiment.

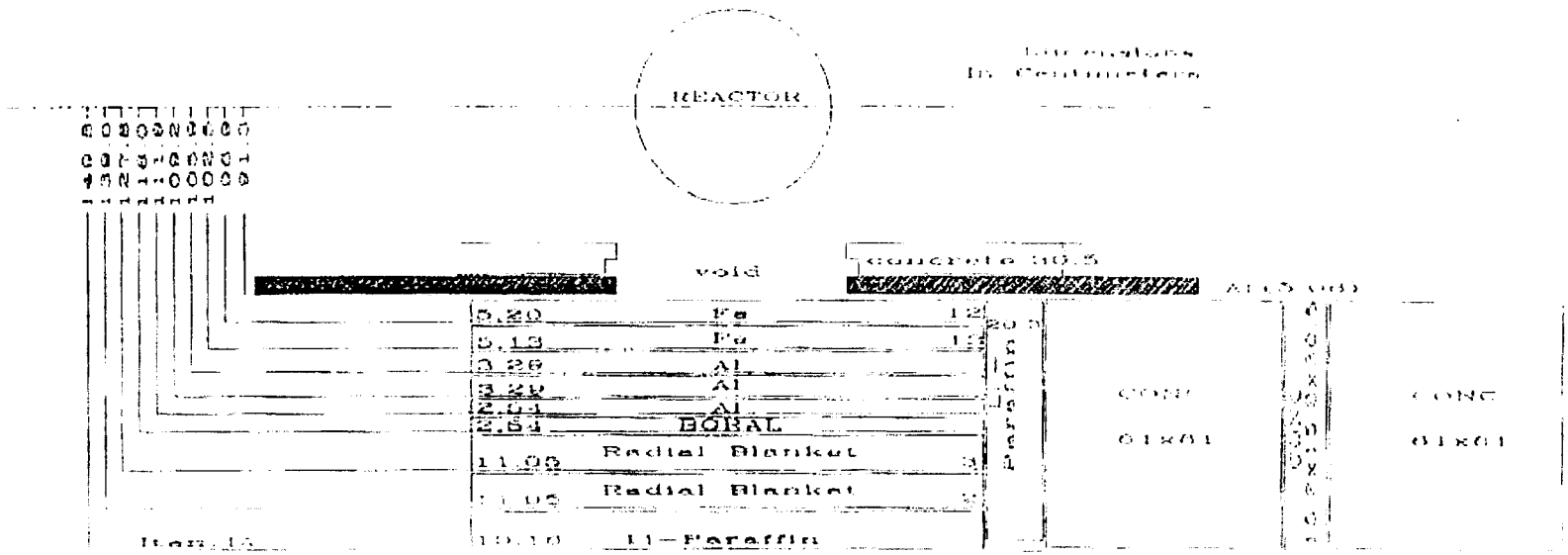

Figure D3. Plan view for the spectrum modifier plus a collimating lithiated-paraffin shield for the remeasurement program for the JASPER Axial Shield Experiment (Configuration I.A).

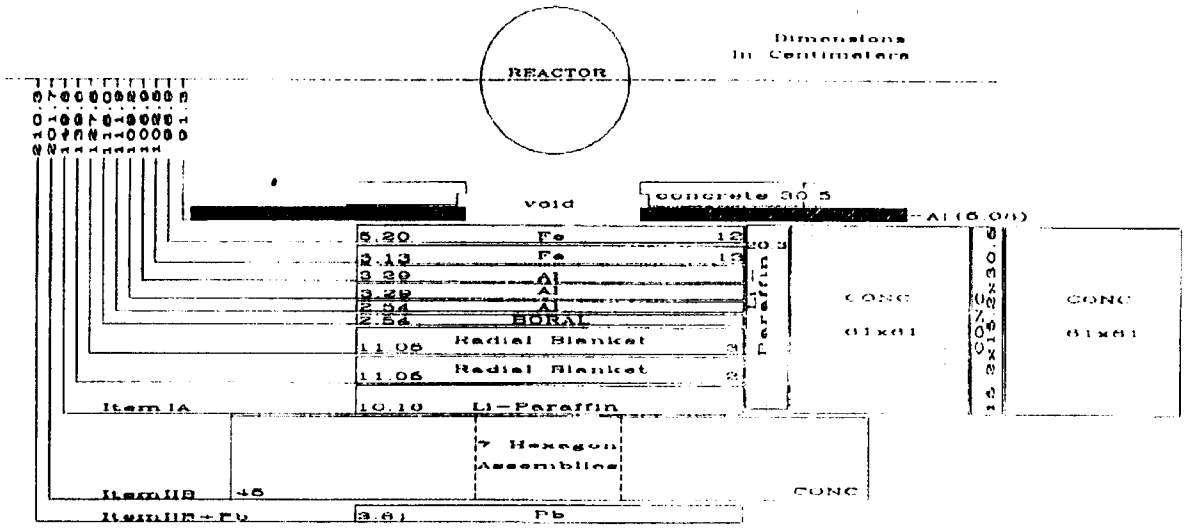

Figure D4. Plan view for the spectrum modifier plus a collimating lithiated-paraffin shield plus the B_4C homogeneous axial shield mockup for the remeasurement program for the JASPER Axial Shield Experiment (Configuration II.B).

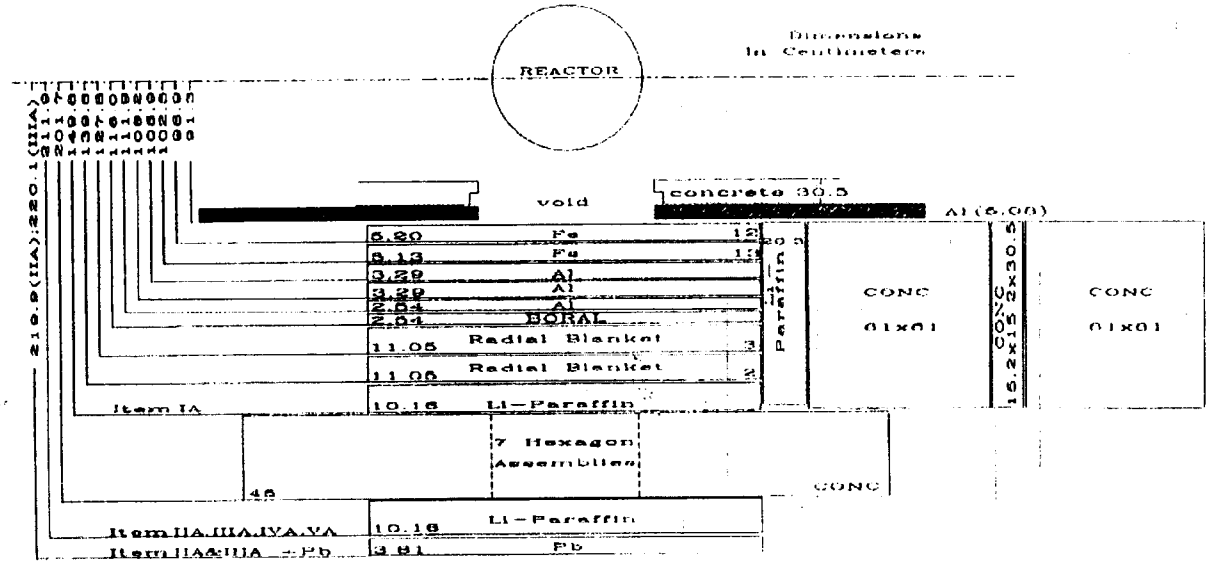

Figure D5. Plan view of configurations consisting of the spectrum modifier plus axial shield mockups preceded and followed by collimating lithiated-paraffin shields for the remeasurement program for the JASPER Axial Shield Experiment (Configurations II.A, III.A, IV.A, and V.A).

Page Intentionally Blank

APPENDIX E

Detector Response Functions

Page Intentionally Blank

Table E1. Bonner Ball count rate response functions (cm^2).

Group	Energy (eV)	3-in. BB	4-in. BB	5-in. BB	8-in. BB	10-in. BB	12-in. BB
1	1.49183E+07	3.43080E-03	3.92840E-02	1.19870E-01	4.29990E-01	5.76450E-01	6.47940E-01
2	1.22140E+07	4.33480E-03	5.05700E-02	1.54190E-01	5.36020E-01	6.96480E-01	7.56230E-01
3	1.00000E+07	5.47290E-03	6.48690E-02	1.97370E-01	6.64810E-01	8.38000E-01	8.80070E-01
4	8.18730E+06	6.81740E-03	8.21780E-02	2.46960E-01	7.83530E-01	9.42800E-01	9.44240E-01
5	6.70320E+06	9.24500E-03	1.07000E-01	3.10000E-01	9.08710E-01	1.04530E+00	1.00480E+00
6	5.48811E+06	1.10220E-02	1.22730E-01	3.49300E-01	9.88020E-01	1.10750E+00	1.03360E+00
7	4.49329E+06	1.34140E-02	1.47880E-01	4.10600E-01	1.07080E+00	1.12830E+00	9.86300E-01
8	3.67879E+06	1.68580E-02	1.78550E-01	4.78240E-01	1.14430E+00	1.14050E+00	9.43510E-01
9	3.01194E+06	2.10080E-02	2.14370E-01	5.57120E-01	1.24290E+00	1.18280E+00	9.33060E-01
10	2.46597E+06	2.41110E-02	2.40630E-01	6.14930E-01	1.32070E+00	1.22530E+00	9.41060E-01
11	2.34570E+06	2.54250E-02	2.50780E-01	6.34850E-01	1.33300E+00	1.21750E+00	9.19740E-01
12	2.23130E+06	2.74860E-02	2.66010E-01	6.63430E-01	1.34410E+00	1.19750E+00	8.81240E-01
13	2.01897E+06	3.18430E-02	2.98370E-01	7.26350E-01	1.39140E+00	1.19280E+00	8.42420E-01
14	1.65299E+06	3.86540E-02	3.44440E-01	8.06550E-01	1.41120E+00	1.13520E+00	7.49240E-01
15	1.35335E+06	4.65630E-02	3.92530E-01	8.82930E-01	1.40870E+00	1.06180E+00	6.53960E-01
16	1.10803E+06	5.56070E-02	4.41840E-01	9.53840E-01	1.38660E+00	9.78880E-01	5.62380E-01
17	9.07180E+05	6.57780E-02	4.91290E-01	1.01760E+00	1.34830E+00	8.91800E-01	4.78500E-01
18	7.42735E+05	7.69570E-02	5.39530E-01	1.07250E+00	1.29750E+00	8.05190E-01	4.04590E-01
19	6.08101E+05	8.77140E-02	5.81040E-01	1.11450E+00	1.24610E+00	7.32460E-01	3.48460E-01
20	5.23397E+05	9.42930E-02	6.04400E-01	1.13600E+00	1.21490E+00	6.92790E-01	3.19920E-01
21	4.97870E+05	1.03720E-01	6.35250E-01	1.16140E+00	1.16940E+00	6.40360E-01	2.84460E-01
22	3.87742E+05	1.20890E-01	6.84390E-01	1.19430E+00	1.08720E+00	5.57720E-01	2.33390E-01
23	3.01974E+05	1.30770E-01	7.10400E-01	1.21050E+00	1.04740E+00	5.20530E-01	2.11960E-01
24	2.98491E+05	1.31340E-01	7.11820E-01	1.21130E+00	1.04510E+00	5.18480E-01	2.10810E-01
25	2.97211E+05	1.31820E-01	7.13010E-01	1.21190E+00	1.04320E+00	5.16770E-01	2.09860E-01
26	2.94518E+05	1.34780E-01	7.20160E-01	1.21560E+00	1.03100E+00	5.06160E-01	2.04010E-01
27	2.73237E+05	1.44330E-01	7.41470E-01	1.22420E+00	9.90760E-01	4.72990E-01	1.86370E-01
28	2.23708E+05	1.58840E-01	7.71230E-01	1.23390E+00	9.35360E-01	4.30170E-01	1.64750E-01
29	1.83156E+05	1.73320E-01	7.97760E-01	1.23970E+00	8.85290E-01	3.94320E-01	1.47640E-01
30	1.49956E+05	1.87720E-01	8.21440E-01	1.24240E+00	8.40280E-01	3.64190E-01	1.33950E-01
31	1.22773E+05	2.06380E-01	8.48860E-01	1.24270E+00	7.88770E-01	3.31940E-01	1.19970E-01
32	8.65169E+04	2.32240E-01	8.82970E-01	1.24100E+00	7.29590E-01	2.97290E-01	1.05610E-01
33	5.65622E+04	2.50080E-01	9.04390E-01	1.23890E+00	6.95220E-01	2.78280E-01	9.80100E-02
34	5.24752E+04	2.65080E-01	9.22400E-01	1.23900E+00	6.71640E-01	2.65520E-01	9.30000E-02
35	3.43067E+04	2.86260E-01	9.47130E-01	1.24010E+00	6.43500E-01	2.50700E-01	8.72660E-02
36	2.85011E+04	2.94300E-01	9.56320E-01	1.24070E+00	6.34080E-01	2.45830E-01	8.54020E-02
37	2.70001E+04	2.97310E-01	9.59830E-01	1.24120E+00	6.30860E-01	2.44170E-01	8.47670E-02
38	2.60584E+04	3.00160E-01	9.63150E-01	1.24160E+00	6.27910E-01	2.42640E-01	8.41850E-02
39	2.47875E+04	3.03500E-01	9.67040E-01	1.24220E+00	6.24540E-01	2.40900E-01	8.35230E-02
40	2.35786E+04	3.18520E-01	9.84130E-01	1.24470E+00	6.10090E-01	2.33550E-01	8.07410E-02
41	1.50344E+04	3.50610E-01	1.01990E+00	1.25100E+00	5.84320E-01	2.20670E-01	7.59140E-02
42	9.11882E+03	3.87190E-01	1.06090E+00	1.26260E+00	5.63080E-01	2.10110E-01	7.19870E-02
43	5.53084E+03	4.21950E-01	1.09620E+00	1.26960E+00	5.43970E-01	2.01010E-01	6.86550E-02
44	3.70744E+03	4.48010E-01	1.12280E+00	1.27670E+00	5.32720E-01	1.95660E-01	6.67010E-02
45	3.03539E+03	4.63430E-01	1.13840E+00	1.28120E+00	5.26840E-01	1.92880E-01	6.56880E-02
46	2.61259E+03	4.76980E-01	1.15200E+00	1.28520E+00	5.22040E-01	1.90620E-01	6.48660E-02
47	2.24867E+03	4.88750E-01	1.16350E+00	1.28830E+00	5.17940E-01	1.88700E-01	6.41750E-02
48	2.03468E+03	5.15190E-01	1.18840E+00	1.29490E+00	5.09270E-01	1.84720E-01	6.27370E-02
49	1.23410E+03	5.66220E-01	1.23210E+00	1.30280E+00	4.92250E-01	1.77160E-01	6.00440E-02
50	7.48518E+02	6.17610E-01	1.26600E+00	1.29790E+00	4.71380E-01	1.68450E-01	5.69820E-02
51	4.53999E+02	6.82050E-01	1.31580E+00	1.30780E+00	4.57370E-01	1.62470E-01	5.48800E-02
52	2.75364E+02	7.43580E-01	1.34890E+00	1.29910E+00	4.37870E-01	1.54680E-01	5.21800E-02
53	1.67017E+02	7.87220E-01	1.34120E+00	1.24890E+00	4.05560E-01	1.42120E-01	4.76910E-02
54	1.01301E+02	7.86080E-01	1.24070E+00	1.22410E+00	4.03010E-01	1.55120E-01	5.93660E-02
55	4.78512E+01	8.23470E-01	1.32500E+00	1.25940E+00	3.94910E-01	1.50690E-01	5.72930E-02
56	2.26033E+01	9.34500E-01	1.34700E+00	1.21860E+00	3.66330E-01	1.39330E-01	5.29340E-02
57	1.06770E+01	1.03770E+00	1.33520E+00	1.15000E+00	3.33150E-01	1.26430E-01	4.80030E-02
58	5.04348E+00	1.13350E+00	1.29210E+00	1.06080E+00	2.98010E-01	1.12960E-01	4.28640E-02
59	2.38237E+00	1.19060E+00	1.18680E+00	9.30950E-01	2.55390E-01	9.67630E-02	3.66940E-02
60	1.12535E+00	1.00810E+00	8.59880E-01	6.42920E-01	1.72980E-01	6.55040E-02	2.47980E-02
61	4.13994E-01	0.00000E+00	0.00000E+00	0.00000E+00	0.00000E+00	0.00000E+00	0.00000E+00
62	1.00001E-05						

Table E2. Hornyak Button response functions (erg · g^{-1} · cm^2) with various energy cutoffs to simulate detector bias settings.

Group	Energy (eV)	E > 120 keV	E > 273 keV	E > 302 keV	E > 498 keV	E > 743 KeV
1	1.49183E+07	6.20000E-07	6.20000E-07	6.20000E-07	6.20000E-07	6.20000E-07
2	1.22140E+07	5.80000E-07	5.80000E-07	5.80000E-07	5.80000E-07	5.80000E-07
3	1.00000E+07	5.41990E-07	5.41990E-07	5.41990E-07	5.41990E-07	5.41990E-07
4	8.18730E+06	5.02990E-07	5.02990E-07	5.02990E-07	5.02990E-07	5.02990E-07
5	6.70320E+06	4.68000E-07	4.68000E-07	4.68000E-07	4.68000E-07	4.68000E-07
6	5.48811E+06	4.36010E-07	4.36010E-07	4.36010E-07	4.36010E-07	4.36010E-07
7	4.49329E+06	4.20010E-07	4.20010E-07	4.20010E-07	4.20010E-07	4.20010E-07
8	3.67879E+06	3.90010E-07	3.90010E-07	3.90010E-07	3.90010E-07	3.90010E-07
9	3.01194E+06	3.50000E-07	3.50000E-07	3.50000E-07	3.50000E-07	3.50000E-07
10	2.46597E+06	3.24160E-07	3.24160E-07	3.24160E-07	3.24160E-07	3.24160E-07
11	2.34570E+06	3.15370E-07	3.15370E-07	3.15370E-07	3.15370E-07	3.15370E-07
12	2.23130E+06	3.07250E-07	3.07250E-07	3.07250E-07	3.07250E-07	3.07250E-07
13	2.01897E+06	2.96960E-07	2.96960E-07	2.96960E-07	2.96960E-07	2.96960E-07
14	1.65299E+06	2.67000E-07	2.67000E-07	2.67000E-07	2.67000E-07	2.67000E-07
15	1.35335E+06	2.44000E-07	2.44000E-07	2.44000E-07	2.44000E-07	2.44000E-07
16	1.10803E+06	2.22000E-07	2.22000E-07	2.22000E-07	2.22000E-07	2.22000E-07
17	9.07180E+05	2.01000E-07	2.01000E-07	2.01000E-07	2.01000E-07	2.01000E-07
18	7.42735E+05	1.77420E-07	1.77420E-07	1.77420E-07	1.77420E-07	0.00000E+00
19	6.08101E+05	1.60360E-07	1.60360E-07	1.60360E-07	1.60360E-07	0.00000E+00
20	5.23397E+05	1.51550E-07	1.51550E-07	1.51550E-07	1.51550E-07	0.00000E+00
21	4.97870E+05	1.40290E-07	1.40290E-07	1.40290E-07	0.00000E+00	0.00000E+00
22	3.87742E+05	1.24170E-07	1.24170E-07	1.24170E-07	0.00000E+00	0.00000E+00
23	3.01974E+05	1.17410E-07	1.17410E-07	0.00000E+00	0.00000E+00	0.00000E+00
24	2.98491E+05	1.16970E-07	1.16970E-07	0.00000E+00	0.00000E+00	0.00000E+00
25	2.97211E+05	1.16600E-07	1.16600E-07	0.00000E+00	0.00000E+00	0.00000E+00
26	2.94518E+05	1.14310E-07	1.14310E-07	0.00000E+00	0.00000E+00	0.00000E+00
27	2.73237E+05	1.07000E-07	0.00000E+00	0.00000E+00	0.00000E+00	0.00000E+00
28	2.23708E+05	9.70020E-08	0.00000E+00	0.00000E+00	0.00000E+00	0.00000E+00
29	1.83156E+05	8.61060E-08	0.00000E+00	0.00000E+00	0.00000E+00	0.00000E+00
30	1.49956E+05	7.59340E-08	0.00000E+00	0.00000E+00	0.00000E+00	0.00000E+00
31	1.22773E+05	0.00000E+00	0.00000E+00	0.00000E+00	0.00000E+00	0.00000E+00
32	8.65169E+04	0.00000E+00	0.00000E+00	0.00000E+00	0.00000E+00	0.00000E+00
33	5.65622E+04	0.00000E+00	0.00000E+00	0.00000E+00	0.00000E+00	0.00000E+00
34	5.24752E+04	0.00000E+00	0.00000E+00	0.00000E+00	0.00000E+00	0.00000E+00
35	3.43067E+04	0.00000E+00	0.00000E+00	0.00000E+00	0.00000E+00	0.00000E+00
36	2.85011E+04	0.00000E+00	0.00000E+00	0.00000E+00	0.00000E+00	0.00000E+00
37	2.70001E+04	0.00000E+00	0.00000E+00	0.00000E+00	0.00000E+00	0.00000E+00
38	2.60584E+04	0.00000E+00	0.00000E+00	0.00000E+00	0.00000E+00	0.00000E+00
39	2.47875E+04	0.00000E+00	0.00000E+00	0.00000E+00	0.00000E+00	0.00000E+00
40	2.35786E+04	0.00000E+00	0.00000E+00	0.00000E+00	0.00000E+00	0.00000E+00
41	1.50344E+04	0.00000E+00	0.00000E+00	0.00000E+00	0.00000E+00	0.00000E+00
42	9.11882E+03	0.00000E+00	0.00000E+00	0.00000E+00	0.00000E+00	0.00000E+00
43	5.53084E+03	0.00000E+00	0.00000E+00	0.00000E+00	0.00000E+00	0.00000E+00
44	3.70744E+03	0.00000E+00	0.00000E+00	0.00000E+00	0.00000E+00	0.00000E+00
45	3.03539E+03	0.00000E+00	0.00000E+00	0.00000E+00	0.00000E+00	0.00000E+00
46	2.61259E+03	0.00000E+00	0.00000E+00	0.00000E+00	0.00000E+00	0.00000E+00
47	2.24867E+03	0.00000E+00	0.00000E+00	0.00000E+00	0.00000E+00	0.00000E+00
48	2.03468E+03	0.00000E+00	0.00000E+00	0.00000E+00	0.00000E+00	0.00000E+00
49	1.23410E+03	0.00000E+00	0.00000E+00	0.00000E+00	0.00000E+00	0.00000E+00
50	7.48518E+02	0.00000E+00	0.00000E+00	0.00000E+00	0.00000E+00	0.00000E+00
51	4.53999E+02	0.00000E+00	0.00000E+00	0.00000E+00	0.00000E+00	0.00000E+00
52	2.75364E+02	0.00000E+00	0.00000E+00	0.00000E+00	0.00000E+00	0.00000E+00
53	1.67017E+02	0.00000E+00	0.00000E+00	0.00000E+00	0.00000E+00	0.00000E+00
54	1.01301E+02	0.00000E+00	0.00000E+00	0.00000E+00	0.00000E+00	0.00000E+00
55	4.78512E+01	0.00000E+00	0.00000E+00	0.00000E+00	0.00000E+00	0.00000E+00
56	2.26033E+01	0.00000E+00	0.00000E+00	0.00000E+00	0.00000E+00	0.00000E+00
57	1.06770E+01	0.00000E+00	0.00000E+00	0.00000E+00	0.00000E+00	0.00000E+00
58	5.04348E+00	0.00000E+00	0.00000E+00	0.00000E+00	0.00000E+00	0.00000E+00
59	2.38237E+00	0.00000E+00	0.00000E+00	0.00000E+00	0.00000E+00	0.00000E+00
60	1.12535E+00	0.00000E+00	0.00000E+00	0.00000E+00	0.00000E+00	0.00000E+00
61	4.13994E-01	0.00000E+00	0.00000E+00	0.00000E+00	0.00000E+00	0.00000E+00
62	1.00001E-05					

APPENDIX F

Tabular Results

Page Intentionally Blank

Table F1. Comparison of calculated and measured 3-inch Bonner ball count rates on centerline 30 cm behind various original configurations.

Configuration	Detector Count Rate ($s^{-1} . W^{-1}$)		C/E[a]
	Measured	Calculated	
I.A[b]	6.00+2[c]	5.20+2	0.87
I.A[d]	6.00+2	6.70+2	1.12
II.A	1.32+0	1.50+0	1.14
II.B	6.10+0	8.04+0	1.32
III.A	1.41+0	1.53+0	1.09
III.B	1.56+0	1.79+0	1.15
III.C	6.69+0	8.52+0	1.27
III.D	8.19+0	1.20+1	1.47
III.E	5.44-1	6.55-1	1.20
IV.A	1.48+0	1.52+0	1.03
IV.B	6.75+0	7.94+0	1.18
V.A	1.69+0	1.61+0	0.95
V.B	8.34+0	9.39+0	1.13

[a]Ratio of calculated to measured result.
[b]Standard weighted uranium cross sections used in analysis.
[c]Read as 6.00×10^2.
[d]Self-shielded uranium cross sections used in analysis.

Table F2. Comparison of calculated and measured 4-inch Bonner ball count rates on centerline 30 cm behind various original configurations.

Configuration	Detector Count Rate ($s^{-1} . W^{-1}$)		C/E[a]
	Measured	Calculated	
I.A[b]	2.09+3[c]	1.91+3	0.91
I.A[d]	2.09+3	2.27+3	1.09
II.A	4.14+0	4.70+0	1.14
II.B	1.82+1	2.21+1	1.21
III.A	4.39+0	4.80+0	1.09
III.B	4.99+0	5.70+0	1.14
III.C	1.94+1	2.30+1	1.19
III.D	2.31+1	3.12+1	1.35
III.E	1.87+0	2.18+0	1.17
IV.A	4.67+0	4.84+0	1.04
IV.B	1.98+1	2.20+1	1.11
V.A	5.34+0	5.24+0	0.98
V.B	2.40+1	2.61+1	1.08

[a]Ratio of calculated to measured result.
[b]Standard weighted uranium cross sections used in analysis.
[c]Read as 2.09×10^3.
[d]Self-shielded uranium cross sections used in analysis.

Table F3. Comparison of calculated and measured 5-inch Bonner ball count rates on centerline 30 cm behind various original configurations.

Configuration	Detector Count Rate ($s^{-1} \cdot W^{-1}$)		C/E[a]
	Measured	Calculated	
I.A[b]	3.03+3[c]	2.79+3	0.92
I.A[d]	3.03+3	3.21+3	1.06
II.A	6.11+0	7.09+0	1.16
II.B	2.41+0	2.88+1	1.20
III.A	6.45+0	7.17+0	1.11
III.B	7.25+0	8.42+0	1.16
III.C	2.60+1	2.96+1	1.14
III.D	3.02+1	3.90+1	1.29
III.E	2.71+0	3.18+0	1.17
IV.A	6.75+0	7.29+0	1.08
IV.B	2.58+1	2.88+1	1.12
V.A	7.67+0	7.97+0	1.04
V.B	3.09+1	3.44+1	1.11

[a]Ratio of calculated to measured result.
[b]Standard weighted uranium cross sections used in analysis.
[c]Read as 3.03×10^3.
[d]Self-shielded uranium cross sections used in analysis.

Table F4. Comparison of calculated and measured 8-inch Bonner ball count rates on centerline 30 cm behind various original configurations.

Configuration	Detector Count Rate ($s^{-1} . W^{-1}$)		C/E[a]
	Measured	Calculated	
I.A[b]	2.17+3[c]	2.07+3	0.95
I.A[d]	2.17+3	2.29+3	1.06
II.A	5.33+0	6.59+0	1.24
II.B	1.56+1	1.79+1	1.15
III.A	5.63+0	6.54+0	1.16
III.B	6.12+0	7.25+0	1.18
III.C	1.68+1	1.82+1	1.08
III.D	1.91+1	2.14+1	1.12
III.E	2.27+0	2.59+0	1.14
IV.A	5.90+0	6.65+0	1.13
IV.B	1.66+1	1.79+1	1.08
V.A	6.08+0	6.97+0	1.15
V.B	1.82+1	2.05+1	1.13

[a]Ratio of calculated to measured result.
[b]Standard weighted uranium cross sections used in analysis.
[c]Read as 2.17×10^3.
[d]Self-shielded uranium cross sections used in analysis.

Table F5. Comparison of calculated and measured 10-inch Bonner ball count rates on centerline 30 cm behind various original configurations.

Configuration	Detector Count Rate ($s^{-1} . W^{-1}$)		C/E[a]
	Measured	Calculated	
I.A[b]	1.14+3[c]	1.08+3	0.95
I.A[d]	1.14+3	1.18+3	1.04
II.A	3.32+0	4.22+0	1.27
II.B	7.55+0	8.65+0	1.15
III.A	3.38+0	4.15+0	1.23
III.B	3.64+0	4.53+0	1.24
III.C	8.16+0	8.81+0	1.08
III.D	9.07+0	9.95+0	1.10
III.E	1.27+0	1.55+0	1.22
IV.A	3.53+0	4.17+0	1.18
IV.B	7.97+0	8.64+0	1.08
V.A	3.55+0	4.22+0	1.19
V.B	8.92+0	9.31+0	1.04

[a]Ratio of calculated to measured result.
[b]Standard weighted uranium cross sections used in analysis.
[c]Read as 1.14×10^3.
[d]Self-shielded uranium cross sections used in analysis.

Table F6. Comparison of calculated and measured 12-inch Bonner ball count rates on centerline 30 cm behind various original configurations.

Configuration	Detector Count Rate ($s^{-1} . W^{-1}$)		C/E[a]
	Measured	Calculated	
I.A[b]	5.45+2[c]	5.19+2	0.95
I.A[d]	5.45+2	5.65+2	1.04
II.A	1.87+0	2.49+0	1.33
II.B	3.41+0	3.84+0	1.13
III.A	1.92+0	2.41+0	1.26
III.B	2.01+0	2.63+0	1.31
III.C	3.71+0	3.90+0	1.05
III.D	4.02+0	4.32+0	1.07
III.E	6.71-1	8.70-1	1.30
IV.A	1.98+0	2.40+0	1.21
IV.B	3.54+0	3.84+0	1.08
V.A	1.97+0	2.42+0	1.23
V.B	3.75+0	4.05+0	1.08

[a]Ratio of calculated to measured result.
[b]Standard weighted uranium cross sections used in analysis.
[c]Read as 5.45×10^2.
[d]Self-shielded uranium cross sections used in analysis.

Table F7. Comparison of calculated and measured 3-inch Bonner ball count rates on centerline 150 cm behind various original configurations.

Configuration	Measured Foreground[a]	Calculated Foreground[a]	C/E[b]	Measured Net[a,c]	Calculated Net (1)[a,c,d]	C/E[b]	Calculated Net (2)[a,c,d]	C/E[b]
I.A[e]	1.08+2[f]	7.90+1	0.73	8.92+1	7.80+1	0.87		
I.A[g]	1.08+2	1.01+2	0.94	8.92+1	9.95+1	1.12		
II.A	3.07-1	2.90-1	0.94	1.59-1	1.70-1	1.07	1.23-1	0.77
II.B	6.94-1	6.78-1	0.98	5.17-1	6.31-1	1.22	5.82-1	1.13
III.A	3.11-1	2.83-1	0.91	1.61-1	1.55-1	0.96	1.10-1	0.68
III.B	3.70-1	2.95-1	0.80	2.29-1	1.67-1	0.73	1.23-1	0.54
III.C	7.71-1	7.01-1	0.91	6.09-1	5.66-1	0.93	5.07-1	0.83
III.D	9.82-1	8.63-1	0.88	8.72-1	7.28-1	0.83	6.70-1	0.77
III.E	1.16-1	7.68-2	0.66	9.73-2	5.63-2	0.58	4.54-2	0.47
IV.A	3.32-1	2.84-1	0.86	1.85-1	1.56-1	0.84	1.11-1	0.60
IV.B	7.87-1	6.82-1	0.87	6.15-1	5.47-1	0.89	4.88-1	0.79
V.A	3.36-1	2.83-1	0.84	1.90-1	1.55-1	0.82	1.11-1	0.58
V.B	8.74-1	7.30-1	0.84	6.96-1	5.95-1	0.85	5.36-1	0.77

[a]Units are $s^{-1} \cdot W^{-1}$.

[b]Ratio of calculated to measured result.

[c]Foreground result minus background result.

[d]For Configuration I.A. Net (1) excludes contributions from radii greater than 85.982 cm. For other configurations, Net (1) excludes contributions from radii greater than 45.26 cm and Net (2) excludes those from radii greater than 37.88 cm. The latter two radii correspond to an equivalent radius of the region shadowed by the background shield and a smaller radius based on imperfect shadowing by the shield (i.e., some neutrons from the shadowed region need only pass through a thin portion of the shield to reach the detector).

[e]Standard weighted uranium cross sections used in analysis.

[f]Read as 1.08×10^2.

[g]Self-shielded uranium cross sections used in analysis.

Table F8. Comparison of calculated and measured 4-inch Bonner ball count rates on centerline 150 cm behind various original configurations.

Configuration	Measured Foreground[a]	Calculated Foreground[a]	C/E[b]	Measured Net[a,c]	Calculated Net (1)[a,c,d]	C/E[b]	Calculated Net (2)[a,c,d]	C/E[b]
I.A[e]	3.52+2[f]	2.84+2	0.81	3.11+2	2.82+2	0.91		
I.A[g]	3.52+2	3.35+2	0.95	3.11+2	3.33+2	1.07		
II.A	7.70-1	6.70-1	0.87	4.82-1	4.49-1	0.93	3.62-1	0.75
II.B	1.86+0	1.66+0	0.89	1.52+0	1.57+0	1.03	1.48+0	0.97
III.A	8.02-1	6.55-1	0.82	5.09-1	4.18-1	0.82	3.35-1	0.66
III.B	9.68-1	6.97-1	0.72	6.90-1	4.60-1	0.67	3.78-1	0.55
III.C	2.05+0	1.72+0	0.84	1.73+0	1.47+0	0.85	1.37+0	0.79
III.D	2.64+0	2.05+0	0.78	2.34+0	1.81+0	0.77	1.70+0	0.73
III.E	3.42-1	2.01-1	0.59	3.05-1	1.62-1	0.53	1.42-1	0.47
IV.A	8.27-1	6.59-1	0.80	5.38-1	4.22-1	0.78	3.39-1	0.63
IV.B	2.08+0	1.68+0	0.81	1.75+0	1.43+0	0.82	1.33+0	0.76
V.A	8.63-1	6.56-1	0.76	5.75-1	4.19-1	0.73	3.37-1	0.59
V.B	2.30+0	1.78+0	0.77	1.96+0	1.54+0	0.79	1.43+0	0.73

[a]Units are $s^{-1} \cdot W^{-1}$.

[b]Ratio of calculated to measured result.

[c]Foreground result minus background result.

[d]For Configuration I.A, Net (1) excludes contributions from radii greater than 85.982 cm. For other configurations, Net (1) excludes contributions from radii greater than 45.26 cm and Net (2) excludes those from radii greater than 37.88 cm. The latter two radii correspond to an equivalent radius of the region shadowed by the background shield and a smaller radius based on imperfect shadowing by the shield (i.e., some neutrons from the shadowed region need only pass through a thin portion of the shield to reach the detector).

[e]Standard weighted uranium cross sections used in analysis.

[f]Read as 3.52×10^{2}.

[g]Self-shielded uranium cross sections used in analysis.

Table F9. Comparison of calculated and measured 5-inch Bonner ball count rates on centerline 150 cm behind various original configurations.

Configuration	Measured Foreground[a]	Calculated Foreground[a]	C/E[b]	Measured Net[a,c]	Calculated Net (1)[a,c,d]	C/E[b]	Calculated Net (2)[a,c,d]	C/E[b]
I.A[e]	5.02+2[f]	4.11+2	0.82	4.55+2	4.08+2	0.90		
I.A[g]	5.02+2	4.70+2	0.94	4.55+2	4.68+2	1.03		
II.A	1.04+0	9.17-1	0.88	6.91-1	6.48-1	0.94	5.41-1	0.78
II.B	2.42+0	2.13+0	0.88	2.02+0	2.03+0	1.00	1.92+0	0.95
III.A	1.09+0	8.94-1	0.82	7.36-1	6.06-1	0.82	5.05-1	0.69
III.B	1.29+0	9.53-1	0.74	9.51-1	6.65-1	0.70	5.64-1	0.59
III.C	2.68+0	2.20+0	0.82	2.31+0	1.90+0	0.82	1.78+0	0.77
III.D	3.33+0	2.56+0	0.77	2.98+0	2.27+0	0.76	2.15+0	0.72
III.E	4.62-1	2.81-1	0.61	4.16-1	2.33-1	0.56	2.09-1	0.50
IV.A	1.11+0	9.01-1	0.81	7.62-1	6.12-1	0.80	5.11-1	0.67
IV.B	2.69+0	2.15+0	0.80	2.31+0	1.86+0	0.81	1.73+0	0.75
V.A	1.18+0	8.95-1	0.76	8.30-1	6.07-1	0.73	5.06-1	0.61
V.B	2.96+0	2.27+0	0.77	2.56+0	1.97+0	0.77	1.85+0	0.72

[a]Units are s^{-1}, W^{-1}.

[b]Ratio of calculated to measured result.

[c]Foreground result minus background result.

[d]For Configuration I.A, Net (1) excludes contributions from radii greater than 85.982 cm. For other configurations, Net (1) excludes contributions from radii greater than 45.26 cm and Net (2) excludes those from radii greater than 37.88 cm. The latter two radii correspond to an equivalent radius of the region shadowed by the background shield and a smaller radius based on imperfect shadowing by the shield (i.e., some neutrons from the shadowed region need only pass through a thin portion of the shield to reach the detector).

[e]Standard weighted uranium cross sections used in analysis.

[f]Read as 5.02×10^2.

[g]Self-shielded uranium cross sections used in analysis.

Table F10. Comparison of calculated and measured 8-inch Bonner ball count rates on centerline 150 cm behind various original configurations.

Configuration	Measured Foreground[a]	Calculated Foreground[a]	C/E[b]	Measured Net[a,c]	Calculated Net (1)[a,c,d]	C/E[b]	Calculated Net (2)[a,c,d]	C/E[b]
I.A[e]	3.52+2[f]	3.05+2	0.87	3.28+2	3.03+2	0.92		
I.A[g]	3.52+2	3.35+2	0.95	3.28+2	3.34+2	1.02		
II.A	8.53-1	8.23-1	0.96	5.83-1	6.11-1	1.05	5.23-1	0.90
II.B	1.62+0	1.43+0	0.88	1.32+0	1.36+0	1.03	1.27+0	0.96
III.A	8.86-1	7.96-1	0.90	6.06-1	5.67-1	0.94	4.84-1	0.80
III.B	1.00+0	8.41-1	0.84	7.35-1	6.12-1	0.83	5.28-1	0.72
III.C	1.77+0	1.46+0	0.82	1.49+0	1.23+0	0.83	1.14+0	0.77
III.D	2.14+0	1.61+0	0.75	1.88+0	1.38+0	0.73	1.29+0	0.67
III.E	3.37-1	2.40-1	0.71	3.00-1	2.01-1	0.67	1.83-1	0.61
IV.A	9.15-1	8.00-1	0.87	6.41-1	5.71-1	0.89	4.88-1	0.76
IV.B	1.78+0	1.44+0	0.81	1.50+0	1.21+0	0.81	1.12+0	0.75
V.A	9.34-1	7.96-1	0.85	6.58-1	5.67-1	0.86	4.84-1	0.74
V.B	1.87+0	1.49+0	0.80	1.58+0	1.26+0	0.80	1.17+0	0.74

[a]Units are $s^{-1} \cdot W^{-1}$.

[b]Ratio of calculated to measured result.

[c]Foreground result minus background result.

[d]For Configuration I.A. Net (1) excludes contributions from radii greater than 85.982 cm. For other configurations, Net (1) excludes contributions from radii greater than 45.26 cm and Net (2) excludes those from radii greater than 37.88 cm. The latter two radii correspond to an equivalent radius of the region shadowed by the background shield and a smaller radius based on imperfect shadowing by the shield (i.e., some neutrons from the shadowed region need only pass through a thin portion of the shield to reach the detector).

[e]Standard weighted uranium cross sections used in analysis.

[f]Read as 3.52×10^2.

[g]Self-shielded uranium cross sections used in analysis.

Table F11. Comparison of calculated and measured 10-inch Bonner ball count rates on centerline 150 cm behind various original configurations.

Configuration	Measured Foreground[a]	Calculated Foreground[a]	C/E[b]	Measured Net[a,c]	Calculated Net (1)[a,c,d]	C/E[b]	Calculated Net (2)[a,c,d]	C/E[b]
I.A[e]	1.84+2[f]	1.60+2	0.87	1.72+2	1.60+2	0.93		
I.A[g]	1.84+2	1.75+2	0.95	1.72+2	1.74+2	1.01		
II.A	5.34-1	5.56-1	1.04	3.54-1	4.14-1	1.17	3.52-1	0.99
II.B	8.54-1	7.82-1	0.92	6.61-1	7.34-1	1.11	6.76-1	1.02
III.A	5.74-1	5.34-1	0.98	3.62-1	3.80-1	1.05	3.22-1	0.89
III.B	5.97-1	5.63-1	0.94	4.22-1	4.08-1	0.97	3.50-1	0.83
III.C	9.29-1	7.92-1	0.85	7.47-1	6.36-1	0.85	5.76-1	0.77
III.D	1.06-0	8.43-1	0.80	8.90-1	6.88-1	0.77	6.28-1	0.71
III.E	1.85-1	1.54-1	0.83	1.61-1	1.27-1	0.79	1.15-1	0.71
IV.A	5.55-1	5.36-1	0.97	3.74-1	3.81-1	1.02	3.23-1	0.86
IV.B	9.10-1	7.83-1	0.86	7.31-1	6.27-1	0.86	5.67-1	0.78
V.A	5.69-1	5.33-1	0.94	3.87-1	3.80-1	0.98	3.21-1	0.83
V.B	9.76-1	8.02-1	0.82	7.83-1	6.46-1	0.83	5.86-1	0.75

[a]Units are $s^{-1} \cdot W^{-1}$.

[b]Ratio of calculated to measured result.

[c]Foreground result minus background result.

[d]For Configuration I.A, Net (1) excludes contributions from radii greater than 85.982 cm. For other configurations, Net (1) excludes contributions from radii greater than 45.26 cm and Net (2) excludes those from radii greater than 37.88 cm. The latter two radii correspond to an equivalent radius of the region shadowed by the background shield and a smaller radius based on imperfect shadowing by the shield (i.e., some neutrons from the shadowed region need only pass through a thin portion of the shield to reach the detector).

[e]Standard weighted uranium cross sections used in analysis.

[f]Read as 1.84×10^{2}.

[g]Self-shielded uranium cross sections used in analysis.

Table F12. Comparison of calculated and measured 12-inch Bonner ball count rates on centerline 150 cm behind various original configurations.

Configuration	Measured Foreground[a]	Calculated Foreground[a]	C/E[b]	Measured Net[a,c]	Calculated Net (1)[a,c,d]	C/E[b]	Calculated Net (2)[a,c,d]	C/E[b]
I.A[e]	8.82+1[f]	7.83+1	0.89	8.29+1	7.81+1	0.94		
I.A[g]	8.82+1	8.47+1	0.96	8.29+1	8.44+1	1.02		
II.A	3.27+1	3.51+1	1.07	2.14+1	2.62+1	1.22	2.20+1	1.03
II.B	4.27+1	4.01+1	0.94	3.06+1	3.81+1	1.25	3.45+1	1.13
III.A	3.29+1	3.37+1	1.02	2.12+1	2.37+1	1.12	1.98+1	0.93
III.B	3.42+1	3.55+1	1.04	2.31+1	2.56+1	1.11	2.16+1	0.94
III.C	4.60+1	4.13+1	0.90	3.45+1	3.13+1	0.91	2.73+1	0.79
III.D	5.17+1	4.28+1	0.83	4.09+1	3.28+1	0.80	2.89+1	0.71
III.E	9.87+2	9.32+2	0.94	8.37+2	7.59+2	0.91	6.81+2	0.81
IV.A	3.30+1	3.37+1	1.02	2.15+1	2.37+1	1.10	1.98+1	0.92
IV.B	4.50+1	4.10+1	0.91	3.41+1	3.10+1	0.91	2.70+1	0.79
V.A	3.29+1	3.36+1	0.98	2.16+1	2.37+1	1.10	1.98+1	0.92
V.B	4.67+1	4.17+1	0.89	3.50+1	3.16+1	0.90	2.77+1	0.79

[a]Units are $s^{-1} \cdot W^{-1}$.

[b]Ratio of calculated to measured result.

[c]Foreground result minus background result.

[d]For Configuration I.A, Net (1) excludes contributions from radii greater than 85.982 cm. For other configurations, Net (1) excludes contributions from radii greater than 45.26 cm and Net (2) excludes those from radii greater than 37.88 cm. The latter two radii correspond to an equivalent radius of the region shadowed by the background shield and a smaller radius based on imperfect shadowing by the shield (i.e., some neutrons from the shadowed region need only pass through a thin portion of the shield to reach the detector).

[e]Standard weighted uranium cross sections used in analysis.

[f]Read as 8.82×10^{1}.

[g]Self-shielded uranium cross sections used in analysis.

Table F13. Comparison of calculated and measured Bonner ball count rates and the integrated spectrum at the spectrum measurement location 179.1 cm behind original Axial Shield Experiment Configuration I.A.

Quantity	Measured Foreground[a]	Calculated Foreground[a]	C/E[b]	Measured Net[a,c]	Calculated Net[a,c]	C/E[b]
Standard-Weighted UO_2						
3 inch BB Count Rate	8.31+1[d]	5.77+1	0.69	6.56+1	5.70+1	0.87
5 inch BB Count Rate	3.79+2	3.00+2	0.79	3.37+2	2.99+2	0.89
10 inch BB Count Rate	1.38+2	1.17+2	0.85	1.27+2	1.17+2	0.92
E > 52.4 keV Neutron Flux	-	1.560+5	-	1.585+5	1.487+5	0.94
Self-Shielded UO_2						
3 inch BB Count Rate	8.31+1	7.39+1	0.89	6.56+1	7.31+1	1.11
5 inch BB Count Rate	3.79+2	3.45+2	0.91	3.37+2	3.43+2	1.02
10 inch BB Count Rate	1.38+2	1.28+2	0.93	1.27+2	1.27+2	1.00
E > 52.4 keV Neutron Flux	-	1.560+5	-	1.585+5	1.555+5	0.98

[a]Units are $s^{-1} \cdot W^{-1}$ for the Bonner ball count rate and $cm^{-2} \cdot s^{-1} \cdot W^{-1}$ for the neutron flux.

[b]Ratio of calculated to measured result.

[c]Foreground result minus background result. The calculated Net results were obtained by limiting contributions to those emerging from radii less than 45.26 cm, which is the nearest radius to the equivalent cylindrical radius of the opening in the shadow shield collar.

[d]Read as 8.31×10^1.

Table F14. Comparison of calculated and measured Bonner ball count rates and the integrated spectrum at the spectrum measurement location 25 cm behind original Axial Shield Experiment Configurations II.A and II.B (with lead).

Quantity	Measured[a]	Calculated[a]	C/E[b]
Configuration II.A			
3-inch BB Count Rate	9.34-1[c]	1.14+0	1.22
5-inch BB Count Rate	4.41+0	5.49+0	1.24
10-inch BB Count Rate	2.41+0	3.27+0	1.36
E > 52.4 keV Neutron Flux	2.707+3	3.374+3	1.25
Configuration II.B (with lead)			
3-inch BB Count Rate	4.91+0	6.17+0	1.26
5-inch BB Count Rate	1.85+1	2.18+1	1.18
10-inch BB Count Rate	5.66+0	6.57+0	1.16
E > 52.4 keV Neutron Flux	6.344+3	6.602+3	1.04

[a]Units are $s^{-1} \cdot W^{-1}$ for the Bonner ball count rates and $cm^{-2} \cdot s^{-1} \cdot W^{-1}$ for the neutron flux.
[b]Ratio of calculated to measured result.
[c]Read as 9.34×10^{-1}.

Table F15. Comparison of calculated and measured Bonner ball count rates and the integrated spectrum at the spectrum measurement location 98.3 cm behind original Axial Shield Experiment Configuration II.B (no lead).

Quantity	Measured Foreground[a]	Calculated Foreground[a]	C/E[b]	Measured Net[a,c]	Calculated Net[a,c] (1)	C/E[b]	Calculated Net (2)[a,c]	C/E[b]
3-inch BB Count Rate	1.35+0[d]	1.44+0	1.07	1.19+0	1.39+0	1.17	1.31+0	1.10
5 inch BB Count Rate	4.75+0	4.77+0	1.00	4.39+0	4.65+0	1.06	4.48+0	1.02
10 inch BB Count Rate	1.61+0	1.68+0	1.04	1.45+0	1.63+0	1.12	1.54+0	1.06
E > 52.4 keV Neutron Flux	-	1.659+3	-	1.683+3	1.610+3	0.96	1.537+3	0.91

[a]Units are $s^{-1} \cdot W^{-1}$ for the Bonner ball count rate and $cm^{-2} \cdot s^{-1} \cdot W^{-1}$ for the neutron flux.

[b]Ratio of calculated to measured result.

[c]Foreground result minus background result. The calculated Net(1) and Net(2) results were obtained by limiting contributions to those emerging from radii less than 45.26 cm and 37.88 cm, respectively, the first radius approximating the equivalent cylindrical radius of the opening in the shadow shield collar.

[d]Read as 1.35×10^{0}.

Table F16. Heterogeneous-to-homogeneous Bonner ball count-rate ratios (streaming factors) for various Axial Shield Experiment original configurations.

Bonner ball	Shield Configuration[a]	Stainless Steel Assemblies		B_4C Assemblies	
		Measured	Calculated	Measured	Calculated
3-inch	A	1.10	1.06	1.07	1.02
	B	1.34	1.49	1.18	1.19
	C	1.11	0.99	1.12	1.01
	D	1.37	1.17	1.28	1.07
4-inch	A	1.07	1.04	1.06	1.02
	B	1.27	1.41	1.21	1.21
	C	1.09	1.00	1.13	1.03
	D	1.32	1.18	1.29	1.11
5-inch	A	1.08	1.03	1.06	1.01
	B	1.25	1.35	1.19	1.19
	C	1.07	1.00	1.10	1.03
	D	1.28	1.19	1.26	1.12
8-inch	A	1.08	1.02	1.06	0.99
	B	1.22	1.20	1.15	1.10
	C	1.06	1.00	1.11	1.01
	D	1.17	1.15	1.14	1.06
10-inch	A	1.08	1.02	1.02	0.98
	B	1.20	1.15	1.10	1.07
	C	1.06	1.00	1.06	0.99
	D	1.18	1.08	1.07	1.00
12-inch	A	1.09	1.02	1.03	0.97
	B	1.18	1.13	1.07	1.06
	C	1.04	1.00	1.06	0.96
	D	1.10	1.05	1.05	0.97

[a]Configurations A: one central blockage assembly + six homogeneous assemblies (III.A and III.C); Configurations B: seven central blockage assemblies (III.B and III.D); Configurations C: one rod bundle assembly + six homogeneous assemblies (IV.A and IV.B); and Configurations D: one central sodium channel assembly + six homogeneous assemblies (V.A and V.B).

Table F17. Comparison of calculated and measured 3-inch Bonner ball count rates on centerline 30 cm behind various remeasurement configurations.

Configuration	Detector Count Rate ($s^{-1} . W^{-1}$)		C/E[a]
	Measured	Calculated	
I.A	6.07+2[b]	5.17+2	0.85
II.A	5.56-1	6.61-1	1.19
II.B	5.50-1	6.83-1	1.24
III.A	6.42-1	7.09-1	1.10
IV.A	5.95-1	6.99-1	1.17
V.A	8.46-1	7.30-1	0.86

[a]Ratio of calculated to measured result.
[b]Read as 6.07×10^2.

Table F18. Comparison of calculated and measured 4-inch Bonner ball count rates on centerline 30 cm behind various remeasurement configurations.

Configuration	Detector Count Rate ($s^{-1} . W^{-1}$)		C/E[a]
	Measured	Calculated	
I.A	1.89+3[b]	1.66+3	0.88
II.A	2.00+0	2.39+0	1.20
II.B	1.94+0	2.38+0	1.23
III.A	2.31+0	2.56+0	1.11
IV.A	2.12+0	2.49+0	1.17
V.A	2.98+0	2.69+0	0.90

[a]Ratio of calculated to measured result.
[b]Read as 1.89×10^3.

Table F19. Comparison of calculated and measured 5-inch Bonner ball count rates on centerline 30 cm behind various remeasurement configurations.

Configuration	Detector Count Rate ($s^{-1} . W^{-1}$)		C/E[a]
	Measured	Calculated	
I.A	2.53+3[b]	2.36+3	0.93
II.A	3.10+0	3.73+0	1.20
II.B	2.95+0	3.70+0	1.25
III.A	3.50+0	3.97+0	1.13
IV.A	3.20+0	3.85+0	1.20
V.A	4.31+0	4.24+0	0.98

[a]Ratio of calculated to measured result.
[b]Read as 2.53×10^3.

Table F20. Comparison of calculated and measured 8-inch Bonner ball count rates on centerline 30 cm behind various remeasurement configurations.

Configuration	Detector Count Rate ($s^{-1} . W^{-1}$)		C/E[a]
	Measured	Calculated	
I.A	1.85+3[b]	1.72+3	0.93
II.A	2.79+0	3.54+0	1.27
II.B	2.74+0	3.52+0	1.28
III.A	2.98+0	3.71+0	1.24
IV.A	2.88+0	3.62+0	1.26
V.A	3.36+0	3.92+0	1.17

[a]Ratio of calculated to measured result.
[b]Read as 1.85×10^3.

Table F21. Comparison of calculated and measured 10-inch Bonner ball count rates on centerline 30 cm behind various remeasurement configurations.

Configuration	Detector Count Rate ($s^{-1} . W^{-1}$)		C/E[a]
	Measured	Calculated	
I.A	9.02+2[b]	9.08+2	1.01
II.A	1.76+0	2.26+0	1.28
II.B	1.66+0	2.26+0	1.36
III.A	1.79+0	2.33+0	1.30
IV.A	1.70+0	2.31+0	1.36
V.A	1.90+0	2.37+0	1.25

[a]Ratio of calculated to measured result.
[b]Read as 9.02×10^2.

Table F22. Comparison of calculated and measured 12-inch Bonner ball count rates on centerline 30 cm behind various remeasurement configurations.

Configuration	Detector Count Rate ($s^{-1} . W^{-1}$)		C/E[a]
	Measured	Calculated	
I.A	4.56+2[b]	4.41+2	0.97
II.A	9.24-1	1.32+0	1.43
II.B	9.26-1	1.33+0	1.44
III.A	9.84-1	1.35+0	1.37
IV.A	9.39-1	1.35+0	1.44
V.A	1.01+0	1.36+0	1.35

[a]Ratio of calculated to measured result.
[b]Read as 4.56×10^2.

Table F23. Comparison of calculated and measured 3-inch Bonner ball count rates on centerline 150 cm behind various remeasurement configurations.

Configuration	Measured Foreground[a]	Calculated Foreground[a]	C/E[b]	Measured Net[a,c]	Calculated Net (1)[a,c,d]	C/E[b]
I.A	5.20-1[e]	6.15+1	1.18	4.69+1	6.04+1	1.29
II.A	7.28-2	6.25-2	0.86	6.71-2	6.10-2	0.91
II.B	1.05-1	1.24-1	1.18	9.38-2	1.15-1	1.23
III.A	8.43-2	6.41-2	0.76	7.75-2	6.26-2	0.81
IV.A	7.88-2	6.29-2	0.80	7.23-2	6.14-2	0.85
V.A	1.04-1	6.28-2	0.60	9.78-2	6.13-2	0.63

[a]Units are $s^{-1} \cdot W^{-1}$.
[b]Ratio of calculated to measured result.
[c]Foreground result minus background result.
[d]The calculated Net excludes contributions from radii greater than 37.88 cm, corresponding to a radius somewhat smaller than the equivalent radius of the region shadowed by the background shield.
[e]Read as 5.20×10^{1}.

APPENDIX G

Graphical Results

Page Intentionally Blank

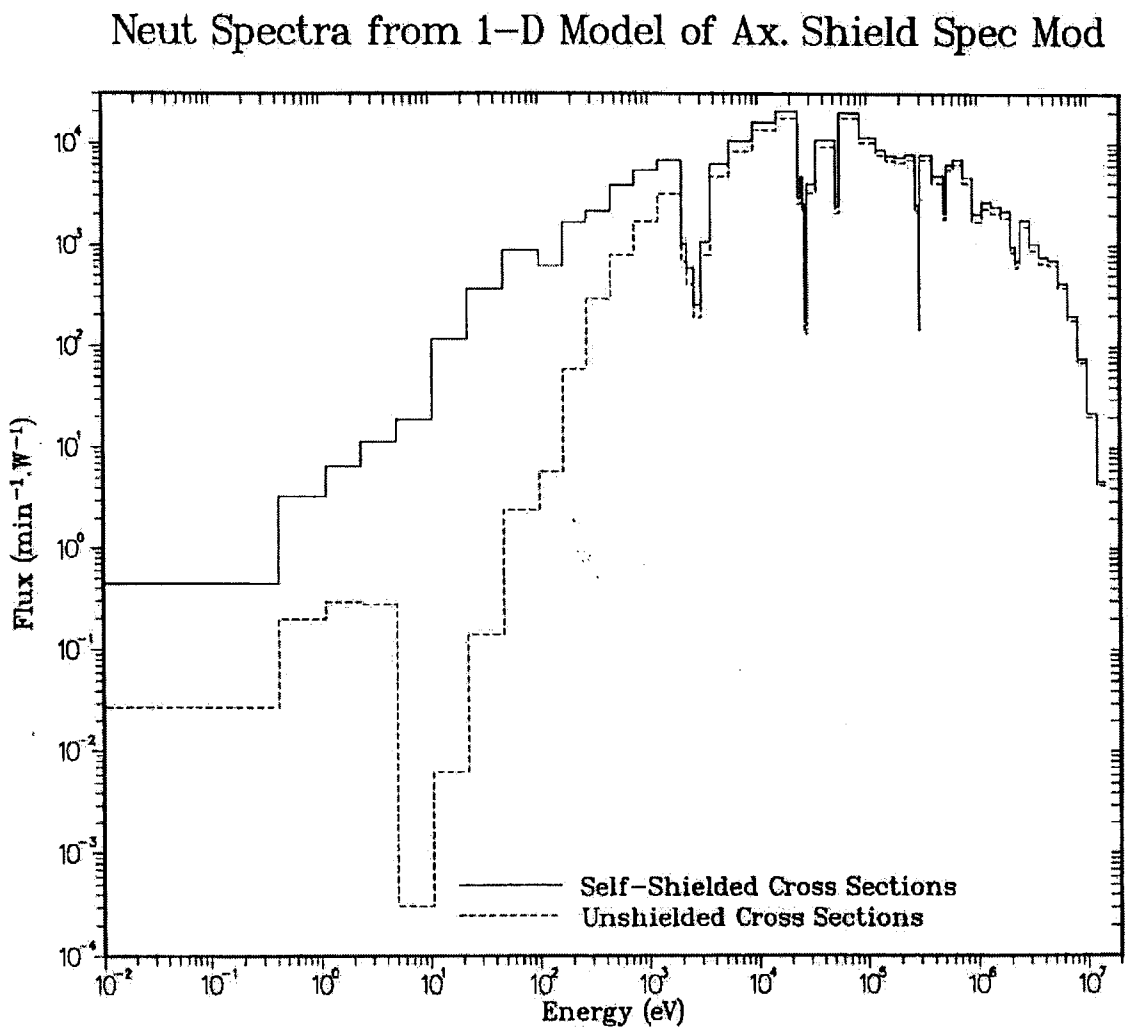

Figure G1. Comparison of neutron spectra behind a one-dimensional model of the spectrum modifier for self-shielded and unshielded UO_2 cross sections.

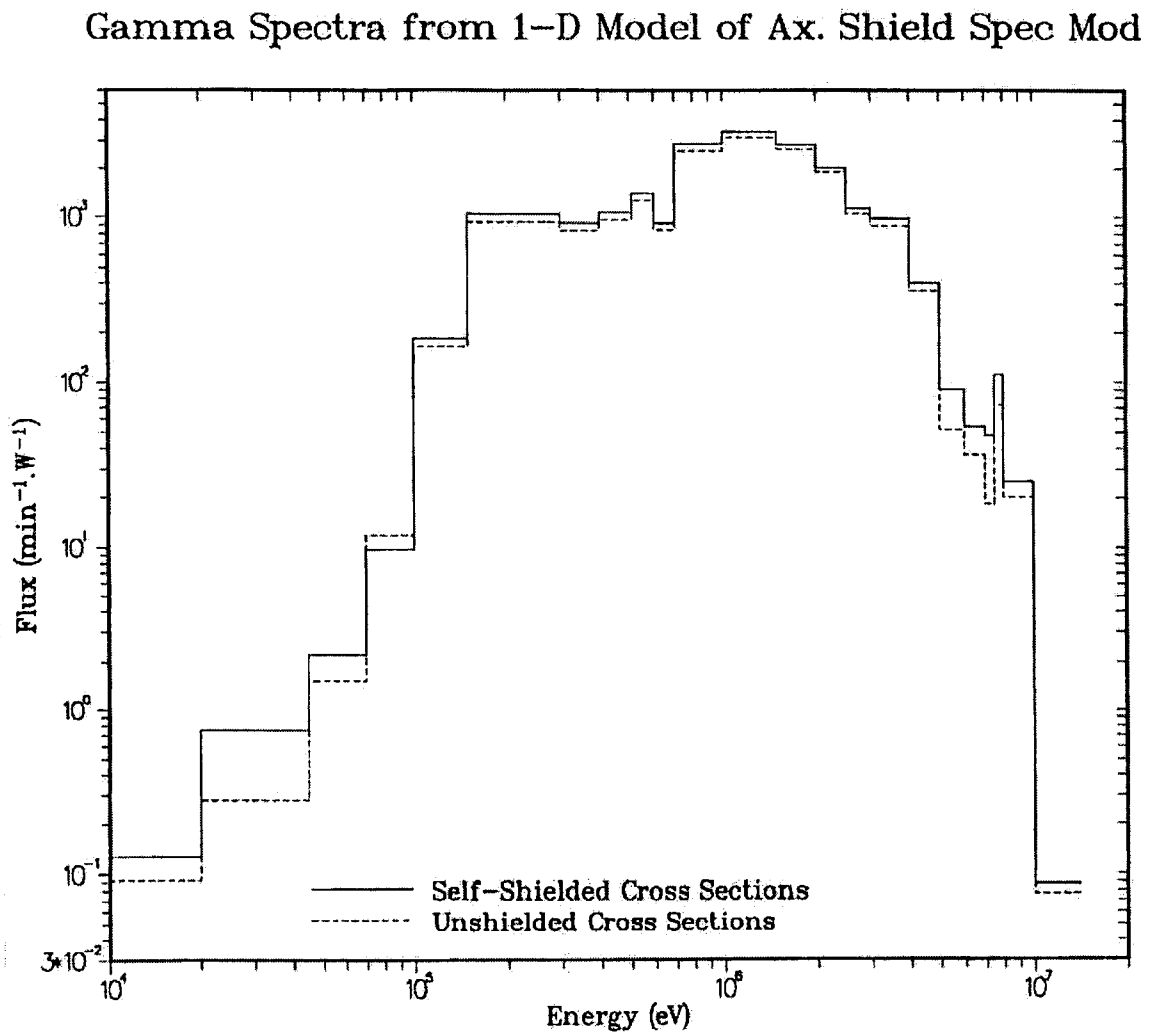

Figure G2. Comparison of gamma-ray spectra behind a one-dimensional model of the spectrum modifier for self-shielded and unshielded UO_2 cross sections.

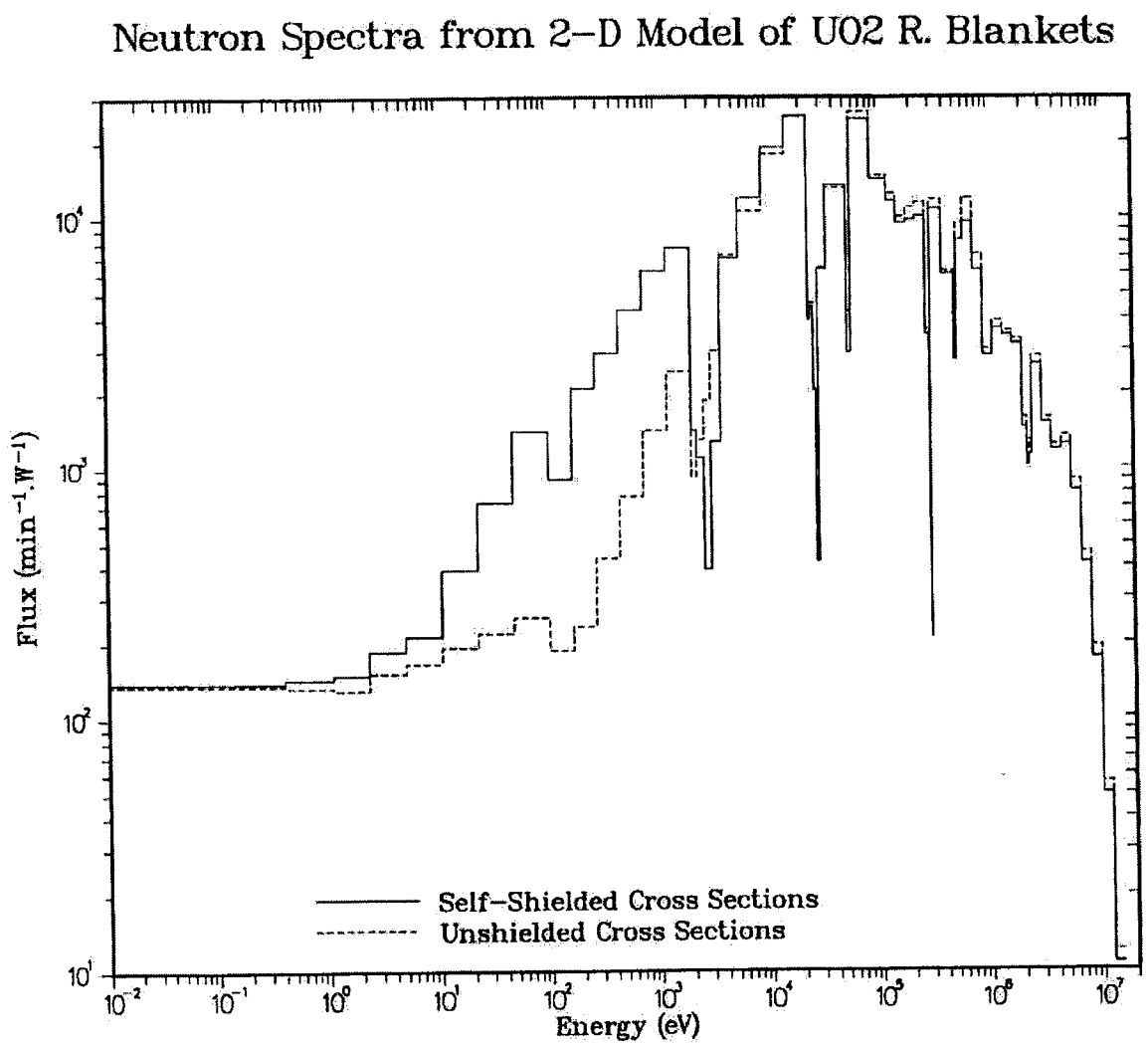

Figure G3. Comparison of neutron spectra behind a two-dimensional model of the spectrum modifier for self-shielded and unshielded UO_2 cross sections.

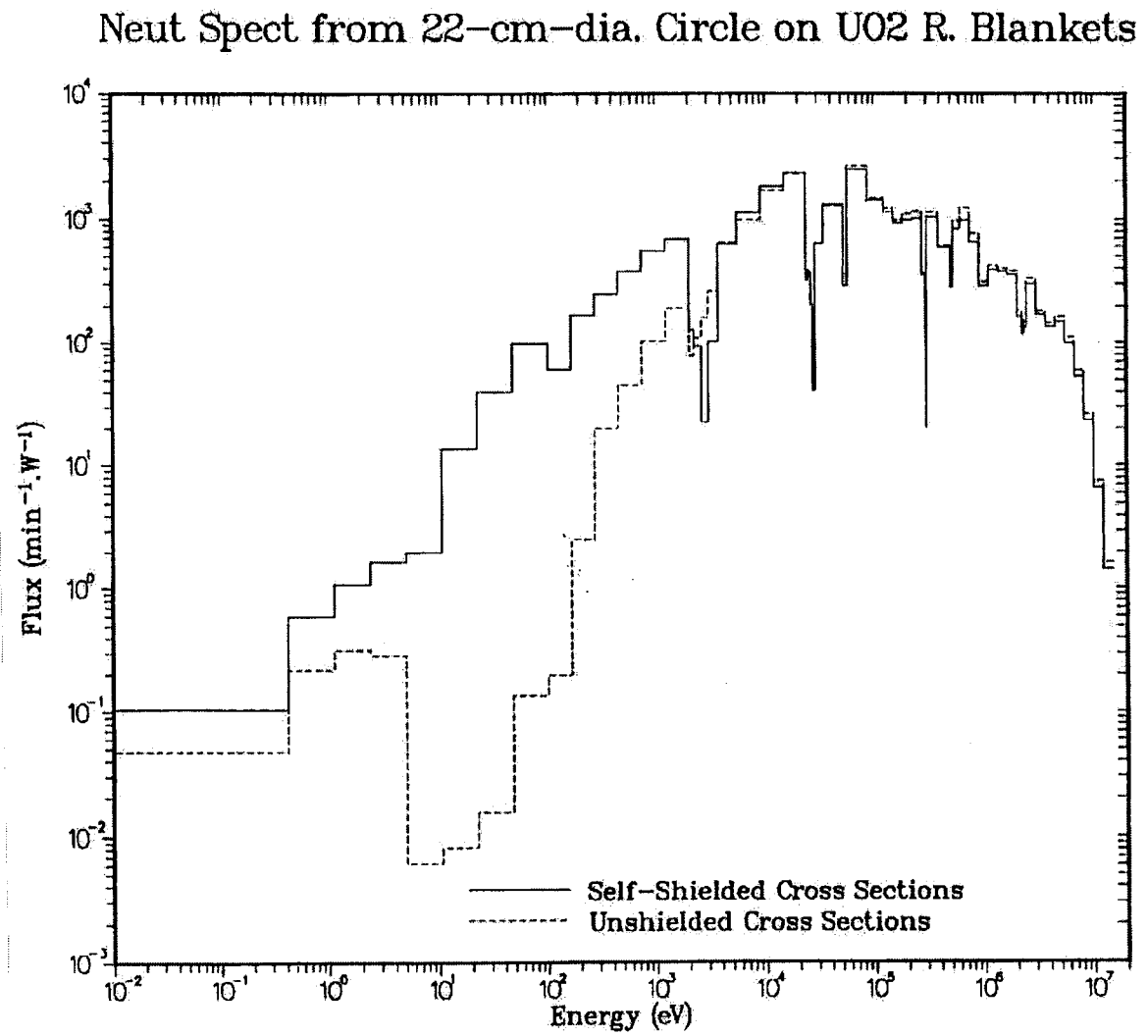

Figure G4. Comparison of neutron spectra due to neutrons from a 22-cm-diameter region of a two-dimensional model of the spectrum modifier for self-shielded and unshielded UO_2 cross sections.

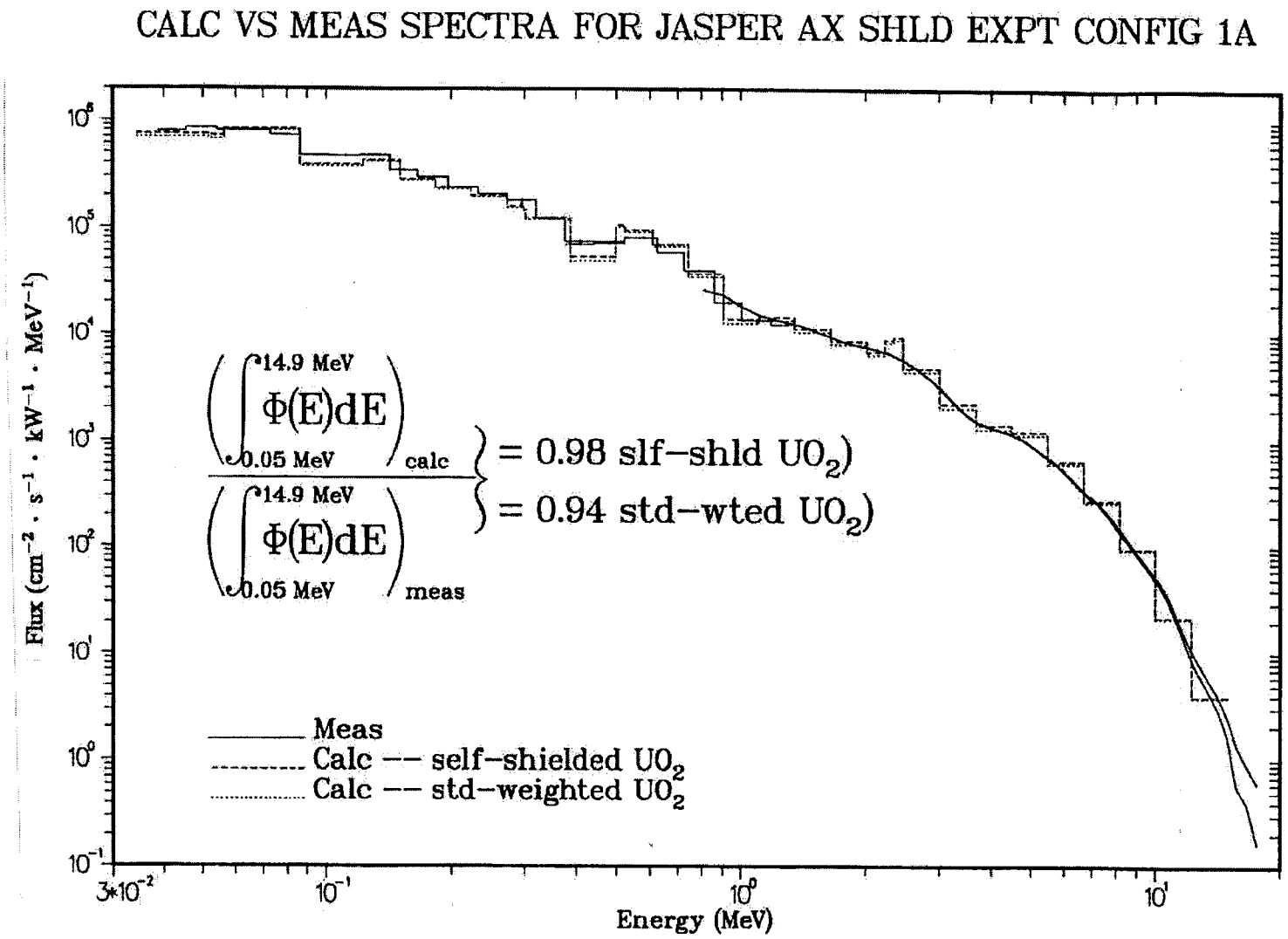

Figure G5. Comparison of calculated and measured neutron spectra behind Jasper Axial Shield Experiment original Configuration I.A.

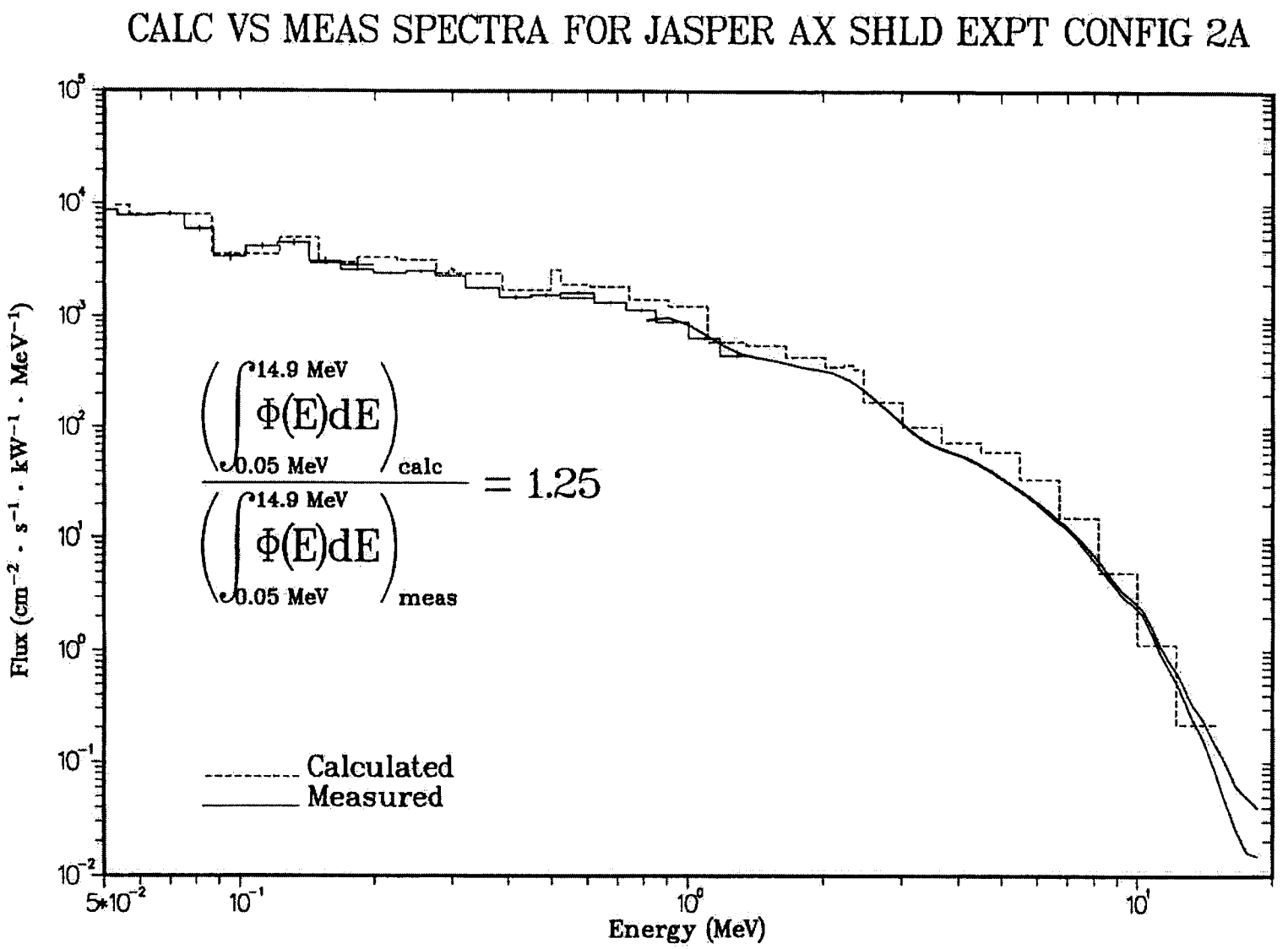

Figure G6. Comparison of calculated and measured neutron spectra behind Jasper Axial Shield Experiment original Configuration II.A.

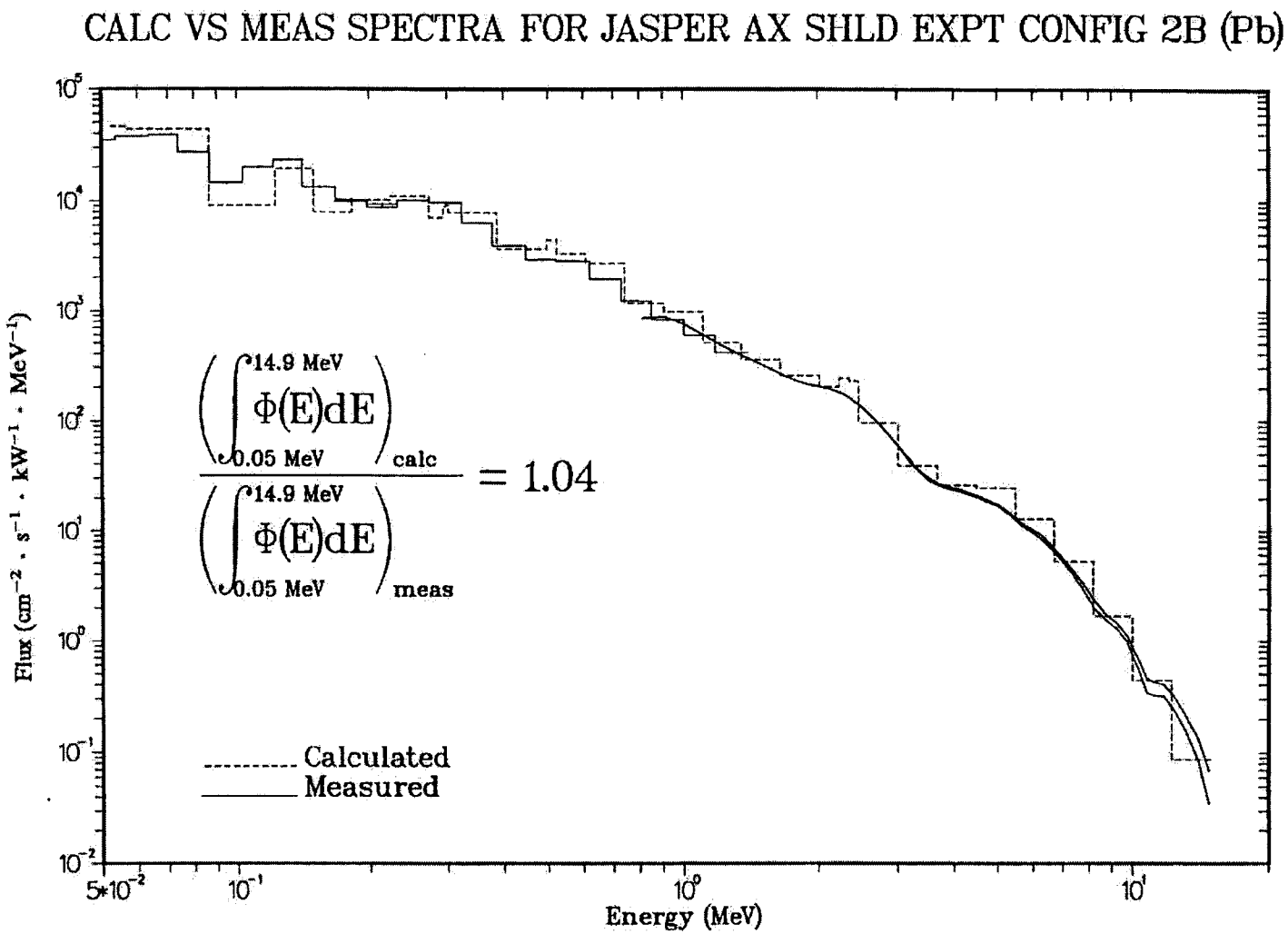

Figure G7. Comparison of calculated and measured neutron spectra behind Jasper Axial Shield Experiment original Configuration II.B with lead slabs.

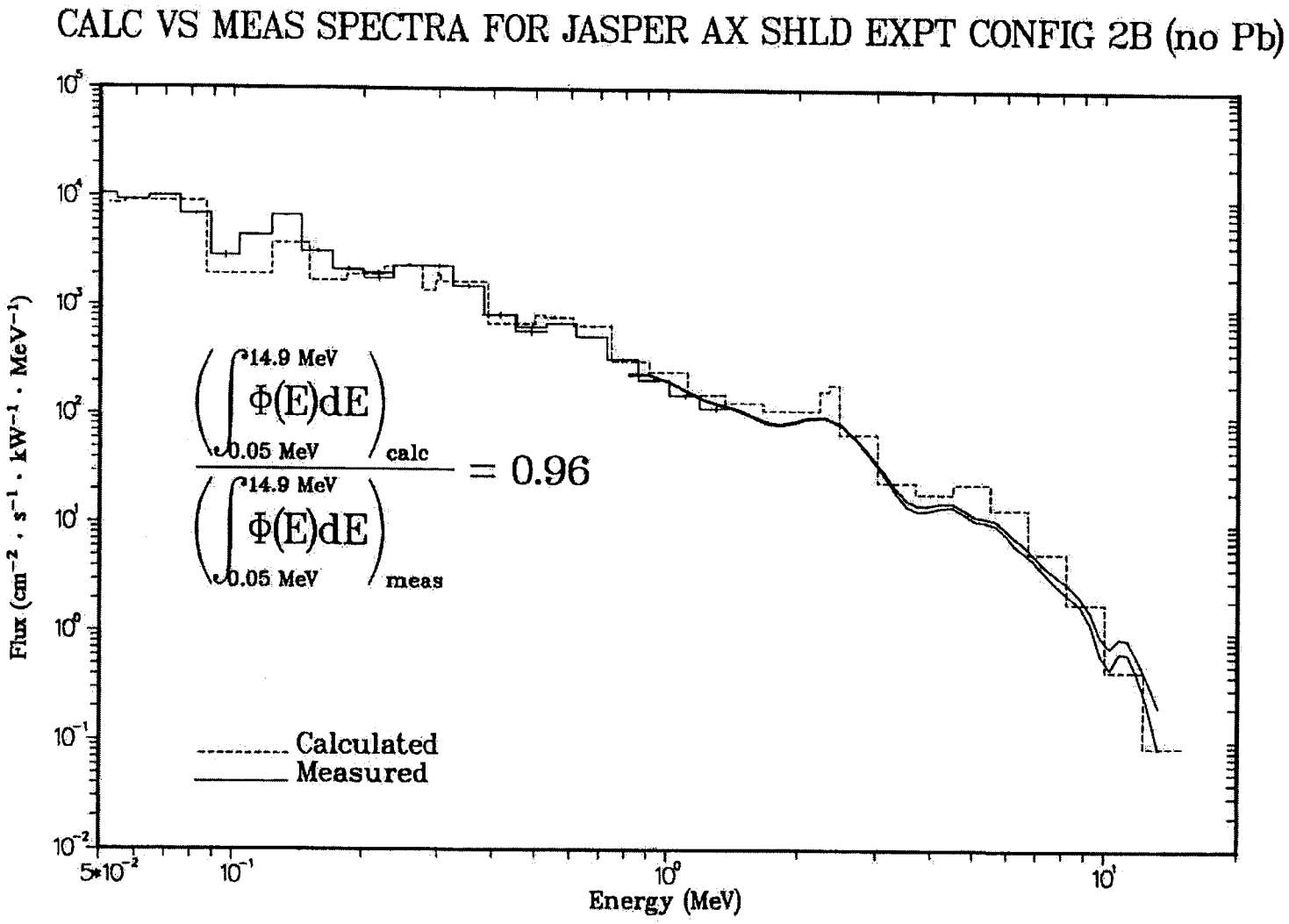

Figure G8. Comparison of calculated and measured neutron spectra behind Jasper Axial Shield Experiment original Configuration II.B without lead slabs.

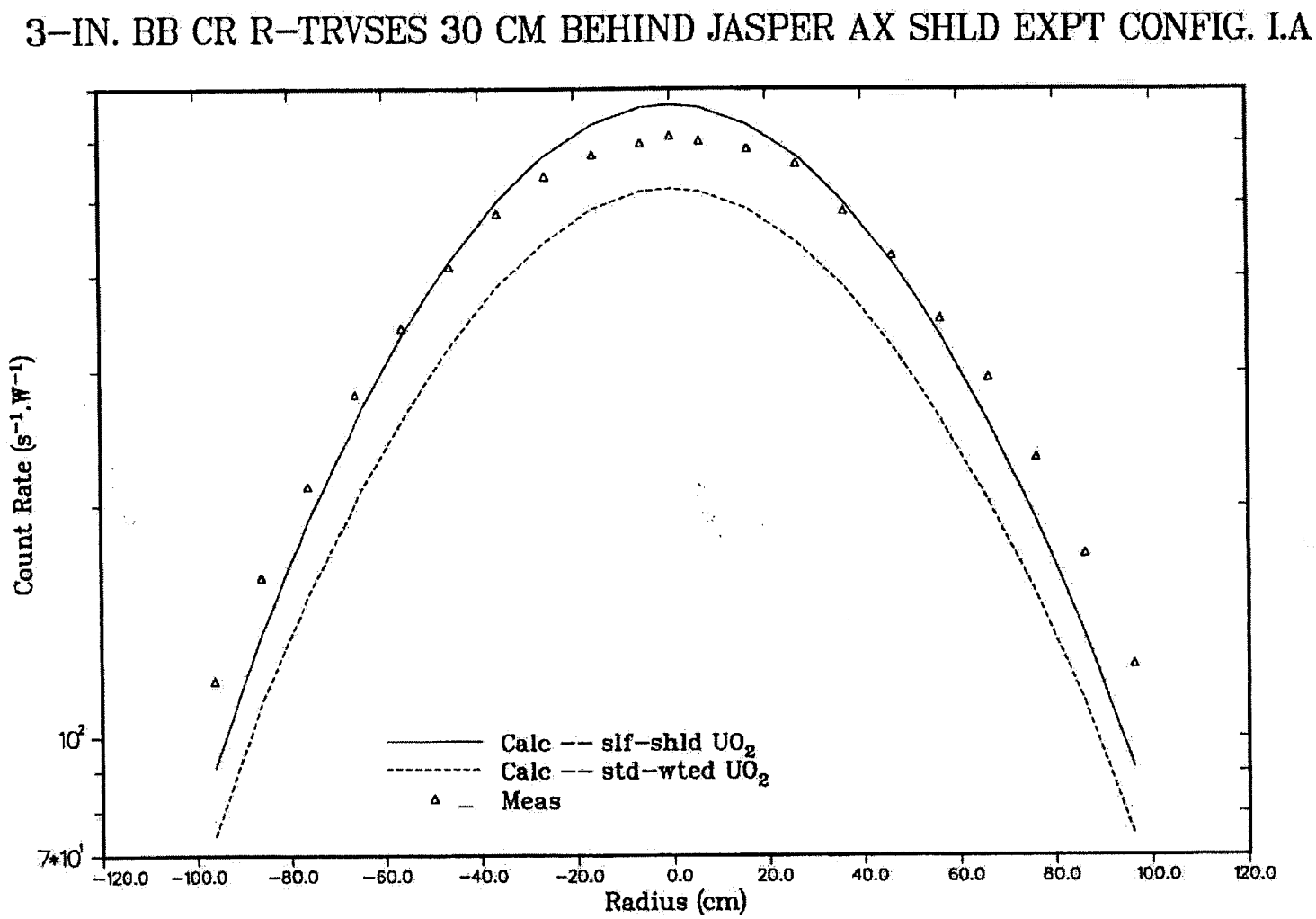

Figure G9. Comparison of calculated and measured 3-inch Bonner Ball count rates for a radial traverse 30 cm behind Jasper Axial Shield Experiment original Configuration I.A.

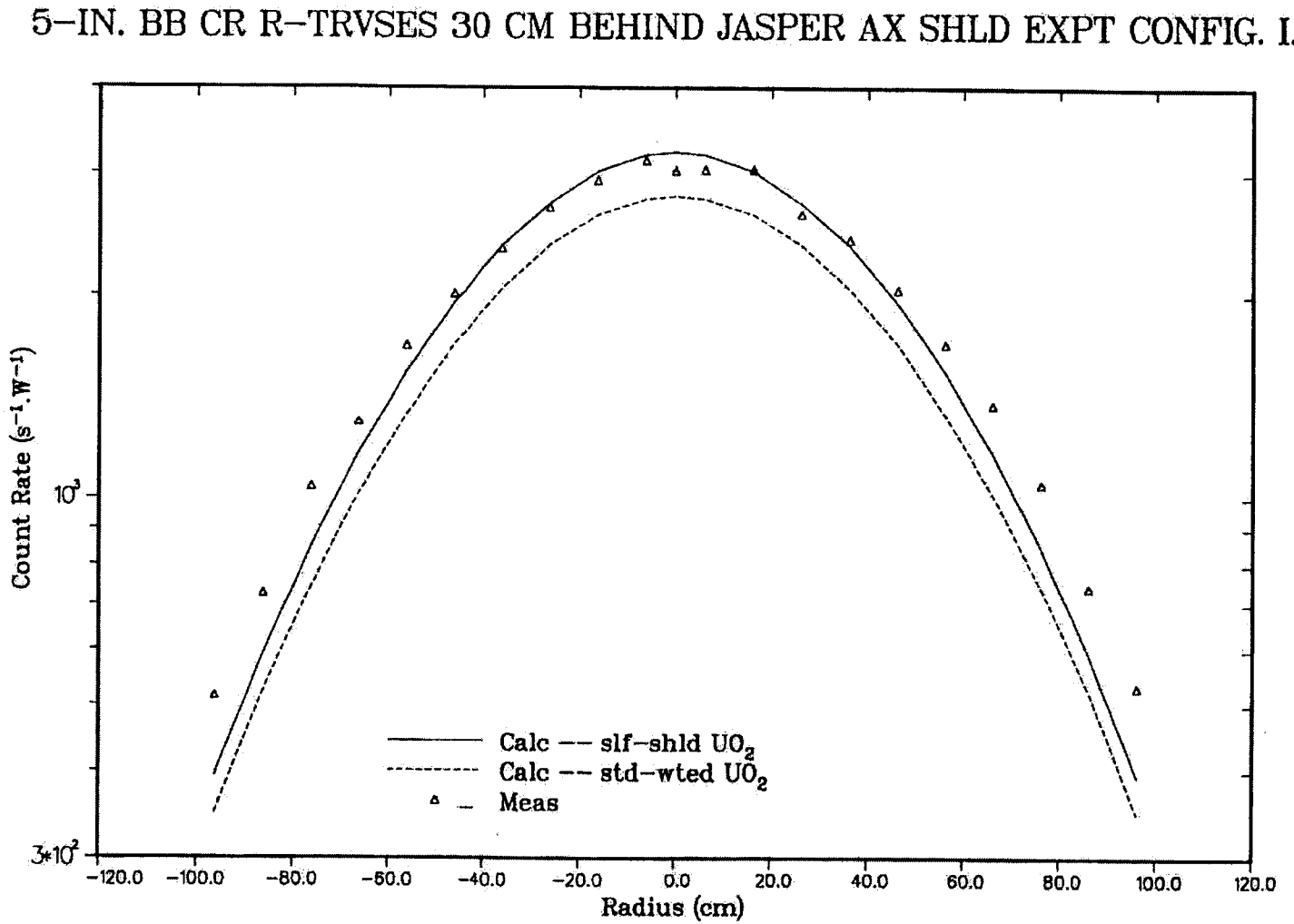

Figure G10. Comparison of calculated and measured 5-inch Bonner Ball count rates for a radial traverse 30 cm behind Jasper Axial Shield Experiment original Configuration I.A.

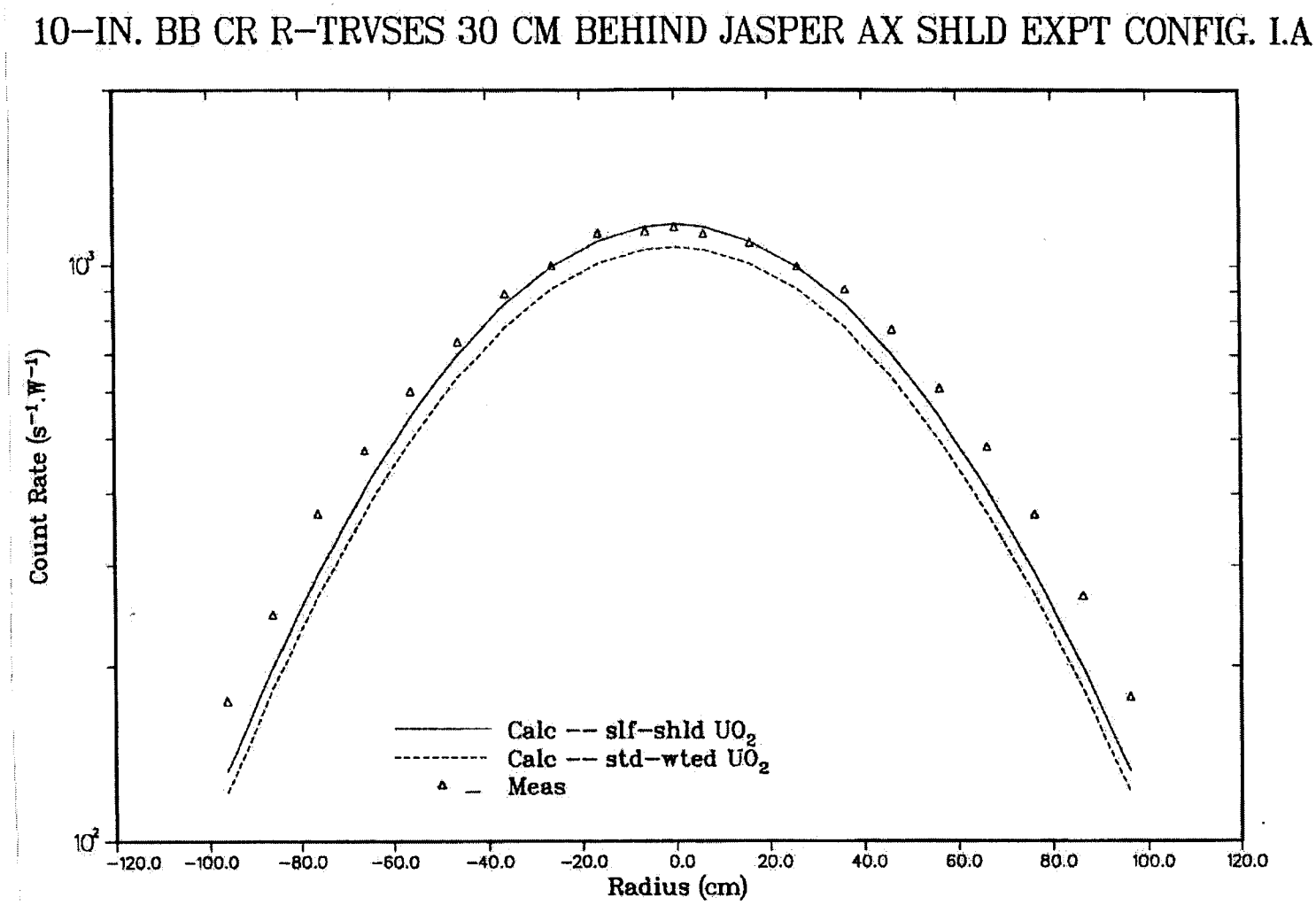

Figure G11. Comparison of calculated and measured 10-inch Bonner Ball count rates for a radial traverse 30 cm behind Jasper Axial Shield Experiment original Configuration I.A.

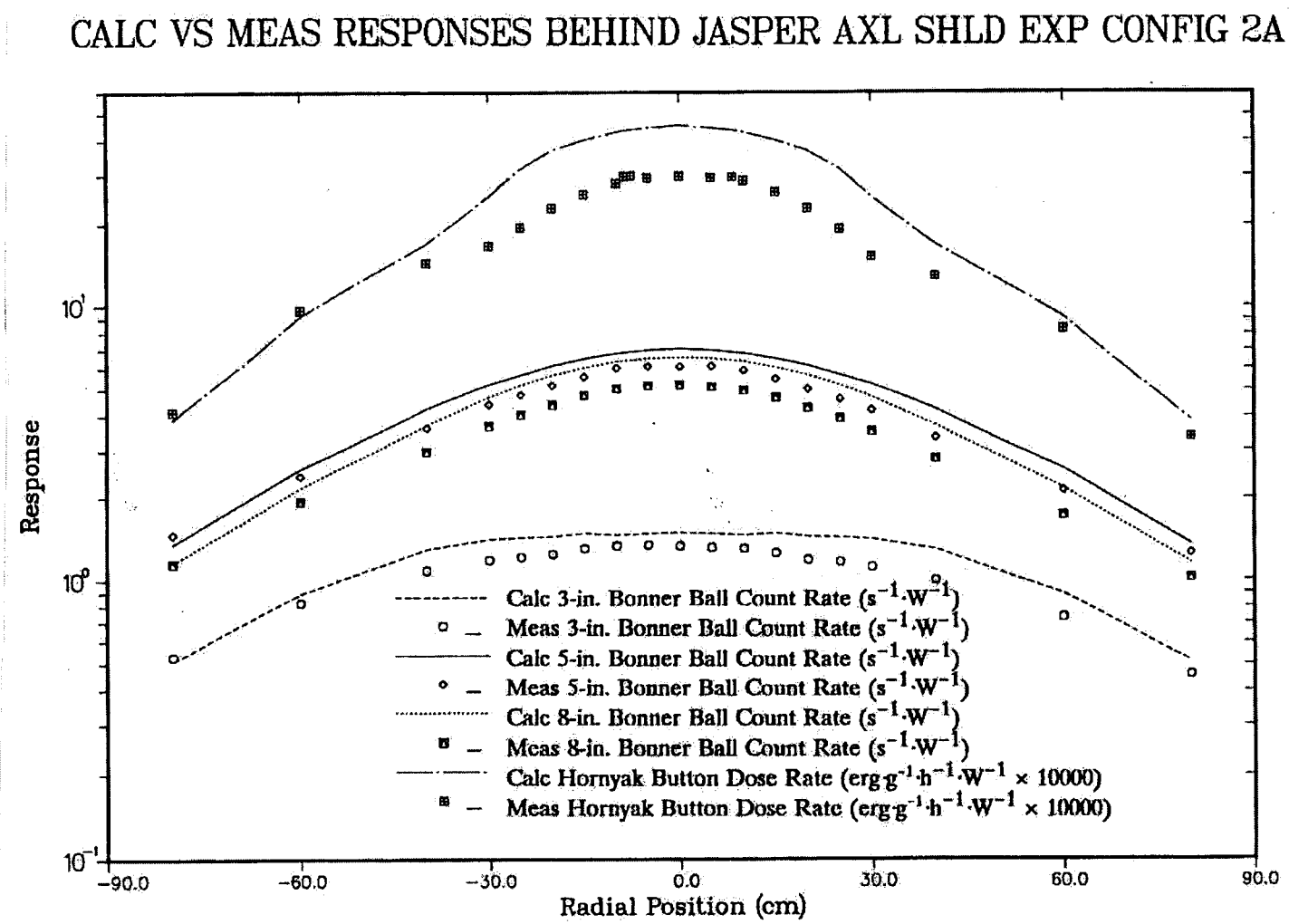

Figure G12. Comparison of calculated and measured Bonner Ball count rates and Hornyak button responses for radial traverses 30 cm behind Jasper Axial Shield Experiment original Configuration II.A and calculations using standard-weighted UO_2 cross sections.

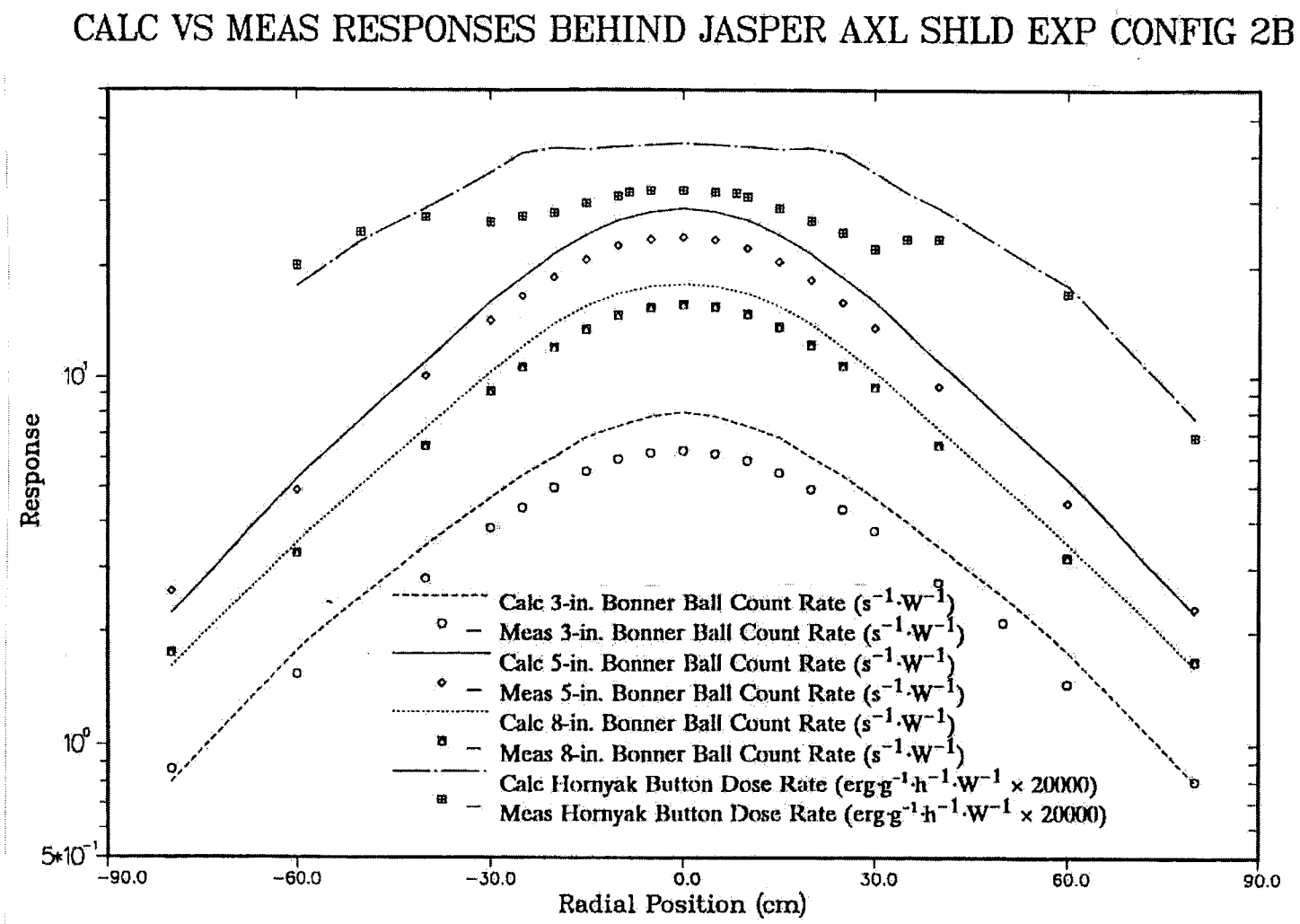

Figure G13. Comparison of calculated and measured Bonner Ball count rates and Hornyak button responses for radial traverses 30 cm behind Jasper Axial Shield Experiment original Configuration II.B and calculations using standard-weighted UO_2 cross sections.

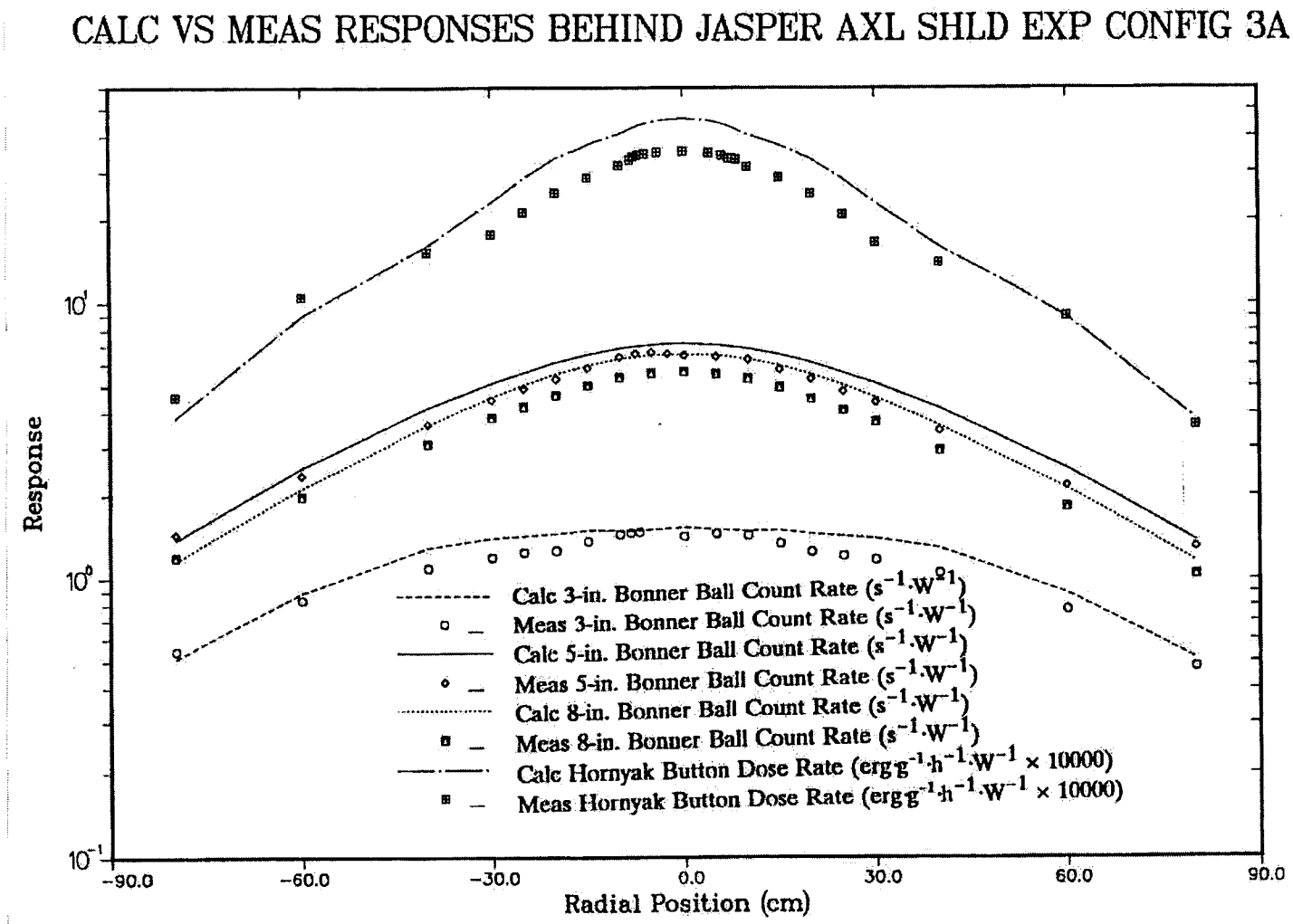

Figure G14. Comparison of calculated and measured Bonner Ball count rates and Hornyak button responses for radial traverses 30 cm behind Jasper Axial Shield Experiment original Configuration III.A and calculations using standard-weighted UO_2 cross sections.

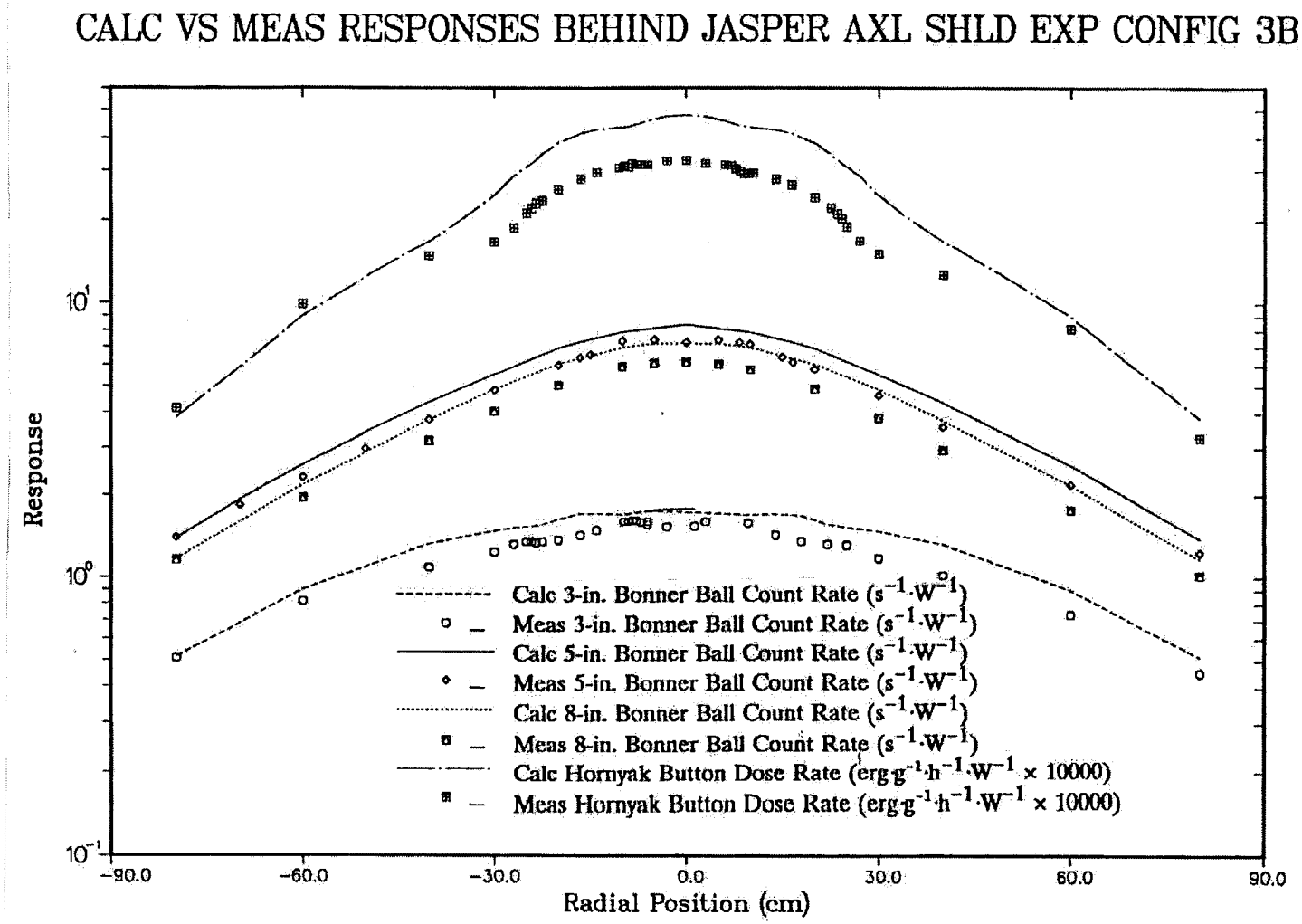

Figure G15. Comparison of calculated and measured Bonner Ball count rates and Hornyak button responses for radial traverses 30 cm behind Jasper Axial Shield Experiment original Configuration III.B and calculations using standard-weighted UO_2 cross sections.

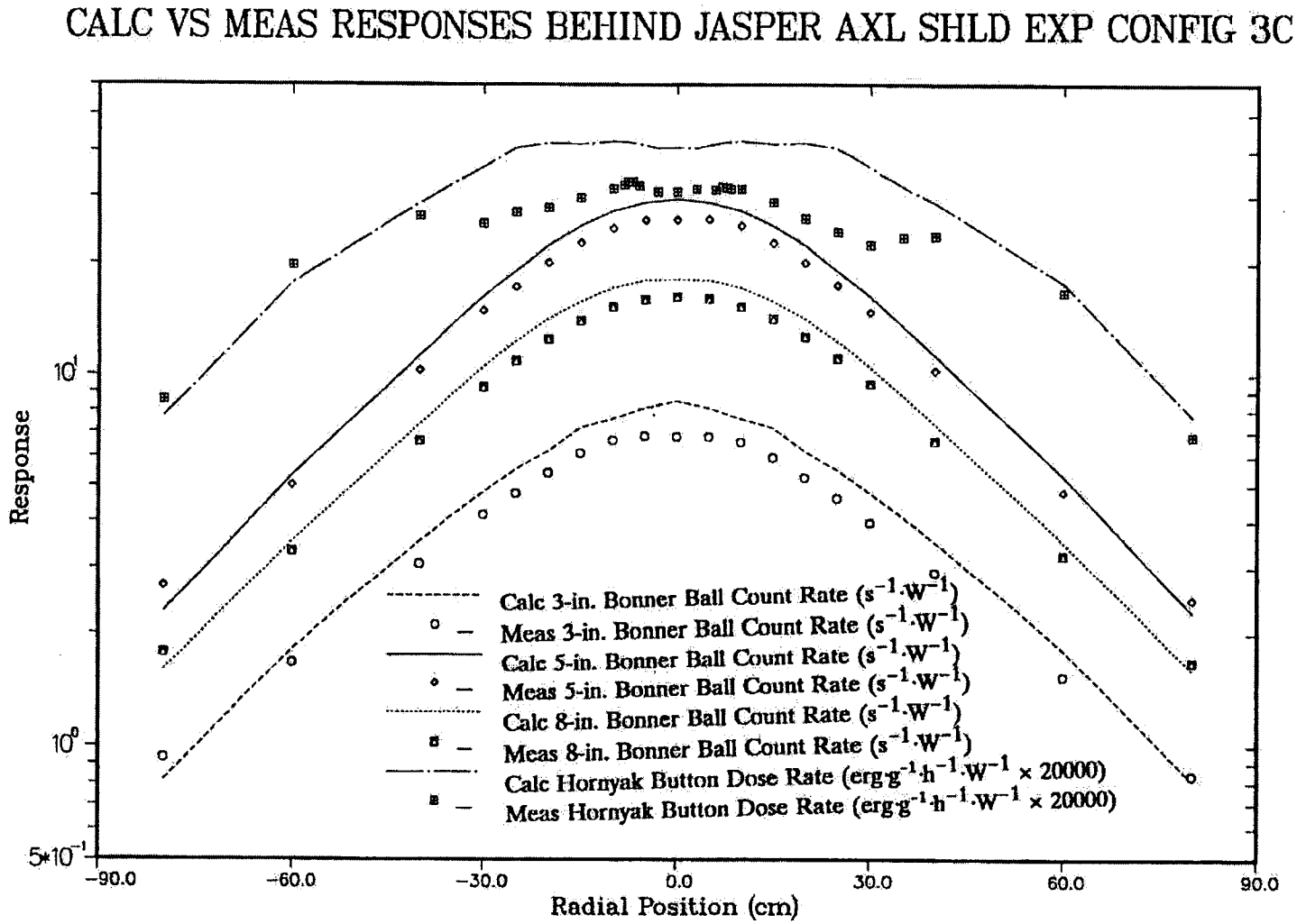

Figure G16. Comparison of calculated and measured Bonner Ball count rates and Hornyak button responses for radial traverses 30 cm behind Jasper Axial Shield Experiment original Configuration III.C and calculations using standard-weighted UO_2 cross sections.

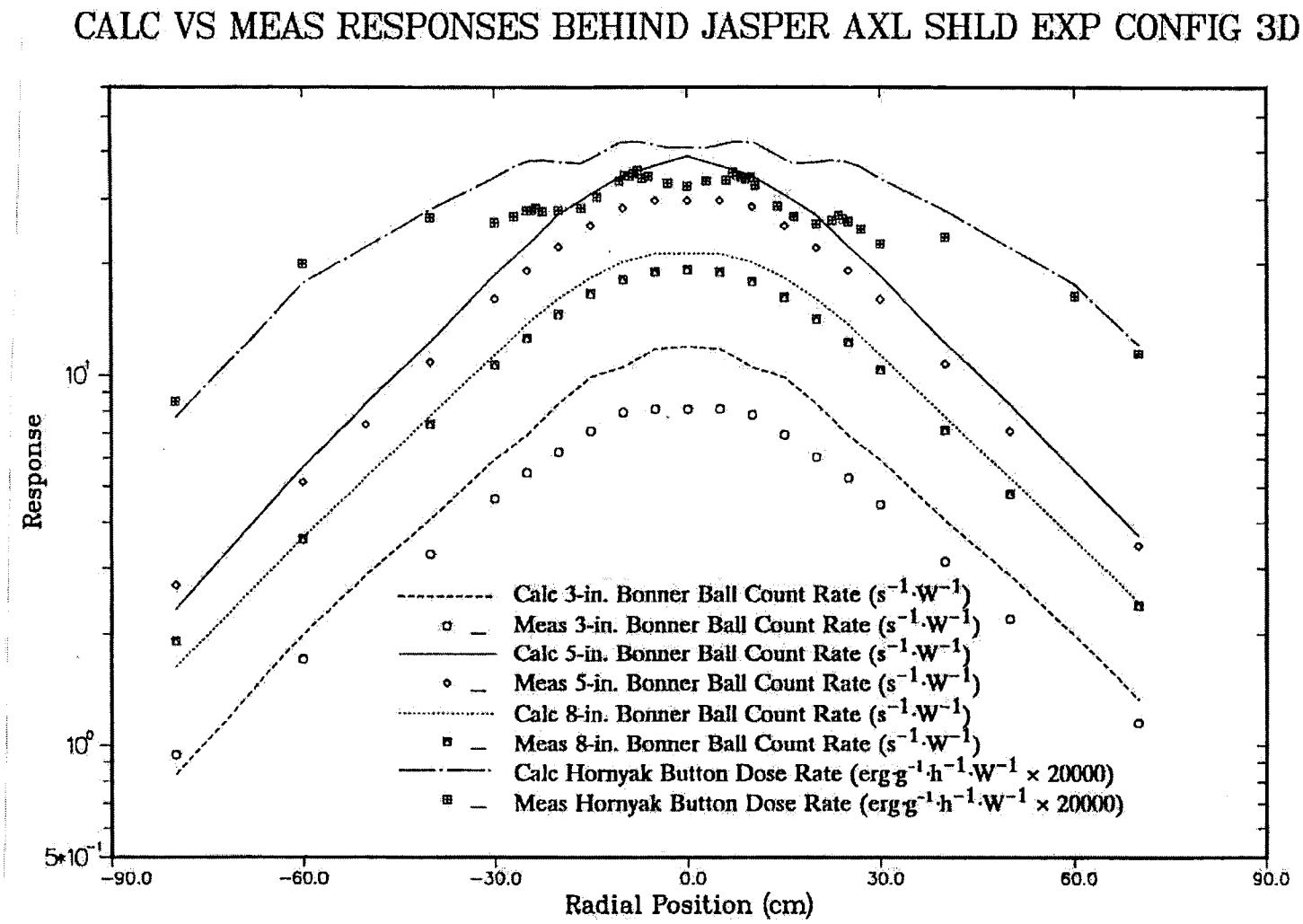

Figure G17. Comparison of calculated and measured Bonner Ball count rates and Hornyak button responses for radial traverses 30 cm behind Jasper Axial Shield Experiment original Configuration III.D and calculations using standard-weighted UO_2 cross sections.

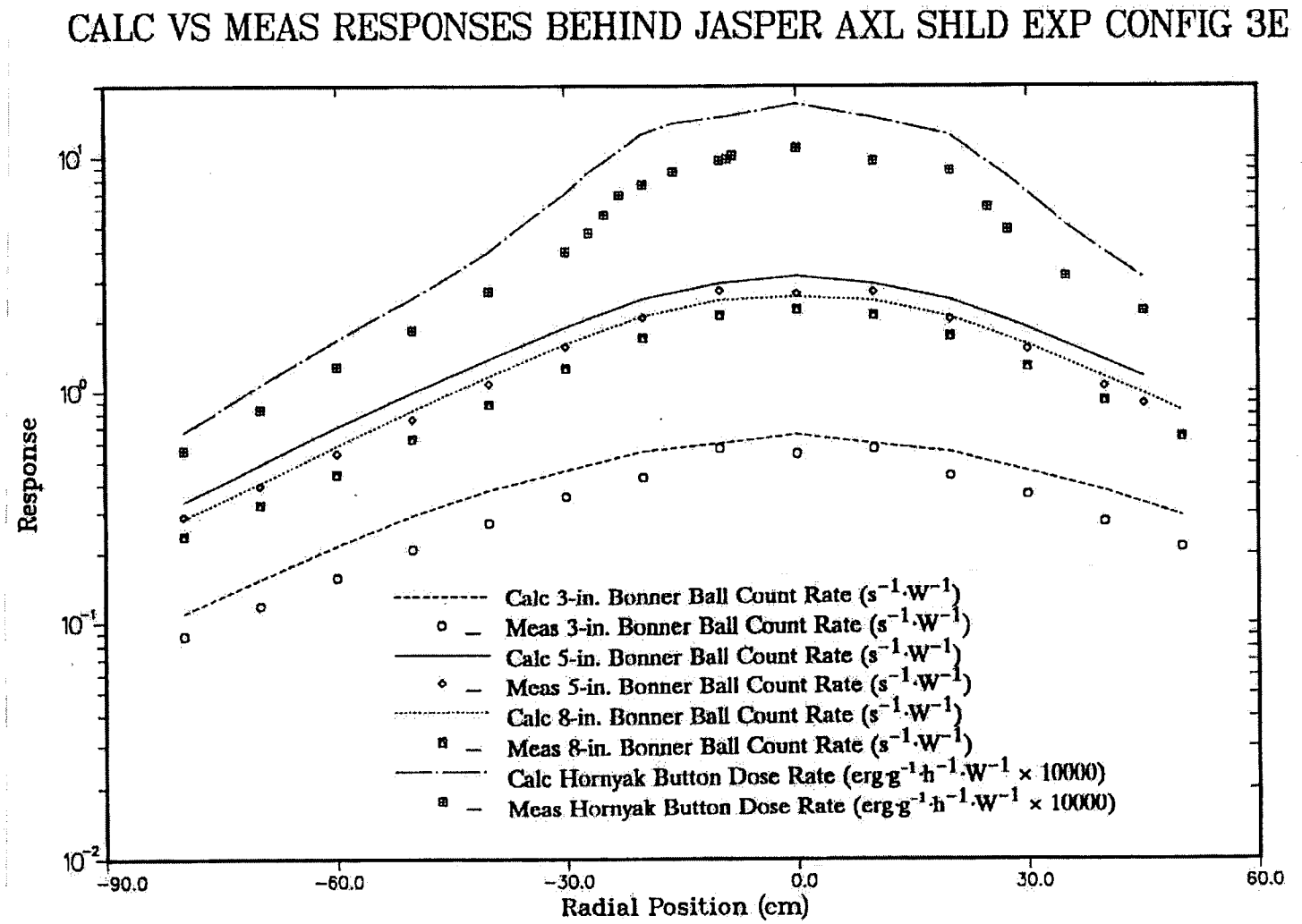

Figure G18. Comparison of calculated and measured Bonner Ball count rates and Hornyak button responses for radial traverses 30 cm behind Jasper Axial Shield Experiment original Configuration III.E and calculations using standard-weighted UO_2 cross sections.

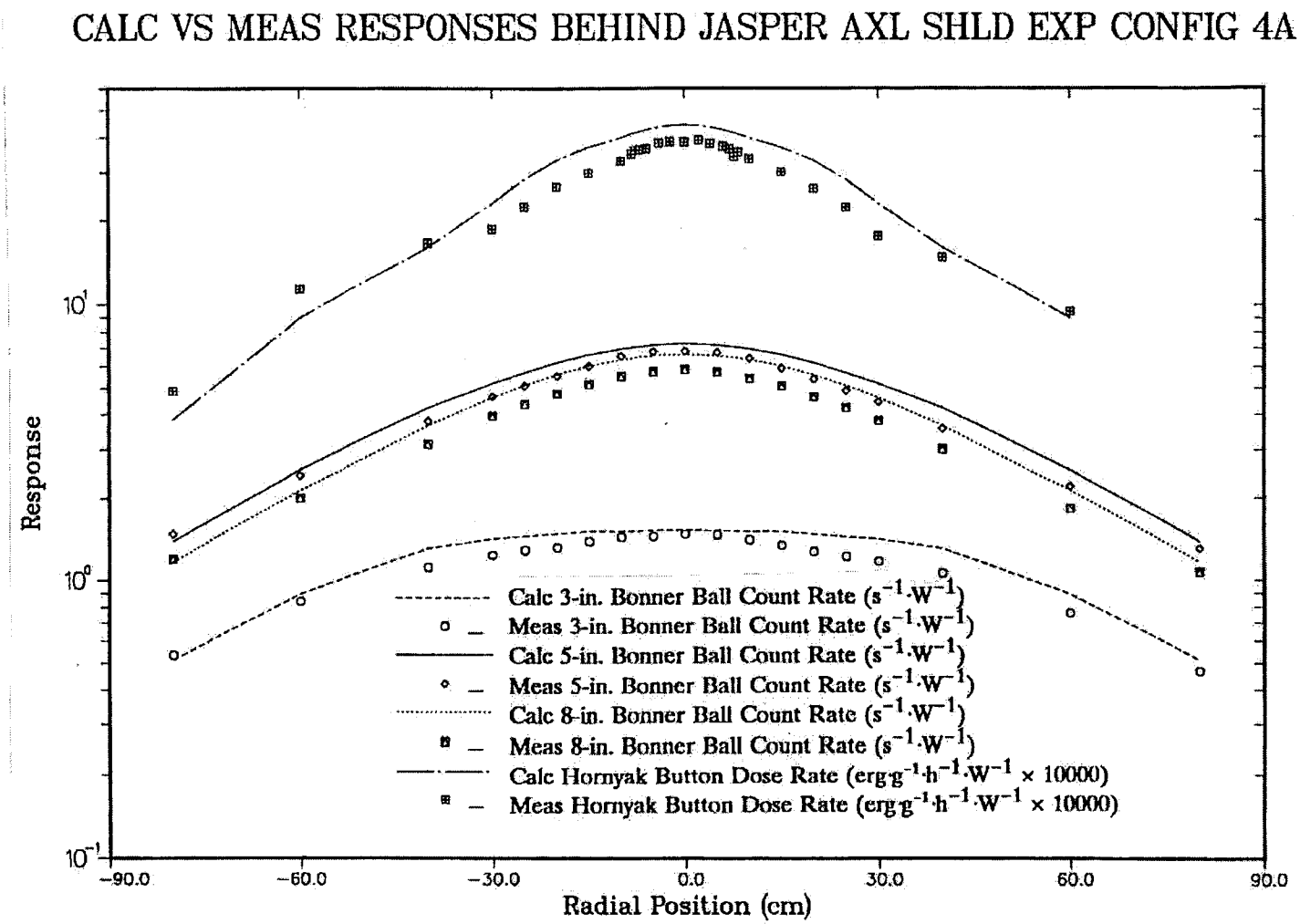

Figure G19. Comparison of calculated and measured Bonner Ball count rates and Hornyak button responses for radial traverses 30 cm behind Jasper Axial Shield Experiment original Configuration IV.A and calculations using standard-weighted UO_2 cross sections.

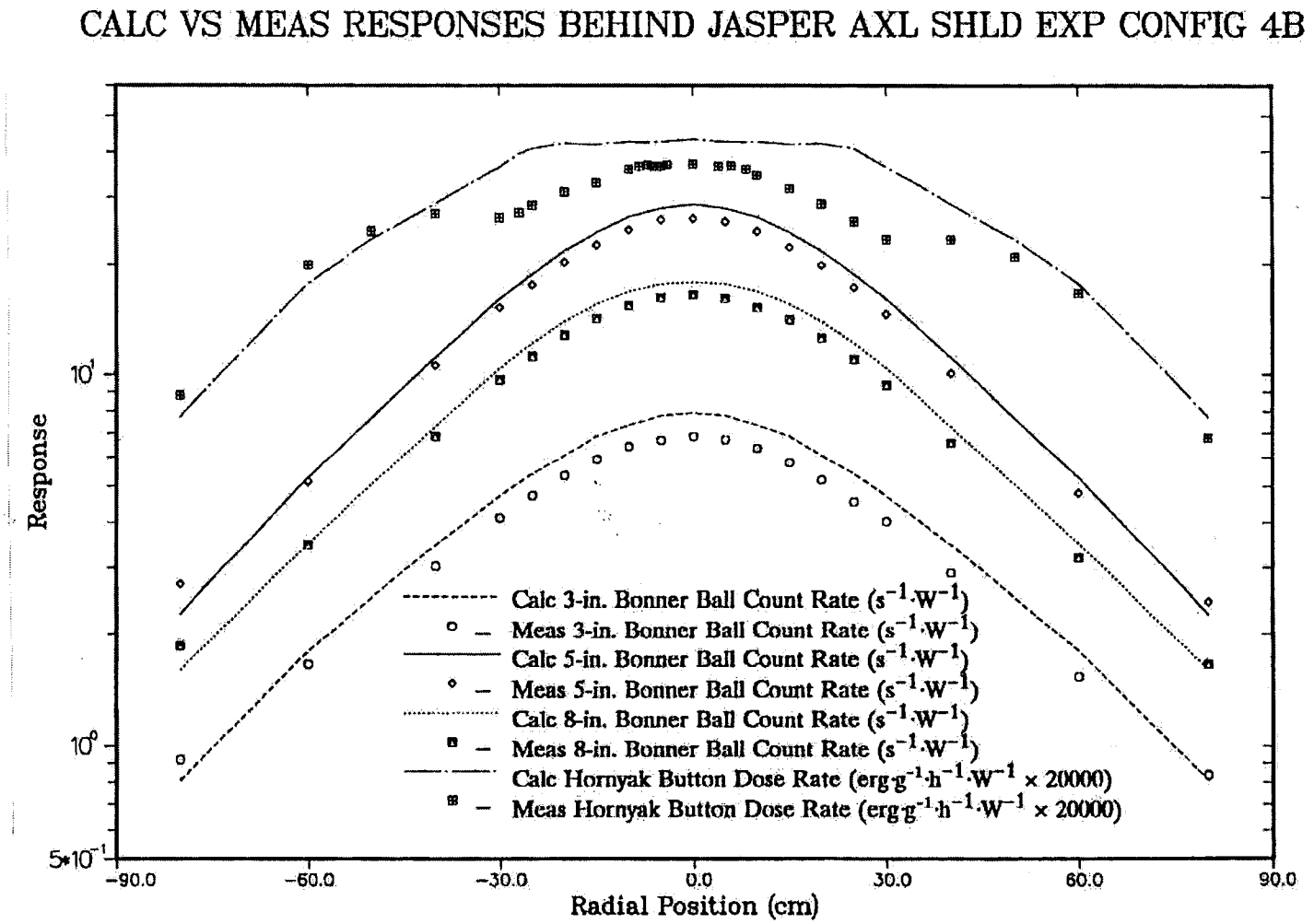

Figure G20. Comparison of calculated and measured Bonner Ball count rates and Hornyak button responses for radial traverses 30 cm behind Jasper Axial Shield Experiment original Configuration IV.B and calculations using standard-weighted UO_2 cross sections.

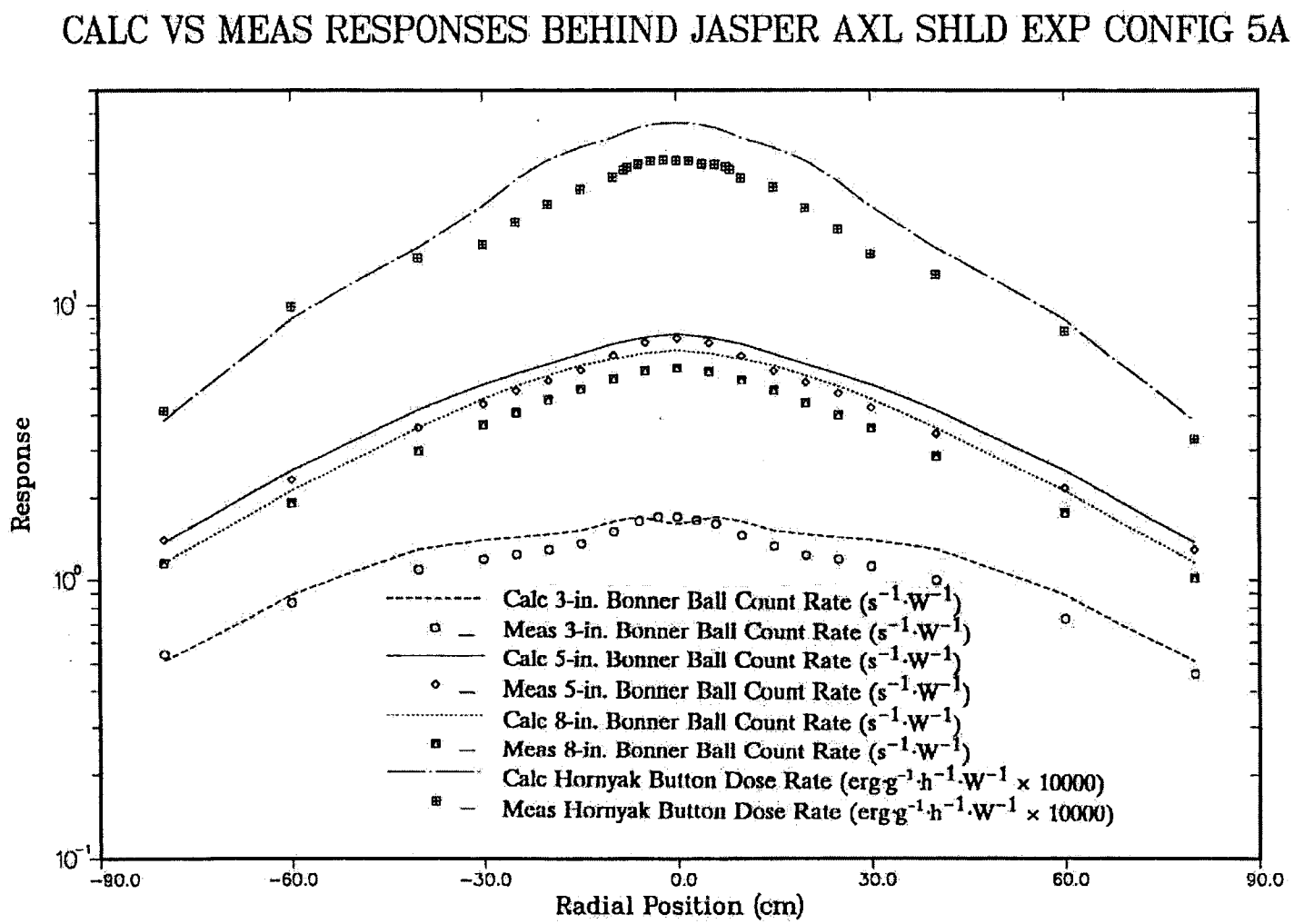

Figure G21. Comparison of calculated and measured Bonner Ball count rates and Hornyak button responses for radial traverses 30 cm behind Jasper Axial Shield Experiment original Configuration V.A and calculations using standard-weighted UO_2 cross sections.

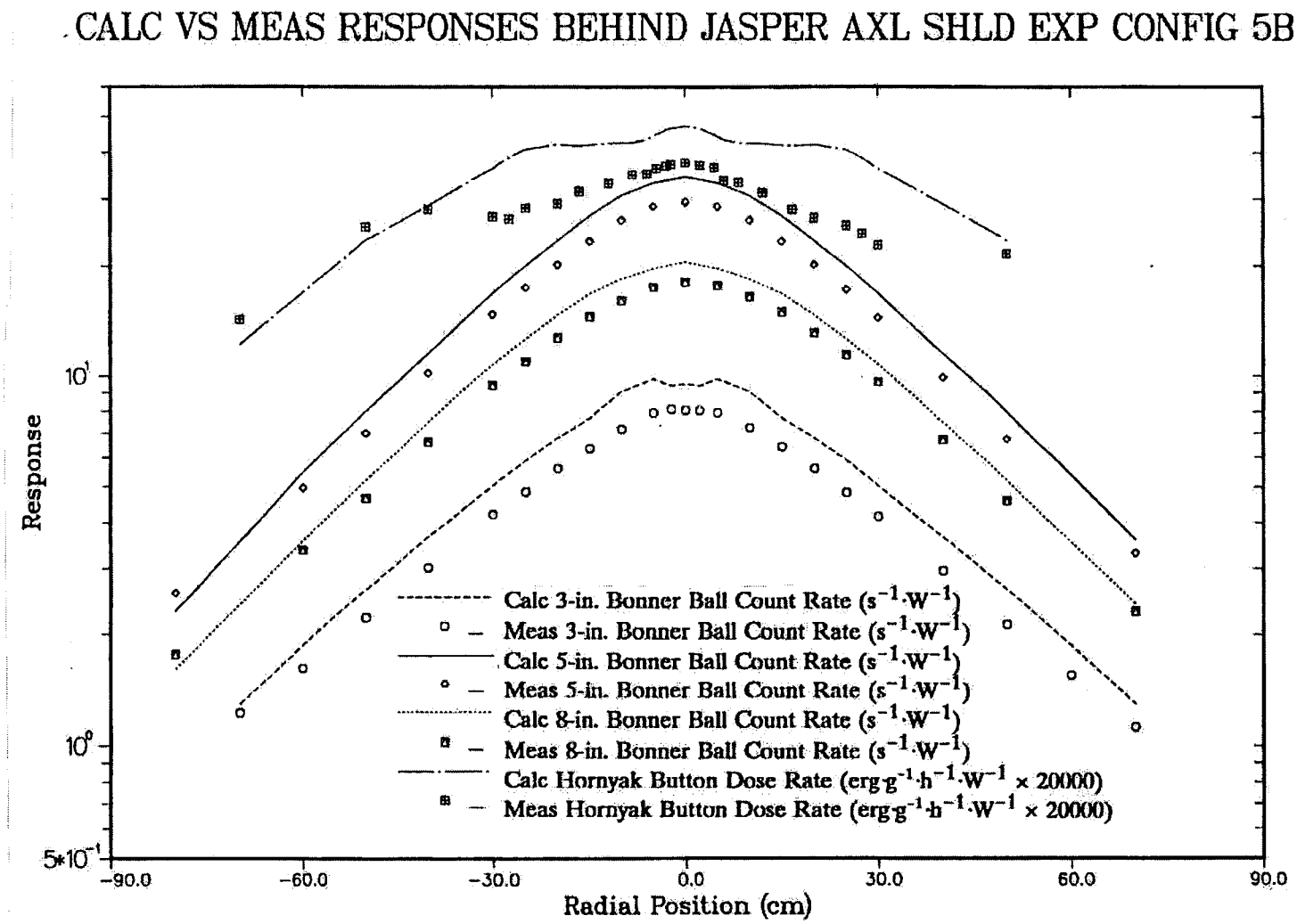

Figure G22. Comparison of calculated and measured Bonner Ball count rates and Hornyak button responses for radial traverses 30 cm behind Jasper Axial Shield Experiment original Configuration V.B and calculations using standard-weighted UO_2 cross sections.

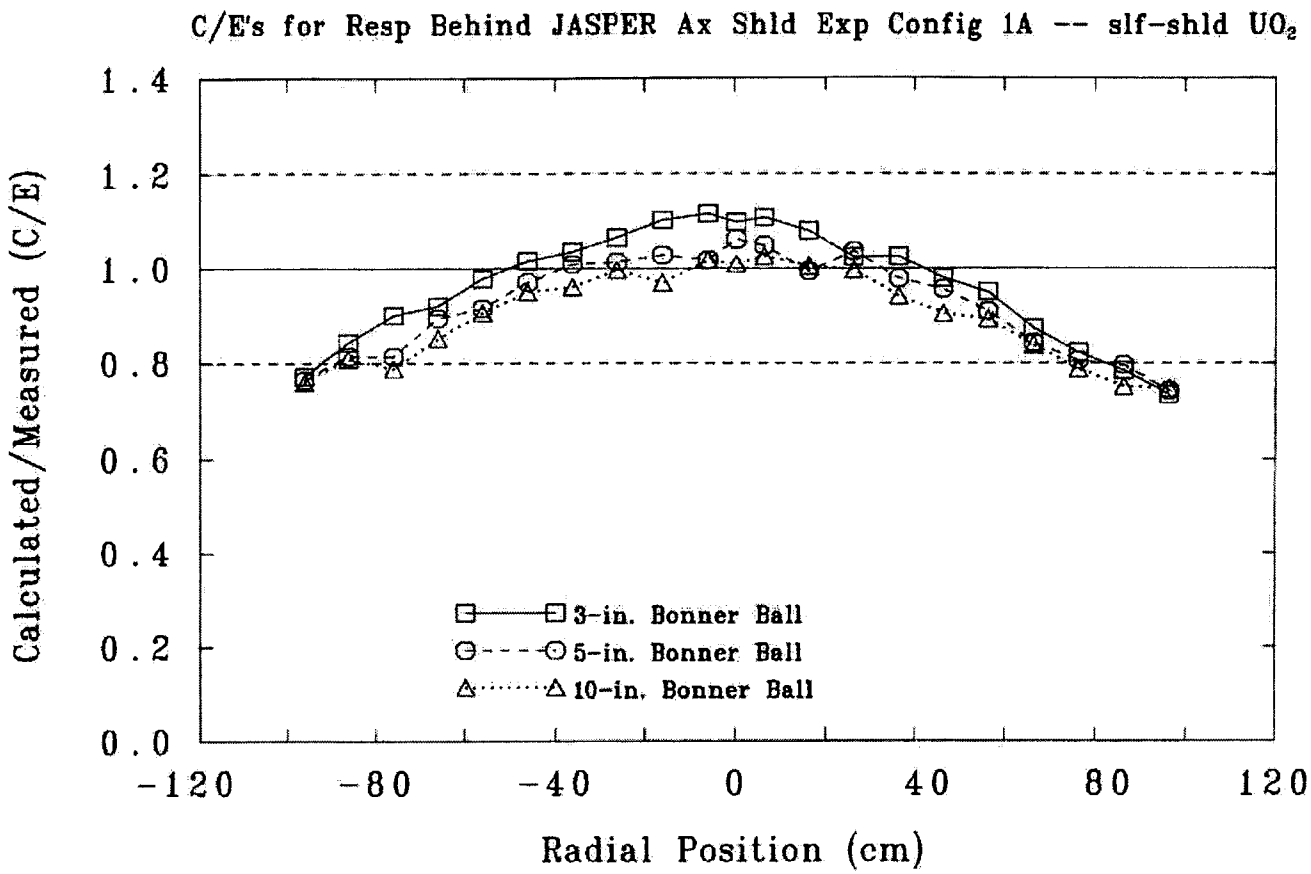

Figure G23. Calculated-to-measured (C/E) response ratios for radial traverses 30 cm behind Jasper Axial Shield Experiment original Configuration I.A and calculations using self-shielded UO_2 cross sections.

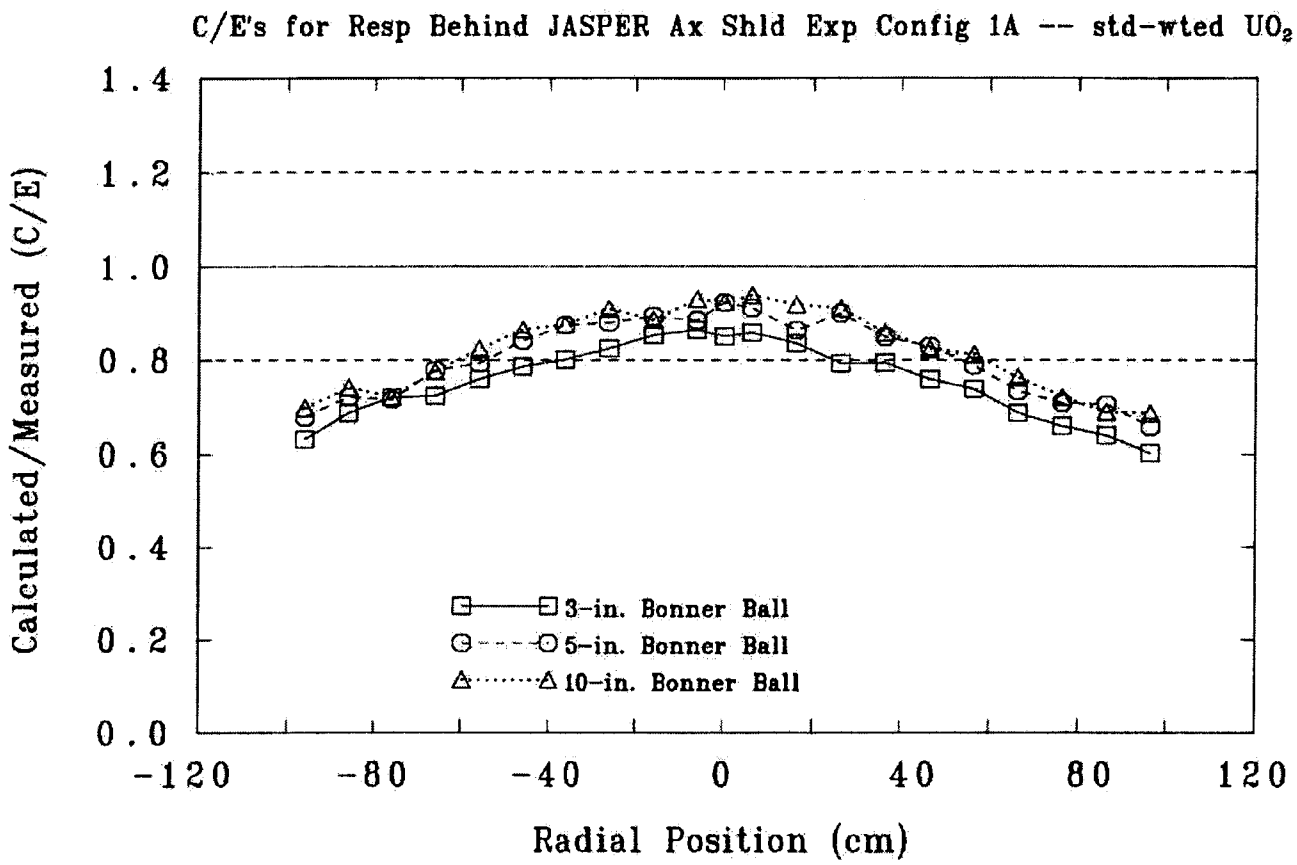

Figure G24. Calculated-to-measured (C/E) response ratios for radial traverses 30 cm behind Jasper Axial Shield Experiment original Configuration I.A and calculations using standard-weighted UO_2 cross sections.

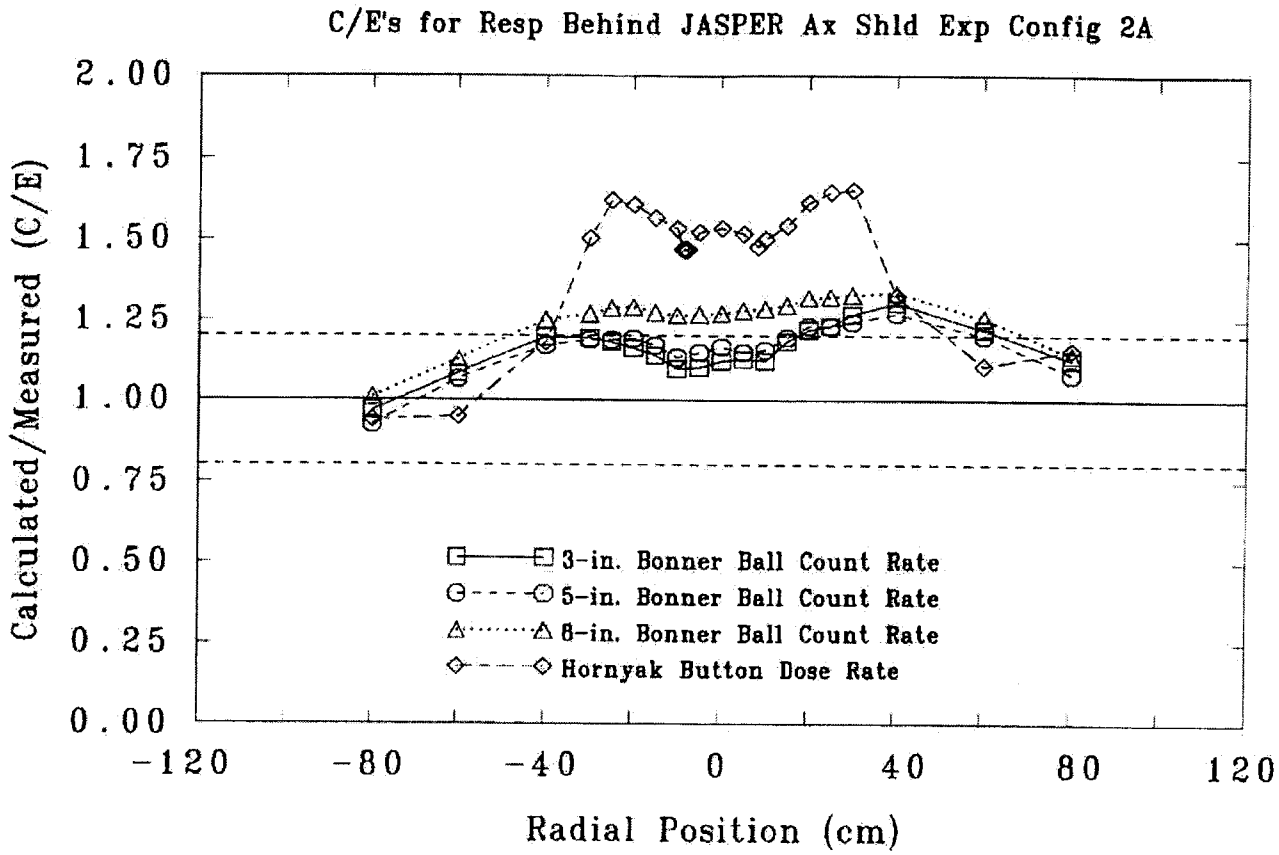

Figure G25. Calculated-to-measured (C/E) response ratios for radial traverses 30 cm behind Jasper Axial Shield Experiment original Configuration II.A and calculations using standard-weighted UO_2 cross sections.

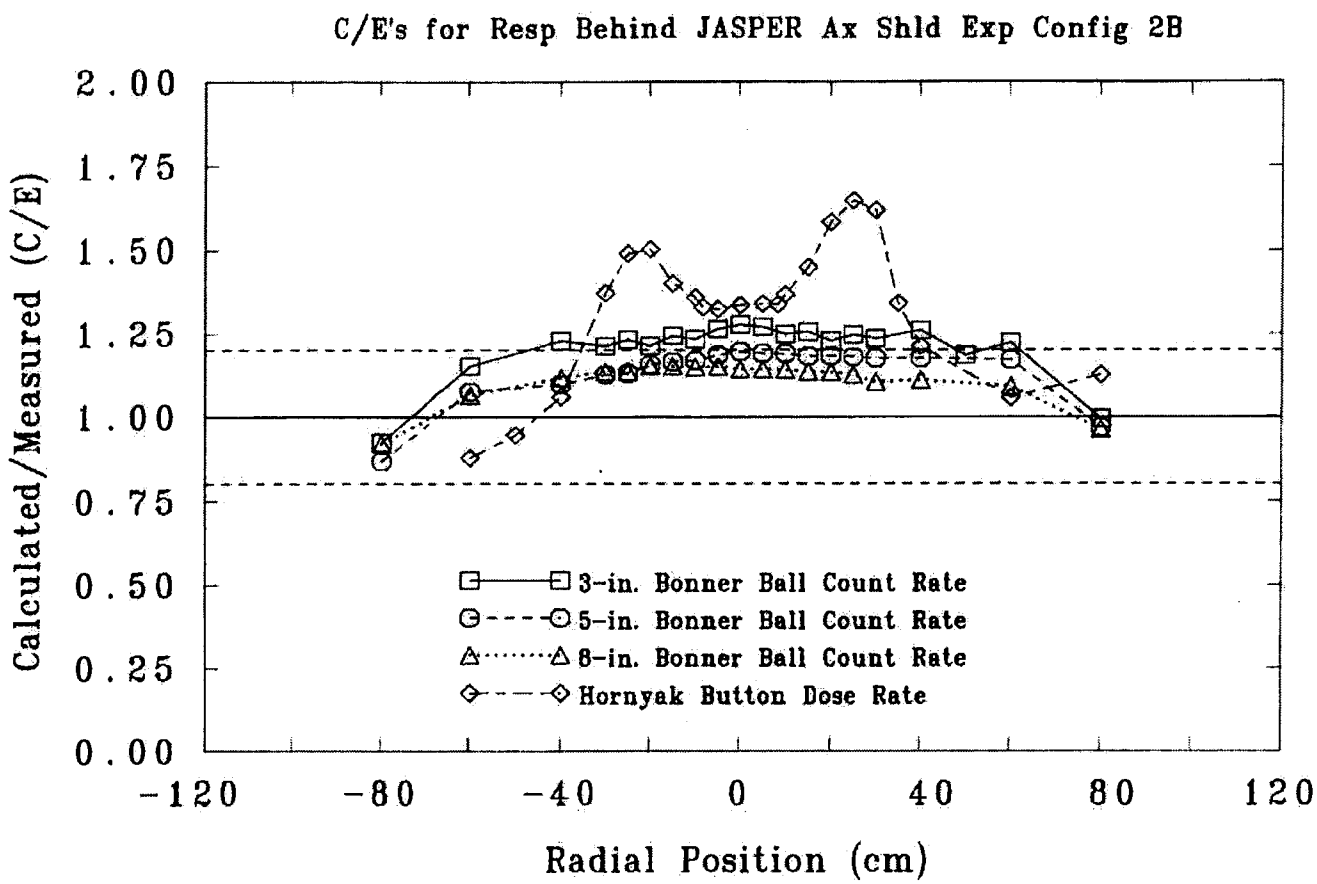

Figure G26. Calculated-to-measured (C/E) response ratios for radial traverses 30 cm behind Jasper Axial Shield Experiment original Configuration II.B and calculations using standard-weighted UO_2 cross sections.

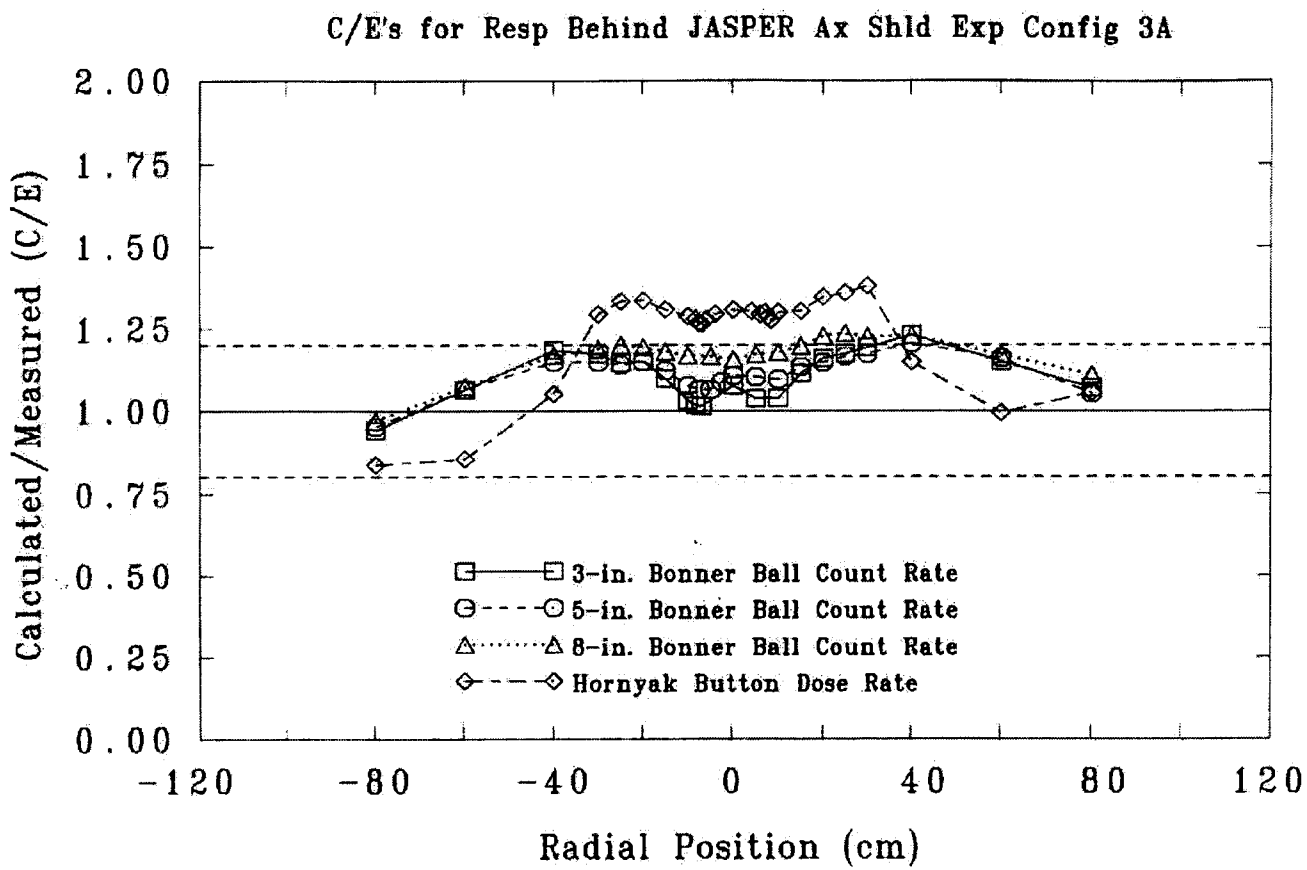

Figure G27. Calculated-to-measured (C/E) response ratios for radial traverses 30 cm behind Jasper Axial Shield Experiment original Configuration III.A and calculations using standard-weighted UO_2 cross sections.

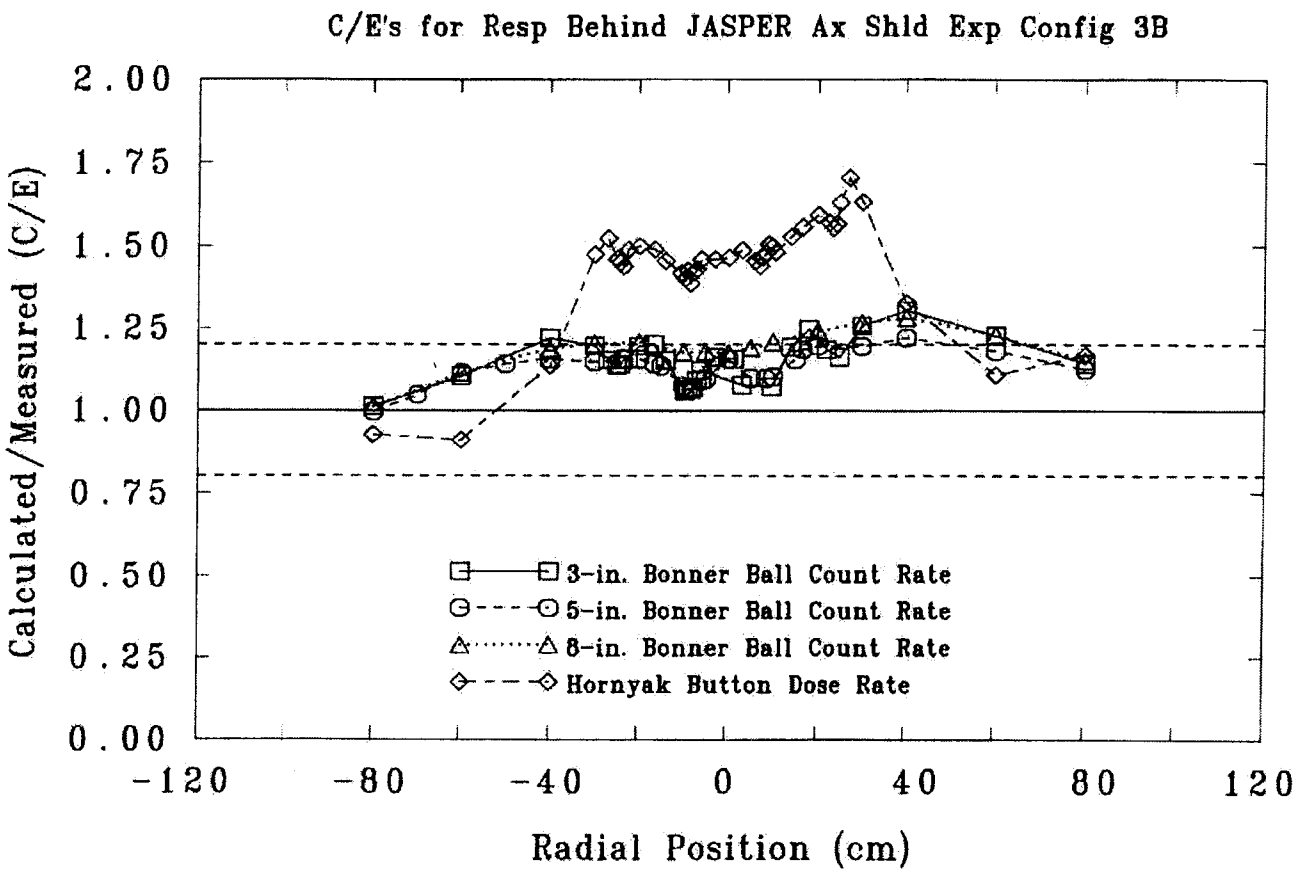

Figure G28. Calculated-to-measured (C/E) response ratios for radial traverses 30 cm behind Jasper Axial Shield Experiment original Configuration III.B and calculations using standard-weighted UO_2 cross sections.

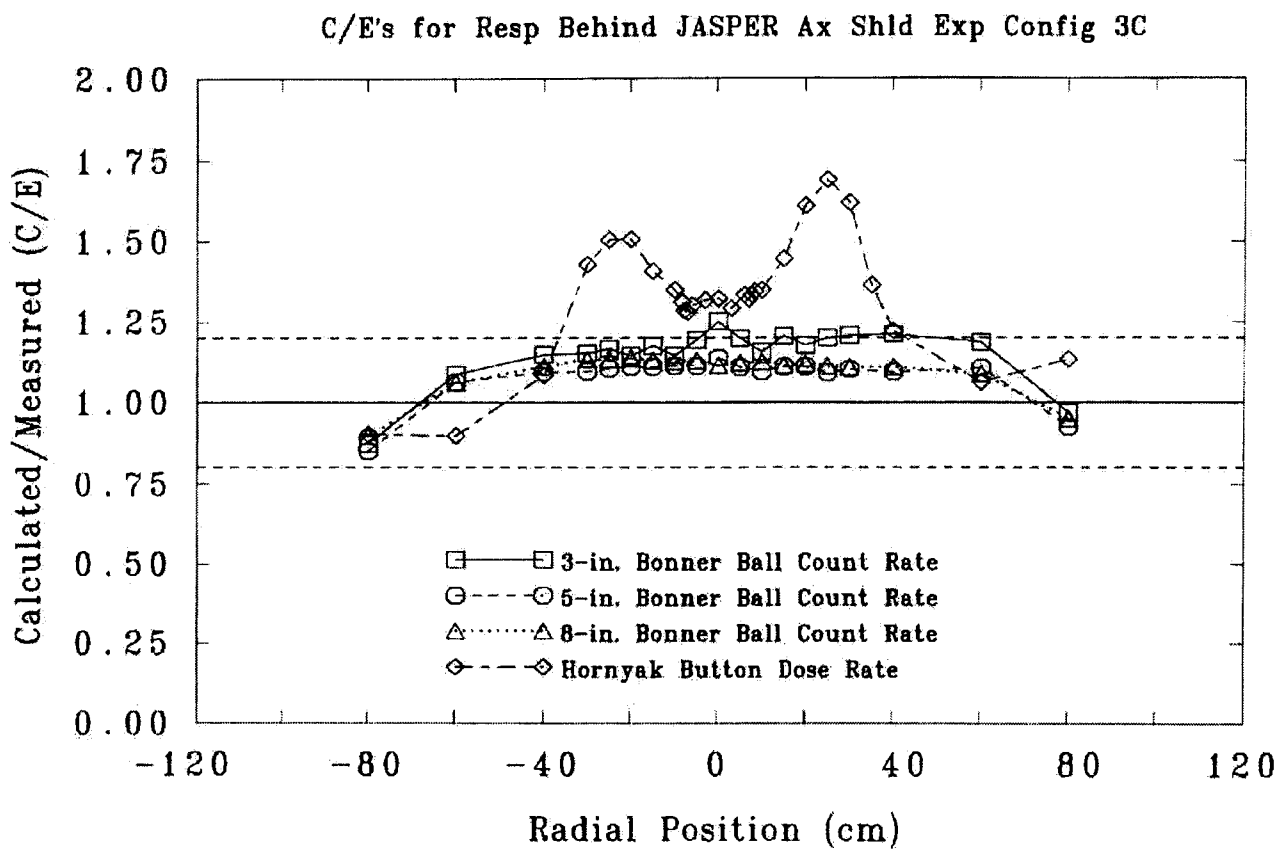

Figure G29. Calculated-to-measured (C/E) response ratios for radial traverses 30 cm behind Jasper Axial Shield Experiment original Configuration III.C and calculations using standard-weighted UO_2 cross sections.

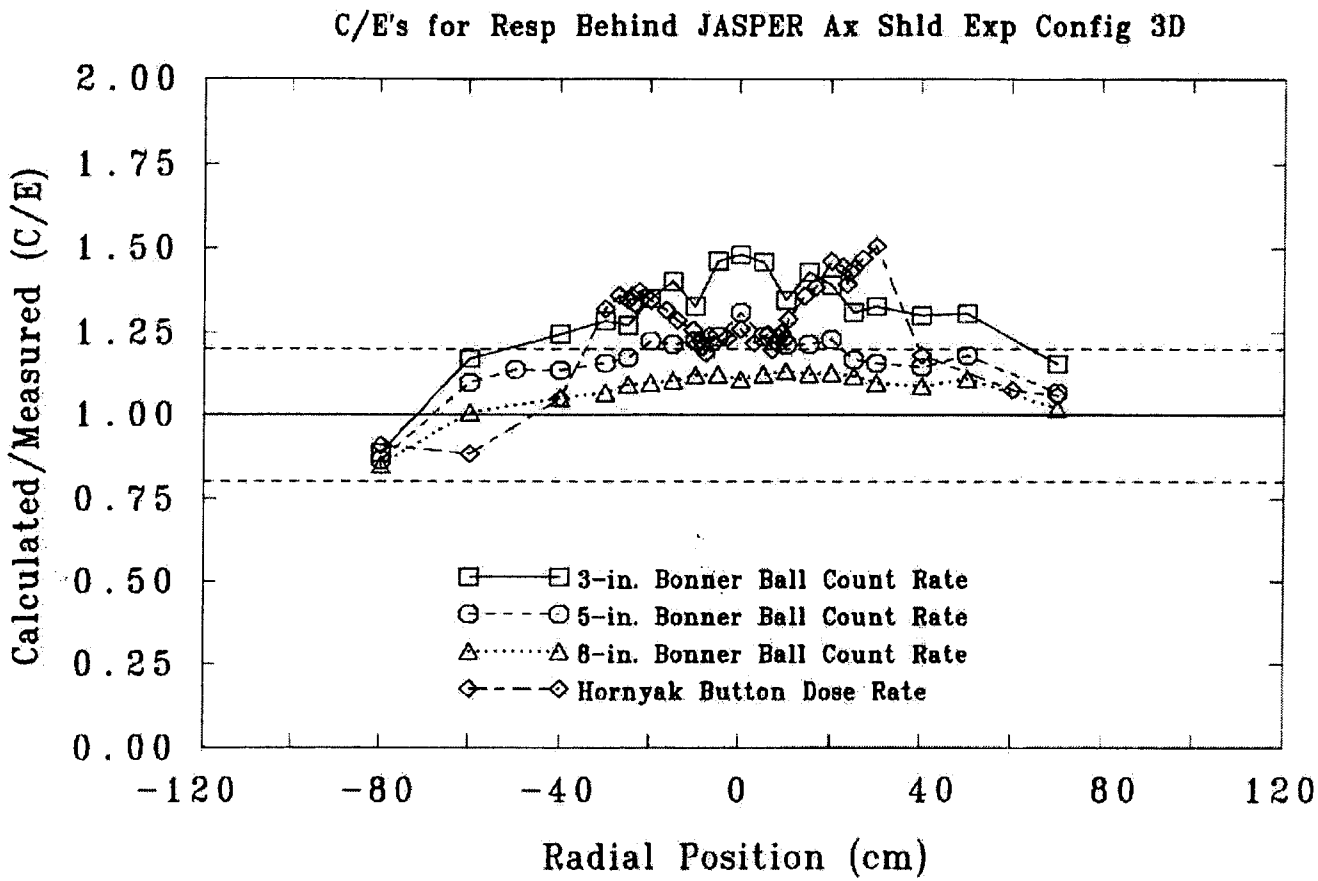

Figure G30. Calculated-to-measured (C/E) response ratios for radial traverses 30 cm behind Jasper Axial Shield Experiment original Configuration III.D and calculations using standard-weighted UO_2 cross sections.

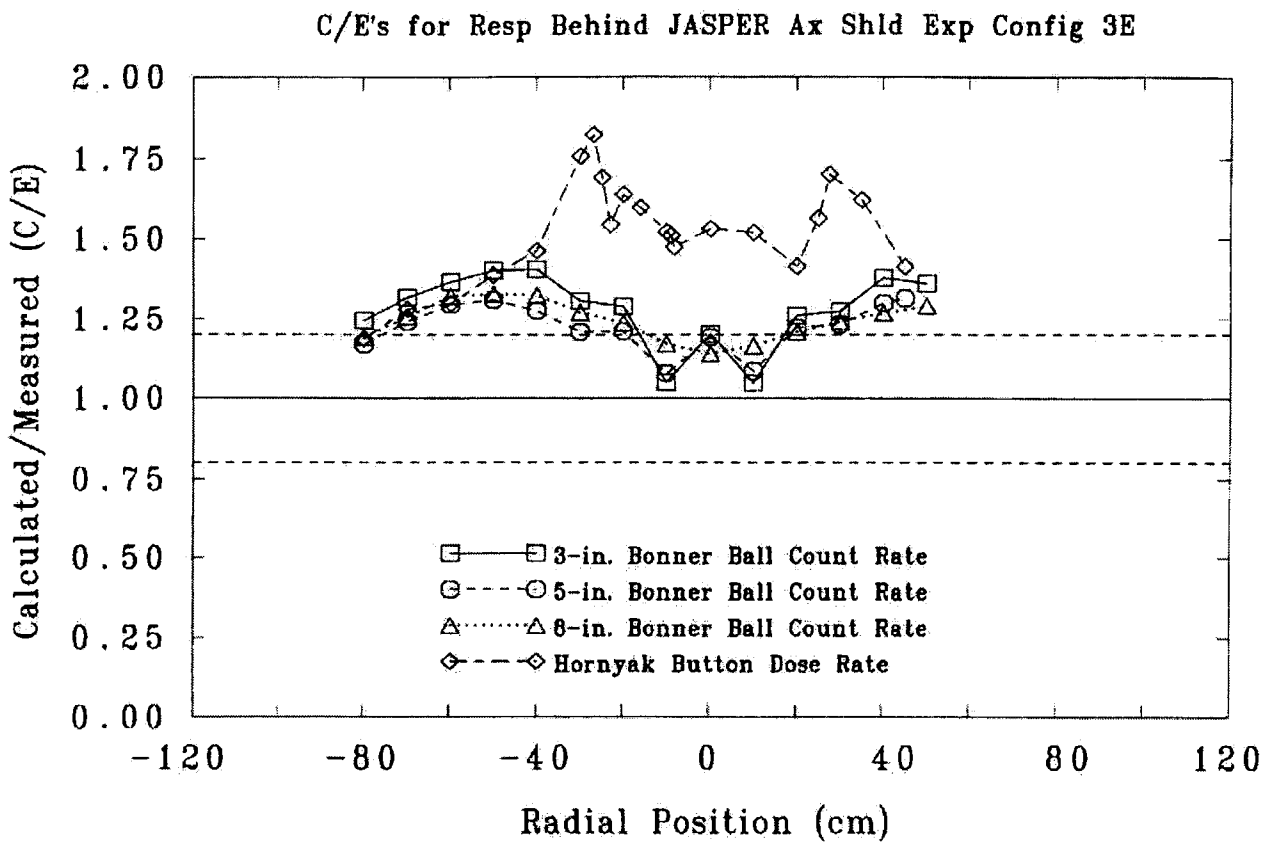

Figure G31. Calculated-to-measured (C/E) response ratios for radial traverses 30 cm behind Jasper Axial Shield Experiment original Configuration III.E and calculations using standard-weighted UO_2 cross sections.

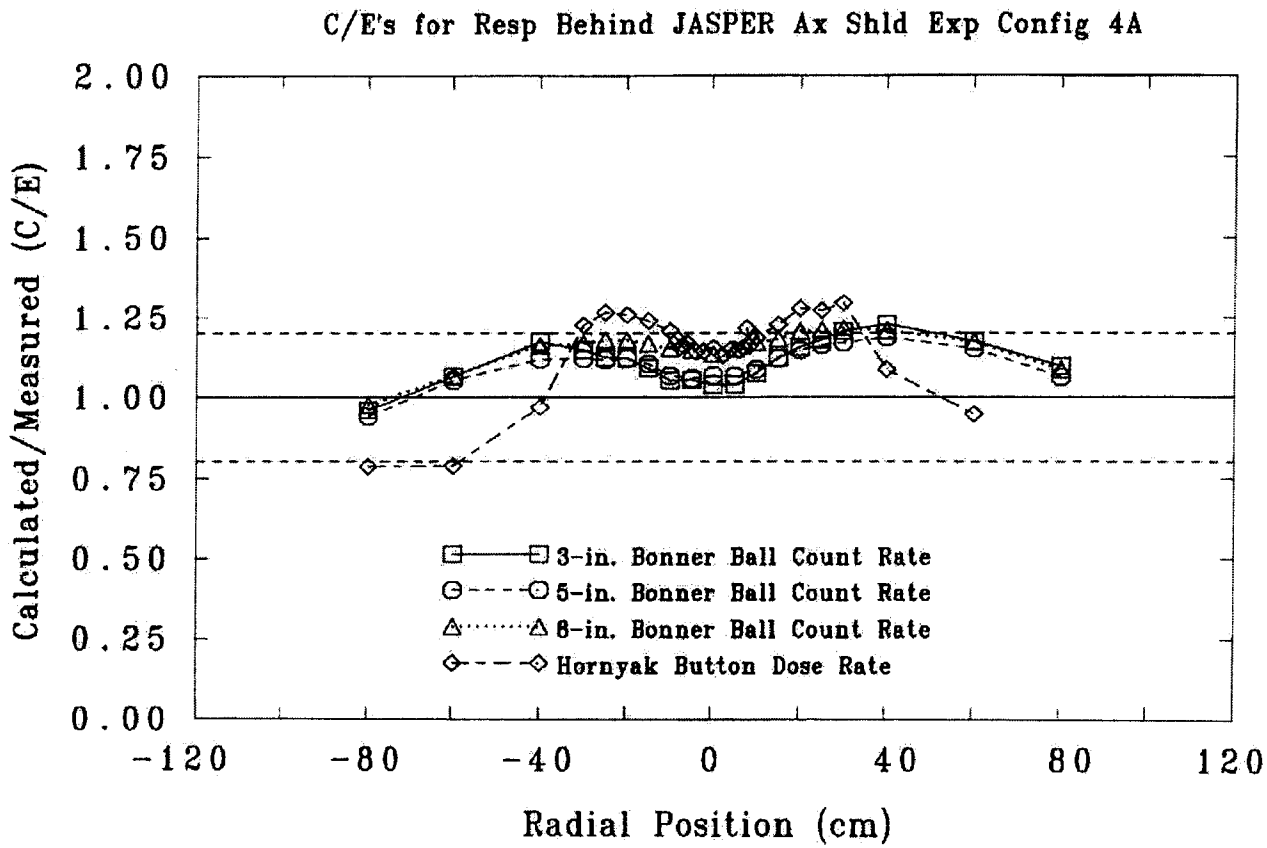

Figure G32. Calculated-to-measured (C/E) response ratios for radial traverses 30 cm behind Jasper Axial Shield Experiment original Configuration IV.A and calculations using standard-weighted UO_2 cross sections.

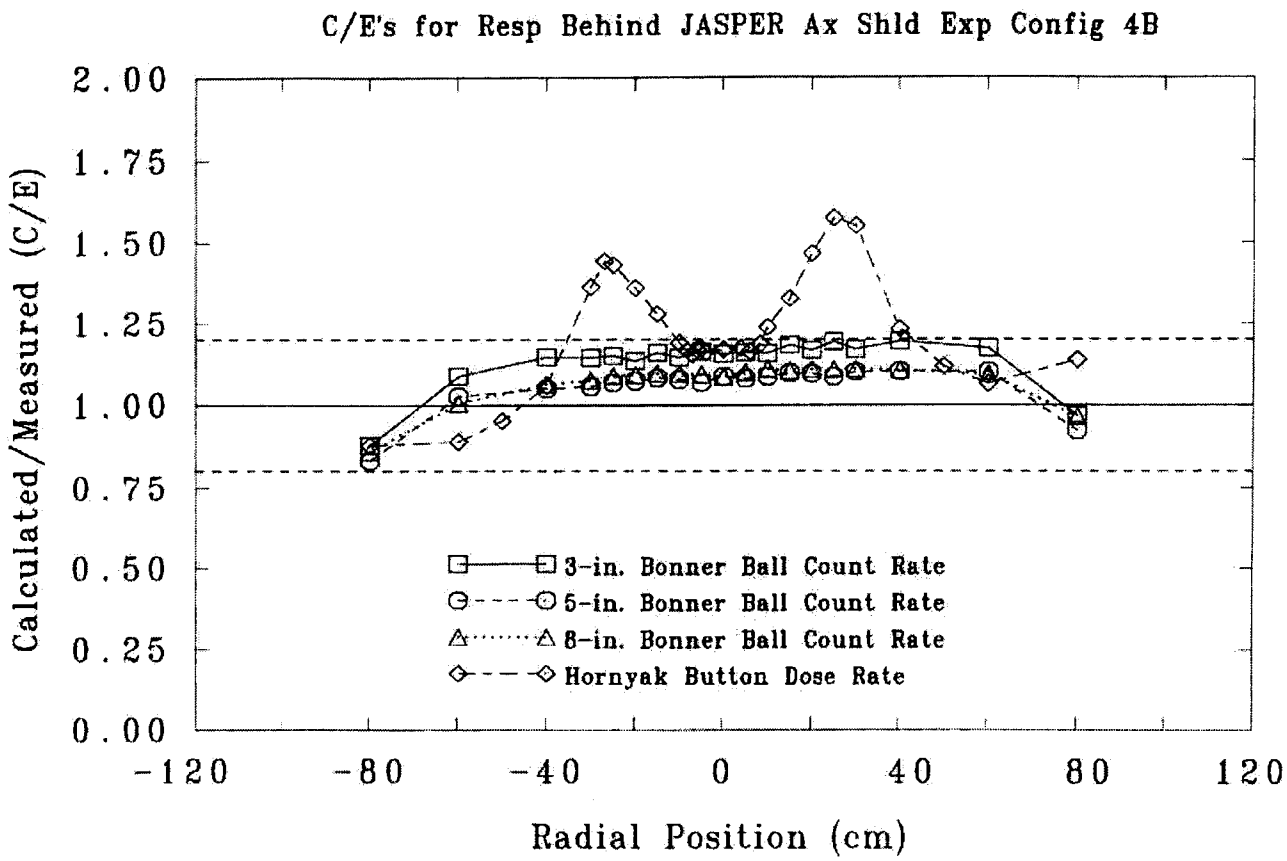

Figure G33. Calculated-to-measured (C/E) response ratios for radial traverses 30 cm behind Jasper Axial Shield Experiment original Configuration IV.B and calculations using standard-weighted UO_2 cross sections.

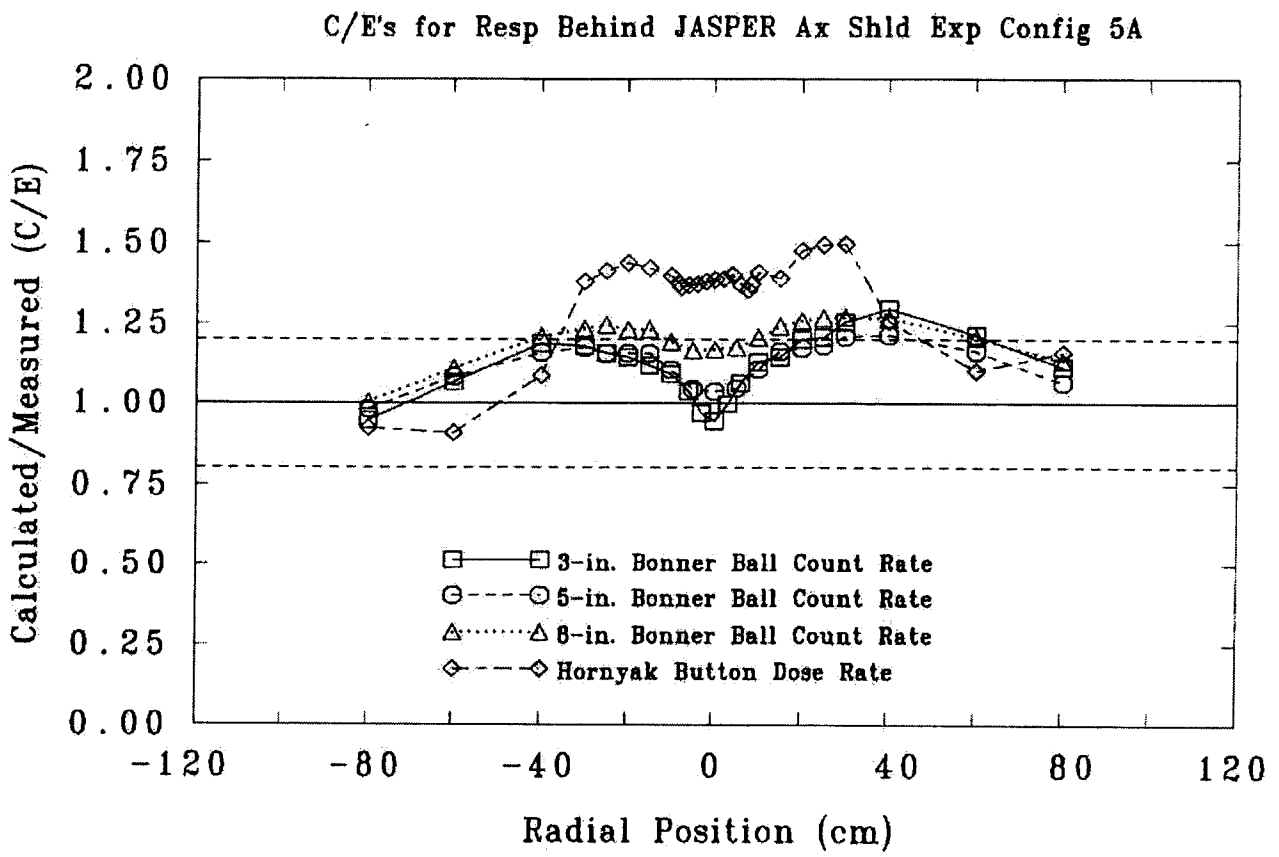

Figure G34. Calculated-to-measured (C/E) response ratios for radial traverses 30 cm behind Jasper Axial Shield Experiment original Configuration V.A and calculations using standard-weighted UO_2 cross sections.

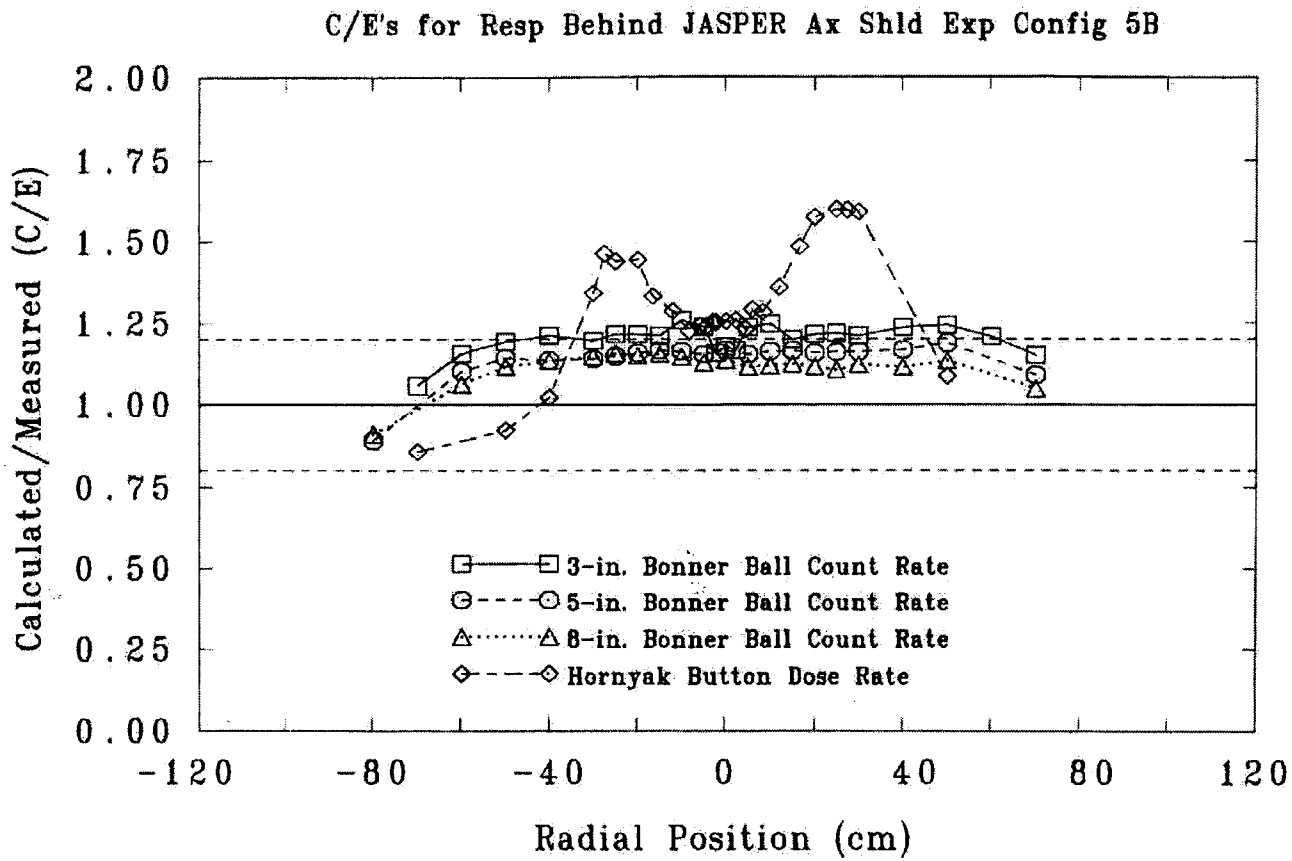

Figure G35. Calculated-to-measured (C/E) response ratios for radial traverses 30 cm behind Jasper Axial Shield Experiment original Configuration V.B and calculations using standard-weighted UO_2 cross sections.

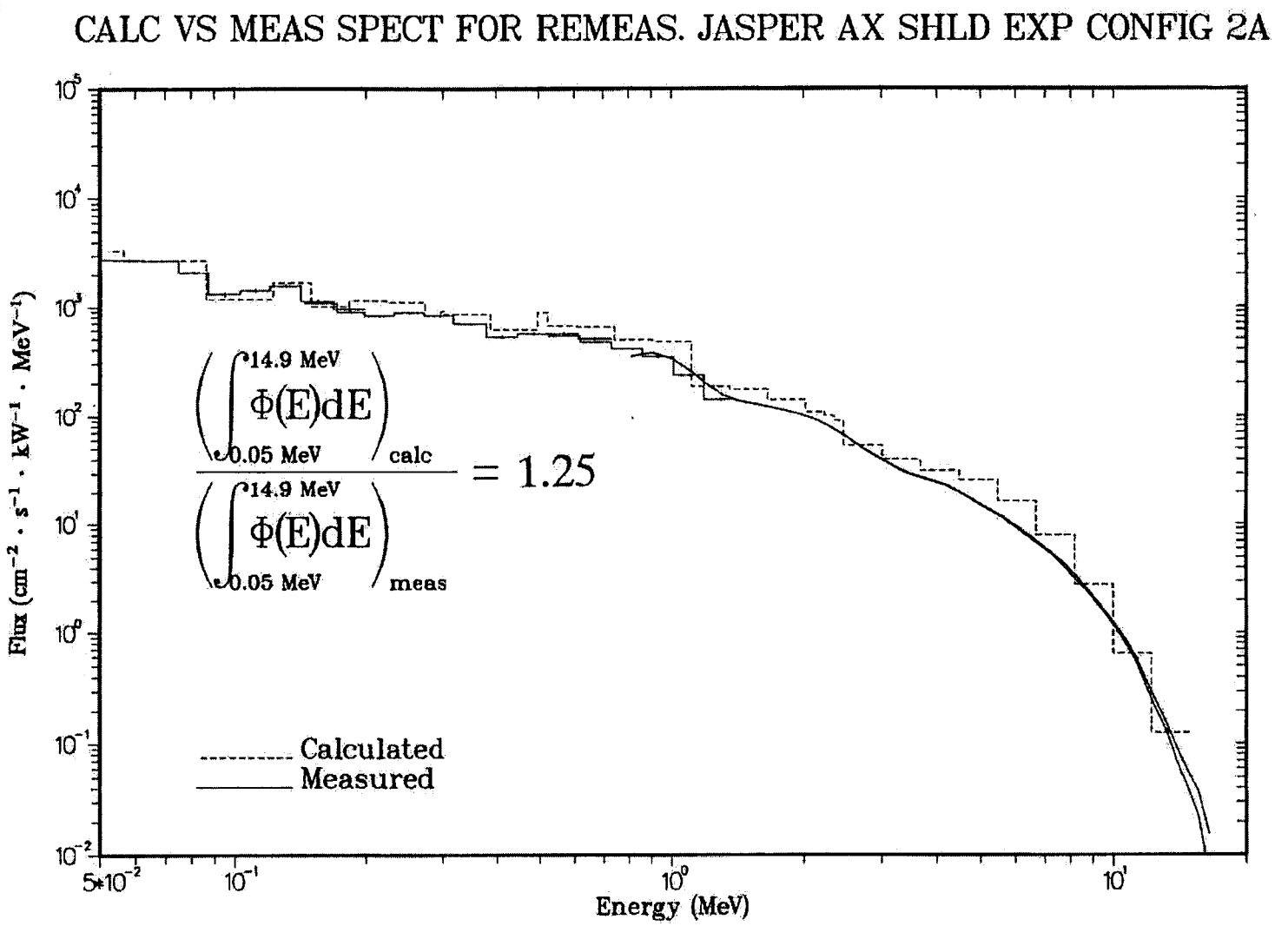

Figure G36. Comparison of calculated and measured neutron spectra behind Jasper Axial Shield Experiment remeasurement Configuration II.A.

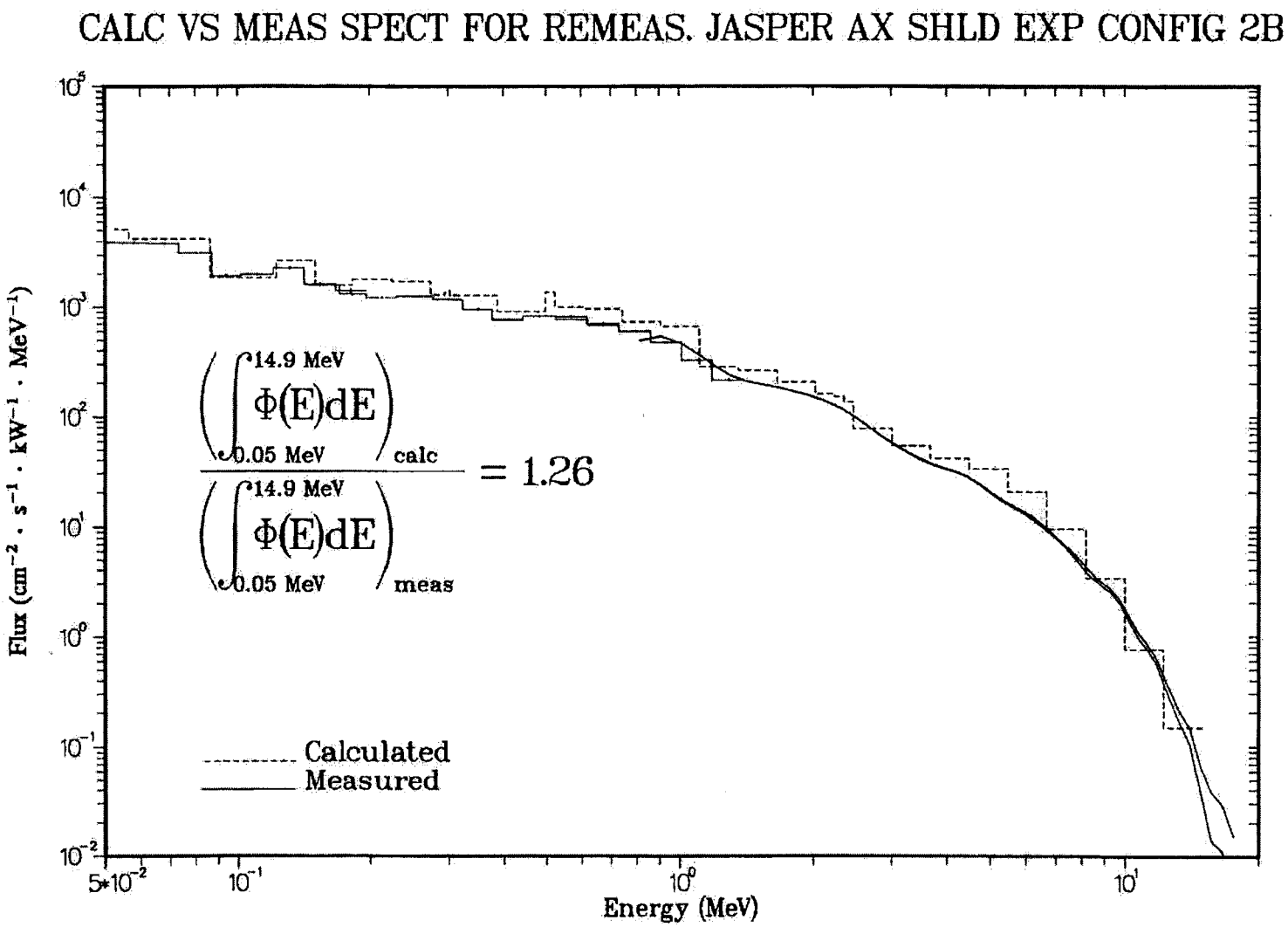

Figure G37. Comparison of calculated and measured neutron spectra behind Jasper Axial Shield Experiment remeasurement Configuration II.B.

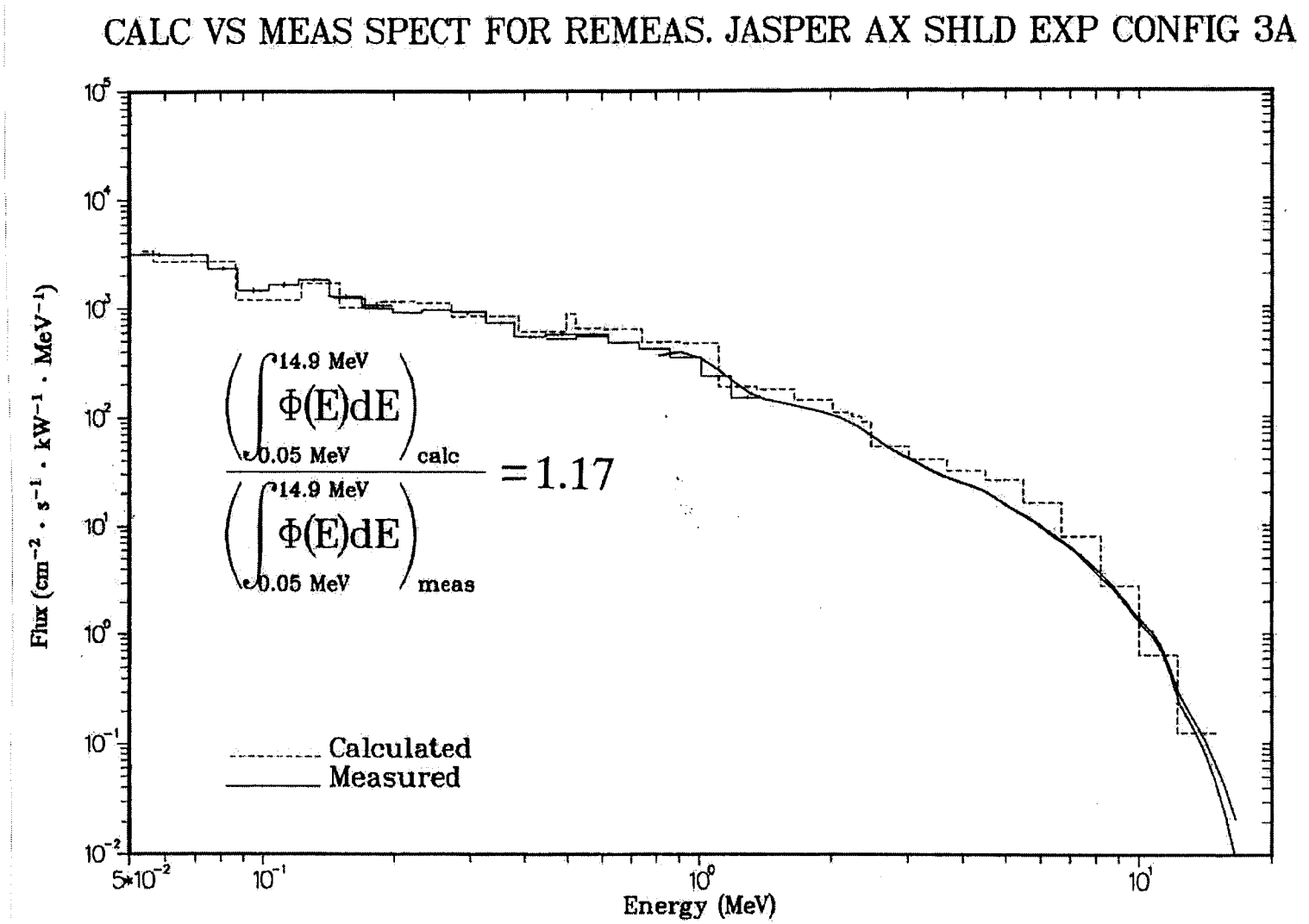

Figure G38. Comparison of calculated and measured neutron spectra behind Jasper Axial Shield Experiment remeasurement Configuration III.A.

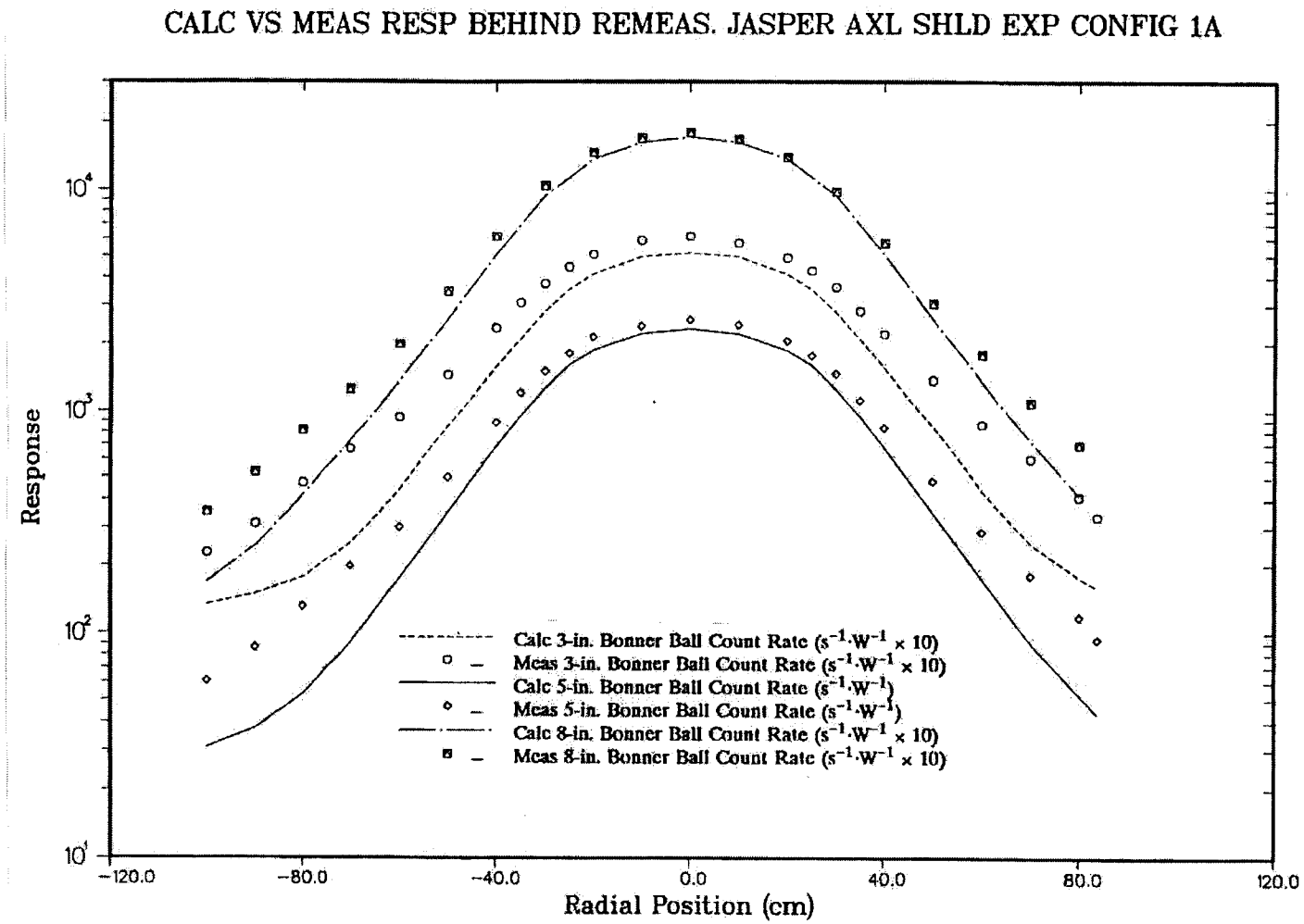

Figure G39. Comparison of calculated and measured Bonner Ball count rates for radial traverses 30 cm behind Jasper Axial Shield Experiment remeasurement Configuration I.A and calculations using standard-weighted UO_2 cross sections.

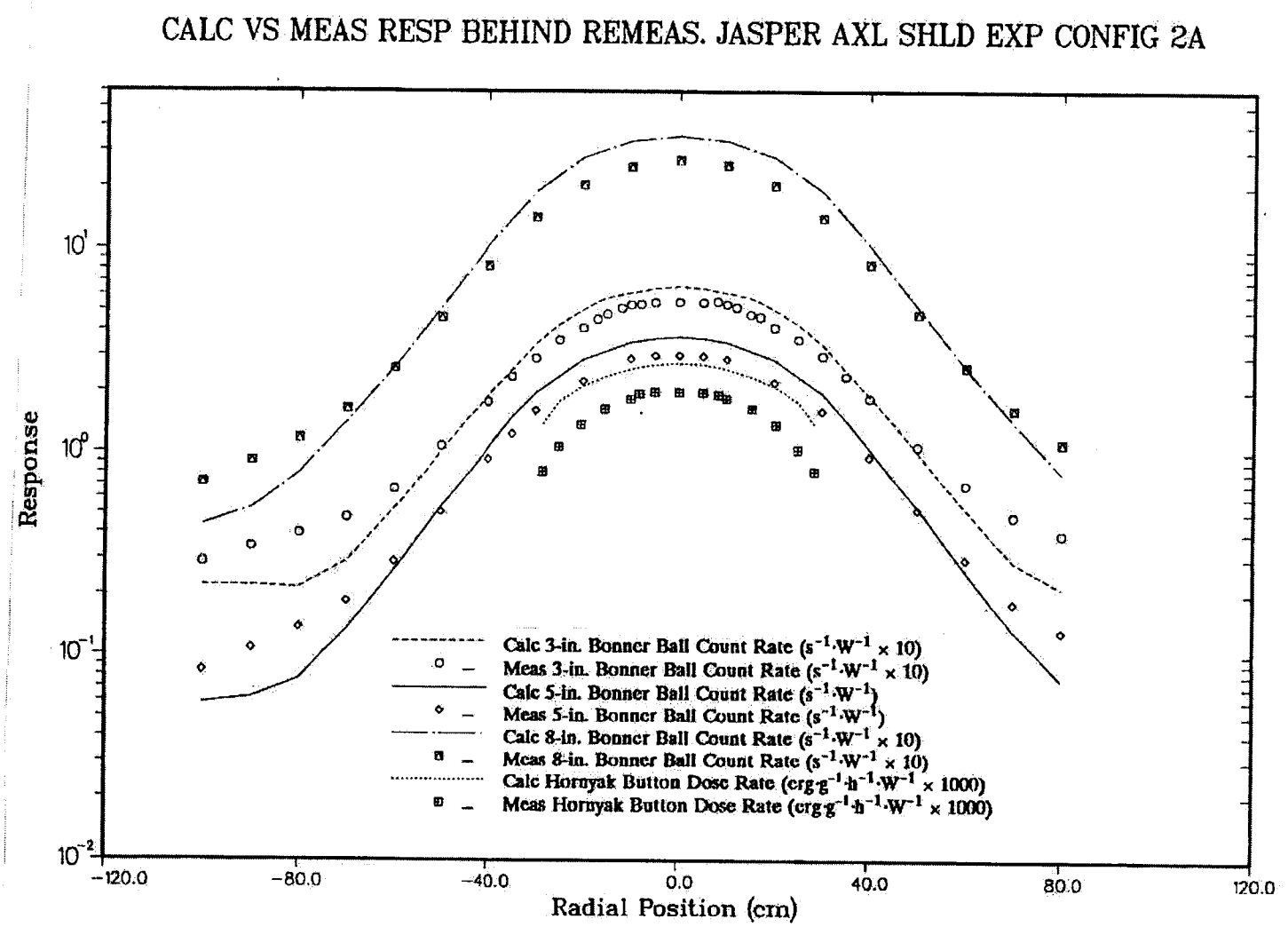

Figure G40. Comparison of calculated and measured Bonner Ball count rates and Hornyak button responses for radial traverses 30 cm behind Jasper Axial Shield Experiment remeasurement Configuration II.A and calculations using standard-weighted UO_2 cross sections.

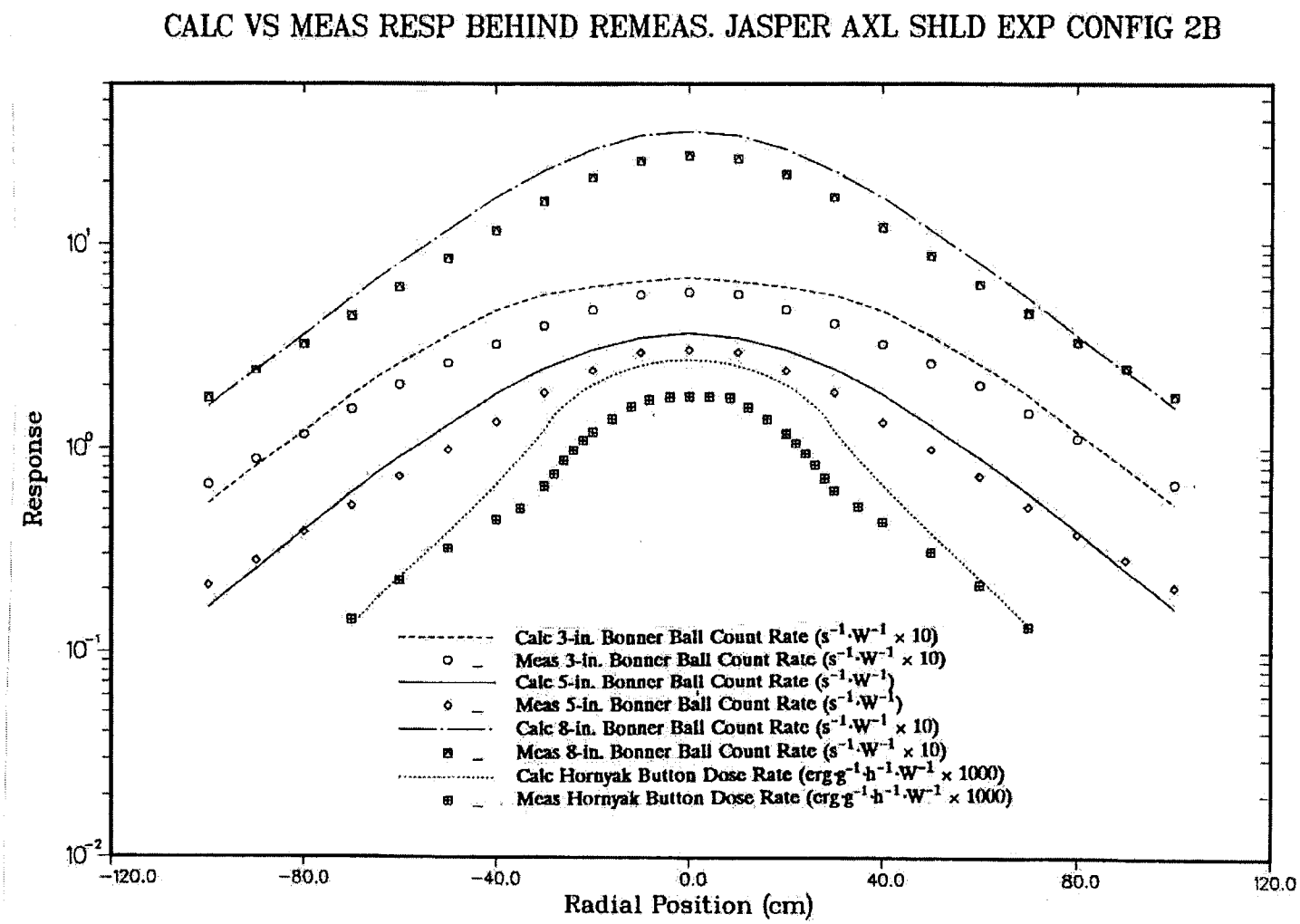

Figure G41. Comparison of calculated and measured Bonner Ball count rates and Hornyak button responses for radial traverses 30 cm behind Jasper Axial Shield Experiment remeasurement Configuration II.B and calculations using standard-weighted UO_2 cross sections.

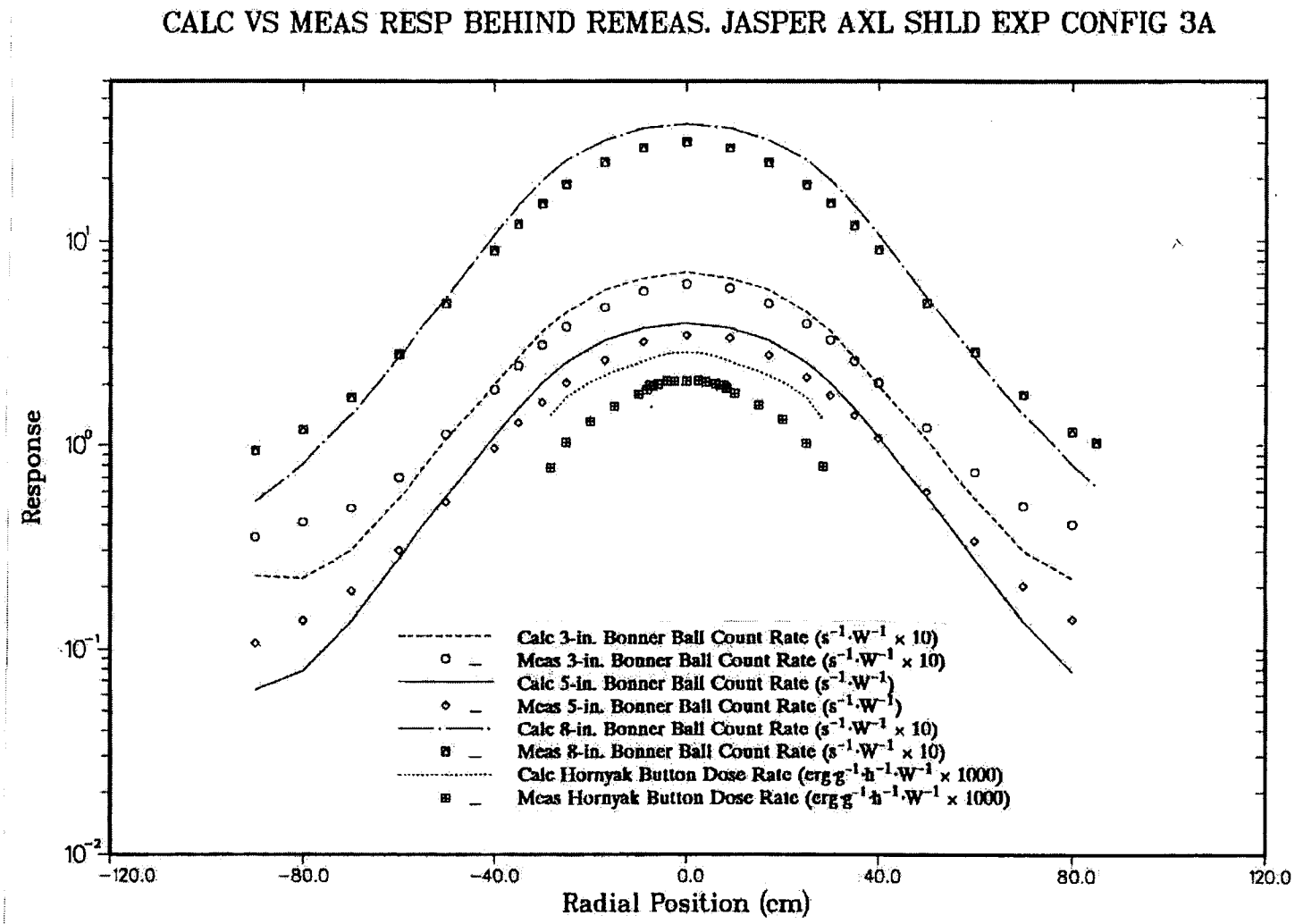

Figure G42. Comparison of calculated and measured Bonner Ball count rates and Hornyak button responses for radial traverses 30 cm behind Jasper Axial Shield Experiment remeasurement Configuration III.A and calculations using standard-weighted UO_2 cross sections.

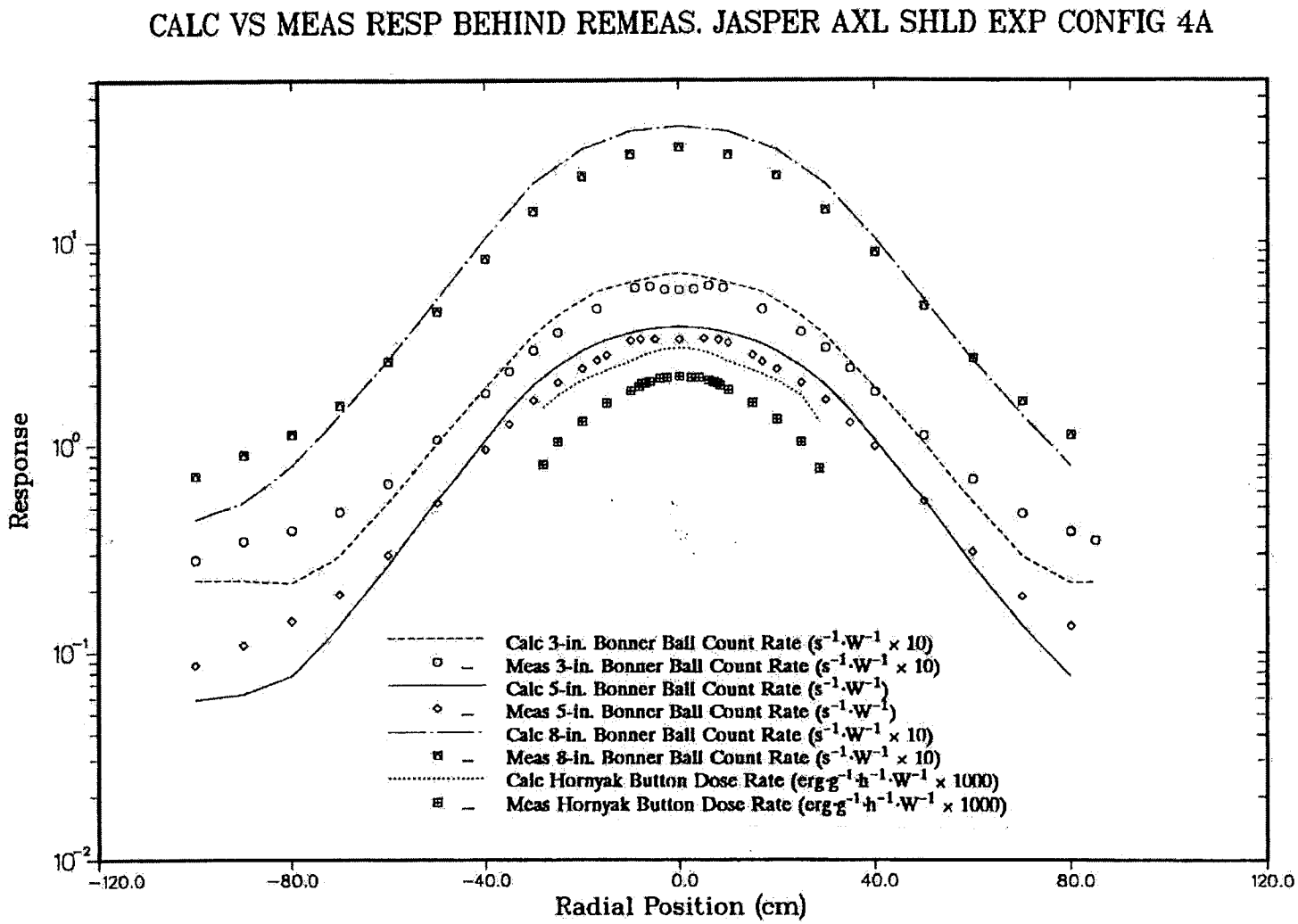

Figure G43. Comparison of calculated and measured Bonner Ball count rates and Hornyak button responses for radial traverses 30 cm behind Jasper Axial Shield Experiment remeasurement Configuration IV.A and calculations using standard-weighted UO_2 cross sections.

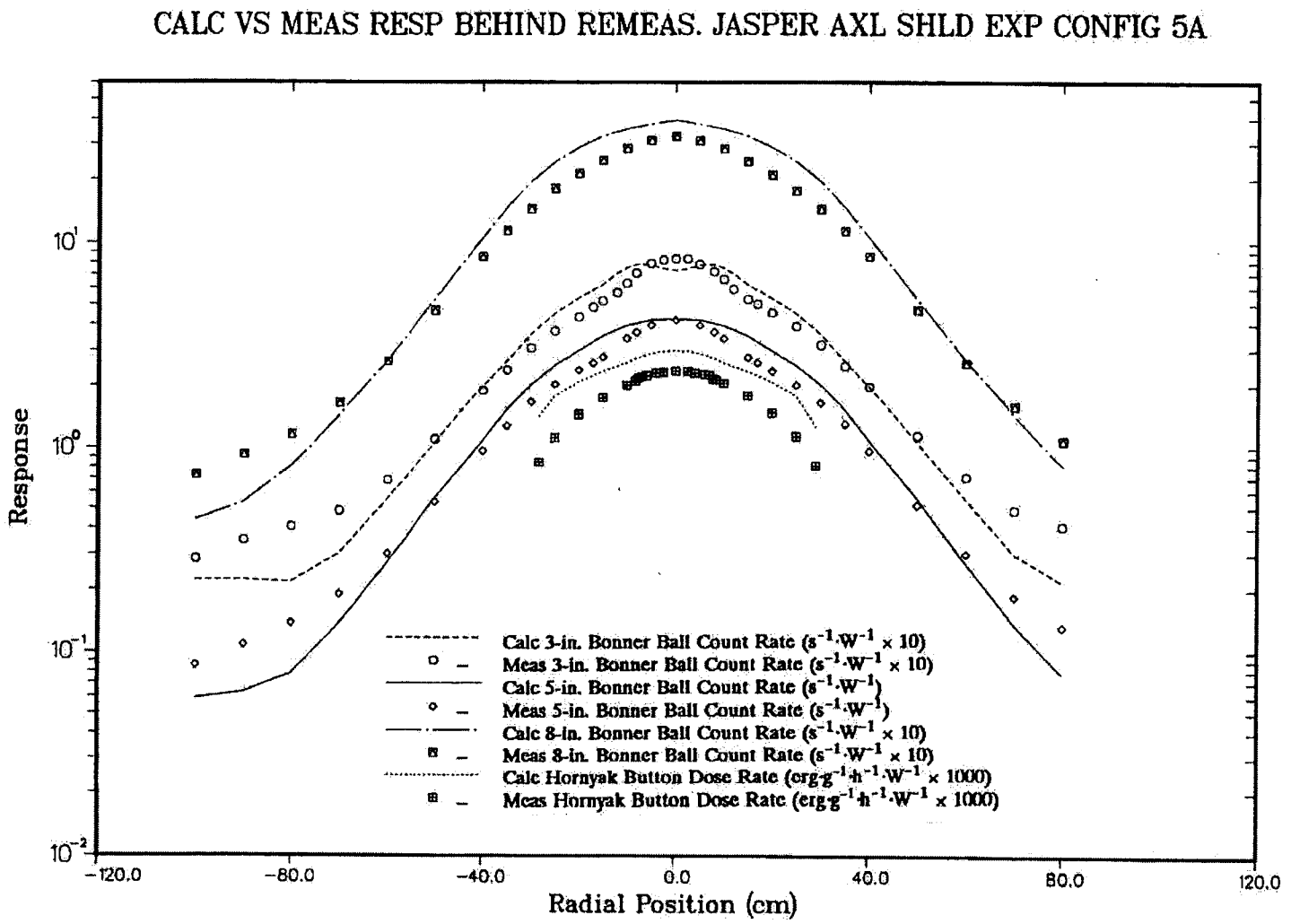

Figure G44. Comparison of calculated and measured Bonner Ball count rates and Hornyak button responses for radial traverses 30 cm behind Jasper Axial Shield Experiment remeasurement Configuration V.A and calculations using standard-weighted UO_2 cross sections.

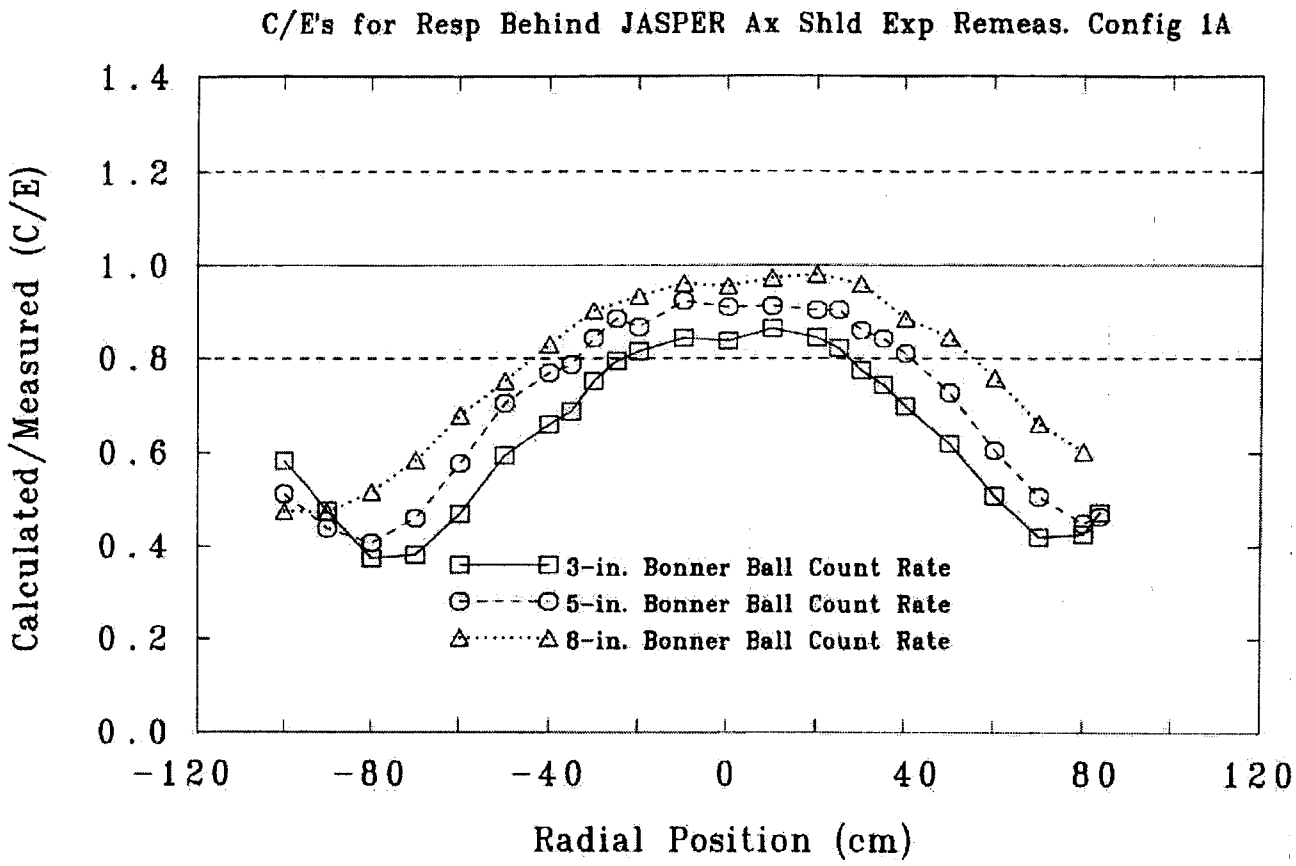

Figure G45. Calculated-to-measured (C/E) response ratios for radial traverses 30 cm behind Jasper Axial Shield Experiment remeasurement Configuration I.A and calculations using standard-weighted UO_2 cross sections.

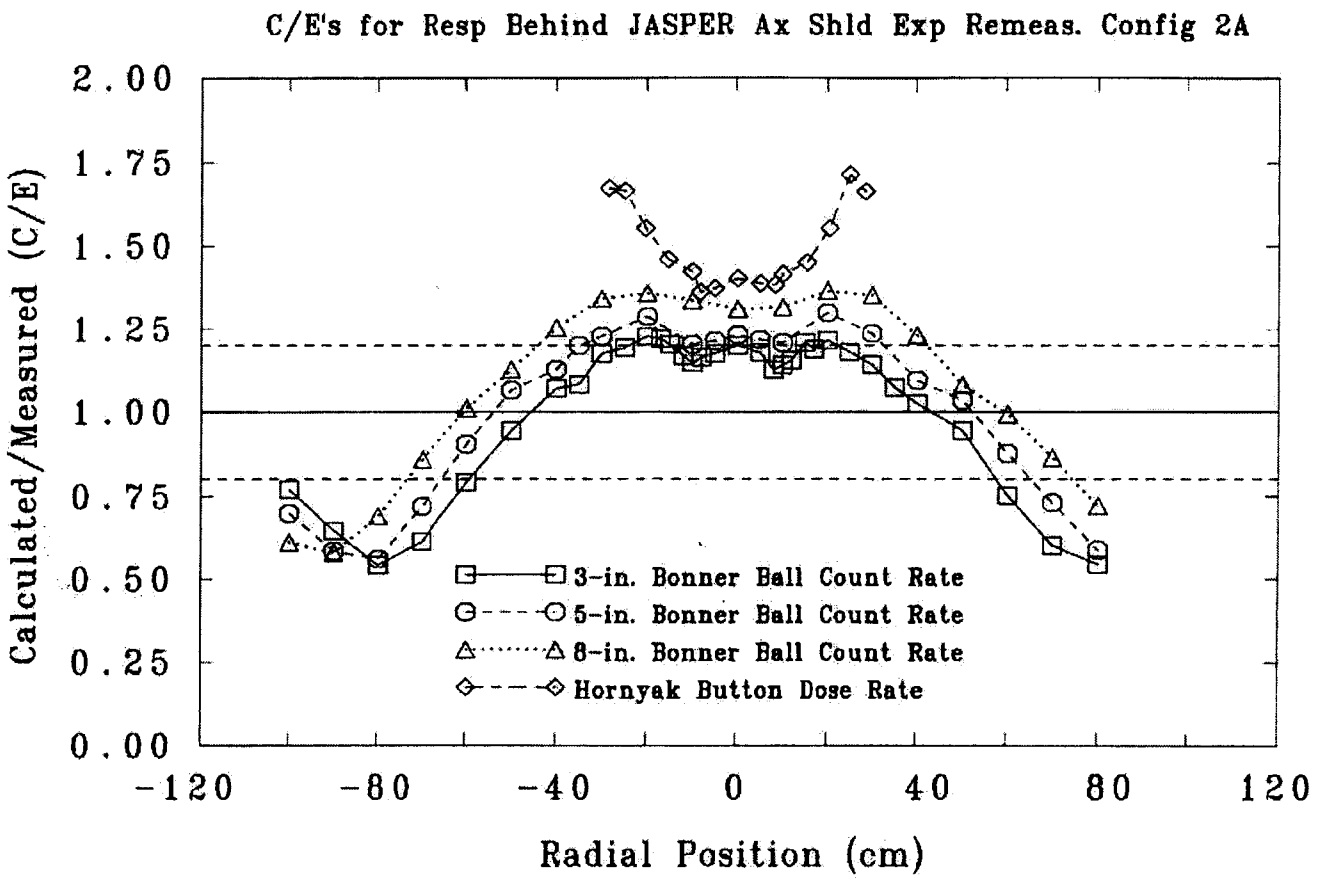

Figure G46. Calculated-to-measured (C/E) response ratios for radial traverses 30 cm behind Jasper Axial Shield Experiment remeasurement Configuration II.A and calculations using standard-weighted UO_2 cross sections.

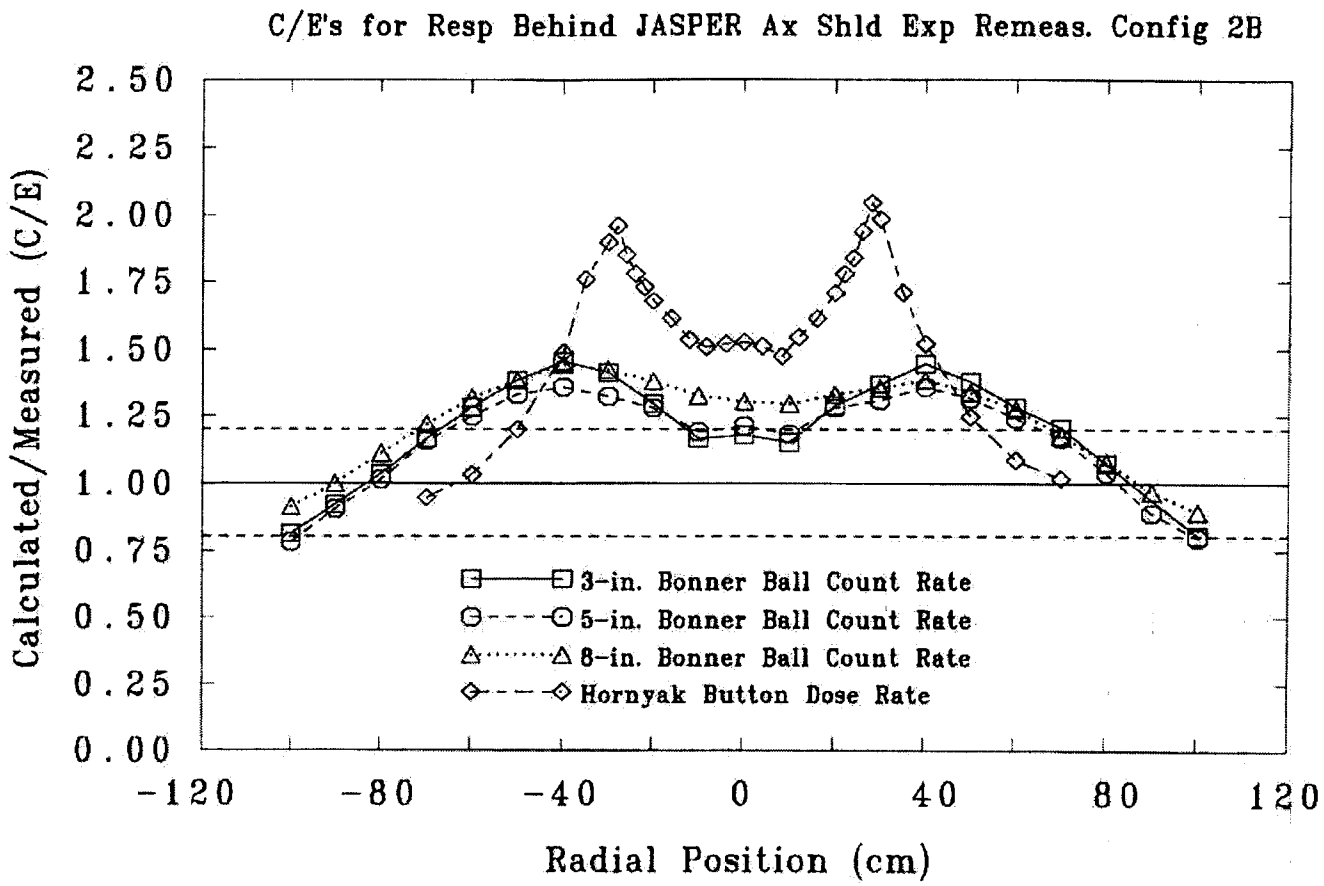

Figure G47. Calculated-to-measured (C/E) response ratios for radial traverses 30 cm behind Jasper Axial Shield Experiment remeasurement Configuration II.B and calculations using standard-weighted UO_2 cross sections.

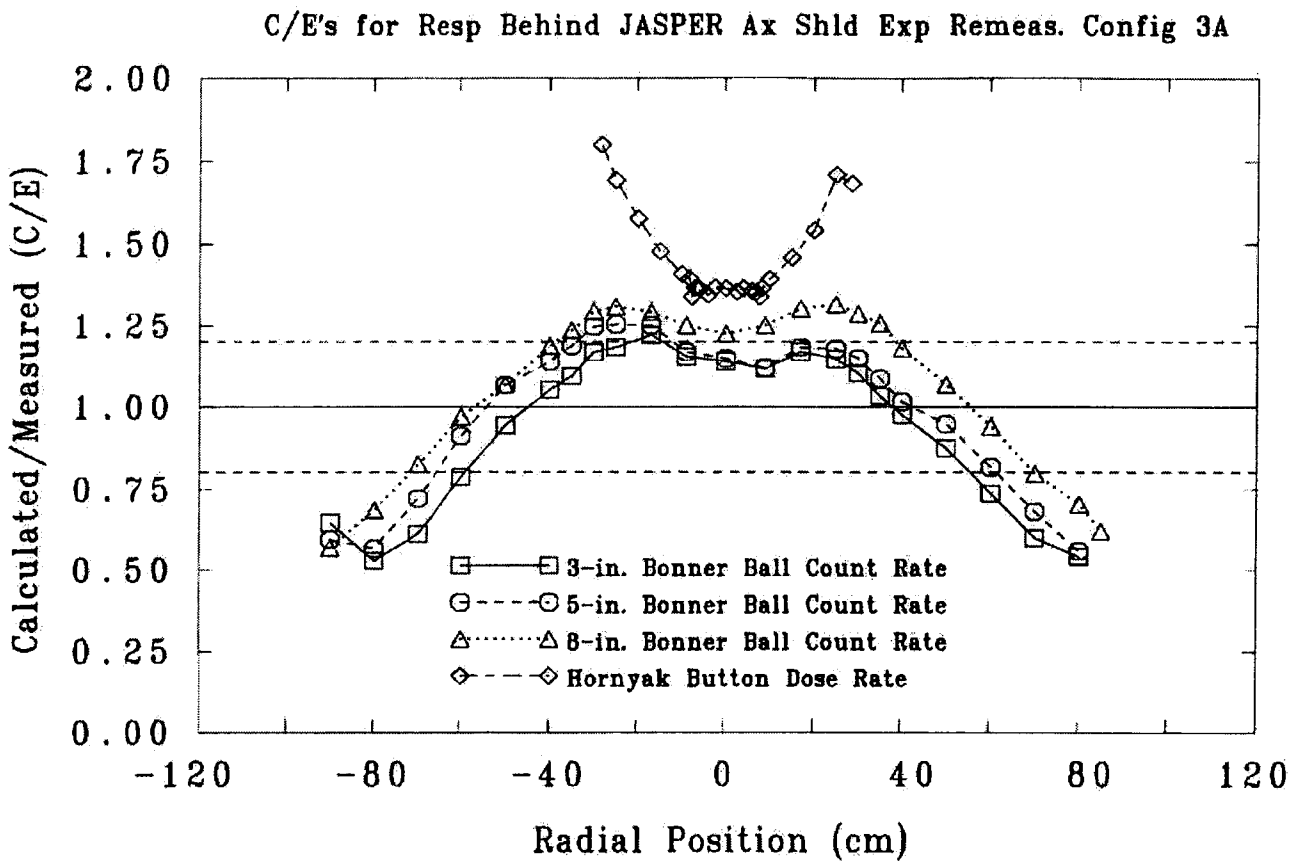

Figure G48. Calculated-to-measured (C/E) response ratios for radial traverses 30 cm behind Jasper Axial Shield Experiment remeasurement Configuration III.A and calculations using standard-weighted UO_2 cross sections.

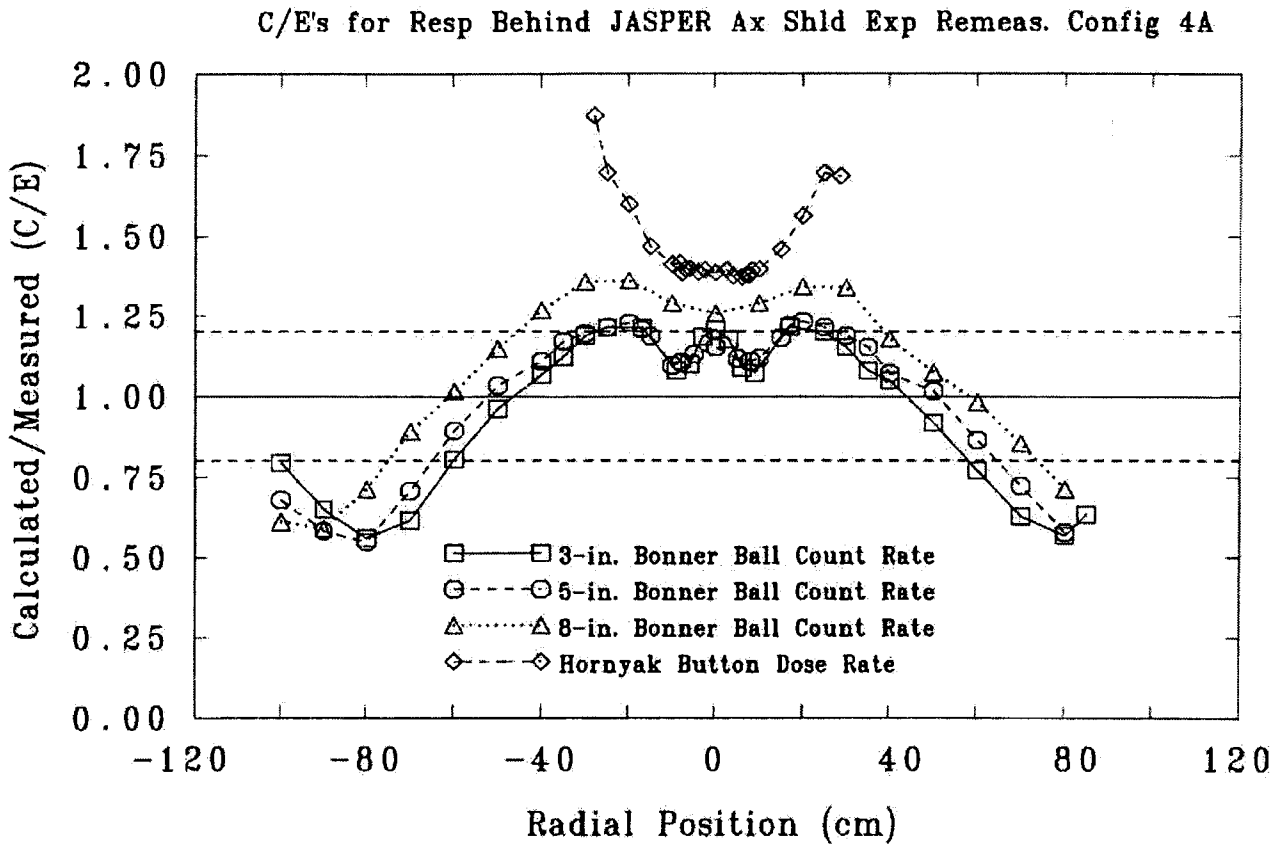

Figure G49. Calculated-to-measured (C/E) response ratios for radial traverses 30 cm behind Jasper Axial Shield Experiment remeasurement Configuration IV.A and calculations using standard-weighted UO_2 cross sections.

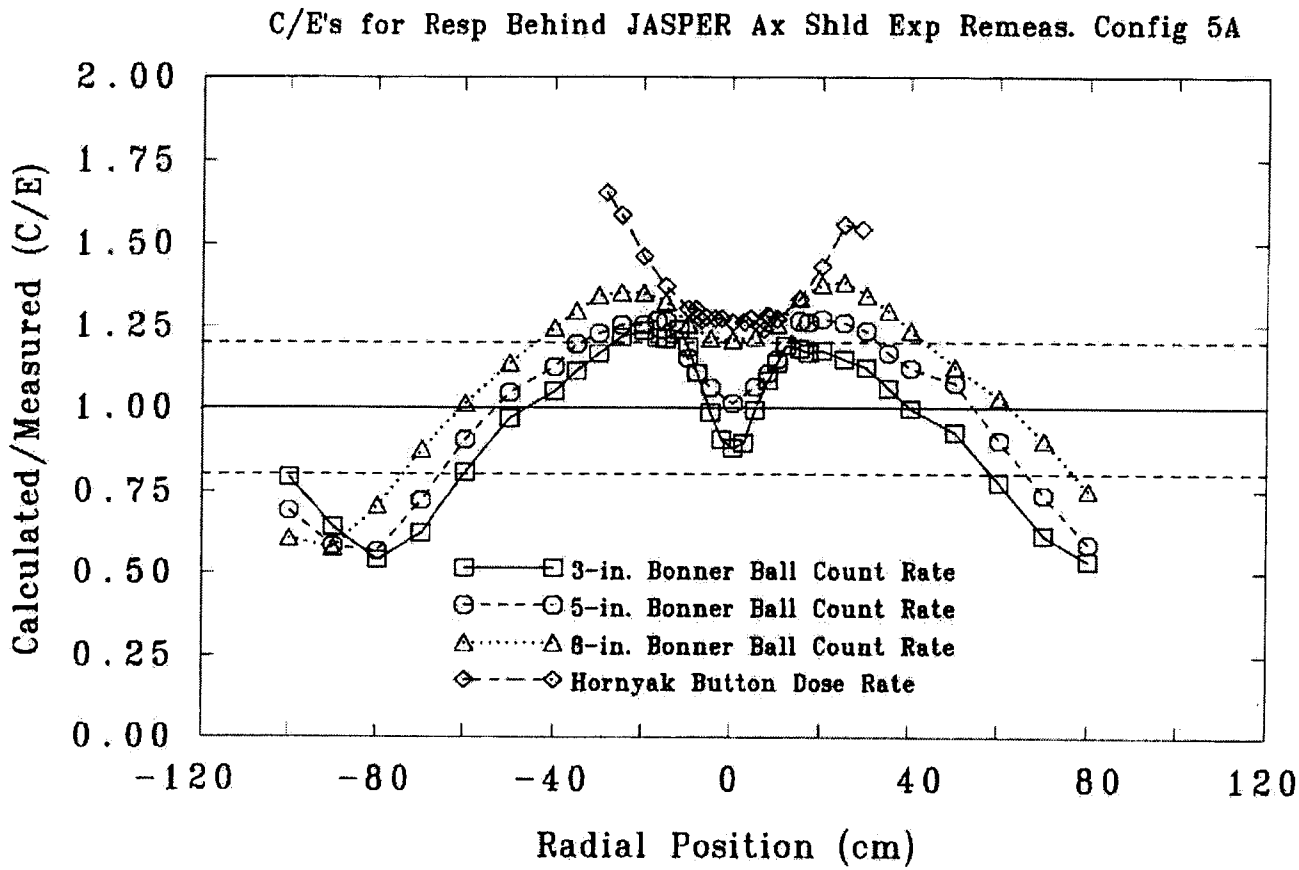

Figure G50. Calculated-to-measured (C/E) response ratios for radial traverses 30 cm behind Jasper Axial Shield Experiment remeasurement Configuration V.A and calculations using standard-weighted UO_2 cross sections.

DISTRIBUTION

1. J. M. Barnes
2. J. A. Bucholz
3. J. N. Herndon
4. D. L. Hill
5. H. T. Hunter
6. D. T. Ingersoll
7. C. O. Slater
8. ORNL Central Research Library
9. NSTD Reports Office
10. Laboratory Records - RC
11. DOE Office of Scientific and Technical Information (OSTI)

EXTERNAL DISTRIBUTION

12. Office of Assistant Manager for Energy Research and Development, DOE-OR, P.O. Box 2008, Oak Ridge, TN 37831-6269/
13. L. F. Blankner, Energy Research and Development, DOE-OR, P.O. Box 2008, Oak Ridge, TN 37831-6269.
14. A. Shono, O-Arai Engineering Center, Japan Nuclear Cycle Development Institute, 4002 Narita, O-Arai-Machi, Higashi-Kbaraki-Gun, Ibaraki-Ken, 311-1393, Japan.
15. K. Chatani, Power Reactor and Nuclear Fuel Development Corporation, 4002 Narita-Cho, O-Arai-Machi, Ibaraki-Ken, 311-13, Japan.
16. N. Ohtani, Director, Research & Development Department, The Wakasa Wan Energy Research Center, 64-52-1, Nagatani, Tsuruga, Fukui, 914-0192, Japan.
17. Morio Takemura, Manager, Nuclear Fuel Cycle Systems Section, Research and Development Department, Power Plant Division, Kawasaki Heavy Industries, Ltd., 6-5, 2 Chome, Minamisuna, Koto-ku, Tokyo 136-8588, Japan.
18. Nakao Makoto, Nuclear Systems Division, Kawasaki Heavy Industries, Ltd., 6-5, 2 Chome, Minamisuna, Koto-ku Tokyo 136-8588, Japan.